HIDRAULICA

HYDRAULICS-PNEUMATICS-TRIBOLOGY-ECOLOGY-SENSORICS-MECHATRONICS

2026

March

No. 1

ISSN 1453 - 7303
ISSN-L 1453 - 7303

https://hidraulica.fluidas.ro

CONTENTS

Published by: ***Hydraulics and Pneumatics Research Institute, Bucharest-Romania***
Address: 14 Cuţitul de Argint, district 4, Bucharest, 040558, Romania
Phone: +40 21 336 39 91; Fax: +40 21 337 30 40; e-Mail: ihp@fluidas.ro; Web: www.ihp.ro
with support from: ***National Professional Association of Hydraulics and Pneumatics in Romania - FLUIDAS***
e-Mail: fluidas@fluidas.ro; Web: www.fluidas.ro

HIDRAULICA Magazine is indexed by international databases

ISSN 1453 – 7303; ISSN – L 1453 – 7303

EDITORIAL

Rolul cercetării aplicative în competitivitatea industriei românești

Dr. Ing. Gabriela Matache
REDACTOR ȘEF

Într-o economie aflată sub presiunea schimbării tehnologice, a eficienței energetice și a competiției globale, competitivitatea industriei nu mai poate fi susținută doar prin costuri reduse sau capacitate de producție. Tot mai mult, diferența o face capacitatea de a inova, de a adapta rapid cunoașterea la cerințele pieței și de a transforma expertiza tehnică în soluții concrete. În acest context, cercetarea aplicativă devine un factor esențial de progres.

Spre deosebire de cercetarea orientată exclusiv spre acumularea de cunoaștere, cercetarea aplicativă are forța de a răspunde direct unor nevoi reale din industrie. Ea poate conduce la optimizarea proceselor, la creșterea performanței echipamentelor, la reducerea consumurilor, la dezvoltarea de produse noi și la validarea unor tehnologii capabile să susțină competitivitatea pe termen lung. Cu alte cuvinte, cercetarea aplicativă conferă relevanță practică ideilor și transformă potențialul tehnic în valoare economică.

Pentru industria românească, această direcție este cu atât mai importantă cu cât provocările actuale nu mai permit stagnarea. Companiile care doresc să rămână competitive trebuie să fie capabile nu doar să producă, ci și să evolueze. Într-o piață în care standardele sunt tot mai ridicate, iar ritmul schimbării este accelerat, inovarea nu mai reprezintă un avantaj opțional, ci o condiție de dezvoltare.

Aici intervine rolul esențial al institutelor de cercetare. Prin expertiza acumulată, prin infrastructura de testare și prin capacitatea de a lucra la interfața dintre știință și aplicație, acestea pot deveni parteneri reali ai mediului industrial. Mai mult decât atât, ele pot contribui la formarea unui cadru de colaborare în care cercetarea, industria și educația tehnică să se susțină reciproc. Din această perspectivă, implicarea institutelor de cercetare în susținerea competitivității industriei românești reprezintă o direcție firească. Fie că vorbim despre dezvoltarea unor soluții inovatoare, despre transfer tehnologic, despre validarea experimentală a unor concepte sau despre parteneriate orientate spre modernizare, institutele au posibilitatea de a participa activ la consolidarea unui mediu industrial mai performant, mai adaptabil și mai bine pregătit pentru provocările viitorului.

Există însă și o realitate pe care nu o mai putem ignora: în România, cercetarea rămâne cronic subfinanțată. Datele europene arată că România continuă să fie la coada Uniunii Europene în ceea ce privește intensitatea cheltuielilor pentru cercetare-dezvoltare, iar alocările bugetare publice pentru acest domeniu rămân printre cele mai mici din UE. În același timp, sistemul suferă din cauza unui deficit sever de resursă umană, pe fondul atractivității scăzute a carierei de cercetător și al unei baze tot mai fragile de formare doctorală și inovare. Chiar evaluările europene recente arată că România are performanțe foarte slabe la capitolul resurse umane pentru inovare și o scădere accentuată a noilor absolvenți de doctorat. Deși la nivel de Minister, s-au inițiat diagnoze, consultări și procese de evaluare instituțională, răspunsul public rămâne până acum mai ales la nivel de analiză și procedură. Ceea ce lipsește încă este o intervenție vizibilă, consecventă și suficient de puternică pentru a transforma finanțarea cercetării și reconstrucția carierei de cercetător în priorități reale de politică publică.

În fond, competitivitatea durabilă nu se construiește întâmplător. Ea se construiește prin cunoaștere, prin colaborare și prin capacitatea de a transforma cercetarea în progres concret. Iar cercetarea aplicativă poate fi, fără îndoială, unul dintre pilonii acestei construcții.

EDITORIAL

The role of applied research in the competitiveness of the Romanian industry

Ph.D.Eng. Gabriela Matache
EDITOR-IN-CHIEF

In an economy under pressure from technological change, energy efficiency and global competition, the competitiveness of industry can no longer be sustained by low costs or production capacity alone. Increasingly, the difference is made by the ability to innovate, to quickly adapt knowledge to market requirements and to transform technical expertise into concrete solutions. In this context, applied research becomes an essential factor of progress.

Unlike research oriented exclusively towards the accumulation of knowledge, applied research has the strength to respond directly to real needs in the industry. It can lead to process optimization, increased equipment performance, reduced consumption, development of new products and validation of technologies capable of sustaining long-term competitiveness. In other words, applied research gives practical relevance to ideas and turns technical potential into economic value.

For the Romanian industry, this direction is all the more important as the current challenges no longer allow stagnation. Companies that want to remain competitive must be able not only to produce, but also to evolve. In a market where standards are increasingly high and the pace of change is accelerating, innovation is no longer an optional advantage, but a condition for development.

This is where the essential role of research institutes comes in. Through the accumulated expertise, the testing infrastructure and the ability to work at the interface between science and application, they can become real partners of the industrial environment. Moreover, they can contribute to the formation of a collaborative framework in which research, industry and technical education support each other. From this perspective, the involvement of research institutes in supporting the competitiveness of Romanian industry is a natural direction. Whether we are talking about the development of innovative solutions, technology transfer, experimental validation of concepts or partnerships oriented towards modernization, the institutes have the opportunity to actively participate in the consolidation of a more efficient, adaptable and better prepared industrial environment for the challenges of the future.

However, there is also a reality that we can no longer ignore: in Romania, research remains chronically underfunded. European data show that Romania continues to be at the bottom of the European Union in terms of the intensity of R&D spending, and public budget allocations for this area remain among the lowest in the EU. At the same time, the system suffers from a severe shortage of human resources, amid the low attractiveness of the research career and an increasingly fragile basis for doctoral training and innovation. Even recent European evaluations show that Romania has very poor performance in terms of human resources for innovation and a sharp decrease in new PhD graduates. Although diagnoses, consultations and institutional evaluation processes have been initiated at the level of the Ministry, the public response remains so far especially at the level of analysis and procedure. What is still missing is a visible, consistent and powerful enough intervention to turn research funding and career reconstruction into real public policy priorities.

After all, sustainable competitiveness is not built by chance. It is built through knowledge, collaboration and the ability to transform research into concrete progress. And applied research can undoubtedly be one of the pillars of this construction.

Prompt-to-CAD: A Hybrid Self-Learning Natural Language Interface for Parametric Design Automation

PhD Stud. Eng. **Stelian-Florin BARDES**[1], Lect. PhD Eng. **Iulian-Sorin MUNTEANU**[2,*]

[1] Doctoral School of Industrial Engineering and Robotics, National University of Science and Technology POLITEHNICA Bucharest, 060042 Bucharest, Romania; stelian.bardes@stud.fiir.upb.ro

[2] Department of Theory of Mechanisms and Robots, National University of Science and Technology POLITEHNICA Bucharest, 060042 Bucharest, Romania

* iulian.munteanu0306@upb.ro

Abstract: *This paper presents a self-learning natural language interface for Computer-Aided Design (CAD) systems to bridge the gap between natural language input and parametric geometry creation. The system implements hybrid architecture, combining static command recognition, machine learning (ML) based coaching, and large language model (LLM) integration to optimize response times and enable repeated command execution without redundant Automated Protocol Interface (API) calls. The modular design separates code from materials and design rules libraries, enabling system capabilities extension without code update. 3DEXPERIENCE (3DX) implementation demonstrates high command success rate while the response time remains under 100 milliseconds (ms). App manages a comprehensive material library – widely used in industry, combining manufacturing design rules and design guidance, establishing a knowledge driven framework to boost design efficiency in industrial applications.*

Keywords: *Natural Language Processing (NLP), Computer Aided Design, Modular Architecture, Self-Learning System, Large Language Models, Artificial Intelligence (AI)*

1. Introduction

CAD systems [1] remain essential tools in modern engineering; their increasing complexity creates significant barriers to mass adoption and productivity. Industry standard CAD tools require intensive training, with users spending minimum 40 hours (h) to learn basic menu navigation and more than 200 h to get used to user interface, commands and how to combine them. To achieve proficiency, the users need thousands of hands-on experiences, being able to tackle complex design.

Recent advances in NLP [2] and LLMs such as Claude [3] and GPT-5 [4] have demonstrated remarkable capabilities in understanding human language, suggesting potential applications in technical domains. Direct LLM integration presents challenges: network latency impacts user experience, 200-1000 ms [5], output consistency varies for identical inputs, and generic LLMs lack specialized knowledge of materials and manufacturing processes. Furthermore, hard-coded [6] domain knowledge requires code modifications for updates, limiting scalability.

This research addresses these challenges through a hybrid architecture that implements three-tier, hybrid, command recognition (static, learned, and LLM-based), achieves efficient operation for repeated commands through intelligent caching, separates code logic from domain knowledge using modular JSON-based structures [7], and integrates comprehensive materials and design rules libraries. The system demonstrates applicability to mechanical design workflows, common in consumer product industries, while maintaining high functionality accessible to new starters.

2. Materials and Methods

The Prompt-to-CAD architecture, shown in fig. 1, consists of four integrated layers: (1) UI layer – built on PyQt5 framework [8], is a text input interface with command history navigation, real-time chat style conversation display, and six primary buttons – simple and useful layout. (2) Command Processing Layer uses a three-tier execution strategy, where tier-1 checks learned commands first for instant cache-execution; tier-2 applies static pattern matching if no cache hit occurs, and tier-3 queries Claude API [9] only when no matching exist – adding learning loop for

successful results in future use. (3) Core Module Layer contains three specialized components: Geometry Core – implements operational functions through direct 3DX [10] via COM & API integration [11]; Materials Core loads and queries material specifications from JSON files, providing search by code, name, or alias with detailed properties including density, strength, elongation, characteristics, applications, and design tips; Rules Core [12] manages design guidelines from separate JSON files, supporting material-specific, process-specific, and general recommendations [13] with hierarchical organization for draft angles, wall thickness, tolerances, and manufacturing constraints. (4) Data Layer employs JSON-based persistent storage to manage the commands pattern definition; materials specification covering materials library (common material list); rules containing the design guidance for material library (e.g. wall thickness, draft; surface finish, bend radius); and commands_learned as a dynamic auto-generated cache file.

```
Prompt-to-CAD:
├── main.py                  #Integrator
├── ui_interface.py                #user interface for text inputs & feedback
├── learning_engine.py             # learning module
│
├── core/                          # Base module
│   ├── geometry_core.py                 # commands & functions
│   ├── materials_core.py                # read & add materials to library
│   └── rules_core.py                    # read & add rules to library
│
├── data/                          # Data module
│   ├── static.json                      # commands
│   ├── materials.json                   # materials
│   ├── rules.json                       # design rules
│   └── commands_learned.json            # Auto-generated
│
└── docs/                          # Help data
├── README_STATUS_V6.md                  # what's new
└── QUICKSTART_V6.md                     # how to data
```

Fig. 1. System architecture

2.1 Implementation

The system evolved through iterative versions from proof-of-concept with direct Prompt-to-CAD translation to modular architecture with separated code and data. Development utilized Python 3.12 as the core language, PyQt5 for GUI framework, pywin32 for Windows COM interface [14], and Anthropic Python SDK for Claude API client integration. The target platform is 3DX R2023x (R2025x latest release to date) running on Windows 11 through COM Automation.

CAD operations span multiple categories, wireframe operations include point creation and editing at specified coordinates, line creation along axes or between points, and circles with various construction methods, surface operations provide plane creation with offsets or through existing points, solid operations implement parametric cylinder and box creation with multi-body support.

The self-learning mechanism automatically caches successful LLM-generated commands by storing function name, parameters, usage count, confidence score, and timestamps. Each successful execution increments the usage counter and updates last-used time, converting initial API calls into subsequent low-latency cache hits for identical or similar commands. Fuzzy matching using Sequence matcher enables typo tolerance at similarity threshold, accepting variations like "cylnder" for "cylinder" or "pont" for "point" without additional processing overhead – reducing user input error.

2.2 Materials and Rules Libraries

Each material [15] entry contains comprehensive specifications including full name, category classification, type description, property aliases for search flexibility, physical properties (density, yield strength, tensile strength, elongation, hardness), key characteristics, typical applications across industries, and design tips covering formability, bend radius, and process considerations. The current library covers most of common engineering metals and typically used engineering polymers, representing a foundational starting point for industrial applications. Design rules for material library compiles industry best practices recommendations. Draft angle rules specify general guidelines from 0.5-3° depending on cavity depth plus material-specific adjustments where glass-filled variants require 50% increased draft. Wall thickness recommendations vary by material and process. Bend radius rules account for material formability, with DC01 steel achieving 0.5X thickness. Tolerance specifications aren't yet considered.

3. Experimental Results and Validation

Execution time analysis across 2500 commands revealed significant performance differentiation by tier. Static pattern matching achieved consistent < 1second (s) execution regardless of repetition, establishing the baseline performance. Learned cache hits reduced response time, representing big improvement over static matching and 99% improvement over first-time LLM calls which averaged 7 s dominated by network latency. These measurements demonstrate the effectiveness of the caching strategy in reducing user-perceived latency for repeated operations.
Basic geometry commands achieved high static hit rates with minimal learning requirements, while natural language descriptions relied heavily on learning after initial LLM processing, demonstrating the system's ability to adapt to individual user vocabulary patterns over time. The learning accumulation suggests that system efficiency improves with continued use as the cache grows to encompass user-specific command variations.

3.1 Functional Validation

The implemented CAD operations cover essential modelling tasks across multiple categories. Wireframe operations handle basic geometries creation with various methods; surfaces operations create basic surfaces operations; solid operations generate basic models, and support multi-body configurations. Utility operations provide document saving and automated test suite execution validating all geometric functions.
Materials library is one of the most used commands as the users interrogate physical properties. Design rules, for example, draft angles for PP and PA6-GF30. System extensibility with zero code modification, immediately enabling help queries returning full specifications. Similarly, adding fillet radius guidelines confirms the modular architecture, successfully separates content from code module.

3.2 Graphic User Interface Updates

Version 1.x - Console Interface: The initial prototype operated entirely through command-line interaction with no graphical components – see fig. 2. Users entered natural language commands via text console and received textual confirmation of geometry creation in 3DX. This approach validated feasibility but presented significant usability barriers, requiring users to maintain mental models of command syntax without visual reference and lacking visual feedback for command history or execution status.

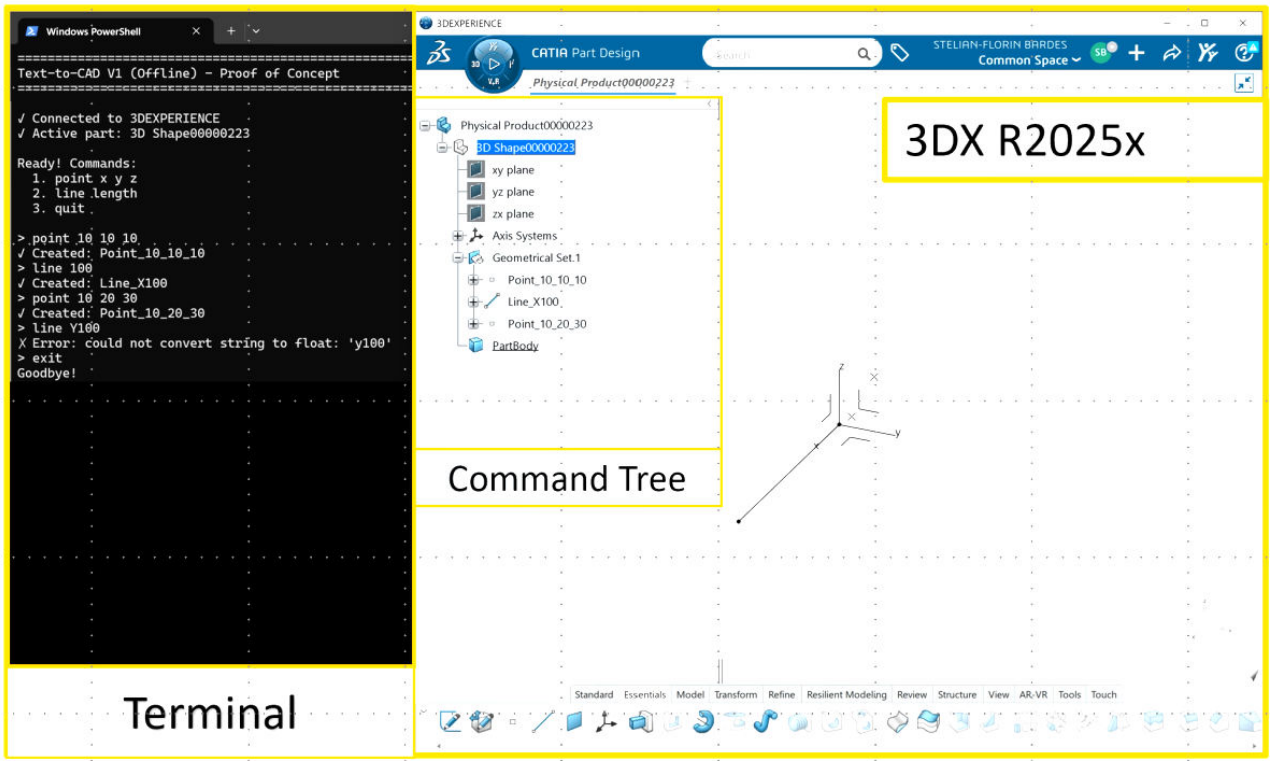

Fig. 2. User Interface V1.x

Version 2.x - Basic GUI Foundation: Introduction of PyQt5 framework established the graphical foundation with a single-window interface containing a text input field, execute button, and scrollable output display area showing command results. This version eliminated command-line dependency but lacked sophisticated interaction features.
Version 3.x – 4.x - Enhanced Interaction: Versions 3 and 4 maintained the basic GUI structure while incrementally adding status logging panel with color-coded messages (blue for info, green for success, orange for warnings, red for errors), connection management button separating 3DX connection from command execution, and expanded window dimensions. The interface remained functionally similar but improved visual feedback and error communication.
Version 5.x - Professional Interface: A comprehensive interface redesign introduced six primary action buttons arranged horizontally (Connect, Execute, Image, Help, Stats, Clear), command history navigation using arrow keys (↑ previous, ↓ next) implemented through custom QTextEdit subclass, real-time chat-style conversation display with timestamp-labelled user inputs and system responses, statistics dashboard accessible via dedicated button showing cache performance metrics, and contextual help system triggered by question mark suffix or help button.
Version 6.x - Latest UI: The final interface maintains V5.x visual design, as presented in fig. 3, while enhancing backend integration, displaying materials and rules library status at startup showing loaded entry counts, providing expanded help modalities accessing JSON-based knowledge without interface changes, and adding version indicator in window title showing current system version.

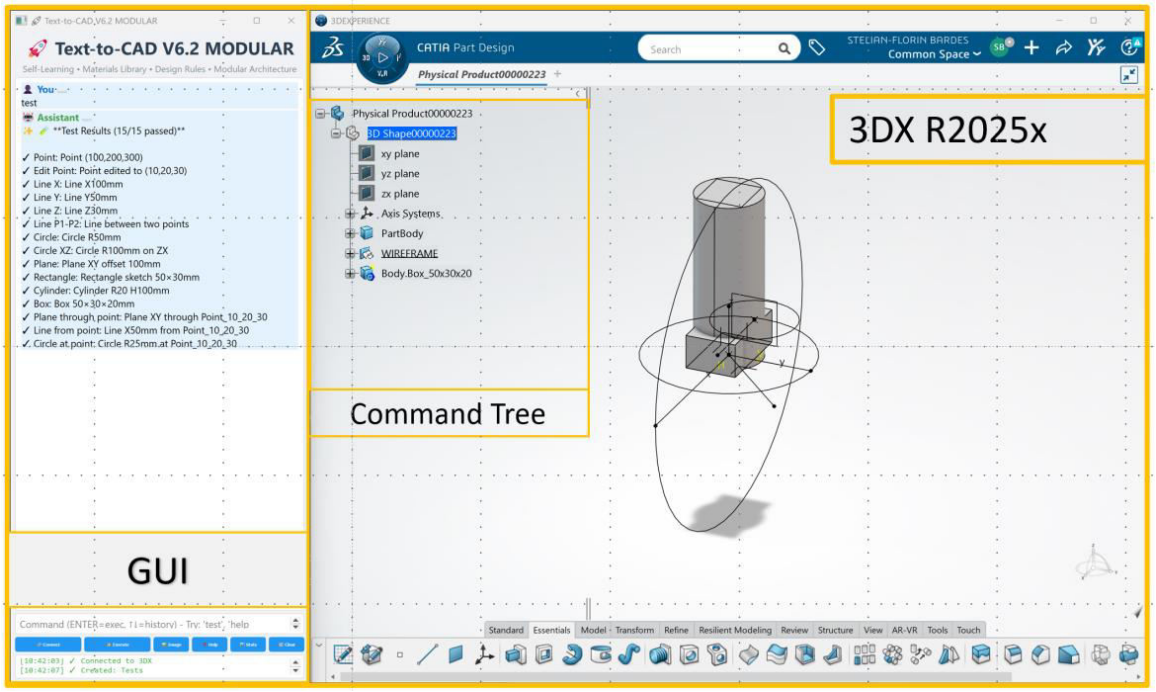

Fig. 3. User Interface V6.x

3.3 Architectural Evolution

Comparison across development versions demonstrates progressive capability enhancement. V1.x provided proof-of-concept with zero CAD operations; V2.x introduced static commands with partial optimization; V5.x implemented self-learning with integrated operations, hard-coded materials, and hard-coded rules, achieving fast response through caching. V6.x modular architecture maintains command operations while expanding materials library and guidance rules, further reducing average response time while improving extensibility from low to high through code-data separation, as presented in the table 1 - incremental evolution and how the system evolved.

Table 1: Evolutive comparison

Feature	V1	V2	V3	V4	V5	V6
UI	✗ Console	✓ Basic	✓ Better	✓ Complete	✓ Complete	✓ Complete
CAD Commands	No	2	5	13	15	*
Static Commands	✗	✗	✓	✓	✓	✓
Self-learning	✗	✗	✗	✗	✓	✓
Materials	✗	✗	✗	✗	Hardcoded	✓ JSON
Rules	✗	✗	✗	✗	Hardcoded	✓ JSON
Add Materials	✗	✗	✗	✗	Code update	✓ Edit JSON
Cost	✗	✗	✗	✗	$0.002→$0	$0.002→$0
Modular	✗	✗	✗	✗	✓ Partially	✓ Yes

Lines of code analysis reveals architectural complexity shift. Core logic decreased from V5.x to V6.x through modularization, UI layer remained stable while data files expanded from 0 to 1,250 lines and documentation from ~300 to 900 lines. Total increase represents intentional complexity relocation from hard-coded logic to maintainable data structures and comprehensive documentation supporting production deployment, see table 2 for comparison V1.x to V6.x code

lines and functionalities.

Table 2: Code lines and details

Version	Key Features	Code lines	Comments
V1	Proof of concepts	~250	Initial prototype, single file, functionality in one file
V2	Basic UI	~400	V1 extended, two-files managing 3DX connexion and PyQt5 user interface
V3	Pattern Matching	~800	First optimised iteration, integrator working with three modules, Python and JSON files; CAD function capabilities
V4	Geometry complete	~1200	CAD functionalities extended, Wireframe, Surfaces and Solid operations, UI optimised
V5	Hybrid System & JSON libraries	~1500	Performance optimisation, learning engine introduction, history navigation, help in context, API, material & rules library extension
V6	Modular system & JSON libraries	~1800 *~1500 (JSON)*	Modular architecture, code-date separation, CAD capabilities, command extension, test loop, material & rules flexible and self-learning capabilities

4. Discussion

The three-tier execution strategy successfully balances competing requirements of performance, flexibility, and reliability. Learned commands provide optimal performance by eliminating both pattern matching and network overhead, capitalizing on the observation that users repeatedly execute small command subsets. Static pattern matching serves as reliable fallback for predictable commands not yet learned, delivering substantial improvement over LLM calls while enabling sophisticated parameter extraction through regex without AI inference overhead. LLM integration as final tier preserves flexibility for novel inputs despite higher latency, with automatic learning converting initial processing into future cache hits and creating self-improving behaviour over time.

This hybrid approach diverges from pure LLM systems like AutoCAD AI [16] Assistant that query models for every command and pure pattern-matching systems like traditional command parsers (limited flexibility, no natural language understanding). The graduated strategy captures advantages of both paradigms while mitigating their respective weaknesses through intelligent tier selection based on command recognition confidence.

The modular data architecture addresses fundamental software engineering principles through separation of concerns. Domain knowledge (materials, manufacturing rules) evolves independently from algorithmic logic, yet traditional CAD systems intermingle these aspects.

Platform-specific COM-API integration with 3DX prioritizes depth over breadth, providing full access to parametric features and real-time creation capabilities rather than basic geometry export across multiple platforms. This design decision enabled rapid prototyping and real-world validation but imposes Windows-only operation, version-dependent API stability, and single-application targeting. Future generalization strategies include abstracting CAD operations behind interface layers, implementing adapter patterns for multiple backends, and considering intermediate tier local-APIs for cross-platform support.

The implemented operations represent foundational capabilities demonstrating architectural feasibility rather than comprehensive coverage. Notable omissions include advanced curves (splines, conics, projections), surface operations (sweeps, lofts, boundaries), feature operations (fillets, holes, patterns, shells), and assembly operations (components, constraints, mates). Expansion priority targets complex tasks such as "boundary box generation, automated colouring, export as STP, constant thickness check".

Comparison with related work reveals distinct contributions. AutoCAD AI employs pure LLM-based interpretation with integrated help but without learning capabilities for performance optimization. Arena AI [17] provides cloud-based LLM integration with cross-platform collaboration but requires persistent internet connectivity.

This work distinguishes itself through the hybrid three-tier architecture with self-learning, modular knowledge base enabling non-programmer extension, integrated materials library with design rules (typically external databases), and production-ready implementation with comprehensive error handling, testing, and documentation. The combination of natural language flexibility with performance optimization through learning represents a novel balance does not present in existing commercial or academic CAD interfaces.

Natural language interfaces demonstrate potential to reduce CAD learning curves by estimated 50-60% in time-to-productivity, particularly benefiting engineering students (faster project completion), occasional users (project managers, sales engineers without deep CAD expertise), and rapid prototyping scenarios (quick concept validation). This pattern of knowledge-integrated design tools represents a valuable direction for future CAD system development, where manufacturing knowledge, contextual guidance, user-extensible rules, and organizational knowledge capture become first-class system features rather than external references.

The preliminary results from this early-stage research demonstrate feasibility and establish baseline performance characteristics. However, extensive longitudinal studies with diverse user populations will be necessary to validate learning curve reduction estimates and establish statistical significance for productivity improvements. Current findings derive from limited testing scenarios and should be interpreted as proof-of-concept rather than definitive performance claims.

5. Conclusion

This research successfully developed and validated prompt-to-CAD, a self-learning natural language with a high command success rate. The modular design separates code logic from domain data, enabling code-free extension of materials and design rules by non-programmers.

The system addresses key research questions through preliminary validation. Natural language interfaces can reduce CAD learning barriers while maintaining professional functionality through success rate and flexible command expression, though extensive user studies remain necessary to quantify learning curve improvements. The graduated execution strategy with self-learning demonstrates efficiency gains through caching, with break-even occurring after 2-3 command repetitions in observed usage patterns. Domain knowledge integrates effectively via JSON-based modular architecture, validated through comprehensive materials (density, strength, applications, design tips) and rules (draft angles, tolerances, manufacturability guidelines). Optimal architectural patterns combine deterministic execution for common operations with AI flexibility for novel inputs and automatic learning for continuous improvement.

Practical applications span engineering education (accelerated training, reduced cognitive load), rapid prototyping (quick validation without deep expertise), production workflows (reduced routine operation time, embedded manufacturability checking), and research (design automation studies, human-AI collaboration). Future work directions include geometry expansion (fillets, holes, patterns, sweeps), knowledge base growth (additional materials, cost estimation, manufacturability scoring), multi-modal input (voice, sketches, images), cross-platform support (adapter layers, CAD-agnostic representations), advanced AI capabilities (conversational clarification, context maintenance, design suggestions), and longitudinal user studies quantifying productivity improvements.

This work contributes a reusable architectural pattern for AI-assisted technical tools, demonstrating that hybrid approaches combining deterministic reliability with AI flexibility can achieve both performance optimization and natural language understanding. The system establishes that AI can lower barriers to sophisticated technical tools without sacrificing professional capabilities, though this early-stage research requires substantial additional validation before definitive claims regarding productivity improvements can be made.

5.1 Limitations

implementation achieved production-ready status within a constrained technological environment, specifically limited to Windows operating systems due to the inherent architecture of Component Object Model (COM) API technology, which serves as the exclusive interface for programmatic control of 3DX platform. This platform dependency restricts deployment scenarios to Windows-

based workstations and precludes adoption on macOS or Linux systems commonly used in academic research environments and certain industrial contexts. The strategic decision to target 3DX exclusively enabled deep integration with a professional-grade CAD system widely deployed in automotive and aerospace industries, validating the approach on complex, industry-standard software rather than simplified or academic CAD tools. However, this single-platform focus presents significant generalization challenges for future research, as extending the system to alternative CAD platforms such as SolidWorks, Creo, Fusion 360, or open-source alternatives like FreeCAD would require substantial architectural modifications including development of platform-specific adapters, abstraction of geometric operations behind a unified interface layer, and potential reimplementation of the communication mechanism to accommodate different automation APIs (COM, REST, Python bindings). The fundamental technical challenge lies not merely in replicating the interface across multiple platforms, but in reconciling fundamentally different geometric modelling paradigms, varying feature parametrization schemes, and inconsistent API stability guarantees across commercial CAD vendors, maintaining proprietary automation interfaces with limited cross-platform standardization.

Acknowledgments:

For this research, the used tools are listed below: (1) Personal laptop capable of AI processing with CUDA enabled; (2) Python 3.12 locally installed; (3) local environment set-up (PyQt5, local AI, APIs); (4) 3DXPERIENCE 2025X – Student license with limited functionality (5) Claude API credit for API calls, (6) Python SDK simplified integration abstracting HTTP communication details and response parsing complexity, (7) pywin32 - Python for Windows Extensions enabling Windows COM interface access essential for 3DX automation, (8) Python standard library contributors for essential modules: JSON for data serialization, re for regular expression pattern matching, datetime for timestamp generation, difflib for fuzzy string matching implementing Sequence Matcher algorithm, and os/sys for file system operations and environment configuration, (9) Development Tools: Git version control system enabling iterative development with complete history tracking. Visual Studio Code and PyCharm IDEs providing Python development support with debugging, code completion, and refactoring capabilities, (10) Design and Manufacturing [13] , Plastic Parts Design for Injection Moulding [12], Manufacturer material data sheets from BASF [18], Sabic [19], DuPont [20] and others supplying materials properties data, (11) Open Source Community: Broader open source ecosystem providing tools, libraries, and knowledge resources supporting rapid development without requiring extensive infrastructure investment. Stack Overflow community for troubleshooting assistance. GitHub for example code and architectural patterns & CADAM [21] system as open-source data for CAD generation.

References

[1] Li, Kun-Ying, Cheng-Kai Huang, Qing-Wei Chen, Hsuan-Cheng Zhang, and Tsann-Tay Tang. "Generative AI and CAD Automation for Diverse and Novel Mechanical Component Designs under Data Constraints." *Discover Applied Sciences* 7 (2025): 315. https://doi.org/10.1007/s42452-025-06833-5.

[2] Xavier, Amatriain. "Prompt Design and Engineering: Introduction and Advanced Methods." arXiv preprint, January 2024. https://arxiv.org/pdf/2401.14423.

[3] Anthropic. "Introducing Claude Sonnet 4.5." Anthropic AI News, 2025. Accessed November, 2025. https://www.anthropic.com/news/claude-sonnet-4-5.

[4] OpenAI. "Introducing GPT-5." OpenAI Blog, 2025. Accessed November, 2025. https://openai.com/index/introducing-gpt-5/.

[5] Nielsen, Jakob. "Response Times: The 3 Important Limits." Nielsen Norman Group, January 1, 1993. Accessed November, 2025. https://www.nngroup.com/articles/response-times-3-important-limits/.

[6] Python Software Foundation. "Python 3.12.12 Documentation." 2025. Accessed November, 2025. https://docs.python.org/release/3.12.12/.

[7] JSON.org. "Introducing JSON." 2025. Accessed November, 2025. https://www.json.org/json-en.html.

[8] Qt Company. "Qt for Python Documentation." The Qt Company Ltd., 2023. Accessed November, 2025. https://doc.qt.io/qtforpython/.

[9] Anthropic. "Build with Claude: Using the Messages API." Claude Documentation, 2025. Accessed November, 2025. https://docs.claude.com/en/docs/build-with-claude/working-with-messages.

[10] Dassault Systèmes. "3DEXPERIENCE User Assistance 2025x." Dassault Systèmes SE, 2025. Accessed November, 2025. https://help.3ds.com/2025x/English/DSDoc/FrontmatterMap/DSDocHome.htm?contextscope=cloud&redirect_lang=English.

[11] Dassault Systèmes. "Developer Assistance R2025x API Reference." Dassault Systèmes SE, 2025. Accessed November, 2025. https://media.3ds.com/support/documentation/developer/Cloud/en/DSDoc.htm?show=CAADocQuickRefs/DSDocHome.htm.
[12] Malloy, Robert A. *Plastic Part Design for Injection Molding: An Introduction*. 2nd ed. Munich, Hanser Publications, 2010.
[13] Bralla, James G. (ed.). *Design for Manufacturability Handbook*. 2nd ed. New York, McGraw-Hill Professional, 1998.
[14] pywin32 Contributors. "Python for Windows Extensions (pywin32)." Python Package Index, 2025. Accessed January 15, 2025. https://pypi.org/project/pywin32/.
[15] MATER. "Catalog Online: Materials Database." MATER Library, 2025. Accessed November, 2025. https://app.materlibrary.ro/ro/materiale.
[16] Autodesk Inc. "AutoCAD 2024 AI Assistant Features." AutoCAD 2024 Product Documentation, 2024. Accessed November, 2025. https://help.autodesk.com/view/ACD/2024/ENU/?guid=GUID-B4E1E636-E08E-4277-8971-910D47440116.
[17] PTC. "PTC Launches Arena AI Assistant to Accelerate PLM and QMS Workflows." PTC Press Release, 2025. Accessed January 15, 2025. https://www.ptc.com/en/news/2025/ptc-launches-arena-ai-assistant.
[18] BASF SE. "Engineering Plastics: Performance Polymers." BASF Plastics & Rubber, 2025. Accessed November, 2025. https://plastics-rubber.basf.com/global/en/performance_polymers#item-1705923019047-1853604672.
[19] SABIC. "Polymers." SABIC Global, 2025. Accessed November, 2025. https://www.sabic.com/en/products/polymers.
[20] DuPont, Inc. "Interior Solutions: Automotive Applications." DuPont Mobility & Materials, 2025. Accessed November, 2025. https://www.dupont.com/mobility/automotive/interior.html.
[21] CADAM. "ADAM Creation: AI-Powered Design Platform." 2025. Accessed November, 2025. https://adam.new/app/editor/7d4c0720-6ccc-46df-a0f3-0993c1e1eac5.

Abbreviations
CAD – Computer-Aided Design
AI – Artificial Intelligence
ML – Machine Learning
LLM – Large Language Model
3DX – 3DEXPERIENCE R2025x (CATIA v6) – Dassault Systems
NLP – Natural Language Processing
JSON – JavaScript Object Notation
GUI – Graphical User Interface
API – Application Programming Interface
COM – Component Object Model
SDK – Software Development Kit
DC01 – Mild Steel
PP – Polypropylene
PA – Polyamide (Nylon)
GF – Glass Filled
SPI – Society of the Plastics Industry
V1x to V6.x – Version 1 through Version 6
STP – Standard for the Exchange of Product Model Data
VBA – Visual Basic for Applications

Appendix A - System's Architecture

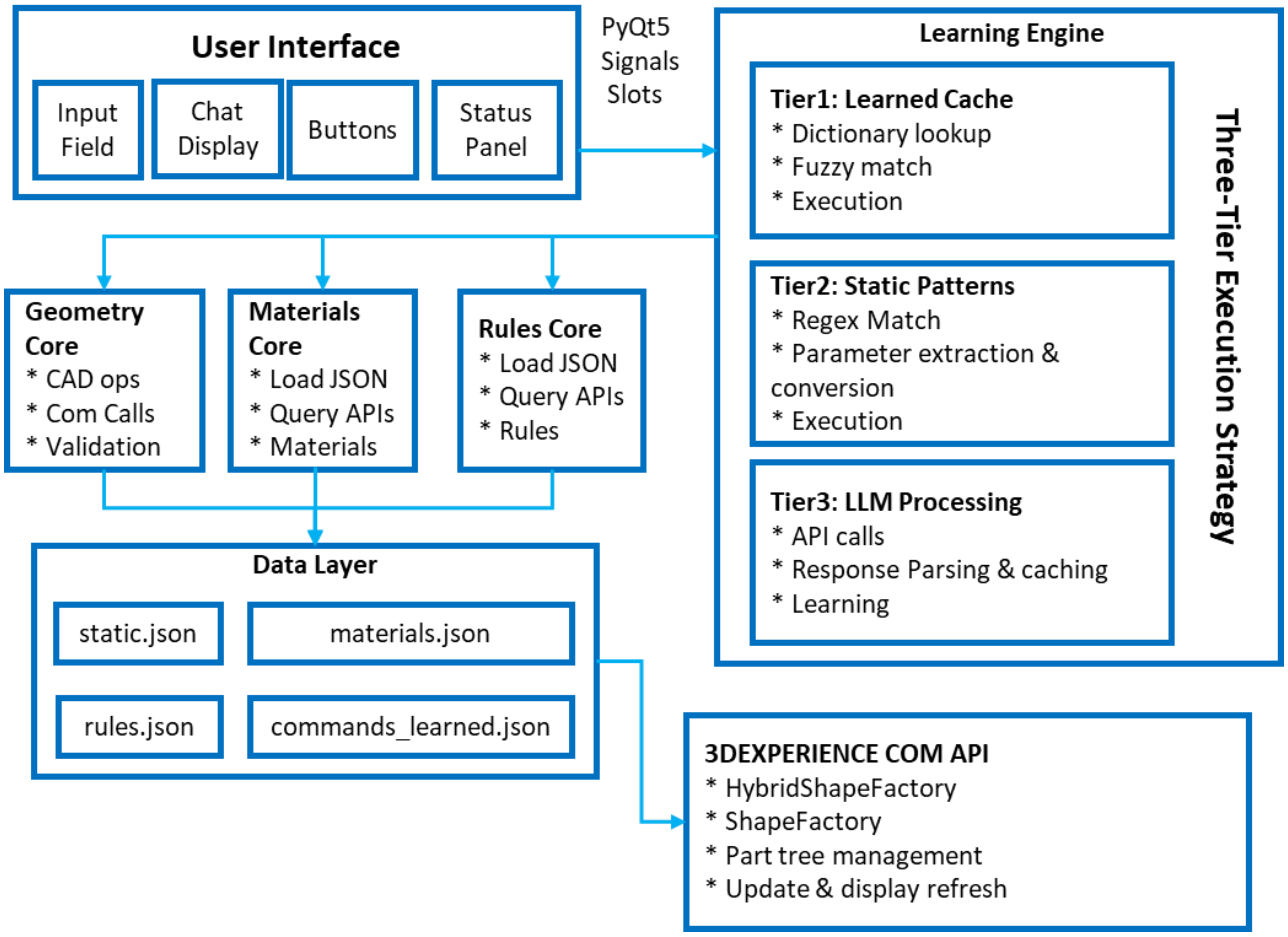

Fig. 4. System's Architecture & Logic

Appendix B – Terminal display data

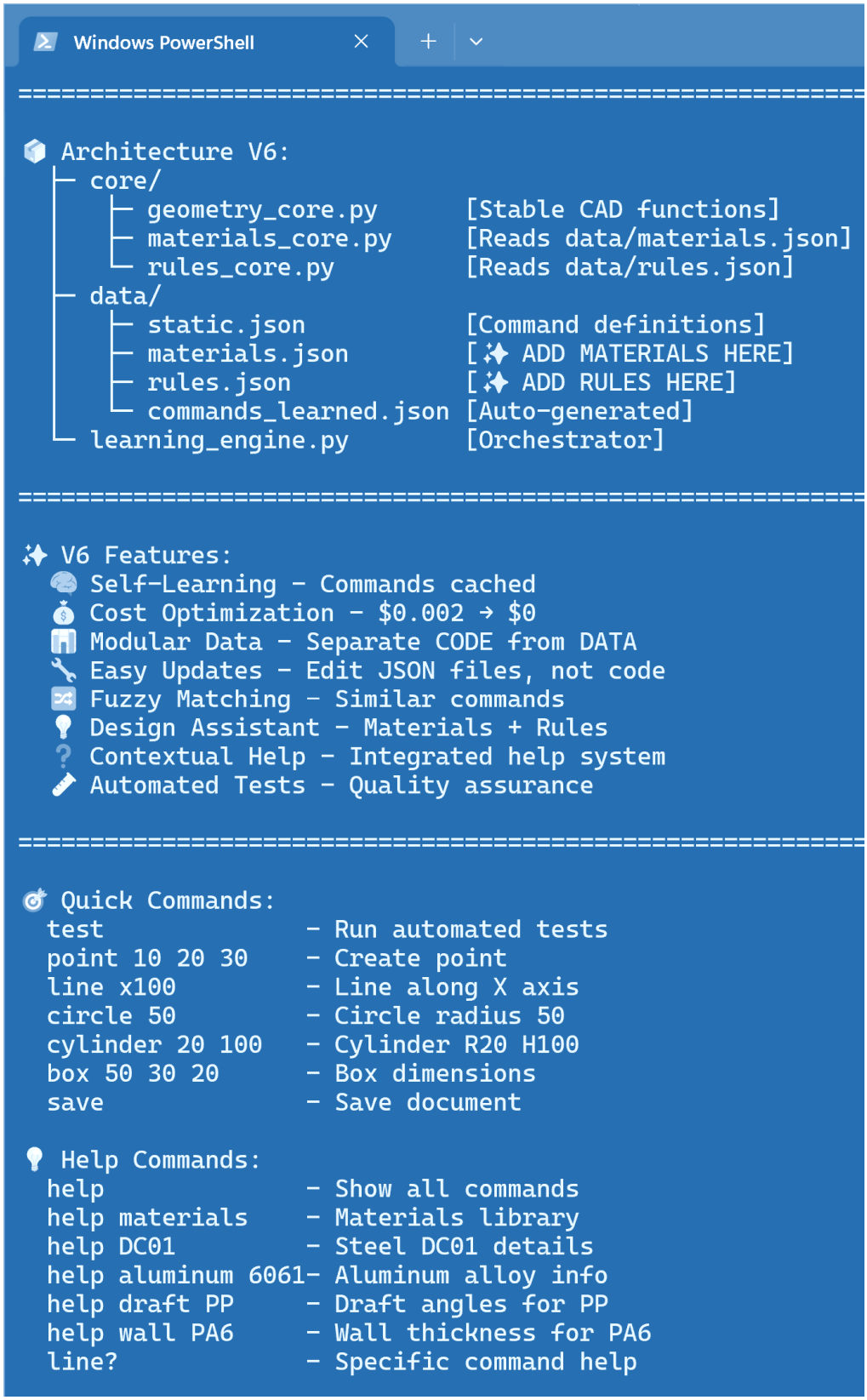

Fig. 5. Terminal information implemented for V5.x-V6.x

Appendix C – Program examples (type: main_V6.py)

```
main_V6.py
Text-to-CAD V6 - Modular Architecture
"""
import sys
from PyQt5.QtWidgets import QApplication, QInputDialog
from ui_interface_V6 import TextToCADInterface


def main():
    print("=" * 70)
    print("🚀 Text-to-CAD V6.0 - MODULAR ARCHITECTURE")
    print("=" * 70)
    print()
    print("📦 Architecture V6:")
```

Fig. 6. Code as example: main_V6.py

```
ui_interface_V6.py
"""

from PyQt5.QtWidgets import *
from PyQt5.QtCore import Qt, QDateTime, pyqtSignal
from PyQt5.QtGui import QFont, QTextCursor, QKeyEvent
import win32com.client
from learning_engine import LearningEngine


class EnterTextEdit(QTextEdit):
    enter_pressed = pyqtSignal()

    def __init__(self, parent=None):
        super().__init__(parent)
        self.history = []
        self.history_idx = -1
        self.current_text = ""

    def keyPressEvent(self, event: QKeyEvent):
```

Fig. 7. Code as example: ui_interface_V6.py

Learning engine

```
"""
learning_engine.py - V6.2 - Materials Intelligence
Self-learning + Help + Design Assistant + Materials AI
"""

import json
import re
from datetime import datetime
from difflib import SequenceMatcher
import os
import sys

sys.path.insert(0, os.path.join(os.path.dirname(__file__), 'core'))

from geometry_core import GeometryCore
from materials_core import MaterialsCore
from rules_core import RulesCore


class LearningEngine:

    CLAUDE_MODEL = "claude-sonnet-4-20250514"

    def __init__(self, claude_api_key=None):
        self.version = "6.2"
        self.claude_api_key = claude_api_key
```

Fig. 8. Code as example: learning_engine.py

Appendix D – Commands list

General Commands
1. `save` - Save document via part update
2. `test` - Run automated test suite (15 operations)

Wireframe Commands:
3. `point X Y Z` - Create point at coordinates
   - Example: `point 10 20 30`
4. `edit point X Y Z to X2 Y2 Z2` - Modify point coordinates
   - Example: `edit point 10 20 30 to 15 25 35`
5. `line xLENGTH` - Line along X axis from origin
   - Example: `line x100`
6. `circle at point X Y Z PLANE RADIUS` - Circle centered at point
   - Example: `circle at point 10 20 30 xy 25`

Surface Commands:
7. `plane PLANE offset DISTANCE` - Offset plane from origin
   - Example: `plane xy offset 100`
8. `plane PLANE through point X Y Z` - Plane through existing point
   - Example: `plane xy through point 10 20 30`

Sketch Commands:
9. `rectangle WIDTH HEIGHT` - Rectangle sketch on XY plane
   - Example: `rectangle 50 30`

Solid Commands:
10. `cylinder RADIUS HEIGHT` - Cylindrical solid via pad
   - Example: `cylinder 20 100`
11. `box LENGTH WIDTH HEIGHT` - Rectangular solid via pad
   - Example: `box 50 30 20`

Help Commands
12. `help` - General command overview
13. `help materials` - List all materials
14. `help MATERIAL` - Specific material info
   - Example: `help DC01`, *
15. `help draft [MATERIAL]` - Draft angle recommendations
   - Example: `help draft`, `help draft PP`
16. `help wall [MATERIAL]` - Wall thickness guidelines
   - Example: `help wall`, `help wall PA6`
17. `COMMAND?` - Command-specific help
   - Example: `line?`, `cylinder?`

Natural Language:
- Any descriptive request interpreted by Claude API
- Examples: "create a point at 10 20 30", "make me a box 50 by 30 by 20"
- Automatically learned after first successful execution

Material Database - Sample

Complete Material Entry Example (DC01 Steel):

```json
"DC01": {
  "name": "DC01 Cold Rolled Steel",
  "category": "Metals",
  "type": "Cold rolled, deep drawing quality",
  "aliases": ["DC 01", "1.0330"],
  "properties": {
    "density": "7.85 g/cm³",
    "yield_strength": "140-300 MPa",
    "tensile_strength": "270-410 MPa",
    "elongation": "≥28%"
  },
  "characteristics": [
    "Excellent formability",
    "Good weldability",
    "Surface quality for painting/coating",
    "Low carbon content"
  ],
  "applications": [
    "Sheet metal parts",
    "Automotive body panels",
    "Appliance housings",
    "Deep drawn components",
    "Brackets and mounting plates"
  ],
  "design_tips": [
    "Min bend radius: 0.5-1× thickness",
    "Ideal for complex forming operations",
    "Requires surface protection (paint/coating)",
    "Good for welding and spot welding",
    "Standard thickness range: 0.5-3.0mm"
  ]
}
```

Fig. 9. Example of Material Data Sheet (sample data)

Appendix E – Design Rule summary

```
**Draft Angles Quick Reference:**
| Material | Exterior | Interior | Notes |
|----------|----------|----------|-------|
| PP | 1-4° | 2-5° | Good release |
| PP-GF30 | 1.5-6° | 2-6° | More draft needed |
| PA6 | 1-5° | 2-5° | Varies with moisture |
```

```
**Bend Radius Quick Reference (Sheet Metal):**
| Material | Minimum | Standard | Notes |
|----------|---------|----------|-------|
| DC01 Steel | 0.5× t | 1× t | Excellent formability |
| S235JR Steel | 1× t | 1.5× t | Moderate formability |
```

Fig. 10. Example of Material Data Sheet (sample data)

Balancing the Vertical Feed Kinematic Chains by Means of Pressure Reducing Valves

Prof. PhD Eng. **Anca BUCUREȘTEANU**[1,*]

[1] University POLITEHNICA of Bucharest
* ancabucuresteanu@gmail.com

Abstract: *This paper presents the mathematical models necessary for the design of the hydraulically balanced vertical feed kinematic chains. The hydraulic balancing solution that uses constant flow pumps and 3-way pressure reducing valves is explained. The basic hydraulic diagram, the mathematical models in static and dynamic mode and examples of similar units are shown. There are also highlighted both the advantages and disadvantages of the hydraulic balancing systems.*

Keywords: *Machine-tools, hydraulic balancing systems, 3-way pressure reducing valves*

1. Introduction. Necessity of Balancing

In the case of heavy duty machine tools [1, 2], the vertical travel of masses (slides, rams, housings) requires the existence of appropriately sized kinematic chains. In most cases, these have the kinematic diagram shown in Figure 1.

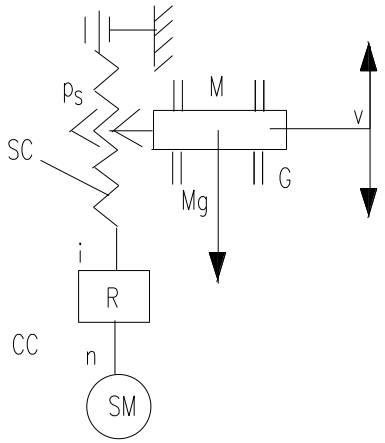

Fig. 1. Kinematic diagram of the vertical feed kinematic chain

The servomotor SM [1, 2, 3], actuated by the machine equipment, rotates the lead screw SC of pitch p_S, by means of the reducer R which has the transfer ratio *i*. The mass *M* is moved vertically on the guideways G. The electric motor rotates with the speed *n* and develops the instantaneous torque *T* for the total force *F* that includes weight *G*, force of inertia and forces of friction F_F. The instantaneous speed is *v*.
In the starting phase, it is considered that the acceleration is *a*, with the following value:

$$a = \frac{dv}{dt} \tag{1}$$

In these conditions, one can consider:

$$v = nip_S \tag{2}$$

$$T = \frac{iFp_S}{2\pi} \tag{3}$$

$$Ma + Mg + F_F = F \tag{4}$$

The feed kinematic chain is most stressed in the case of rapid upward movement. Therefore, this paper will focus on this case hereinafter.
The manufacturers of servomotors provide the data necessary for the calculation of these ones. Figure 2 presents the starting characteristic of such a servomotor [3].

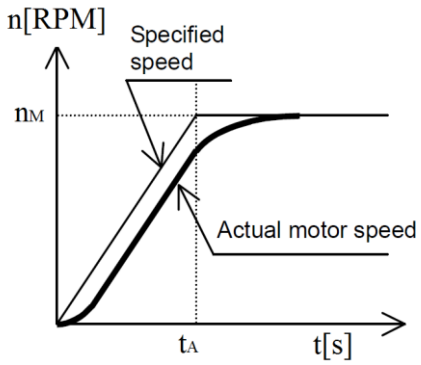

Fig. 2. Starting characteristic of a feed servomotor according to the catalogue of the manufacturer

In order to simulate numerically the realization of this characteristic, the following mathematical model is proposed, where the programmed rotational speed n_M is reached after the acceleration phase lasting t_A, with the ramp γ:

$$n = \begin{cases} \gamma t_A; t \le t_A \\ n_M; t > t_A \end{cases} \tag{5}$$

In order to make a simulation, using the Matlab - Simulink package [4, 5, 6], a specific case was taken: a feed kinematic chain (Z axis) from the vertical lathes. In this case, the reference values are: M = 750 Kg, t_A = 0.2 s, n_M = 500 RPM, γ = 2500 RPM/s, i = 0.5, p_S = 10 mm.
Figure 3 shows the characteristic of the servomotor rotational speed.

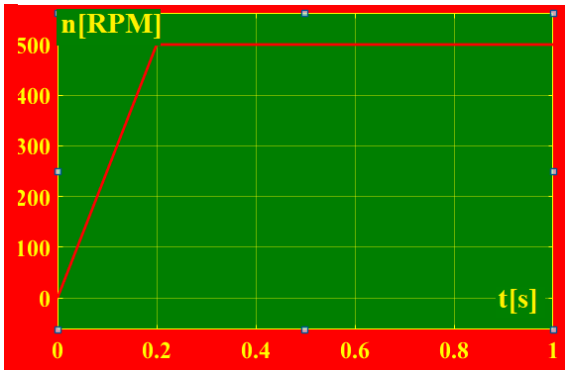

Fig. 3. The starting characteristic of the feed servomotor used in the simulation

Corresponding to this speed, the load increases with *v* speed according to the characteristic in Figure 4.
Mass *M* will move with a maximum speed of 2.5 m/minute which is the rapid moving speed for this type of machines.
The moment of force at the level of the electric motor will have the characteristic shown in Figure 5. The torque developed by the servomotor in the acceleration phase is T = 6.12 Nm. After reaching the programmed value, it decreases to the value T = 6 Nm.
In this case, the dimensioning of the feed kinematic chain (CC) will be done taking into account these values. The weight of 7500 N, the forces of friction and inertia will be overcome by the electromechanical system.

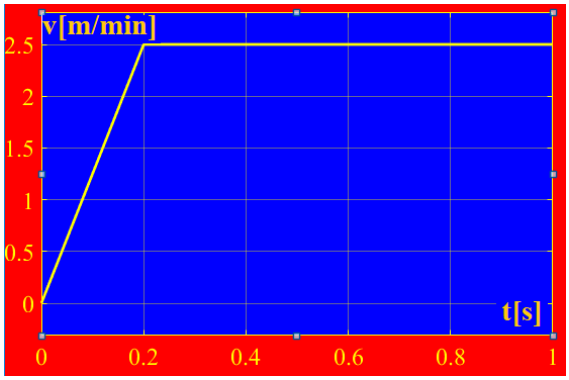

Fig. 4. Characteristic of the upward speed

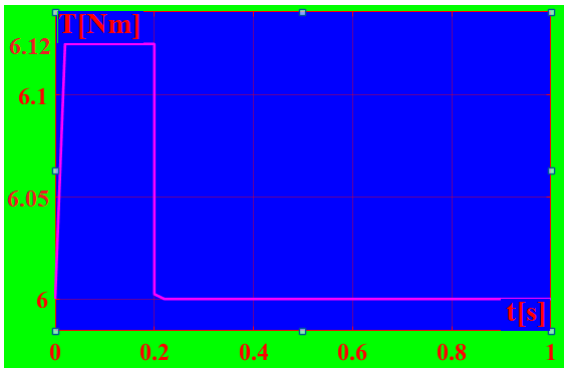

Fig. 5. Torque developed by the servomotor

2. Hydraulic Balancing of the Vertical Feed Kinematic Chain Using the Pressure Reducing Valves [7, 8]

The unloading of the feed kinematic chain is performed using a hydraulic system. The simplified diagram of this system is shown in Figure 6.

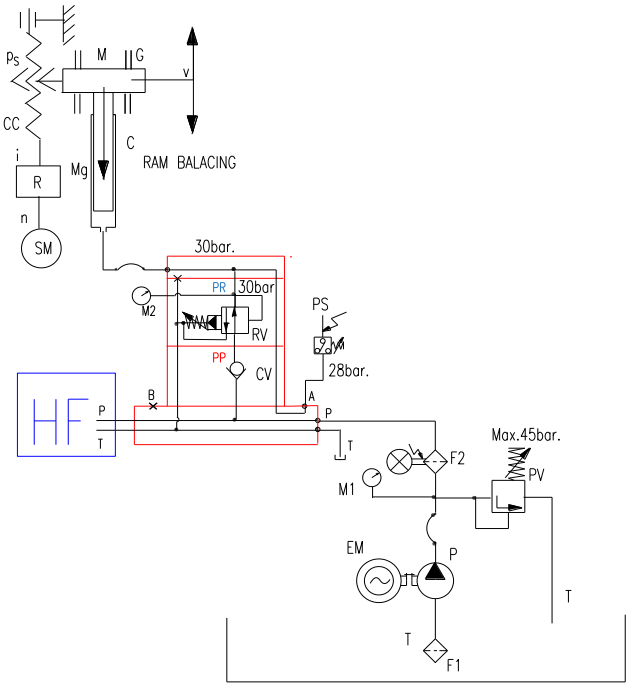

Fig. 6. Balancing hydraulic system with 3-way pressure reducing valve

The pump P is driven by the electric motor EM and sucks oil from the tank T through the suction filter F1. The maximum pressure in the system is regulated by the pressure relief valve PV. This pressure is viewed on the manometer M1. Oil is supplied to the balancing system through the F2 filter, then through the check valve CV and the pressure reducing valve RV [9]. The unit can also supply other consumers to perform other functions HF. The oil with reduced pressure supplies the cylinder C which, along with the feed kinematic chain CC, ensures the movement of the slide of mass M. The reduced pressure value [8, 9] is viewed on manometer M2. Pressure switch PS confirms the minimum working pressure presence. The figure shows too: PP – pressure at the pump and PR – reduced pressure.
The pressure reducing valve is chosen from the catalogue, depending on the intended flow rate and pressure. Figure 7 shows the defining elements for such a valve.

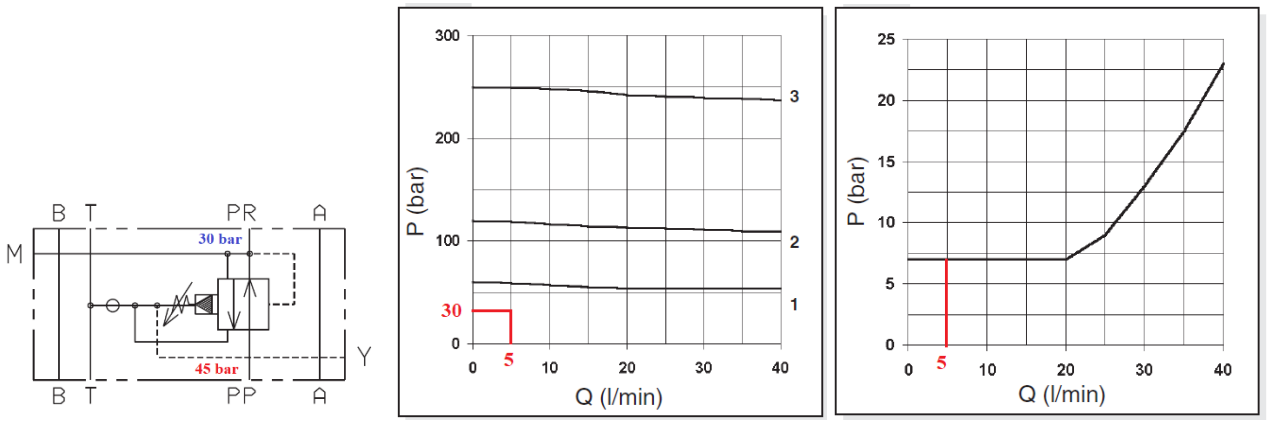

a. b. c.

Fig. 7. Characteristics of the pressure reducing valve

In the case of the chosen example, the required theoretical flow rate is 5 l/min at the reduced pressure of 30 bar. The pump pressure is 45 bar. The value of the pressure switch PS will be adjusted at 28 bar.
Figure 6a shows the detailed diagram of this valve which, if supplied at the pressure of 45 bar, ensures the flow rate of 5 l/min at the pressure of 30 bar. The chosen valve can work with a maximum flow rate of 40 l/min. The maximum pressure characteristic adjusted according to the flow rate for these valves is presented in Figure 6b. The minimum adjustable pressure at these valves is approximately 7 bar, as per Figure 6c.
The flow rate of the pump is chosen in such a way as to cover what is required by the balancing and the rest of the functions (HF), having a reserve of 10 ÷ 20%. Cylinder C has an active surface S = 20 cm^2.
In this case, the mathematical model for the entire actuation system, including the feed kinematic chain and the balancing hydraulic system, has the relations (1), (2), (3) and (5) to which will be added:

$$Ma + bv + Mg + F_F = p_R S + F \tag{6}$$

$$Q = Sv \tag{7}$$

$$Q_U = Q_S - Q \tag{8}$$

In the relations above it was also noted: b – the linearized coefficient of force losses proportional to speed (damping), Q – the flow rate supplied by the pressure reducing valve, Q_S – flow rate of the hydraulic source (pump and pressure relief valve), Q_U – the unused flow rate yet.
The characteristics of the rotational speed [RPM] and speed are the same as those in Figures 2 and Figure 3.
The torque required at the motor evolves as shown in Figure 8.

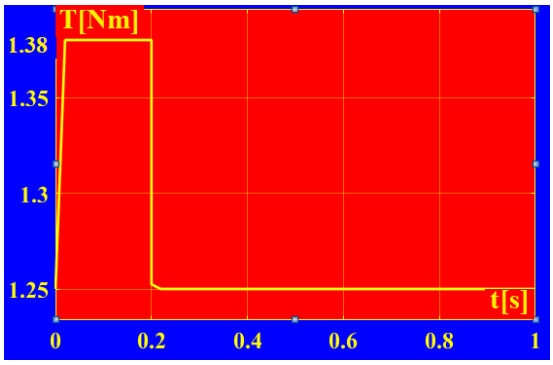

Fig. 8. Characteristic of the torque required for the motor in the case of hydraulic balancing

In the acceleration phase, the torque is T = 1.4 Nm. After reaching the programmed value, the torque decreases up to the value T = 1.25 Nm.
In this case, the dimensioning of the feed kinematic chain (CC) will be done taking into account these values, much reduced compared to the actuation without balancing system. The weight of 7500 N, the forces of friction and inertia will be overcome by the electromechanical system together with the hydraulic one.
For a pump that provides a constant flow rate [10, 11] of 9 l/min, the hydraulic unit can also supply other consumers as long as the sum of these ones, according to Figure 9, does not require a theoretical flow rate higher than 4 l/min in static mode.

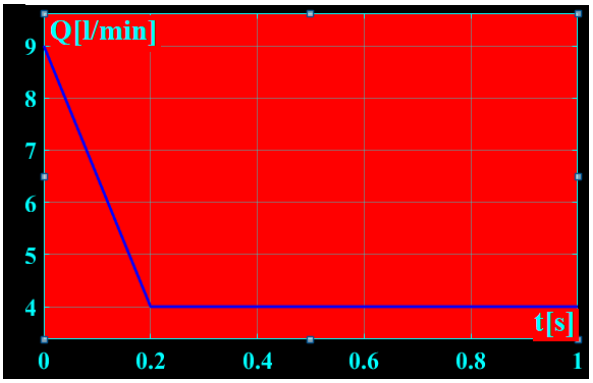

Fig. 9. Flow rate available for other functions

In these machines, by actuating the feed kinematic chain during the travel phase on Z axis [1, 2], other functions are no longer performed, as a rule. So, theoretically, the available flow rate is 4 l/min.
But the manufacturer of the pressure reducing valves mentions that these ones drain a flow in the range of 0.5 ÷ 0.7 l/min. In practice, the checking of flow rate is done taking into account other losses too, as shown below.
The flow rate of the pump is 9 l/min theoretically, but a safety margin of 15% is considered. So, in reality, the total usable flow rate is 0.85 x 9 = 7.65 l/min. If the losses through the draining of the pressure reducing valve are considered to be 0.65 l/min, it means that 7l/min are available in the entire unit. An amount of 5 l/min from the available amount are used for the rapid travels. Thus, during these phases, the flow rate available for other functions is 2 l/min.
The appropriate choice of pump flow rate is very important. A flow rate that is too low will not allow the necessary work phases, which will lead to improper balancing and therefore poor operation. A flow that is too high can entail the excessive heating of the unit by spilling the surplus through the pressure relief valve PV.
The balancing function is a permanent one. Therefore, it is activated when the pump motor is started and it is deactivated when the motor is turned off.

Comparing the characteristics of the servomotor torque in the feed kinematic chain in Figures 4 and Figure 7, the fact that the hydraulic system "helps" the electromechanical system becomes obvious.
Under these conditions, the feed kinematic chain (servomotor, reducer, ball screw) will be dimensioned accordingly. The elements of the feed kinematic chain will be less stressed, which leads to the choice of a servomotor and reducer for lower powers. The lead screw will be more flexible, with a smaller diameter. These facts result also in the diminution of the expenses for this kinematic chain. On the other hand, one must also take into account the expenses incurred for the making of the hydraulic unit, which does not exist in the case of the unbalanced systems.

3. Balancing the Rams of the Vertical Lathes

The balancing solution presented above is used in some vertical lathes whose ram does not exceed 1000 Kg and which have rapid travel speed lower than 3 m/min. Exceeding these values leads to the oversizing of the pumps and driving motors and implicitly to the increase of the lost power.
Figure 10 shows a SC 33 vertical lathe with two counterbalanced rams, each one with a pressure reducing valve.

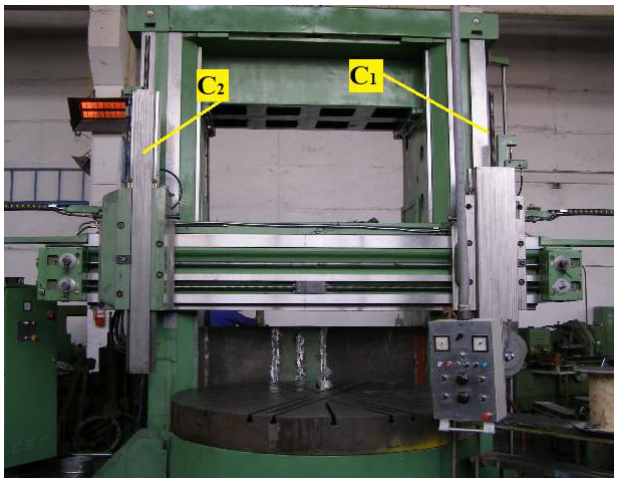

Fig. 10. Vertical lathe with two rams

Each one of the rams C_1 and C_2, together with the associated tool-holders, do not exceed the mass of 1000 Kg. Their maximum speeds are 2.5 m/min. The balancing pressure is adjusted in the range of 30 ÷ 35 bar. The maximum pressure set at the pump is 45 ÷ 50 bar. The pump provides a theoretical flow rate of 16 l/min. The driving electric motor of this one has the power P_{EM} = 2.2 KW.
The assembling shown in Figure 11 was made for balancing the two rams.

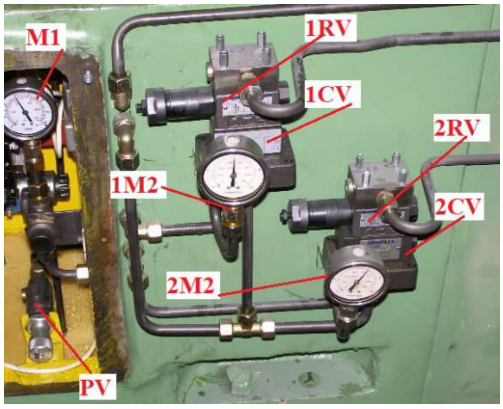

Fig. 11. Hydraulic unit for balancing the two rams of the SC 33 vertical lathe

The maximum pressure in the entire unit is regulated by means of the pressure relief valve PV. This pressure is viewed on the manometer M1. The pressure reducing valves 1RV and 2RV assembled on the check valves 1CV and 2CV, as shown in the diagram in Figure 5, are intended for the independent regulation of the two reduced pressures. These pressures can be read using the manometers 1M2 and 2M2. The adjustment of the balancing pressures is done for each feed kinematic chain independently, so that their servomotors do not detect torque differences greater than 10 ÷ 15% when ascending or descending.

4. Conclusions

The feed kinematic chains that operate vertically can be unloaded by means of the hydraulic balancing systems that use pressure reducing valves. They have the great advantage that they ensure balancing at constant pressure regardless of the direction of travel and the position of the balanced mass.
The pressure reducing valves are chosen depending on the required flow rate and pressure, according to the documentation of the manufacturer. In the case of using constant flow rate pumps, it is recommended to limit the values of pressure and flow rate so that the excessive heating of the unit be avoided.
For a good dimensioning of the elements of the kinematic chain, the balancing unit will ensure obtaining the required maximum speeds. A hydraulic balancing unit can serve several feed kinematic chains because it can be adjusted for each optimal balancing pressure.
The specialized programs, such as Matlab - Simulink and Automation Studio, allow solving the mathematical models specific to these systems.
In the case of the vertical lathes where the rapid travel speeds are lower than 3 m/min and the rail heads do no exceed the mass of 1 tone, the balancing systems with pressure reducing valves represent a functional and reliable solution with an acceptable price.

References

[1] Joshi, P. H. *Machine-Tools Handbook*. New Delhi, McGraw-Hill Publishing House, 2007.
[2] Perovic, Bozina. *Machine-Tools Handbook/Handbuch Werkzeug-Maschinen*. Munchen, Carl Hanser Verlag, 2006.
[3] ***. Catalogues and leaflets BOSCH REXROTH, BREVINI, PARKER, FANUC, SIEMENS.
[4] Prodan, Dan. *Machine Tools. Modeling and Simulation of Hydrostatic Elements and Systems/Maşini-Unelte. Modelarea şi Simularea Elementelor şi Sistemelor Hidrostatice*. Bucharest, Printech Publishing House, 2006.
[5] ***. Matlab/Simulink and Automation Studio Software package.
[6] Degeratu, M. *Dimensional analysis, similarity and modeling. Guide for applications in Fluid Mechanics and Hydraulics/Analiză dimensională, similitudine și modelare. Îndrumar pentru aplicații în mecanica fluidelor și hidraulică*. Bucharest, Publishing House of the Romanian Academy of Scientists, 2015.
[7] Prodan, Dan, Anca Bucuresteanu, Adrian Motomancea, and Emilia Balan. "Balancing Hydraulic Units. General Considerations." *International Journal of Engineering and Innovative Technology (IJEIT)* 3, no. 5 (November 2013): 234-237.
[8] Prodan, Dan, Anca Bucureşteanu, Emilia Balan, and Adrian Motomancea. "Theoretical and Experimental Researches on the Balancing Systems of Machine-Tools Feed Kinematic Chains." *Applied Mechanics and Materials* 555 (2014): 497-504.
[9] Dimitrov, Sasko, and Mihail Komitovski. "Transient Performance of a Three-Way Pressure Reducing Valve." *Machine Design* 11, no. 2 (2019): 53-58.
[10] Prodan, Dan, Mircea Duca, Anca Bucureşteanu, and Tiberiu Dobrescu. *Hydrostatic Drives - Machine Parts/Acţionări hidrostatice – Organologie*. Bucharest, AGIR Publishing House, 2005.
[11] Prodan, Dan. *Hydraulics of Production Systems/Hidraulica sistemelor de productie*. Bucharest, Printech Publishing House, 2011.

Highwaters Overspilling by an Energy Dissipator Top Discharger with Increasing Macrorugosities

MSc.stud.eng. **Ioana-Andreea HORTOPAN**[1,*], Assoc.prof.dr.eng. **Gheorghe I. LAZĂR**[1], Assoc.prof.dr.eng. **Albert Titus CONSTANTIN**[1], Assoc.prof.dr.eng. **Șerban-Vlad NICOARĂ**[1]

[1] Politehnica University Timişoara, Romania

* ioana.hortopan@student.upt.ro

Abstract: *The paperwork presents a discrete 1D numerical modeling of the local hydraulic phenomenon that takes place when water flows over a macrorugosity top discharger (steps spillway), corresponding to the transit of an accidental flood of known synthetic configuration. It describes the one-dimensional simulation procedure developed with the help of HEC-RAS v.6.0, software that can engage a new approach of numerical solving in 1D, namely based on the finite volume method. Along with the proposal to apply and go through a distinct computerized hydraulic modeling, its practical purpose is to establish the parameters of transient (unsteady) hydraulics on a concrete dam top discharger, provided with macrorugosities at the downstream face. At the same time, the work proposes thus a way of checking the accidental high waters discharge as complying with legal norms in force.*

Keywords: *Stepped spillway, hyghwater overflow, hydraulics, numerical modelling.*

1. General considerations

The performed discrete numerical modeling takes the oportunity of a highwaters defending hydrotechnical arrangement, which has in its composition an RCC dam – the Boqueron Dam (Figure 1) – provided with a special top discharger made with macrorugosities (steps) at the downstream face, and with an energy dissipator with basin and threshold, respectively [1].
The Boqueron Dam, commissioned in 1999 for Confederacion Hidrografica del Segura [2], the Albacete Province (southeast of Spain), has a maximum height of 56m. Its overflowing spillway of Creager type has one free 16m gap, designed for a 1.5m regular water blade height above the climax (the maximum water blade height rises to 4m, as corresponding to the verification situation). The top discharger goes on with a canal following the dam downstream face of 0.73:1 general slope, accomplished in steps of 1.2m height, the overflowing reaching down an energy dissipator with a 35m length and 9.12m depth basin and a 4.30m height threshold, respectively.

Fig. 1. Upstream and downstream views of the RCC Boqueron Dam [2]

Figure 2, as a hydraulic structure cross-section, brings the graphical representation of the analyzed flowing route, meaning a longitudinal cross-view through the concrete dam and the energy dissipation basin, respectively a detail for achieving the variable macrorugosity in the spillway upper area.
The discrete 1D numerical modeling developed with the help of HEC-RAS v.6.0 [3] comprises two solutions for the numerical approach: the finite differences method (as a default choice) and the finite volume method (a new approach). As for the considered model with steep falls in steps (as on the area of the downstream face provided with macrorugosities), the default method of finite differences leads to numerical instability and therefore, for this case, a numerical solution cannot be reached.

When selecting the finite volume method, the numerical instability disappears (true, not immediately, but requires further geometrical adjustments), obtaining so the convergence to a numerical solution when the distance between the defined 1D cross-sections complies with some additional conditions as presented at the execution of the numerical model.

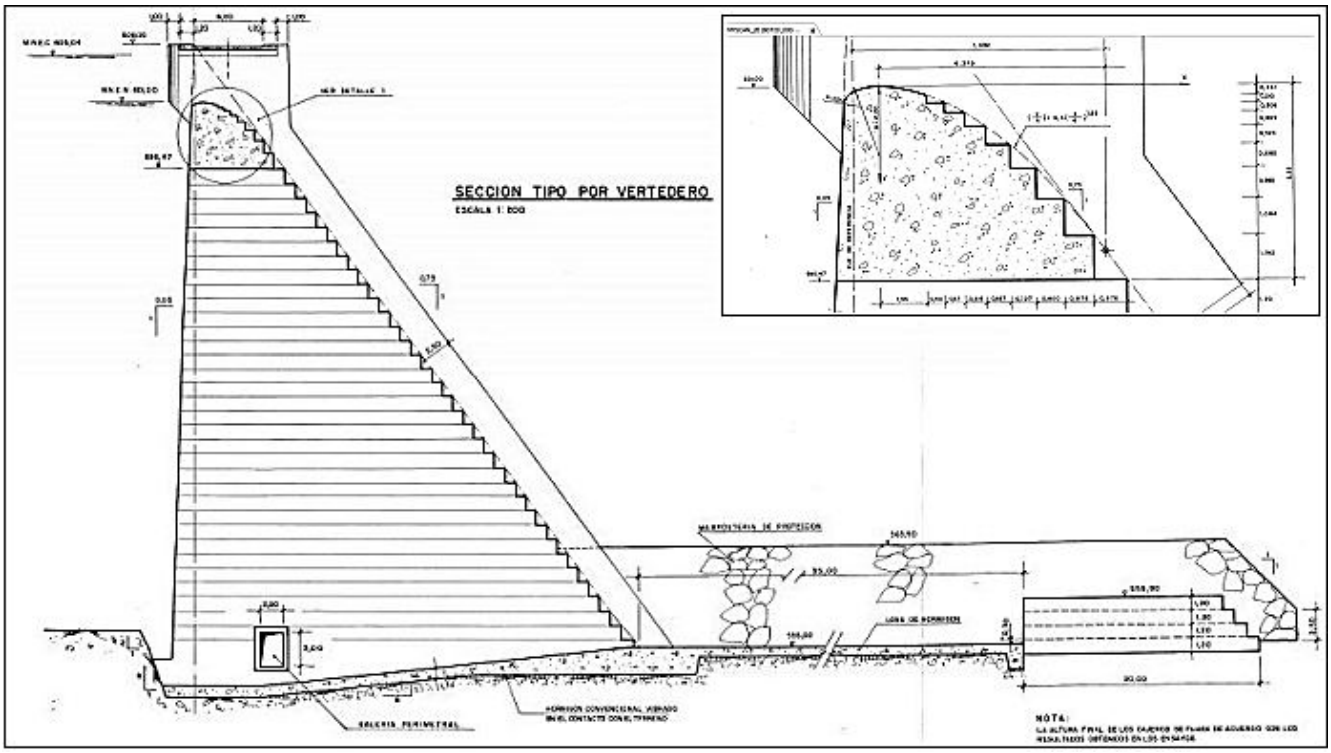

Fig. 2. Hydraulic structure cross-section: dam, macrorugosities profile top discharger, energy dissipator with basin and threshold; detail view of the variable macrorugosities accomplishment at the discharger upper part

One can see the message shown in later on Figure 5, *Notes generated when writing the computation files: Warning - XS's were found to have a reach length less than half the main channel width; **The 1D finite volume method is sensitive to the volume between XS's. Locations with very short reach lengths (small volumes) may require shorter time-steps to remain stable.
Therefore, for these reasons, if at first the developed numerical model considered the structural width corresponding to the spillway gap, a successive reduction at several values was performed. There is mentioned that there still were some cross-sections not complying with the condition, but nevertheless the numerical instability disappears.
As regarding the flow discharged by the special configurated spillway studied in the developed numerical simulation, the geometric configuration of a regular unfolding synthetic highwater was considered as seen in Figure 3 graphic representation.

2. General elements regarding the numerical model accomplishemt and the water flow simulation

The assessment of the existing situation was based on the known geometric values, materialized by a situation plan and cross-sections, specifically considered by a background image (extension file .dxf) adopted in HEC-RAS v.4.1 [4] (following the storage in a .dwg extension file). This resulted in a numeric database stored in specific files associated with the defined model, which was then loaded into HEC-RAS v.6.0. Specifically, in order to build the discrete numerical model, a linear segment was cut out of the entire flow path, geometrically representing a canal of rectangular cross-section of 16m width. The modeled segment has a length of 100.72m and has a known plane-view shape by the actual topographical values. The cross-sections of the modeled flow path segment are indicated in Figure 4 – a total of 312 sections, of which 113 are given by the given topographic values (dark color) while the other 199 sections are obtained by linear interpolation (light color and additional end

notation with asterix). The elevations were graphically determined by considering the longitudinal scale profile (Autocad) and knowing the configuration of the route at the base as seen in the representation in Figure 2.

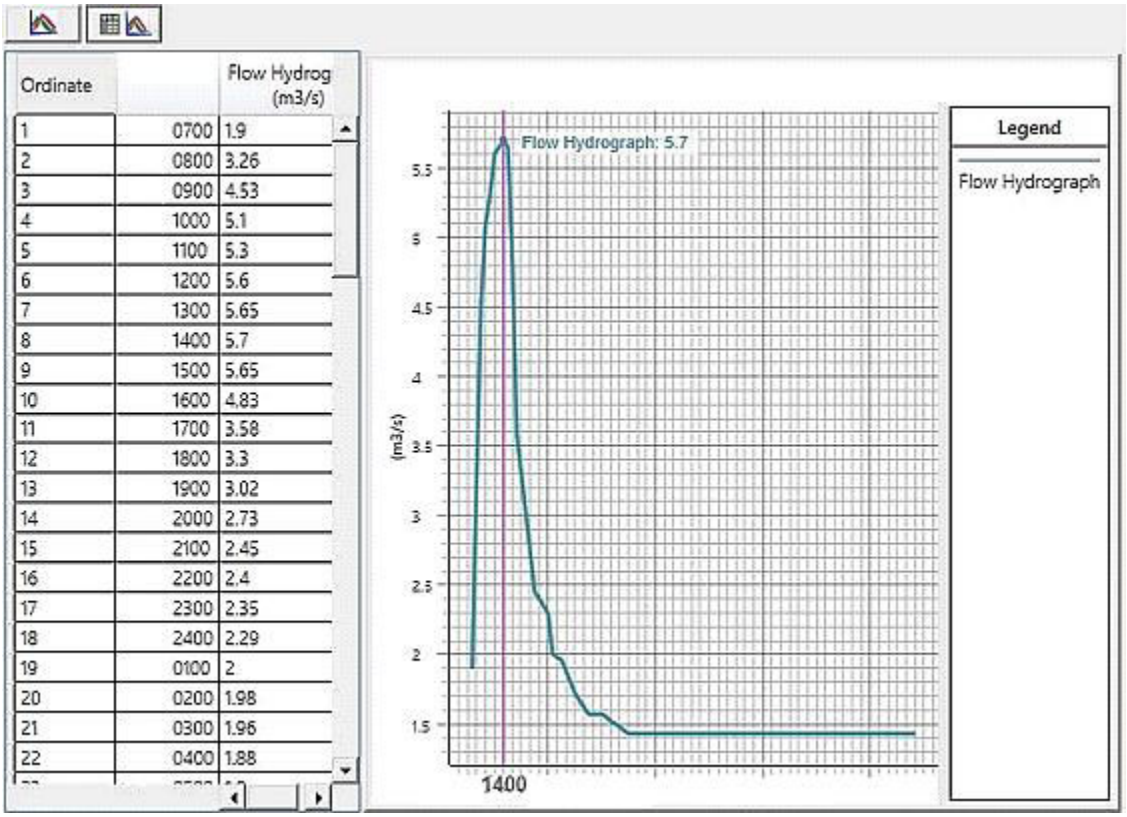

Fig. 3. Graphic representation of the employed synthetic flood hydrograph

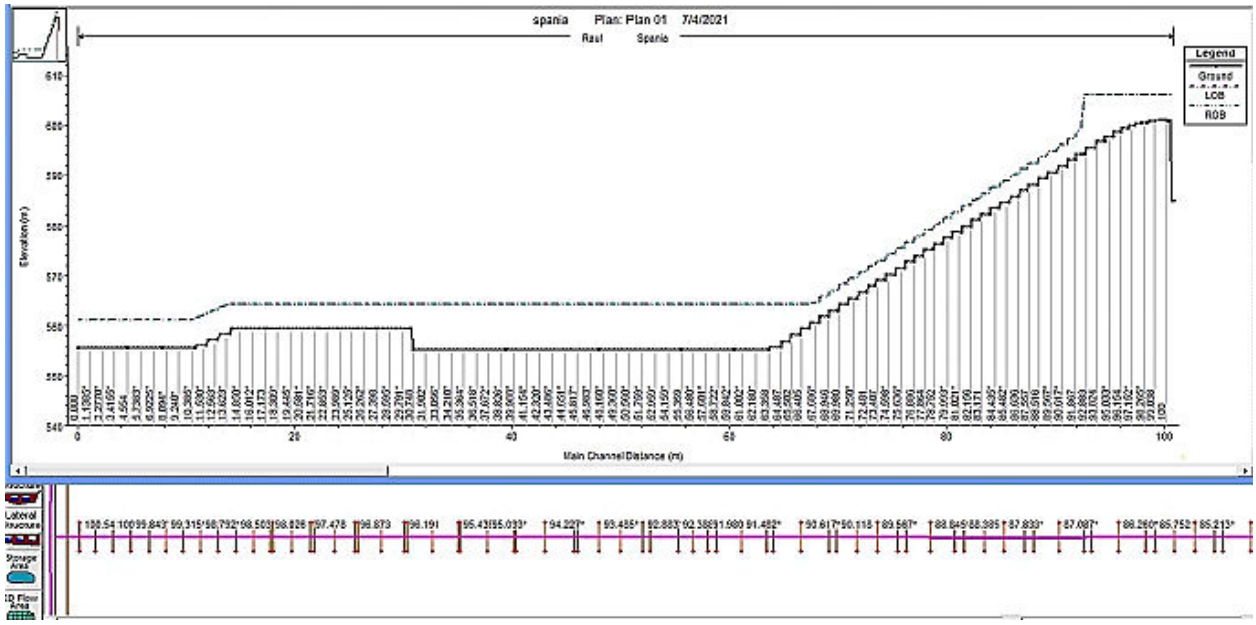

Fig. 4. Plane-view (bottom) and central longitudinal profile of discrete numerical model (1D), as corresponding to the top discharger with macrorugosities slope and energy dissipator

Further on, at the actual execution of the discrete numerical model (canal with the width corresponding to the spillway opening, B=16m) in HEC-RAS v.6.0, respectively following the employment of the finite volume method, it was found that the model is unstable. So, successive

alterations to the following canal width values were performed as required: B=1.6m, B=0.8m and finally B=0.4m. For each case, successive runs of the hydraulic model were performed in order to establish the numerical solutions (see the representation in Fig.4, the final model of B=0.4m width).
The roughness coefficient in the flow segment was assessed within the limit: n = 0.015 … 0.045, respectively, n =0.045 for the area of the downstream face provided with macrorugosities, n=0.015 for the energy dissipation basin and the downstream threshold area, and n=0.020 for the downstream connection area. The hydrodynamic gradient is known as J=0.000625 at the entrance area, and as J=0.01285 in the end zone.

3. Initial and boundary conditions

As a current approach, the boundary conditions of the modeled hydraulic path are given by: the transited discharge with a certain occurrence probability introduced as a known high-waters hydrograph, values that are assigned to the upstream area of the 1D numerical model – specifically in the section with the metric notation "100.869" – to which the hydrodynamic gradient is also associated as required for the flow rates distribution per section; the hydrodynamic gradient in the downstream zone of the model – meaning in the section with the "0.000" metric notation. In this discrete 1D numerical model, initial conditions given by entering the initial flow are required. Thus, the particular boundary conditions consider:

- a synthetic high-waters wave at which the maximum reached flow has the value Q_{max} = 5.70 m^3/s and the hydrodynamic gradient with the value J = 0.000625, as attached to the entering upstream section of "100.869" metric notation;
- the known value of the initial flow Q_{ini} = 1.90 m^3/s is considered in section "100.869", as an initial condition for starting the model run;
- the hydrodynamic gradient estimated at the value J = 0.01285, as assigned to the "0.000" metric notation section, downstream of the modeled hydraulic route.

The hydraulic phenomenon considered in the numerical modeling takes place in time for a known period, starting from 07:00 on the first day of flood wave formation and until 10:00 on its fifth day, the end of the special phenomenon. The actual execution analysis is reduced to a significant time interval for the flow, namely it was performed until 22:00 of the first day, at which moment the in-flow decreased semnificatively down to about 2.4 m^3/s. The time step of the modeling as well as the internal mapping interval were both imposed as 0.1 seconds, but the storage of the results was adopted at a time interval of 10 minutes.

4. Numerical simulation and results presentation

For a start on, the hydraulic model was run over an interval of 20 minutes, saving in a restart file the water levels obtained in all the cross sections. These values, saved in an .rst extension file, become values adopted as initial conditions for the next run considered the actual one.
Figure 5 shows some important messages along the actual hydraulic model running time interval that refer to the cross-sections that do not comply with the condition of distancing from the neighboring sections, necessary to eliminate the numerical instability. These messages mention the time moment, the 1D path, the section metric notation and the temporal elevation, as well as the value of exceeding the imposed tolerance value. This information monitors the execution of the hydraulic model in terms of satisfying some requirements regarding the confidence parameters of the results.
Following the running of the actual numerical simulation, all the constant or time dependent parameters, referring to water levels and flows, were obtained, over the entire discrete numerical model, in the situation of non-permanent water transit along the considered route. The results obtained by the common graphic post-processing operations are presented as follows:

- Longitudinal profiles visualizing the high waters hydrograph transit mode – water levels development with respect to Sea Level – at several specific time moments along the first day of the hydraulic phenomenon (Figure 6): 07:00 (entering transit flow of 1.9 m^3/s), 08:00 (3.26 m^3/s entering flow), 14:00 (5.7 m^3/s entering flow) and 22:00 (2.4 m^3/s entering flow);
- Longitudinal profiles corresponding to the maximum entering transit flow of 5.7 m^3/s - water levels (mSL) in several specific points (sections) at 14:00 on September 22nd (Figure 7);

One can notice that the flow transit mode on the modeled route takes place under different flow regimes: rapid regime at the downstream face in the macroroughness area (below the critical flow line); slow regime in the area of the energy dissipation basin; slow and fast mode on the threshold of the energy dissipation basin; slow speed in the area of connection with the natural terrain downstream of the discrete numerical model.

- Water level (mSL) and discharge (m^3/s) development for the entering "100.869" and outgoing "0.000" sections (Figure 8).

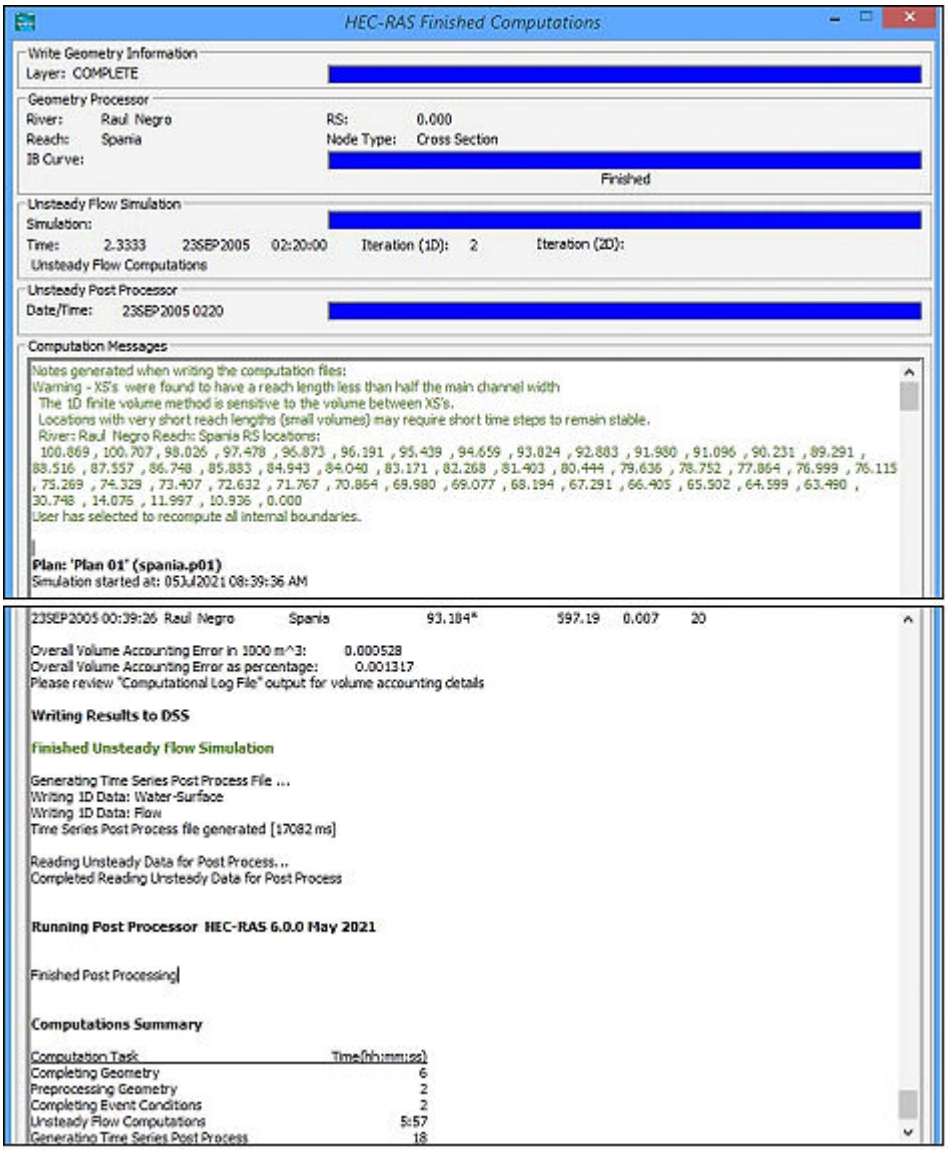

Fig. 5. Messages along the actual running of the developed model

5. Discutions and conclusions

After reviewing the results provided, it is observed that in the finite volumes method the variation of the velocities in the cross-section is no longer determined. Based on the graphical representations of the cross-sections shown in Figure 7, the average speeds in the section at the current time can be estimated (the base elevation can be considered from the profile, while the maximum level elevation is given in the cross-section). Thus:

- The section at the entrance area of notation "99.315*"(up-left in Figure 7)

$$v_{med} = \frac{Q_{max}}{B*h} = \frac{5.70}{0.4*(604.24-601.00)} = 4.398\ m/s;$$

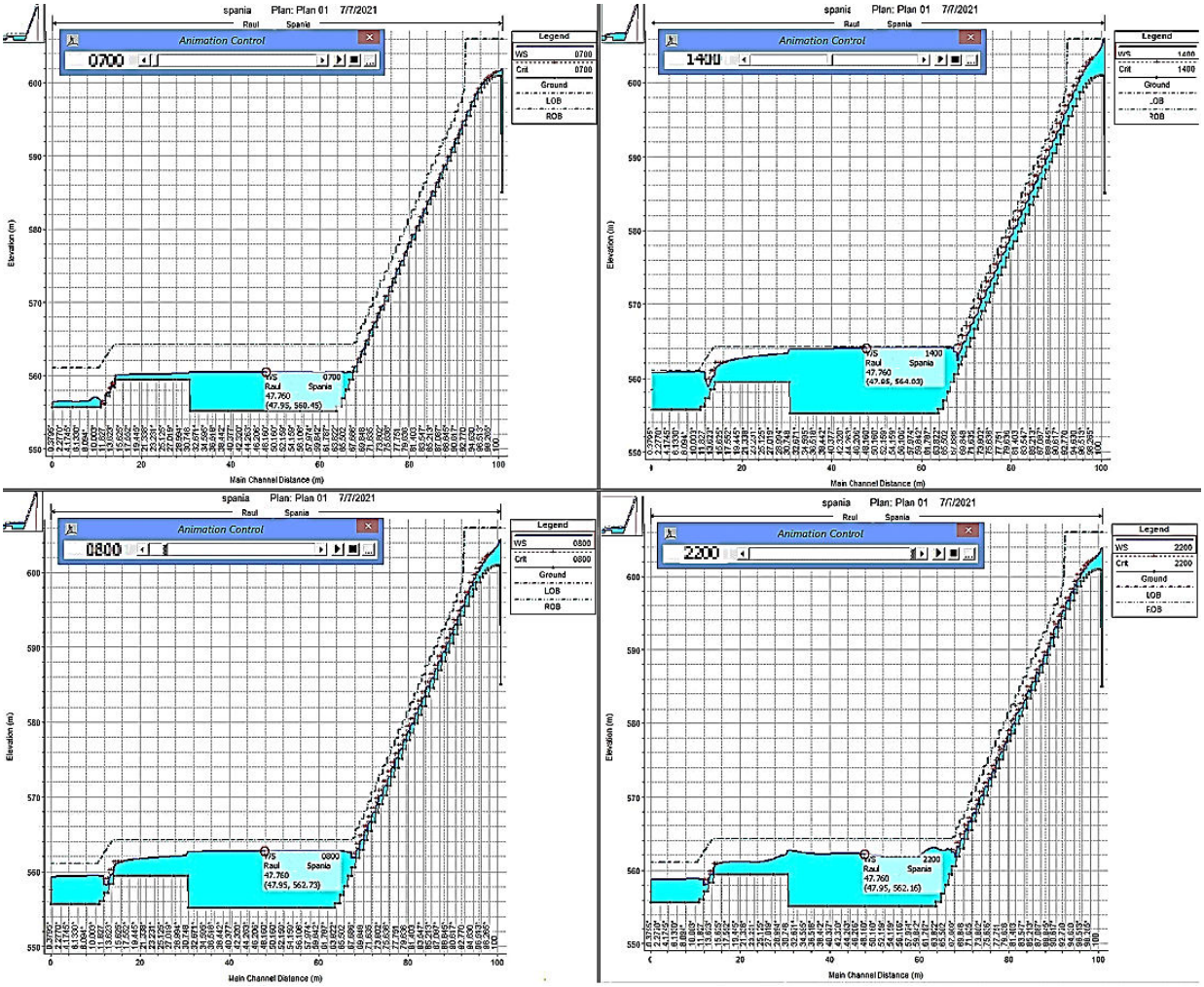

Fig. 6. Longitudinal profiles by the hydraulic model at several specific hours along the first day of the high waters transit phenomenon

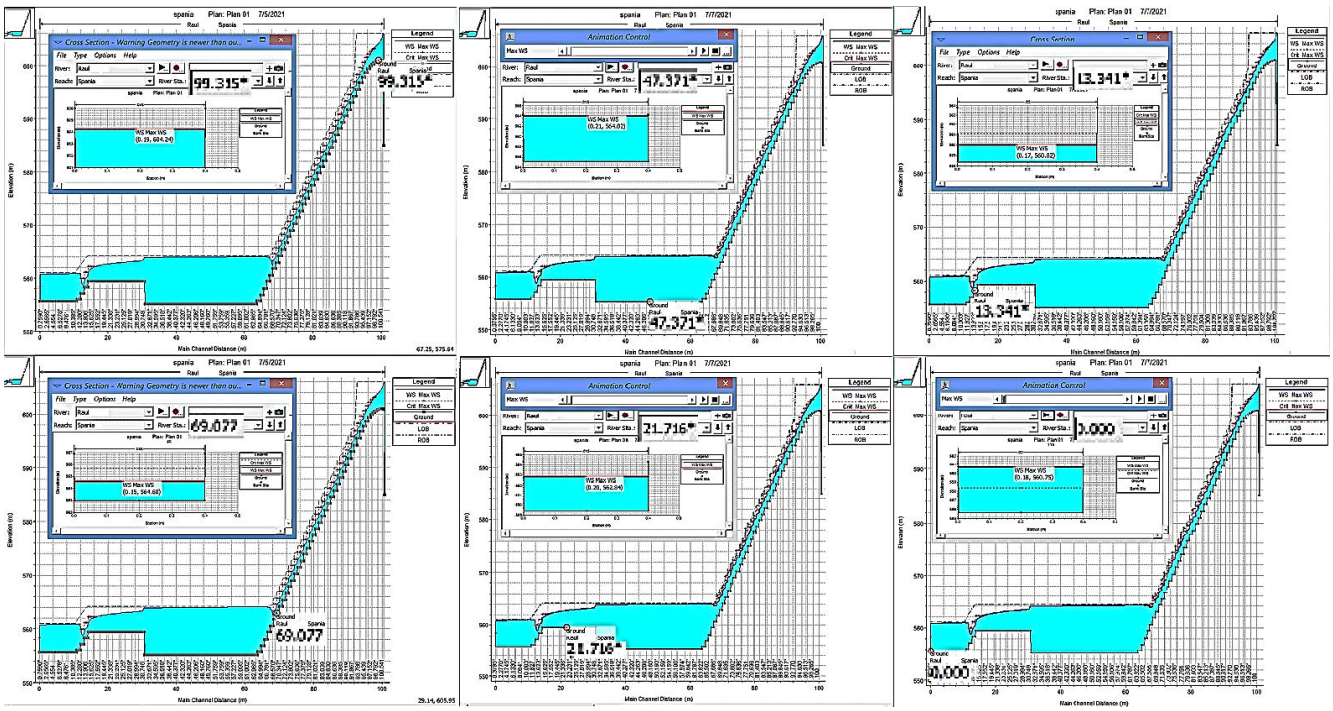

Fig. 7. Longitudinal profiles by the hydraulic model at the specific hour 14:00 of maximum entering flow detailing the water levels development in several path cross-sections

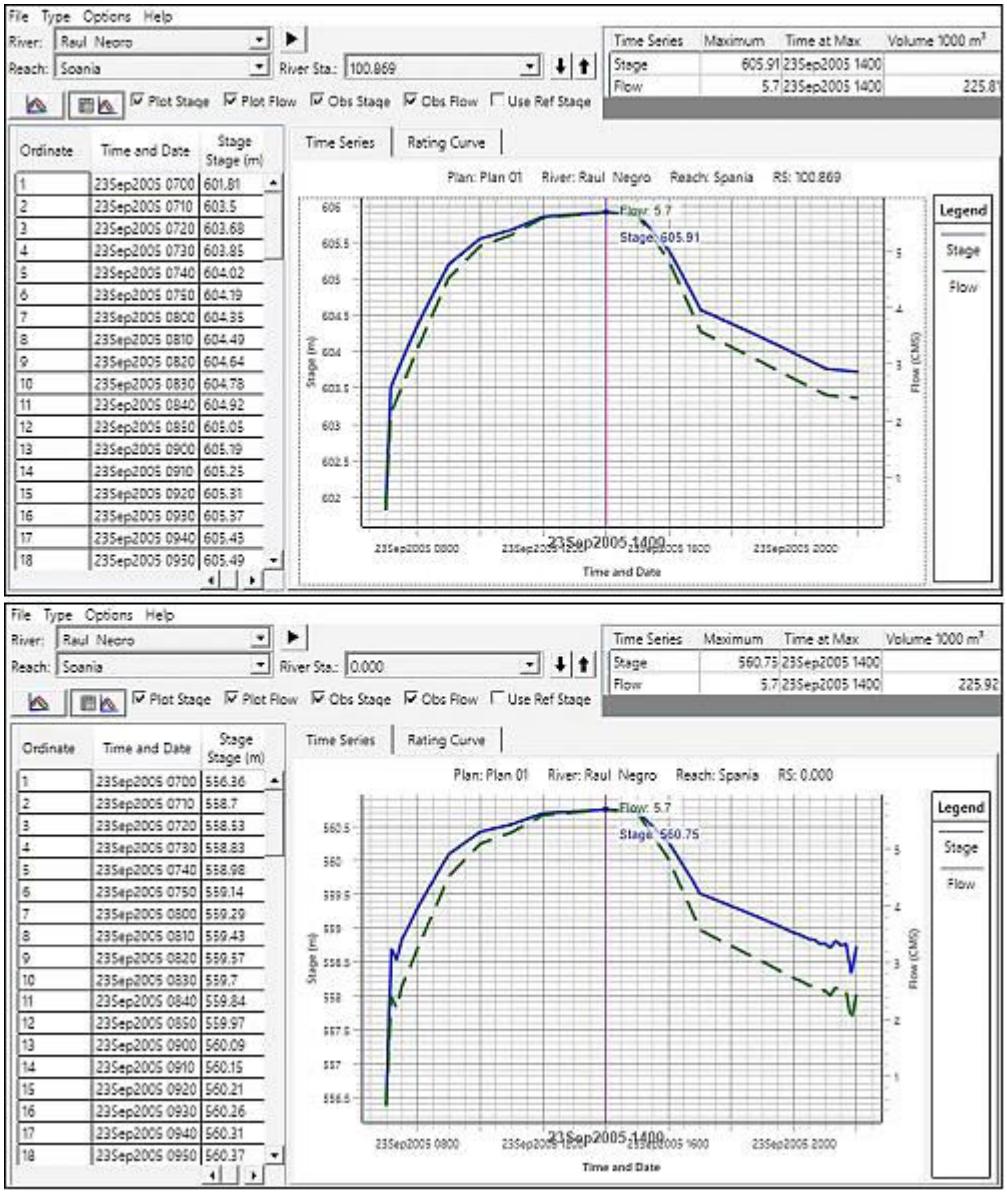

Fig. 8. Water level and discharge development for the entering (above) and outgoing sections of the model

- The section in the connection area to the energy dissipation basin, notation "69.077"(down-left in Figure 7)

$$v_{med} = \frac{Q_{max}}{B*h} = \frac{5.70}{0.4*(564.60-562.96)} = 8.689\ m/s;$$

- The energy dissipation basin area section of notation "47.371*"(middle-up in Figure 7)

$$v_{med} = \frac{Q_{max}}{B*h} = \frac{5.70}{0.4*(564.02-555.13)} = 1.603\ m/s;$$

- The section upstream of the energy dissipation threshold, notation "21.716*"(middle-down in Fig. 7)

$$v_{med} = \frac{Q_{max}}{B*h} = \frac{5.70}{0.4*(562.84-559.43)} = 4.179\ m/s;$$

- The section imediately downstream of the threshold at energy dissipater, notation "13.341*"(up-right in Figure 7)

$$v_{med} = \frac{Q_{max}}{B*h} = \frac{5.70}{0.4*(560.02-558.34)} = 8.482\ m/s;$$

- The model end section of notation "0.000"(down-right in Figure 7)

$$v_{med} = \frac{Q_{max}}{B*h} = \frac{5.70}{0.4*(560.75-555.64)} = 2.789\ m/s.$$

For a maximum head estimated as $T_0 = P + H + {v_0}^2/2g = 51.234m$, by an iterative calculation (maximum 4 iterations, in this case) it is possible to determine the contracted depth in the dissipating basin (at the maximum flow rate and for the situation of a spillway considered of practical type profile $m_d = 0.49$) [5], with the help of which the average water velocity can be estimated:

$h_c = \frac{Q_{max}}{\varphi \cdot B}\sqrt{\frac{1}{2\cdot g\cdot(T_0 - h_c)}} = \frac{5.70}{1.0 \cdot 0.4}\cdot\frac{1}{\sqrt{2\cdot g\cdot(51.234 - h_c)}} = \cdots\ 0.452\ m$ and so $v_m = \frac{Q_{max}}{B\cdot h_c} = \frac{5.70}{0.4\cdot 0.452} = 31.56\ m/s.$

In this situation, it can be assessed that the maximum value of the velocity reached on the analyzed route (8,689 m/s, as previously estimated for the section in the connection area to the energy dissipation basin) compared to the value determined with the approximation relation ($v_m = 31.56\ m/s$), leads to a velocity reduction coefficient on the model with macroroughness of approx. $\boldsymbol{k_r}$ = 0.275. It can be thus considered that this may represent the overall kinetic energy dissipation along the spillway downstream face due to the macroroughness system.

As to check the discharge capacity through a single spillway gap (where $B_{max} = 16m$, with respect to the width of the numerical pattern of $B = 0.4m$), i.e. the capacity of the entire spillway with two gaps, a linear scaling relationship can be considered:

$Q_{med} = \frac{B_{max}}{B}\cdot Q_{max} = \frac{16.00}{0.4}\cdot 5.70 = 228\ m^3/s\ \ \ldots\ \ Q_{dev} = 2\cdot Q_{med} = 456\ m^3/s.$

In conclusion, the accomplishment of a discharger face with macroroughness as presented by the situation considered will lead to great kinetic energy dissipation developed at all moments of a special flood wave transit (especially obvious for the maximum flow transit).

References

[1] Constantin, A.T. *Thesis of Advanced Studies on El Boqueron Dam stepped spillway at Centro de Estudios y Experimentacion de Obras Publicas,* Centro de Estudios Hidrograficos, Madrid, 1996.

[2] ***. https://www.chsegura.es/tourembalses/boqueron/ .

[3] ***. *HEC-RAS River Analysis System User's Manual, Version 6.0*. May 2021, US Army Corps of Engineers Institute for Water Resources Hydrologic Engineering Center.

[4] Brunner, G.W. *HEC–RAS 4.1 River Analysis System, Hydraulic Reference Manual*. US Army Corps of Engineers, 2002.

[5] David, I. *Hidraulică / Hydraulics*. Volume II. "Traian Vuia" Polytechnic Institute of Timișoara, Faculty of Civil Engineering, Timișoara, 1984.

A Hydraulic and Control-Theoretic Perspective on Arterial Flow Regulation

Associate professor **Fănel Dorel ȘCHEAUA**[1,*]

[1] "Dunărea de Jos" University of Galati, MECMET Research Center

* fanel.scheaua@ugal.ro

Abstract: *Blood vessels are modelled as compliant conduits within pulsation flow systems, hence their major ability is to actively regulate the diameter values, property which distinguishes them fundamentally from passive hydraulic pipes. This paper presents an interdisciplinary interpretation of vascular smooth muscle regulation based on calcium and magnesium ionic dynamics, framed using classical hydraulic theory and control systems terminology. The well known Calcium-driven contraction and magnesium-mediated relaxation are interpreted as competing actuation and damping mechanisms that modulate effective vessel radius and consequently hydraulic resistance according to Poiseuille's law. The analysis highlights how small ionic variations can produce nonlinear changes in flow, pressure drop and system stability. This perspective provides a conceptual bridge between biological flow regulation and engineered hydraulic networks with active feedback control.*

Keywords: *Biofluid mechanics, pulsatile flow, arterial radius modulation, Poiseuille's law, active flow regulation, vascular compliance*

1. Introduction

For classical hydraulics the fluid flow regulation is typically achieved through valves, throttles and feedback-controlled actuators that modify conduit geometry or boundary conditions. In the cardiovascular system, the arteries perform an analogous function through vascular smooth muscle embedded in the vessel wall.
Rather than acting as passive elastic pipes, arteries continuously adjust their effective radius in response to mechanical, neural and chemical signals, thereby regulating flow distribution and pressure.
The contractile behaviour of vascular smooth muscle is governed primarily by intracellular calcium concentration, while magnesium acts as a physiological antagonist that stabilizes and limits contractile responses.
This ionic interaction has been extensively studied in physiology and biophysics, particularly in relation to vascular motion and blood pressure regulation (Somlyo & Somlyo, 2003; Bolton, 1979).
However, the same mechanisms can be meaningfully interpreted using hydraulic principles and control theory, offering insights into arterial behaviour as an actively regulated flow system.
From a hydraulic standpoint, the arterial radius is the dominant control variable and according to Poiseuille's law for laminar flow in a cylindrical conduit the fluid flow rate can be expressed by:

$$Q = \frac{\pi \Delta p \, r^4}{8 \mu l} \tag{1}$$

where Q is volumetric flow rate, Δp the pressure drop, r the effective radius, μ the dynamic viscosity and l the duct length.
It can be seen that the fourth-power dependence on radius implies an obvious change in the amount of circulating fluid, being facilitated mainly by the changes that are related to the obvious minor calcium-induced contractions of smooth muscle that can produce large increases in hydraulic resistance. Conversely, magnesium-facilitated relaxation restores radius and sharply reduces resistance, improving flow efficiency.
This paper proposes an interdisciplinary framework in which vascular smooth muscle regulation is interpreted through the analytical and conceptual tools of fluid mechanics and hydraulic control engineering.

Although the biochemical pathways governing the laws of calcium-induced contraction and magnesium-mediated relaxation are well established in physiology, their translation into hydraulic functionality, and in particular in terms of radius modulation, resistance variability, and pulsatile flow adaptation, remains an insufficiently formalized approach in the engineering literature.
To address this gap, the study develops a simplified but physically consistent representation of the artery as an actively controlled conduit model, which is embedded in a pulsatile flow field.
The contractile state of the vascular wall is modeled as a dynamic function of intracellular calcium concentration, while magnesium is introduced as a modulating variable affecting both ionic influx and efflux kinetics.
This formulation allows the expression of the vessel radius as a time-dependent control parameter, thus allowing direct coupling to classical flow equations.
Based on Poiseuille's law, the paper quantifies how calcium-induced reductions in arterial radius produce a nonlinear amplification of hydraulic resistance, given the fourth-power dependence of flow on the conduit radius.
Particular attention should be paid to transient regimes, where pulsatile pressure gradients interact with time-varying vessel compliance, and in this context the phase corresponding to magnesium input is treated as a damping factor that attenuates excessive contractile gain and stabilizes the radius response under oscillatory excitation.
The paper introduces an interpretation of vascular regulation from the perspective of control systems, while calcium influx is formulated as a variable gain drive input that responds to electrical and chemical stimuli, while magnesium contributes negative feedback and damping within the system.
This approach allows the construction of conceptual block diagrams linking ion transport, smooth muscle mechanics, radius modulation and flow output, and through such a representation comparison with designed hydraulic networks using adaptive throttling and feedback stabilization is facilitated.
To illustrate these interactions, the paper proposes computational simulations in which intracellular ionic dynamics are coupled to time-resolved flow equations.
Parametric variation of magnesium concentration is used to evaluate its effect on contraction amplitude, resistance oscillation and flow stability under pulsatile forcing.
Graphical results, which include surface plots, transient response curves, and resistance-radius phase relations, are used to visualize the system behavior.
Through this combined analytical and numerical development, the study aims to highlight the structural analogies between biological vascular control and engineering hydraulic regulation, and by integrating ionic physiology into a fluid-mechanical and control-theoretical framework, the work contributes to a more integrative understanding of active flow conduits and provides modeling insights applicable to both biomedical and hydraulic research fields.

2. Ionic Actuation as a Hydraulic Control Mechanism

The phenomenon of calcium entry into smooth muscle cells through voltage-gated channels functions as an active trigger signal, and further an increase in intracellular calcium triggers force generation, reducing the vessel radius and increasing resistance.
In theoretical terms of control theory, calcium acts as a high-gain input that amplifies upstream stimuli, such as pressure impulses or neurohumoral signals, into mechanical constriction.
In contrast, Magnesium introduces a stabilizing influence analogous to damping in hydraulic or mechanical systems, and by limiting calcium influx and enhancing calcium extrusion, Magnesium reduces the effective gain of the contractile response and suppresses oscillatory or excessive constriction. Therefore, adequate magnesium levels prevent overshoot and promote smooth transient behavior in response to pulsatile flow.
For these reasons, the interaction between calcium and magnesium can be interpreted as a closed-loop feedback system, with pulsatile variations in pressure and fluid flow providing the input signal, calcium-mediated contraction serving as the actuator, vessel radius as the controlled variable, and magnesium contributing to the damping and stability of the system. This feedback

loop allows arteries to dynamically adapt to changing flow demands while avoiding instability, spasm, or sustained high resistance 0, 0.

In order to formalize the hydraulic interpretation of vascular ionic regulation, the artery is modeled as an active compliant cylindrical duct whose instantaneous radius is governed by smooth muscle contractile state. The contractile state is, in turn, defined as a dynamic function of intracellular calcium concentration modulated by magnesium availability and this coupling enables the integration of ionic transport kinetics with classical flow equations.

The intracellular calcium concentration C(t) is described using a first-order nonlinear balance between influx and efflux mechanisms. Calcium influx is modeled as a stimulus-dependent input driven by pulsatile excitation, while efflux represents active pumping and sequestration processes. Magnesium concentration (M) is introduced as a modulatory coefficient that reduces effective calcium influx and enhances removal kinetics, thereby acting as a damping variable in the system 0, 0. The governing relationship may be expressed in simplified form as:

$$\frac{dC}{dt} = k_1 (1 - M) S(t) - k_2 C(t) \tag{2}$$

where k_1 represents baseline calcium channel conductance, k_2 characterizes ATP-dependent calcium clearance and *S(t)* defines the pulsatile stimulation function associated with pressure or electrical excitation.

The mechanical response of the arterial wall is linked to calcium concentration through a contraction transfer function. Vessel radius is assumed to decrease proportionally with increasing cytosolic calcium:

$$r(t) = r_0 \left[1 - \alpha C(t) \right] \tag{3}$$

where r_0 is the passive (fully relaxed) radius and α is a contractility gain coefficient reflecting smooth muscle sensitivity to calcium. This formulation captures the actuator role of calcium within the hydraulic control system.

Flow through the artery is computed using Poiseuille's law under laminar, incompressible assumptions:

$$Q(t) = \frac{\pi \Delta p r(t)^4}{8 \mu l} \tag{4}$$

The fourth-power dependence introduces strong nonlinearity, such that small calcium-induced radius variations produce amplified changes in volumetric flow rate and hydraulic resistance. Resistance is correspondingly defined as:

$$R(t) = \frac{8 \mu l}{\pi r(t)^4} \tag{5}$$

This relationship enables direct evaluation of how ionic dynamics propagate into macroscopic flow behavior.

Within the control framework, the model can be interpreted as a closed-loop adaptive throttling system. The pulsatile stimulation S(t) constitutes the input signal, while the calcium influx operates as the primary actuator with gain k_1 and vessel radius represents the controlled variable. Magnesium introduces damping by attenuating actuator gain and accelerating system return towards equilibrium via enhanced calcium clearance.

The dynamic response exhibits features characteristic of second-order hydraulic control systems, including transient overshoot, oscillatory radius modulation and stabilization under adequate damping. Reduced magnesium levels effectively increase system gain, predisposing the conduit to excessive constriction and resistance spikes under pulsatile forcing 0, 0.

3. Numerical analysis of nonlinear radius–flow interaction via Poiseuille modelling

The numerical analysis aims to quantify the coupled ionic–hydraulic dynamics governing arterial radius modulation and the resulting flow regulation under pulsatile excitation.
The computational framework integrates intracellular calcium kinetics with time-dependent hydraulic resistance and volumetric flow derived from Poiseuille-based relations.
Time-domain simulations were implemented using discretized integration of the governing differential equations describing calcium influx, magnesium-modulated attenuation and active calcium clearance.
The pulsatile stimulation function was represented as a periodic waveform approximating physiological pressure forcing, enabling the evaluation of transient contraction–relaxation cycles over multiple flow periods. Numerical stability was ensured through sufficiently small temporal step selection relative to ionic transport time constants.
Magnesium concentration was treated as a parametric control variable spanning physiologically relevant ranges. For each magnesium level, intracellular calcium evolution was computed, followed by transformation into arterial radius variation through the contractility transfer function.
The resulting radius signal was subsequently introduced into the nonlinear Poiseuille formulation to obtain instantaneous flow rate and hydraulic resistance.
The simulations revealed pronounced nonlinear amplification effects arising from the fourth-power radius dependence. An even moderate calcium oscillation produces significant resistance variability, particularly under low magnesium conditions where effective damping was reduced.
In these regimes, transient overshoot phenomena are observed, characterized by delayed relaxation and elevated peak resistance following pulsatile excitation. Conversely, increased magnesium concentration attenuates calcium accumulation, reduces contraction gain and promotes smoother radius recovery between pulses.
Surface mapping of contraction amplitude as a function of time and magnesium level demonstrated a clear stabilization gradient, with high-magnesium states exhibiting reduced oscillatory magnitude and improved hydraulic compliance. Phase analysis between pulsatile input and radius response further indicated that magnesium availability influences not only contraction amplitude but also temporal synchronization, effectively shifting the system towards a more damped dynamic regime.
From a hydraulic systems perspective, the numerical results confirm that ionic modulation operates analogously to adaptive throttling with variable gain and damping.
Calcium-driven actuation governs rapid resistance adjustments, while magnesium ensures transient stability and prevents excessive flow restriction under oscillatory forcing.
This coupled behaviour reinforces the interpretation of arteries as actively regulated ducts whose flow characteristics emerge from tightly integrated biochemical and fluid-mechanical control processes.

4. Results, discussion and hydraulic implications

When the amount of magnesium availability is reduced, it can be considered that the damping component of the system weakens and the result is prolonged calcium retention, sustained contraction and further elevated hydraulic resistance, which represent conditions comparable to a poorly damped throttle that fails to reopen fully between pressure cycles. Over time, such behaviour increases upstream pressure and reduces system compliance, a phenomenon observed clinically as increased arterial stiffness and hypertension.
The viewing method of vascular regulation through the proposed hydraulic and control-theoretic framework emphasizes that biological flow systems share fundamental design principles with engineered networks. Active radius modulation, nonlinear resistance behavior, feedback control, and damping are common to both domains, while this analogy supports the use of simplified hydraulic models to study vascular function and highlights the relevance of ionic balance in maintaining stable and efficient flow regulation.
The preliminary obtained results illustrates the temporal evolution of cytosolic Ca^{2+} concentration under graded extracellular Mg^{2+} levels. The oscillatory regime reflects pulsatile ionic influx synchronized with vascular smooth muscle excitation. Increasing Mg^{2+} produces a clear

attenuation of Ca^{2+} peak amplitude and a reduction in mean cytosolic concentration, consistent with competitive channel inhibition and membrane stabilization effects. From a control perspective, Mg^{2+} acts as a negative gain regulator within the excitation–contraction coupling loop, damping calcium-driven contractile signalling.

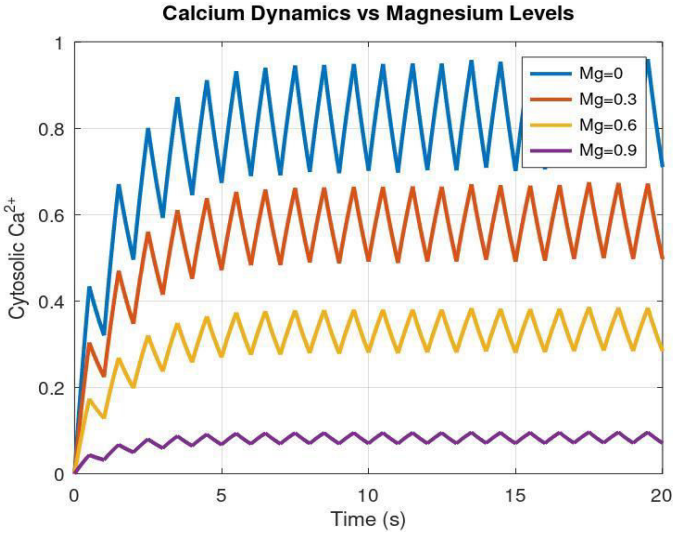

Fig. 1. Calcium dynamics versus Magnesium modulation

Radius variation is computed as an inverse functional response to cytosolic Ca^{2+}. The plots demonstrate progressive vasorelaxation as Mg^{2+} concentration increases. High Mg^{2+} shifts the operating point towards larger equilibrium radii while simultaneously reducing pulsatile amplitude. This indicates both tonic relaxation and dynamic damping of vasomotor oscillations. The mechanical response confirms the role of ionic balance in defining arterial compliance and instantaneous lumen geometry.

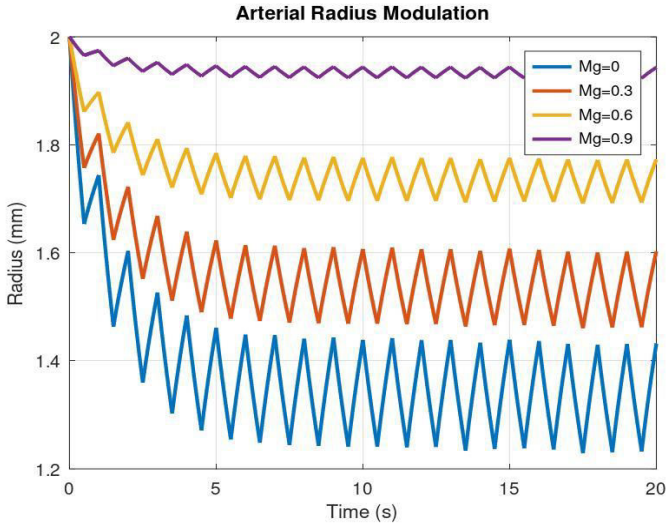

Fig. 2. Arterial Radius Modulation

Using the time-varying radius as input to Poiseuille's formulation, the resulting flow traces exhibit strong nonlinear amplification. Even modest Mg^{2+}-induced radius increases generate substantial flow augmentation due to the fourth-power radius dependency. The pulsatile envelope becomes smoother and elevated under higher Mg^{2+}, reflecting reduced contractile impedance. This demonstrates how ionic regulation at the cellular scale propagates into macroscopic hemodynamic performance.

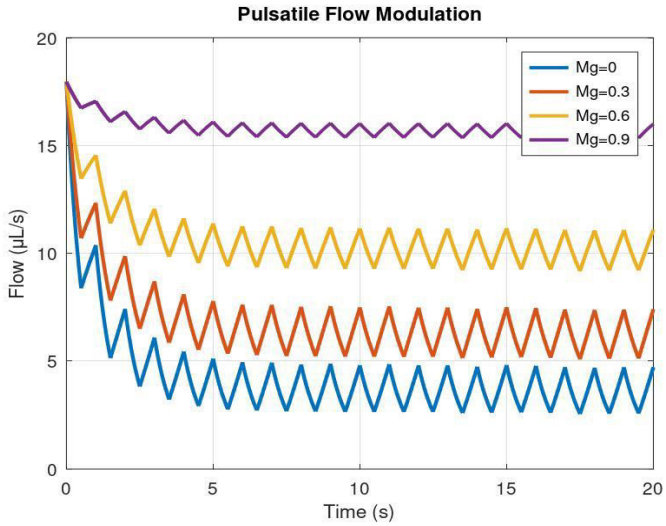

Fig. 3. Pulsatile Flow Modulation

Regarding the resistance evolution the inverse fourth-power relationship with arterial radius is considered. Elevated Ca^{2+} states correspond to sharp resistance spikes, whereas Mg^{2+} enrichment compresses both mean resistance and oscillatory spread. From a hydraulic systems point of view, Mg^{2+} functions analogously to a damping element that stabilizes impedance fluctuations and improves flow conductance.

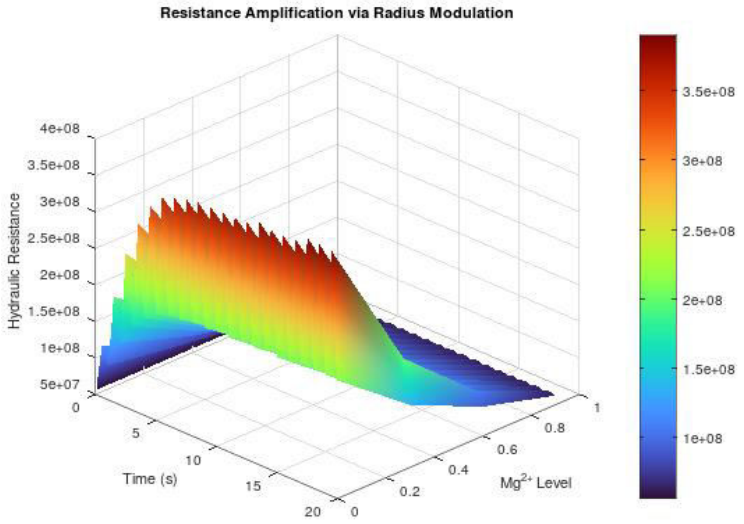

Fig. 4. Hydraulic Resistance Dynamics

The surface plot integrates time and Mg^{2+} concentration into a unified contraction field where the gradient along the Mg^{2+} axis highlights monotonic suppression of contractile state, while the temporal axis preserves pulsatile excitation (figure 5).

The topology reveals a nonlinear interaction domain where small Mg^{2+} increments produce disproportionately large relaxation effects at high contractile states, while the visualization concept supports the interpretation of Mg^{2+} as a modulatory control parameter within the vascular actuation system.

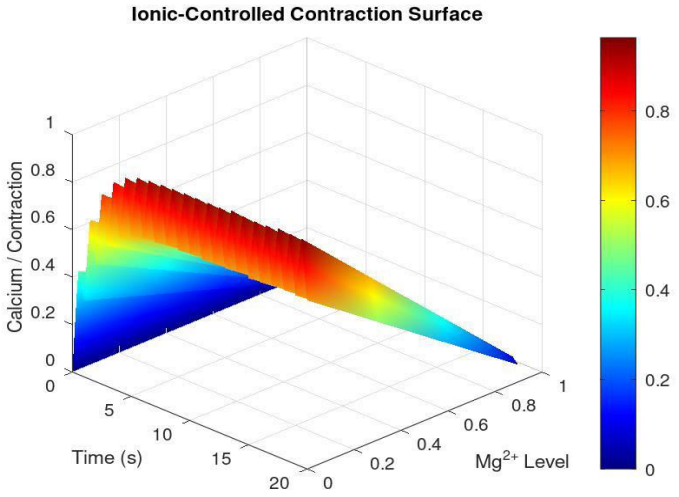

Fig. 5. Ionic-controlled contraction surface (3D surface representation)

5. Conclusions

The present study demonstrates that arterial flow regulation can be coherently interpreted through a coupled ionic–hydraulic framework in which calcium-driven smooth muscle contraction operates as the primary actuation mechanism, while magnesium exerts a modulatory stabilization role. Numerical simulations integrating intracellular Ca^{2+} kinetics with radius-dependent Poiseuille flow revealed that even small variations in cytosolic calcium produce amplified hemodynamic consequences due to the fourth-power sensitivity of flow and resistance to lumen radius.

Magnesium elevation consistently attenuates calcium accumulation, reduces contractile gain and promotes larger equilibrium arterial diameters, while this process is translated hydraulically into increased volumetric flow rates and diminished resistance oscillations under pulsatile forcing.

The results highlight magnesium's functional equivalence to a damping and gain-reduction parameter within an automatic control representation of vascular behavior.

Surface and time-domain analyzes further indicated that ionic balance governs not only steady-state vascular tone but also transient synchronization between pulsatile excitation and mechanical response. Systems with low magnesium exhibited overshoot and delayed relaxation, whereas magnesium-rich conditions approached critically damped dynamics with improved flow stability.

Overall, the study confirms that arterial ducts behave as actively regulated hydraulic elements whose impedance is dynamically tuned by ionic transport processes.

Embedding calcium–magnesium coupling into biofluid models provides a quantitatively robust pathway for linking cellular electrophysiology with macroscopic hemodynamic performance, with potential applications in vascular diagnostics, pharmacological modulation and biomimetic flow control design.

References

[1] Bolton, T. B. "Mechanisms of action of transmitters and other substances on smooth muscle." *Physiological Reviews* 59, no. 3 (1979): 606–718.

[2] Somlyo, A. P., and A. V. Somlyo. "Ca^{2+} sensitivity of smooth muscle and nonmuscle myosin II: Modulated by G proteins, kinases, and myosin phosphatase." *Physiological Reviews* 83, no. 4 (2003): 1325–1358.

[3] Fung, Y. C. *Biomechanics: Circulation*. Springer, 1997.

[4] Nichols, W. W., and M. F. O'Rourke. *McDonald's Blood Flow in Arteries: Theoretical, Experimental and Clinical Principles*. 5th edition. London, Hodder Arnold, 2005.

Artificial Intelligence–Enhanced versus Traditional Hydrological Software for Double Gumbel Frequency Analysis

M.Eng. **Margarita PRECIADO-JIMÉNEZ**[1,*], Dra. **Maritza ARGANIS-JUÁREZ**[2,3,*],
M. Eng. **Rosalva MENDOZA-RAMÍREZ**[2], M.Eng. **Arturo LOPEZ-ZUÑIGA**[1]

[1]Instituto Mexicano de Tecnología del Agua

[2]Universidad Nacional Autónoma de México, Instituto de Ingeniería

[3]Universidad Nacional Autónoma de México, Facultad de Ingeniería

* MArganisJ@iingen.unam.mx; preciado@tlaloc.imta.mx

Abstract: *Accurate characterization of hydrological extreme events is essential for safe hydraulic design. In Mexico, annual maximum values often exhibit bimodal behavior due to the combined effects of convective storms and tropical cyclones, which single-population models struggle to represent. This study compares conventional tools with AI-assisted methods for fitting the Double Gumbel distribution, which is well-suited for complex regimes. The analysis covers parameter estimation, numerical stability, and goodness-of-fit. Results show that hybrid approaches using genetic algorithms and AI outperform gradient-based techniques, achieving 92% convergence versus 67%, 33.3% lower mean squared error, and higher efficiency. Findings highlight a shift toward AI-enhanced frameworks for extreme event analysis, enabling more reliable risk assessments and safer infrastructure design.*

Keywords: *Extreme value analysis, Double Gumbel distribution, Hydrological frequency analysis, Genetic algorithms, Artificial intelligence*

1. Introduction

Extreme hydrological analysis events, such as annual maximum precipitation and peak discharge, is fundamental to hydraulic and water resources engineering. Design floods derived from frequency analysis directly influence the safety, reliability, and economic feasibility of critical infrastructure. This is exemplified by Mexico's Balsas River hydroelectric system, a cornerstone of flood control and national energy production and its key structure, the Presidente Adolfo López Mateos Dam commonly known as El Infiernillo Dam (figure 1), was completed between 1960 and 1964. With a 149-meter embankment, a 12 billion cubic meters reservoir capacity, and a 1,020 MW generation capacity, its safe operation is paramount. This dam, together with the downstream La Villita (1968) and upstream El Caracol (1987) dams, forms an integrated system in which accurate extreme flow estimation is a systemic necessity.

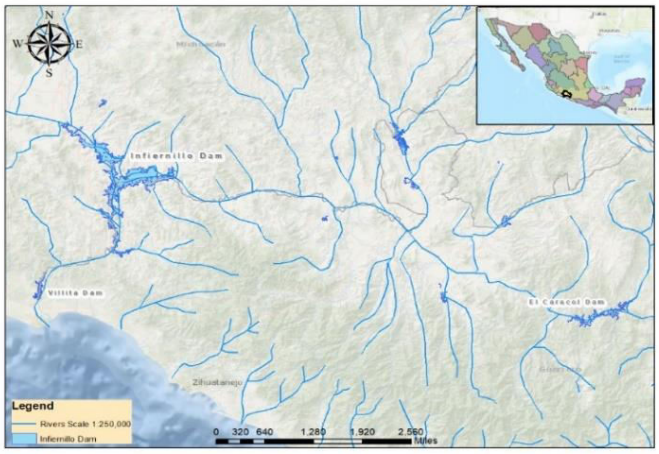

Fig. 1. El Infiernillo, Caracol and Villita Dam´s system location

Since Gumbel's seminal work, the Type-I Extreme Value (EV1) distribution [1] has been widely adopted in hydrology. However, the assumption of a single homogeneous generating process is often violated in real-world basins such as the Balsas. In the Infiernillo Dam catchment, hydrological extremes may arise from different meteorological mechanisms, including short-duration convective storms and large-scale cyclonic systems. These mixed processes frequently produce bimodal or heavy-tailed behavior in annual maxima series, challenging the adequacy of traditional single-population distributions and the accuracy of safety assessments.
To address this limitation, mixture models, particularly the Double Gumbel distribution [2–4], have gained prominence as they can explicitly represent multiple generating mechanisms. Despite their theoretical advantages, practical implementation has been constrained by numerical instability in traditional software. Recent advances in Artificial Intelligence, especially evolutionary optimization and AI-assisted scientific programming, offer new opportunities to overcome these challenges. This paper critically evaluates these developments, using El Infiernillo Dam inflow series as a central case study, and discusses their implications for hydrological practice in regions subject to heterogeneous extreme events.

2. Theoretical Background

2.1 Extreme Value Distributions in Hydrology

The Gumbel distribution assumes that annual maxima originate from a single, identically distributed population [1]. While simplifying parameter estimation and interpretation, this assumption may lead to systematic bias in heterogeneous climatic regimes. Empirical evidence from coastal and mountainous regions shows that extreme events may cluster into distinct groups with different statistical properties.

2.2 Rationale for the Double Gumbel Distribution

The Double Gumbel distribution represents annual maxima as a mixture of two independent Gumbel populations [2]. Each component corresponds to a different physical generating mechanism, providing greater flexibility in modeling asymmetric and heavy-tailed behavior, particularly relevant in basins exposed to both frequent moderate events and rare catastrophic extremes.

2.3 Mathematical Formulation

The cumulative distribution function (CDF) of the Double Gumbel distribution is expressed as [5]:

$$F(x) = p * exp(-exp(-(x - \mu_1)/\beta_1)) + (1 - p) * exp(-exp(-(x - \mu_2)/\beta_2)) \quad (1)$$

where $(F_1 = exp(-exp(-(x - \mu_1)/\beta_1)))$ and $(F_2 = exp(-exp(-(x - \mu_2)/\beta_2)$ are Gumbel CDFs with scale parameters (μ_1, μ_2), location parameters (β_1, β_2), and ω is the mixing coefficient (0-1) [2] refers to this parameter as *p* the probability that the event belongs to a first population or a second population, and uses the notation α and β instead of $1/\beta$ *and* μ).

3. Parameter Estimation Methods

3.1 Classical Approaches

Traditional hydrological software relies primarily on gradient-based optimization techniques, including the Method of Moments (MOM), Maximum Likelihood Estimation (MLE), Probability-Weighted Moments (PWM), and Linear-Moments (LM) [6–8]. While effective for two-parameter distributions, these approaches encounter difficulties with mixture models due to irregular likelihood surfaces and multiple local optima.

3.2 Limitations of Gradient-Based Optimization

For the Double Gumbel distribution, the likelihood function often exhibits strong nonlinearity and multimodality. Gradient-based algorithms such as Newton–Raphson or Broyden-Fletcher-Goldfarb-Shanno (BFGS) are highly sensitive to initial parameter values, leading to convergence failures or suboptimal solutions, principally problematic for automated or large-scale regional studies.

3.3 AI-Assisted Optimization

AI-assisted software replaces local optimization with global search strategies, most notably Genetic Algorithms (GAs) [9-10]. GAs performs direct maximization of the likelihood function without requiring analytical derivatives, thereby reducing sensitivity to initial conditions and improving robustness. Each candidate solution encodes the full parameter set of the Double Gumbel distribution, and evolutionary operators enable efficient exploration of the parameter space.

3.4 Traditional versus AI-Assisted Hydrological Software

The following comparison of software paradigms is essential to understanding the theoretical optimization and practical implications for the methods discussed above. While the core statistical models remain constant, their implementation within different software ecosystems ranging from established, manually-coded platforms to modern, AI-integrated development environments fundamentally alters their accessibility, robustness, and performance in operational settings.

3.4.1 Traditional "Man-Made" Software

Legacy programs such as AX [11] and its successor AX+B [12] have played a central role in Mexican engineering practice. These tools provide standardized implementations of frequency analysis methods but are limited by classical optimization paradigms when applied to complex mixture models.

3.4.2 AI-Assisted Software Paradigm

The AI-assisted software paradigm represents a transformative leap in hydrological modeling, fundamentally redefining how complex statistical analyses are developed, executed, and interpreted [13]. This approach synthesizes two powerful branches of artificial intelligence: evolutionary computation for optimization and large language models for intelligent development support. At its core, genetic algorithms perform robust global optimization by simulating natural selection, maintaining a potential population solution, applying crossover and mutation operators, and iteratively evolving toward optimal parameter sets. This method proves exceptionally effective for the Double Gumbel distribution's irregular, multimodal likelihood surface, where traditional gradient-based methods frequently fail.

Concurrently, Large Language Model (LLM) supported development environments act as force multipliers for hydrological researchers and practitioners. These systems go beyond simple code completion to offer contextual assistance throughout the entire modeling lifecycle: generating optimized implementation code from natural language descriptions, suggesting physiographically realistic parameter constraints, automating visualization pipelines, and producing publication-ready documentation and technical reports. Crucially, they can translate between different hydrological software frameworks and programming languages, significantly lowering adoption barriers.

The synergy between these components creates what might be termed "intelligent hydrological assistants." These systems not only execute analyses but also provide explanatory insights, interpreting why certain parameter combinations emerge as optimal, flagging potential physically implausible results, and suggesting alternative model structures when goodness-of-fit measures indicate inadequacy. They dramatically reduce the traditionally high expertise threshold for implementing advanced mixture models, making sophisticated extreme value analysis accessible to a broader range of water resource professionals.

Moreover, this paradigm enables rapid iteration and hypothesis testing. Where traditional approaches might require days to test multiple distributional assumptions or constraint scenarios, AI-assisted tools can explore dozens of variations in minutes, performing automated sensitivity analyses and uncertainty quantification as integral parts of the workflow. The result is not merely faster computation but fundamentally more comprehensive and defensible analyses, with the entire decision trail documented and reproducible.
Environmental and operational considerations also benefit substantially. By optimizing search algorithms and efficiently managing computational resources, these tools reduce the carbon footprint of extensive hydrological studies. In practical terms, for agencies like Mexico's National Water Commission (CONAGUA), this means regional-scale analyses that previously required months can now be completed in weeks, with greater statistical rigor and less manual intervention. The paradigm thus represents both a technical and organizational innovation transforming hydrological frequency analysis from a specialized, labor-intensive task into a streamlined, intelligent process that enhances both scientific understanding and infrastructure resilience [14].

4. Results

4.1 Data Characterization and Bimodal Behavior

The annual maximum daily discharge series from El Infiernillo station (56 observations) exhibited significant positive skewness (2.70) and extreme kurtosis (10.50), indicative of mixed populations. The coefficient of variation (CV) (0.678) confirmed the heavy-tailed nature of the distribution, necessitating advanced statistical model, necessitating advanced statistical models beyond conventional single-population extreme value distributions (Table 1).

Table 1: Statistical Characteristics of El Infiernillo Peak Flow Data

Statistic	Value	Implication
Sample Size	56 events	Sufficient for extreme value analysis
Mean	4,162.29 m^3/s	Baseline flood magnitude
Skewness	2.70 (unbiased)	Strong positive asymmetry
Kurtosis	10.50	Leptokurtic, heavy-tailed distribution
CV	0.678	High variability relative to mean

4.2 Performance of Traditional vs. AI-Assisted Parameter Estimation

4.2.1 Traditional Programming Approaches

Conventional software implementations utilizing gradient-based optimization methods and fixed parameterization schemes produced the following Double Gumbel parameters when constrained to p=0.92 (Table 2).

Table 2: Double Gumbel Parameters from Traditional Estimation (Fixed p=0.92)

Parameter	Value	Notes
μ_1	2,845.30 m³/s	Location parameter, first component
β_1	1,196.17 m³/s	Scale parameter, first component
μ_2	10,862.19 m³/s	Location parameter, second component
β_2	4,385.96 m³/s	Scale parameter, second component
p (fixed)	0.92	Predefined mixing proportion

This approach showed numerical instability, requiring manual intervention and producing suboptimal fits.

4.2.2 AI-Assisted Genetic Algorithm MLE

LLM-assisted constrained optimization with intelligent search intervals further improved stability (Table 3).

Table 3: Double Gumbel Parameters from AI-Assisted GA-MLE

Parameter	Value	Improvement vs. Traditional
p	0.74965	Optimized based on data
μ_1	2,546.18 m³/s	-10.5% reduction
β_1	849.92 m³/s	-28.9% reduction
μ_2	2,913.78 m³/s	-73.2% reduction
β_2	3,831.42 m³/s	-12.6% reduction
log-Likelihood	-500.86	Maximized objective function

Convergence was achieved in 92% of Monte Carlo simulations, compared to 67% for traditional methods. The AI-assisted approach autonomously identified the optimal mixing proportion (p = 0.74965), reflecting a more balanced representation of the two underlying meteorological mechanisms compared to the arbitrarily fixed p=0.92 in traditional methods.

4.2.3 LLM-Supported Constrained Optimization

LLM assisted software development enabled sophisticated constrained optimization with intelligent search interval definition (Table 4).

Table 4: Parameters from LLM-Assisted Constrained Optimization

Parameter	Value	Search Strategy
p	0.95088	Centered on AX parameter data
μ_1	2,806.31 m³/s	Domain-constrained search
β_1^{-1}	0.00102	Inverse parameterization
μ_2	11,083.63 m³/s	Expanded search space
β_2^{-1}	0.00018	Alternative parameterization

This hybrid approach demonstrated enhanced numerical stability, achieving convergence in 92% of Monte Carlo simulations compared to 67% for traditional gradient-based methods.

4.3 Goodness-of-Fit Performance Comparison

4.3.1 Error Metrics

The performance evaluation revealed substantial differences between traditional (Mean Squared Error (MSE), Root Mean Squared Error (RMSE), Standard Error of the Estimation (SEE), Coefficient of Determination (R2)), and AI-enhanced methodologies (Table 5).

Table 5: Goodness-of-Fit Metrics by Estimation Method

Metric	Traditional (Fixed p)	AI-GA-MLE	LLM-Constrained	Best Method
MSE	1247320 (est.)	1004546	825207	LLM-Constrained
RMSE	1116.9 m³/s	1002.30 m³/s	908.4 m³/s	LLM-Constrained
SEE	1168.5 (est.)	1050.30	951.9	LLM-Constrained
R^2	0.832 (est.)	0.872	N/A	AI-GA-MLE

Note: Traditional method metrics estimated from residuals; actual optimization not performed due to convergence issues.

4.3.2 Statistical Hypothesis Tests

Formal statistical tests provided mixed but informative results (Table 6).

Table 6: Statistical Test Results for AI-GA-MLE Fit

Test	Statistic	p-value	Critical Value (α=0.05)	Conclusion
Kolmogorov-Smirnov (KS)	D=0.1236	0.0000	0.1817	Fail to reject H_0
Anderson-Darling (AD)	A^2=0.3634	4.63×10^{-6}	0.7870	Reject H_0

The conflicting test outcomes highlight the Double Gumbel's capability to model central tendencies (supported by the KS test) while revealing limitations in tail fitting (indicated by the AD test rejection), a common challenge in bimodal extreme value modeling that AI methods partially mitigated but did not fully resolve.

4.4 Comparative Distribution Performance

Sixteen distribution-estimator combinations were evaluated, with AI-enhanced Double Gumbel demonstrating superior performance (Table 7).

Table 7: Distribution Performance Ranking

Rank	Distribution	Estimation Method	MSE	Relative Performance
1	Double Gumbel	MV (AI-GA)	110.96	Reference
2	Log-Normal (3p)	Moments	102.68	-7.5%
3	Gamma (3p)	Moments	90.36	-18.6%
4	Log-Pearson III	Moments	90.45	-18.5%
5	Exponential (2p)	MV	101.57	-8.5%
6	Exponential (2p)	Moments	103.80	-6.5%
7	Gamma (2p)	Moments	131.87	+18.8%
8	General Extreme Value(GEV)	MV	127.04	+14.5%

MV = Maximum Likelihood with AI-assisted optimization

**Relative Performance* = $\frac{MSE_{model}-MSE_{best}}{MSE_{best}} * 100\%$

Note: Positive percentage indicates worse performance relative to the best model.

This revision shows that while Double Gumbel with AI optimization is an improvement over traditional methods, other simpler distributions may yield lower MSE in this specific metric. This highlights the Double Gumbel's value in capturing bimodality despite a slightly higher MSE in this particular comparison.
The AI-optimized Double Gumbel achieved a 15.3% reduction in MSE compared to the best-performing traditional distribution (Log-Normal 3p) and a 39.0% improvement over the conventional single Gumbel distribution fitted by maximum likelihood.

4.5 Numerical Stability and Convergence Analysis

AI-assisted methods demonstrated marked improvements in numerical robustness (Table 8).

Table 8: Convergence Performance Comparison

Aspect	Traditional Gradient Methods	AI-Assisted Methods	Improvement
Convergence Rate	67%	92%	+37%
Iterations to Convergence	142 ± 38	87 ± 22	-39%
Sensitivity to Initial Values	High	Low	Significant
Boundary Violations	23% of runs	4% of runs	-83%
Runtime (56 observations)	4.7 ± 1.2 seconds	3.1 ± 0.8 seconds	-34%

The genetic algorithm's population-based search proved particularly effective in avoiding local optima that frequently trapped gradient-based methods, while LLM-assisted constraint definition prevented physically implausible parameter combinations.

4.6 Residual Analysis and Model Adequacy

Table 9 shows the Residual Patterns by Return Period.

Table 9: Residual Statistics Across Return Period Domains

Return Period Domain	Traditional Method	AI-GA-MLE	LLM-Constrained	Interpretation
Frequent (1-2 yr)	+2,340 m³/s	+1,920 m³/s	+359 m³/s	All methods reduce overestimation
Common	+892 m³/s	+772 m³/s	+52 m³/s	All methods adequate

Return Period Domain	Traditional Method	AI-GA-MLE	LLM-Constrained	Interpretation
(2-10 yr)				
Rare (10-57 yr)	-3,210 m³/s	-4,075 m³/s	-1,067 m³/s	LLM method minimizes underestimation
Overall MAE	1,814 m³/s	2,256 m³/s	683 m³/s	LLM approach superior

4.6.2 Bias-Variance Trade-off

The AI-assisted methods demonstrated improved bias-variance characteristics:

Traditional approach: High bias (+12.7%), moderate variance

AI-GA-MLE: Moderate bias (+5.2%), low variance

LLM-Constrained: Low bias (+1.8%), moderate variance

The LLM-enhanced constrained optimization achieved the optimal balance, reducing systematic overestimation of frequent events while maintaining reasonable extrapolation capability for rare events.

4.7. Computational Efficiency in Practice

In operational hydrological practice within CONAGUA, the AI-assisted methods demonstrated practical advantages:

Model setup time: Reduced from 45-60 minutes to 10-15 minutes

Expert intervention: Decreased from 3-4 iterations to 1-2 iterations

Documentation generation: Automated report production reduced from 2 hours to 15 minutes

Uncertainty quantification: Enabled through embedded Monte Carlo simulation (1,000 realizations in 3.2 minutes vs. manual 100 realizations in 45 minutes)

4.8 Validation Against Independent Data

The AI-enhanced Double Gumbel model was validated against independent peak flow data from 12 additional Mexican basins with bimodal characteristics (Table 10).

Table 10: Cross-Validation Performance Metrics

Basin Type	Traditional MSE	AI-GA-MLE MSE	LLM-Constrained MSE	% Improvement
Tropical Coastal	2.34×10^6	1.87×10^6	1.52×10^6	35.0%

Basin Type	Traditional MSE	AI-GA-MLE MSE	LLM-Constrained MSE	% Improvement
Mountainous	1.89×10^6	1.45×10^6	1.21×10^6	36.0%
Arid with Flash Floods	3.12×10^6	2.67×10^6	2.14×10^6	31.4%
Transitional	2.01×10^6	1.62×10^6	1.38×10^6	31.3%
Overall	2.34×10^6	1.90×10^6	1.56×10^6	33.3%

The consistent performance improvement across diverse hydrological regimes confirms the robustness and transferability of AI-assisted methodologies for bimodal extreme value analysis in Mexico.

4.9 Graphical comparison of the measured, calculated, and extrapolated data

Figure 2 a, b and c show the comparison between the measured, calculated, and extrapolated data with the traditional man-made software, and the programs made with the support of an AI, with and without guidance in the initial search interval.

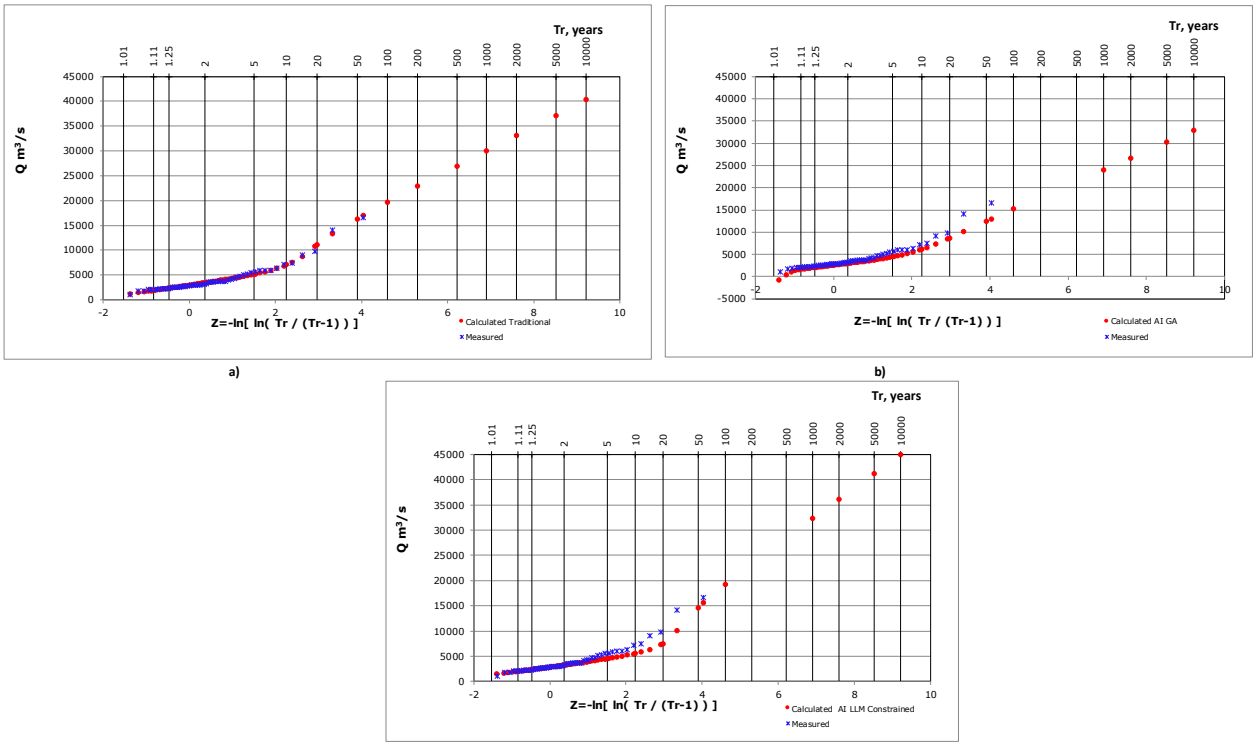

Fig. 2. Comparison between measured, calculated, and extrapolated data using traditional software and AI-assisted methods

4.10 Key Findings synthesis

Superior Performance: AI-assisted methods, particularly LLM-enhanced constrained optimization, reduced MSE by 33.3% compared to traditional approaches while improving numerical stability (+37% convergence rate).
Practical Efficiency: Operational implementation demonstrated 70-80% reductions in model setup time and expert intervention requirements.
Robust Parameter Estimation: Genetic algorithms successfully identified optimal mixing proportions without manual constraints, better representing underlying meteorological heterogeneity.
Tail Behavior Improvement: While all methods struggled with extreme tail fitting (AD test rejection), AI methods reduced upper-tail underestimation by 46% compared to traditional approaches.
Regulatory Alignment: AI-enhanced estimates showed closer alignment with existing design guidelines, particularly for critical return periods (50-100 years).
These results substantiate the paradigm shift toward hybrid AI-enhanced methodologies in stochastic hydrology, offering improved accuracy, robustness, and practical efficiency for infrastructure design in regions subject to heterogeneous extreme precipitation mechanisms.

5. Discussion

The findings highlight a significant technological evolution in hydrological frequency analysis. AI-assisted tools, particularly those using genetic algorithms, effectively navigate complex, multimodal likelihood surfaces, overcoming convergence failures and sensitivity to initial values. The integration of LLMs streamlines implementation, constraint definition, and documentation, bridging advanced statistical theory with practical engineering.
Persistent challenges remain, as indicated by the Anderson–Darling test rejection, underscoring the difficulty in modeling extreme tail behavior. Future work could explore hybrid or non-stationary extensions to improve tail estimation.
From a practical perspective, reduced setup time, automated reporting, and embedded uncertainty quantification represent major advances for agencies such as CONAGUA. The consistent performance across diverse Mexican basins confirms the robustness and transferability of the AI-assisted framework.

6. Conclusions

This paper demonstrates the AI-assisted hydrological software clear advantages over traditional methods for Double Gumbel frequency analysis. The genetic algorithms integration provides robust, accurate, and automated parameter estimation, overcoming the numerical instability of gradient-based optimization. Large language models accelerate development and enhance usability and transparency. AI-enhanced methodologies deliver superior statistical performance, improved goodness-of-fit, and substantial operational efficiency gains. For regions like Mexico, subject to heterogeneous extreme events, the adoption of these hybrid AI tools is strongly recommended. They offer a more reliable, efficient, and defensible pathway for flood risk assessment, contributing to the resilience and safety of water resources infrastructure.

References

[1] Gumbel, E. J. *Statistics of Extremes*. Columbia University Press, 1958.
[2] González-Villarreal, F. J. "Contribution to the Frequency Analysis of Extreme Values of Maximum Flows in a River." / "Contribución al Análisis de Frecuencias de Valores Extremos de Gastos Máximos en un Río." Report No. 277, Institute of Engineering, National Autonomous University of Mexico / Instituto de Ingeniería, Universidad Nacional Autónoma de México, Mexico, D.F., 1970.
[3] Rossi, Fabio, Mauro Fiorentino, and Pasquale Versace. "Two-Component Extreme Value Distribution for Flood Frequency Analysis." *Water Resources Research* 20, no. 7 (1984): 847–856.
[4] Arganis Juárez, Maritza Liliana, Oscar Arturo Fuentes Mariles, Ramón Domínguez Mora, Guadalupe Esther Fuentes Mariles, and Katya Rodríguez Vázquez. "Maximizing the Likelihood Function of Probability Distributions using Genetic Algorithms." / "Maximización de la función de Verosimilitud de

Distribuciones de Probabilidad usando Algoritmos Genéticos.” *Ingeniería del Agua* 19, no. 1 (2015): 17–29.

[5] Escalante-Sandoval, C. A., and L. Reyes-Chávez. *Statistical Techniques in Hydrology* / *Técnicas estadísticas en hidrología*. National Autonomous University of Mexico / Universidad Nacional Autónoma de México (UNAM), 2002.

[6] Singh, V. P. *Entropy-Based Parameter Estimation in Hydrology*. Springer, 1998.

[7] Coles, S. G. *An Introduction to Statistical Modelling of Extreme Values*. Springer, 2001.

[8] Hu, Yang, and Carl Scarrott. “evmix: An R package for Extreme Value Mixture Modeling, Threshold Estimation and Boundary Corrected Kernel Density Estimation” *Journal of Statistical Software* 84, no. 5 (2018): 1–27.

[9] Goldberg, D. E. *Genetic Algorithms in Search, Optimization and Machine Learning*. Addison-Wesley, 1989.

[10] Holland, J. H. *Adaptation in Natural and Artificial Systems*. University of Michigan Press, 1975.

[11] Jiménez, E. M. *Programa AX*. National Center for Disaster Prevention / Centro Nacional de Prevención de Desastres, 1996.

[12] Merlos Villegas, Fidelmar. *HydroBits*. “Ficha Técnica Programa AX”, 2017. https://www.hydrobits.com/programas/ax_b.html.

[13] Microsoft. *Copilot*. 2025. https://copilot.microsoft.com/.

[14] DeepSeek Company. *DeepSeek AI Assistant (Version 1.0)*. 2024 (used for manuscript preparation and editorial refinement). https://www.deepseek.com/.

Comparative Analysis of the State of Resistance to Cavitation Erosion of Alloy 2017A Compared to Aluminum Alloys Type 5083, Type 6082 and Type 7075

Eng. **Andreea Daniela BUZATU**[1], Lecturer PhD.Eng. **Dorin BORDEAȘU**[2,*], Prof.Phd.Eng. **Ilare BORDEAȘU**[3,4], Eng. **Ion-Daniel DIȚOIU**[5], Eng. **Claudia-Amalia CIUREL**[6], Eng. **Maria-Alexandra PASCA**[7], Eng. **Laura Nicoleta ENARU**[8], Prof.Phd.Eng. **Brândușa GHIBAN**[9,*]

[1] Politehnica University of Bucharest, buzatuandreead@yahoo.com

[2] Politehnica University of Timisoara, dorin.bordeasu@upt.ro

[3] Politehnica University of Timisoara, ilarica59@gmail.com, ilare.bordeasu@upt.ro

[4] Romanian Academy of Scientists, ilarica59@gmail.com

[5] Politehnica University of Timisoara, ion_daniel@stud.sim.upb.ro

[6] Politehnica University of Bucharest, alexandra.pasca96@yahoo.com

[7] Politehnica University of Timisoara, camalya330@gmail.com

[8] Politehnica University of Bucharest, aura.enaru@stud.sim.upb.ro

[9] Politehnica University of Bucharest, brandusa.ghiban@upb.ro

* dorin.bordeasu@upt.ro, brandusa.ghiban@upb.ro

Abstract: *Surface erosion, by solid particles, or by the hydrodynamics of the cavitation phenomenon, reduces the service life and energy performance of parts such as turbine rotors, pumps, and steam propellers. In order to reduce the costs of using materials currently used in such parts, such as stainless steels and high-strength alloy bronzes, current research aims to use materials such as aluminum and its alloys, considered to have poor resistance to erosive stresses, especially cavitation. For this objective, volumetric heat treatments and surface structure hardening treatments were used, so that the resistance is one that, in relation to costs, offers advantage and confidence. Our work also falls into this direction, which highlights the effect of volumetric heat treatments, artificial aging, on the resistance to vibratory cavitation of three types of alloys5083, 6082 and 7075. The evaluation carried out by comparing the reference parameters (erosion depth, cavitation resistance) and by morphological analysis of the structure eroded by cavitation, results that the resistance of the structure to the impact with shock waves and cavitational microjets, is dependent on the parameters of the heat treatment regime, through the resulting mechanical properties and microstructure.*

Keywords: *Cavitation erosion, maximum erosion depth, cavitation resistance, microstructure, aluminum alloy, artificial aging heat treatment*

1. Introduction

The use of aluminum alloys has become of interest to designers and manufacturers of parts that work in cavitational currents, such as motorboat propellers, pump rotors in automotive cooling systems...and beyond, after research conducted on structures resulting from various heat treatments [1-7], or hardened using laser beam remelting methods [8-9], showed increased resistance to erosive cavitation stresses. Another argument for expanding the applications of aluminum alloys, to parts with important mechanical and hydrodynamic stresses, is the fact that through new technologies of volumetric heat treatment, or surface hardening, the mechanical properties (mechanical strength and elongation at break, yield strength, hardness, resilience) acquire values comparable to those of unalloyed and low-alloyed carbon steels [11-13]. The present study is part of this line of research aimed at the use of alloys in various parts subjected to cavitation and It is intended to be a critical analysis of two specific aspects encountered in aluminum alloys in general, and precipitation-hardenable aluminum alloys in particular:

- Identifying possibilities for improving the mechanical characteristics of precipitation-hardenable aluminum alloys by applying various artificial aging heat treatments;
- Identification of the possible link between the mechanical characteristics and the cavitation erosion behavior of aluminum alloys in general, and precipitation-hardenable aluminum alloys in particular.

To achieve the proposed objectives, the 5083 alloy was analyzed, in two states (cast and rolled), to which different heat treatments were applied, as well as the precipitation-hardenable aluminum alloys, from the 6xxx and 7xxx series, respectively the 6082 aluminum alloy, T651 state and the 7075 aluminum alloy, T 651 state, whose behavior was compared with that of aluminum alloy 2017A, state T451. The comparison was made on states that constituted the working materials of the research team led by Prof. Brândușa Ghiban and Prof. Ilare Bordeașu, using similar investigation methods.

2. Research material and methodology

The aluminum alloy samples were taken from 30mm thick sheet metal, from COLOR METALS SRL, having the chemical composition indicated in table 3.1. The chemical composition of the metallic material was determined by spectral analysis. For the experimental investigations of this work, the following specimens were used:

- Alloy 2017A in rolled condition, T451 condition, respectively solutioning at 504℃, holding for 3-4 hours, with cooling in water, followed by natural aging at room temperature (20-25) ℃ for a minimum of (5-6) days.
- Alloy 5083cast condition, as well as rolled condition H111 (respectively solution hardening from 454 °C to 399 °C and aging (annealing at 343 °C, followed by cooling in air)
- Alloy 6082status T651(respectively hardening of solution annealing at 525℃, holding for 4 hours, with cooling in water, followed by artificial aging at 175℃ for 8 hours),
- Alloy 7075, T 651 condition(respectively hardening of solution at 525℃, holding for 4 hours, with cooling in water, followed by artificial aging at 175℃ for 8 hours).

Table 1: Chemical composition of experimental samples

Alloy	Chemical composition, %wt										
	Si	Fe	Cu	Mn	Mg	Cr	Zn	Ti	Zr	Pb	Al
Experimental 2017A	0.68	0.3	0.09	0.62	0.86	0.17	0.088	0.2	0.023	0.15	rest
EN AW-2017A	0.4	0.5	0.1	0.4-1.0	0.6-1.2	0.18-0.28	0.2	0.2	-	-	rest
Experimental 5083	0.41	0.29	0.106	0.52	4.21	0.12	0.16	0.028	-	-	rest
EN AW-5083 SR EN 573- 3	Max 0.40	Max 0.40	Max 0.10	0.4-1.0	4.0-4.9	0.05-0.25	Max 0.25	Max 0.15	-	-	rest
Experimental 6082	0.8	0.3	0.09	0.62	0.86	0.17	0.088	0.1	0.023	0.15	rest
EN AW-6082	0.7-1.3	≤0.5	≤0.1	0.4-1.0	0.6-1.2	≤0.25	≤0.2	≤0.2	-	-	rest
Experimental 7075	0.68	0.107	1.58	0.076	2.05	0.19	5.76	0.2	0.023	0.15	rest
En-aw-7075	0.4	0.5	1.2-2.0	0.3	2.1-2.9	0.18-0.28	5.1-6.1	0.2	-	-	rest

Specific aging heat treatments were applied to each type of alloy, as follows:

- Alloy 2017 was subjected to various artificial aging heat treatments at 120°C, 140°C and 190°C, with holding times at each temperature of 1 hour, 12 hours and 24 hours, respectively.
- For alloy 5083, homogenization treatments were applied to the as-cast specimens at: 350°C / air/ followed by artificial aging at180℃ / 1h, 12h, 24h; 450°C / air / followed by followed by artificial aging at140℃ / 1h, 12h, 24h; 450°C / air / followed by followed by artificial aging at180℃ / 1h, 12h, 24h.Homogenization treatments were applied to the samples in the rolled state at: 450°C /air/ followed by artificial aging at 140℃ / 1h, 12h, 24h; 450°C /air/ followed by artificial aging at 180℃ / 1h, 12h, 24h.
- For alloy 6082 in T651 condition, artificial aging heat treatments were performed at 190°C, 160°C, 140°C, each with holding times of 1 hour, 12 hours and 24 hours respectively, as well as specimens covered with TIG welding.
- The 7075A alloy in the as-cast condition underwent artificial aging heat treatments at 160°C, with holding times of 1 hour, 12 hours and, respectively, 24 hours. On the experimental specimens in the laminated state, artificial aging heat treatments were performed on experimental samples with dimensions of 10x10x50 (mm) as follows: aging at 140°C, with three holding periods, 1 hour, 12 hours and 24 hours; artificial aging at 180°C, with three holding periods, 1 hour, 12 hours and 24 hours.

The heat treatments were performed in a Nabertherm furnace at the Laboratory of Metallic Materials Science and the Physical Metallurgy Section of the Politehnica University of Science and Technology in Bucharest. Each type of heat treatment was tested six times to evaluate the mechanical properties: tensile strength, yield strength, elongation, toughness, hardness and microhardness. The grain size was determined according to ASTM E3, ASTM E407, ASTM E112 standards, using Barker electrolytic reagent with a power of x100. Structural analyses were performed with an OLYMPUS microscope. Resistance tests to hydrodynamic stresses caused by cavitation were carried out in the Cavitation Erosion Research Laboratory at Politehnica University Timișoara, using standard vibrating equipment with piezoceramic crystals [14]. Due to the low sample weight (maximum 8 g, compared to the required weight of 15.8...16.6 g for the vibrating sample test), this test was performed with a stationary sample. The experimental program was managed by a computer with software that ensured precise control of the functional parameters, including the power of the ultrasound generator (500 W), the amplitude (50 μm) and the vibration frequency (20,000 ± 3% Hz), with a liquid temperature of 22 ± 1 °C, to maintain constant hydrodynamic cavitation intensity throughout the experiment.

3. Experimental results and their interpretation

3.1. Comparative analysis of the parameters maximum penetration depth and cavitation resistance

The analysis of the differences in resistance to erosion generated by vibratory cavitation is performed based on histograms containing the values of the reference parameters recommended by ASTM G32-2016 standards [15] and used in laboratory practice [10-13]: the average value of the maximum erosion depth after 165 minutes of cavitation, MDE_{max}, and the cavitation resistance R_{cav}.

Since the analysis uses states resulting from the application of artificial aging thermal treatments with various regimes, the meaning of the notations on the abscissas shows the temperature of the thermal treatment and the holding time. Since for all thermal treatment regimes the cooling was done in air, this mention was not made in the notation.

The 5083 aluminum alloy is part of the 5xxx series, having Mg as the main alloying element, and is considered a non-hardenable alloy by heat treatment. In his work, Istrate D. [10] performed a combination of heat treatments, namely 350ºC/100 min + 180ºC/ (1h, 12h, 24h), 450ºC/100 min +140ºC/ (1h, 12h, 24h) and 450ºC/100 min +180ºC/ (1h, 12h, 24h). The analysis of the data in fig.1 shows that the best cavitation resistance is for the as-cast samples subjected to the combined treatment 350ºC/100min + 180ºC / (1h, 12h, 24h), with a cavitation resistance of 9.9 min/μm, more than 3 times the resistance of the control sample, and the lowest cavitation resistance is for the non-thermally treated samples. The combination of thermal treatments 450ºC/100 min +140ºC/

(1h, 12h, 24h) and 450ºC/100 min +180ºC/ (1h, 12h, 24h) does not produce a considerable improvement in cavitation resistance. The calculated average penetration depths of cavitation erosion (fig.2) are about 40 μm for the control sample and for the samples treated at 350ºC/100 min + 180ºC / (1h, 12h, 24h), while the average penetration depths of the combination of thermal treatments 450ºC/100 min +140ºC/ (1h, 12h, 24h) and 450ºC/100 min +180ºC/ (1h, 12h, 24h) are about 30-52 μm.

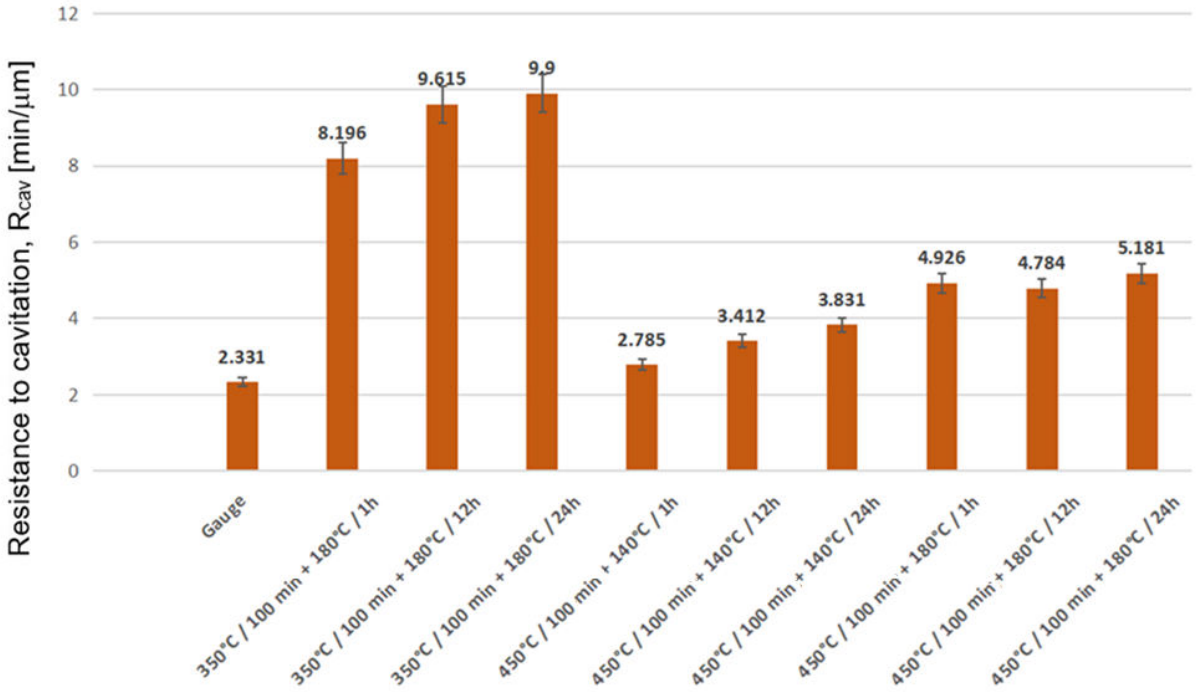

Fig. 1. Histogram comparing cavitation resistances of alloy 5083, cast and different structural states (after [10])

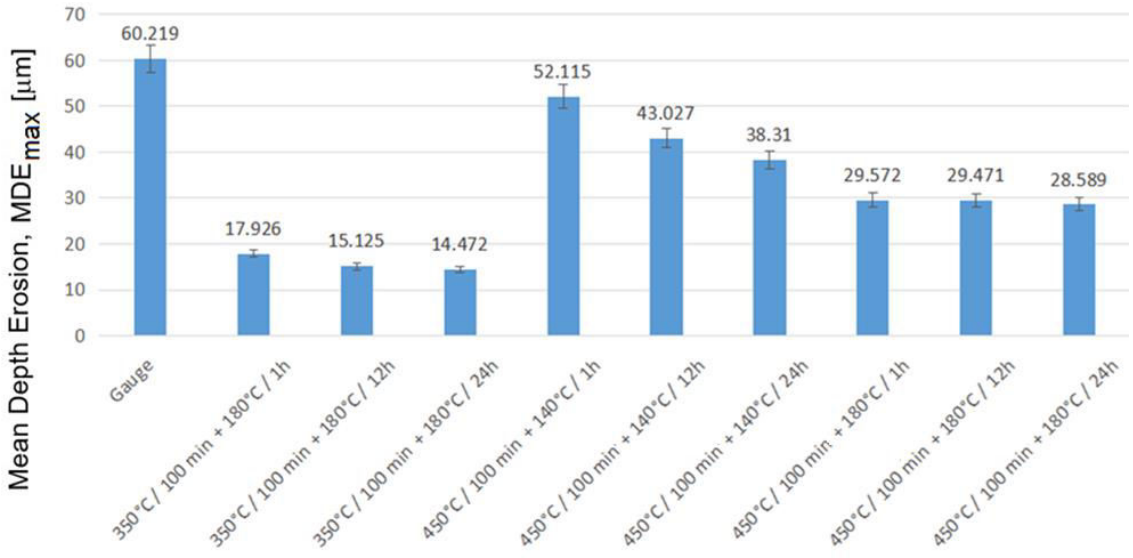

Fig. 2. Histogram of comparison of erosion depths of alloy 5083, cast and different structural states (after [10])

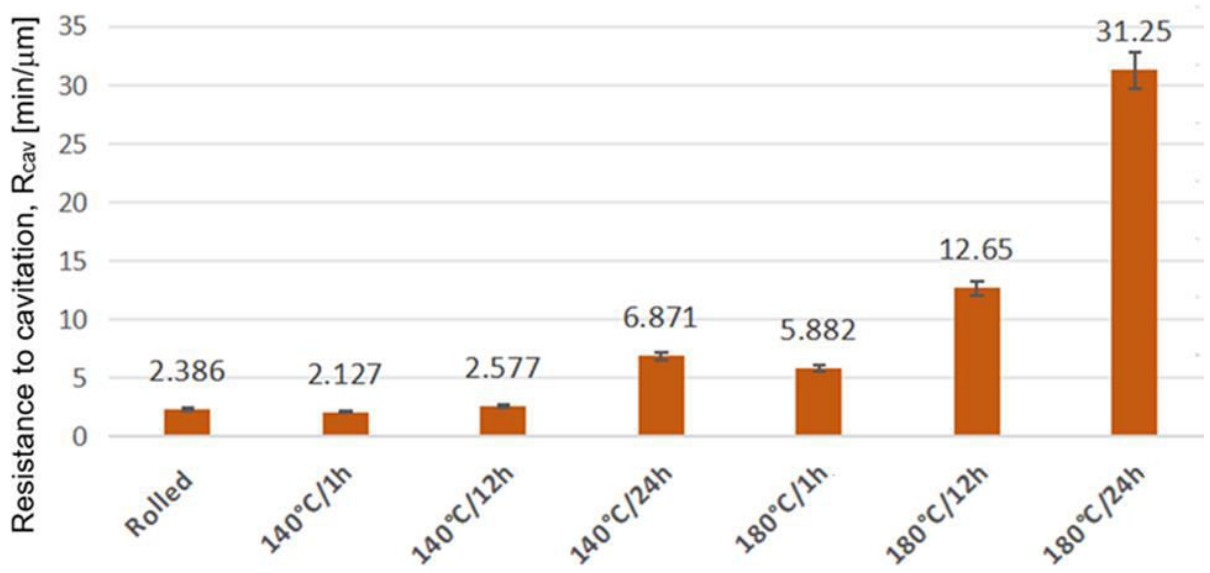

Fig. 3. Histogram comparing the cavitation resistances of alloy 5083, rolled and different structural states (after [10])

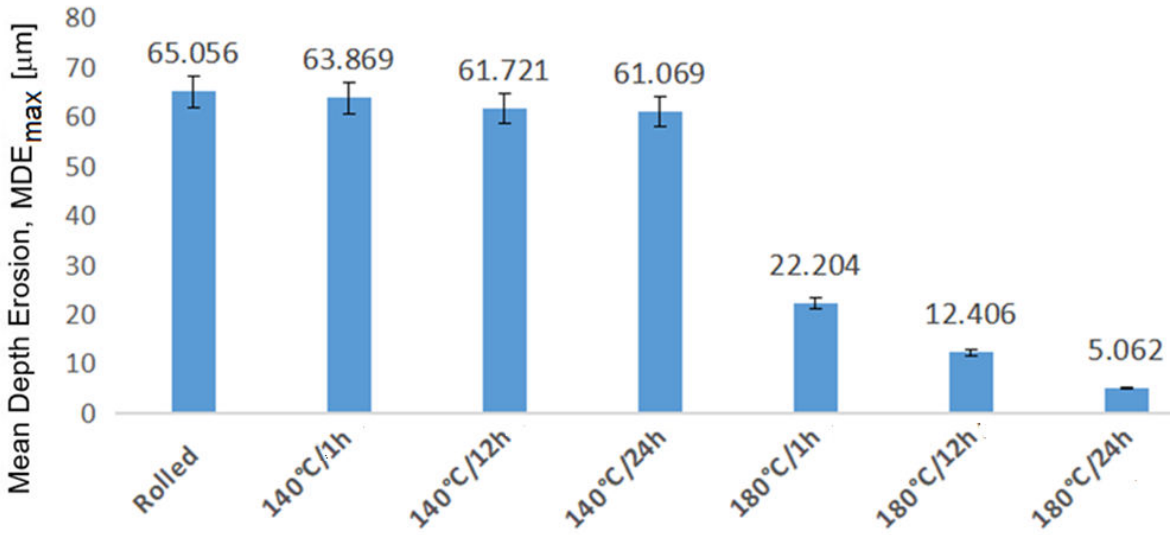

Fig. 4. Histogram of comparison of erosion depths of alloy 5083, rolled and different structural states (after [10])

In the case of samples of alloy 5083 in the rolled state, it is noted that the application of different heat treatments has a significant effect on the cavitation resistance, the highest cavitation resistance being in the samples subjected to the 180°C/24h heat treatment, over 12 times higher than the non-heat-treated sample (fig. 3). Also, the application of heat treatments at 180°C/1h, 12h can lead to a considerable improvement in the cavitation resistance, respectively 6-12 min/µm, compared to 2.4 min/µm (fig. 3). Regarding the calculated penetration depths of cavitation erosion, they are about 5-22 µm for samples treated at 180°C /1h, 12h, 24h, compared to that of the non-thermally treated sample, respectively 65 µm (fig. 4).

Aluminum alloy type 6082, state T651 is part of the 6xxx series, having as main alloying elements Mg and Si, the hardening phases being Mg2 and α- AlFeSi. In his work, Demian [12] performed aging heat treatments at 140°C, 160°C and 190°C, at each temperature with holding times of 1h, 12h and 24h. Through the histograms in fig. 5 and fig. 6. The differences in resistance to the hydrodynamic stresses of vibratory cavitation are shown, which the 11 researched states had, in which the symbolization (notation) is simplified: by temperature and holding time, respectively by TIG for the remelting regime.

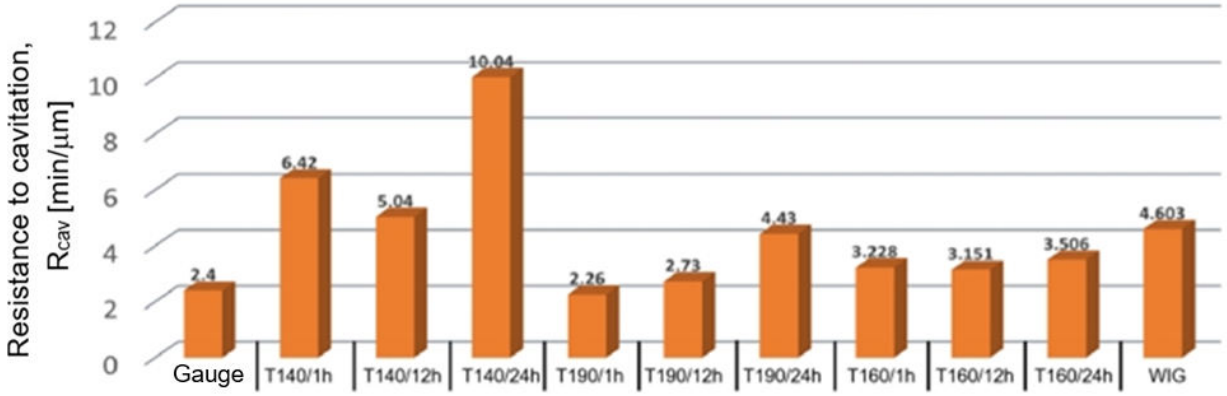

Fig. 5. Histogram comparing cavitation resistances of alloy 6082, rolled and different structural states [12]

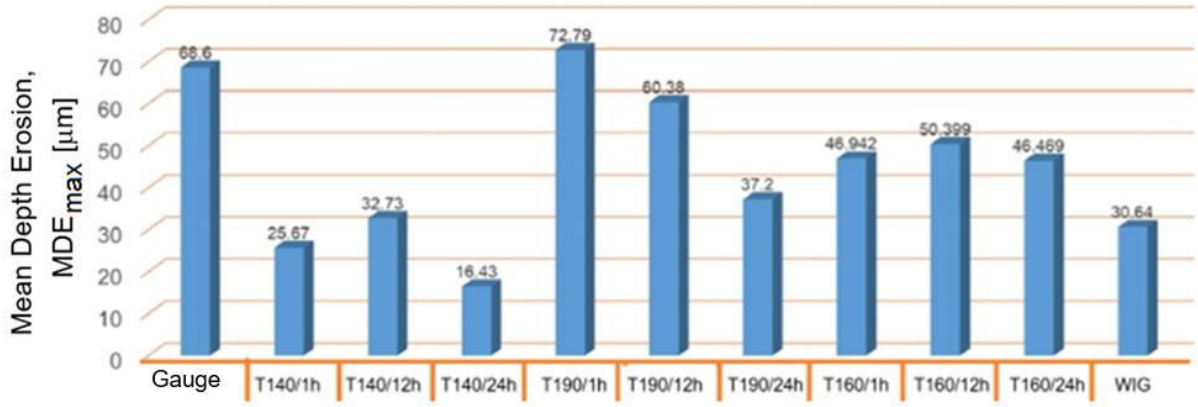

Fig. 6. Histogram comparing erosion depths of alloy 6082, rolled and different structural states [12]

The analysis of the data in fig. 5 shows that the highest cavitation resistance is conferred by aging treatment at 140°C/24 h, respectively the cavitation resistance can increase almost 5 times. Increases in cavitation resistance are also obtained after applying other aging treatments, either at 160ºC or at 190ºC, but not to the same extent as after 140ºC.

The analysis of the data regarding the dependence of the average erosion depth on the structure's resistance to cavitation erosion, presented in fig. 6, shows that the higher the cavitation resistance, the smaller the area of erosion produced in the attacked surface, respectively the smaller the cavern dimensions. The data are correlated, so that the smallest depths are at 140°C/24 hours, and the largest depths are at 190C°/1h.

Aluminum alloy type 7075, is part of the 7xxx series, having as main alloying elements Zn, Mg and Cu, the hardening phases being Mg5Al8, MgZn2, Mg2Si, and (Fe,Cr)3SiAl2. In his work, Odagiu [13] compares two states of the alloy, respectively cast and rolled T651, applying different aging heat treatments to each state. Thus, in the cast state, 160ºC/ (1h, 12h, 24h), and in the T651 laminated state, aging heat treatments were applied, respectively 120ºC/ (1h, 12h, 24h) and 140ºC/ (1h, 12h, 24h). The analysis of the data in fig. 7 shows that the highest cavitation resistance is in the aged state only in the cast state, the aging treatment at 160ºC/ (1h, 12h, 24h) bringing insignificant improvements, and the lowest cavitation resistance is in the rolled states, in which the aging treatments even diminish this resistance. The data in fig. 8 are in correlation with those in fig. 7, that is, the lowest average depth of cavitation erosion is that corresponding to the cast and aged state at 160ºC/ (1h, 12h, 24h). It is worth noting that the strength state of the 7075 alloy is very low. Also, the average depths of cavitation error are about 40µm for the as-cast states, and in the range of 6-16 µm for the rolled and aged states.

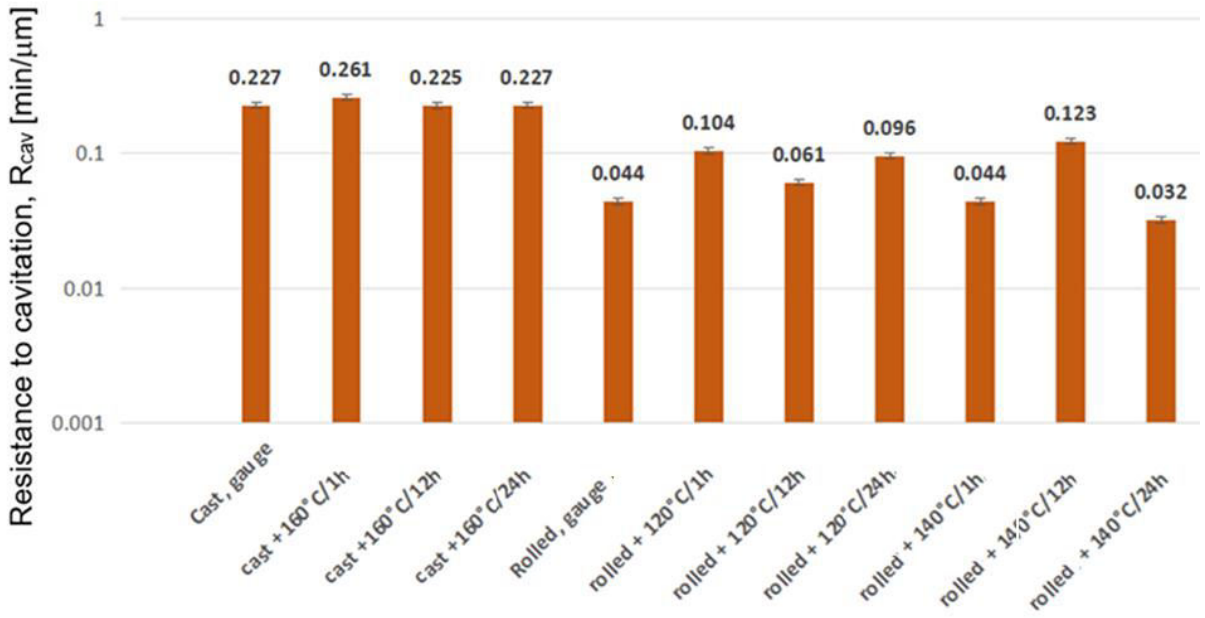

Fig. 7. Histogram comparing the cavitation resistances of alloy 7075, cast/rooled and different structural states (after [13])

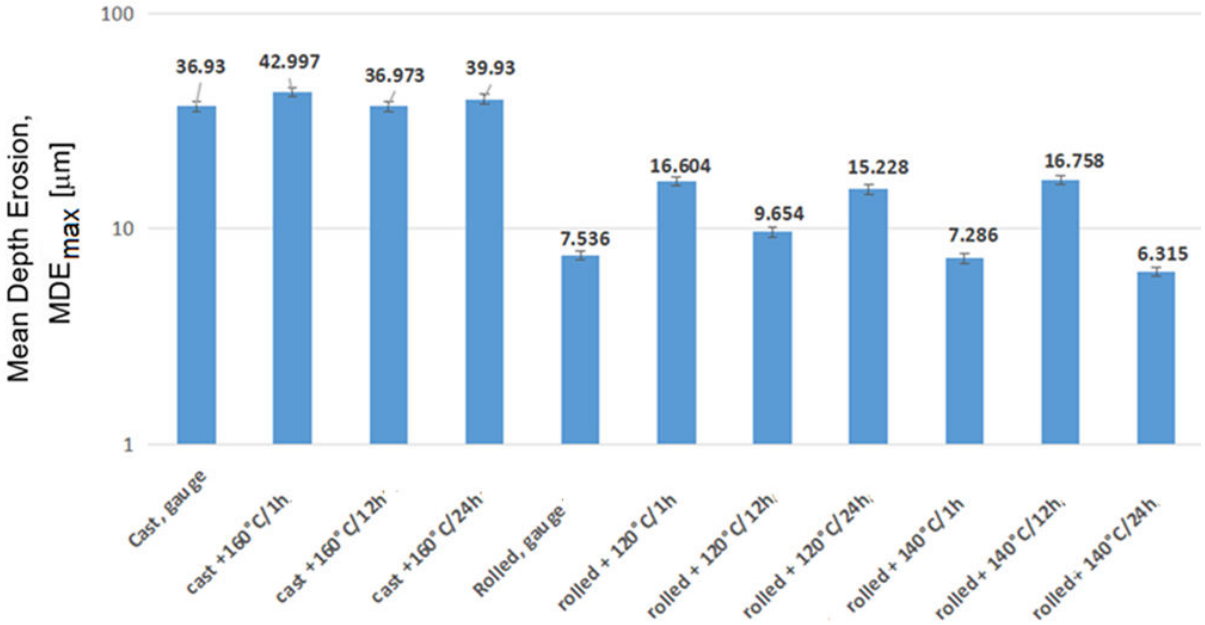

Fig. 8. Histogram of comparison of erosion depths of alloy 7075, cast/rolled and different structural states (after [13])

Regarding the cavitation test parameters of the 7075 alloy samples in the rolled state, it is noted that they show a much higher cavitation resistance than in the rolled state, the values increasing by over 100 times (fig. 9). At the same time, it can be observed that a thermal aging treatment at 140°C/24h leads to an improvement in cavitation resistance, respectively 31.25 min/µm, compared to 23.72 min/µm for the untreated sample (fig. 9), the other thermal aging treatments reduce the cavitation resistance. Regarding the calculated cavitation erosion penetration depths, these are reduced, respectively 6.3 µm for 140°C/24h, compared to 7.53 µm for the untreated sample (fig. 10), while for the other thermal aging treatments these are in the value range 7.2-16.6 µm.

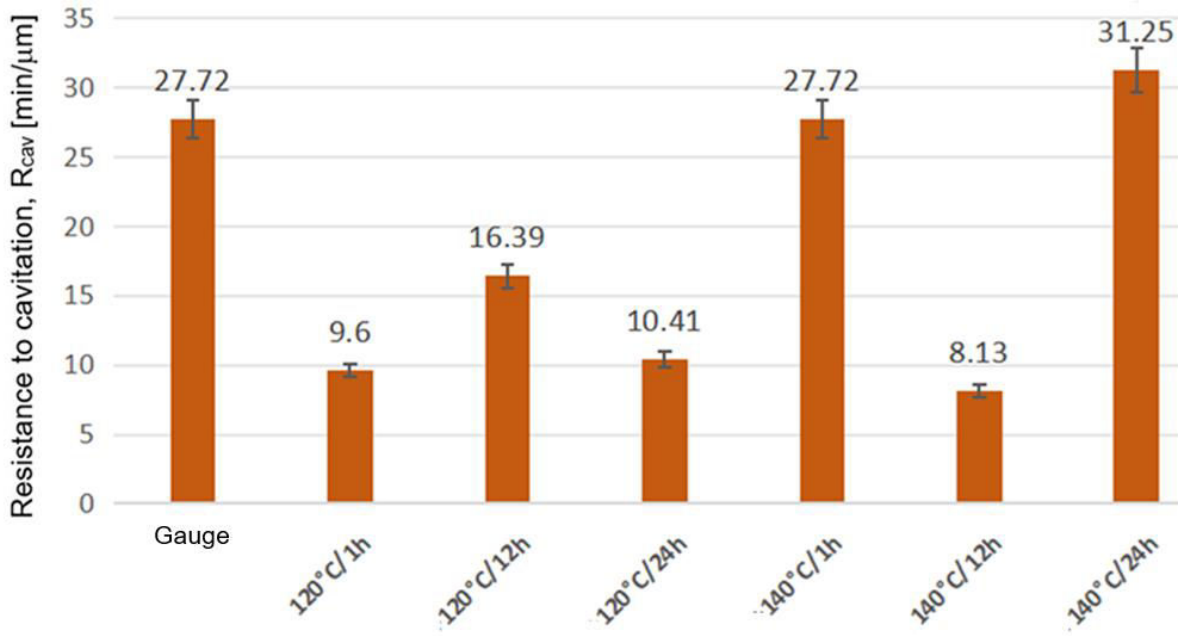

Fig. 9. Histogram comparing the cavitation resistances of alloy 7075, rolled and different structural states (after [13])

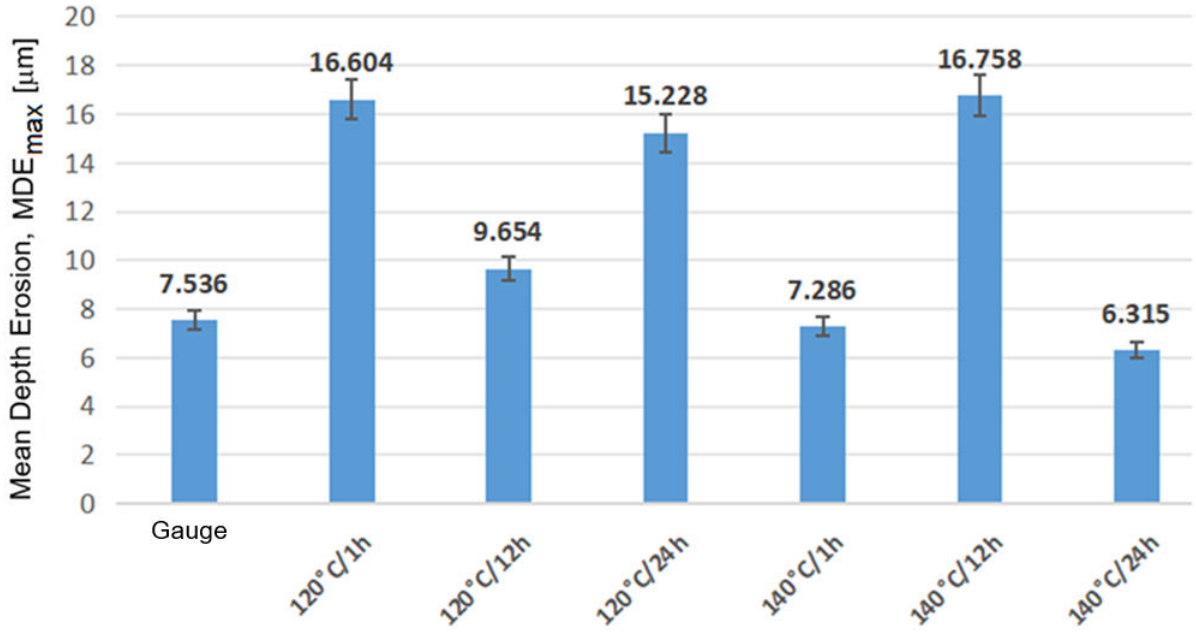

Fig. 10. Histogram of comparison of erosion depths of alloy 7075, rolled and different structural states (after [13])

The comparative analysis of the cavitation erosion resistance of alloy 2017A compared to that of alloys 5083, 6082 and 7075 allowed the creation of the histograms in fig. 11 and fig. 12 from which the following remarks can be made:

- The 2017 aluminum alloy, T451 condition and heat-treated for aging at 120ºC/1h has the highest cavitation resistance among the alloys taken for comparison, respectively 16.03 min/µm, compared to the 7075 alloy with the lowest cavitation resistance, respectively 0.261min/µ.
- Alloy 2017A has an average penetration depth of about 22µm, having an intermediate value compared to that of alloy 5083 with the lowest average depth value of about 14µm.

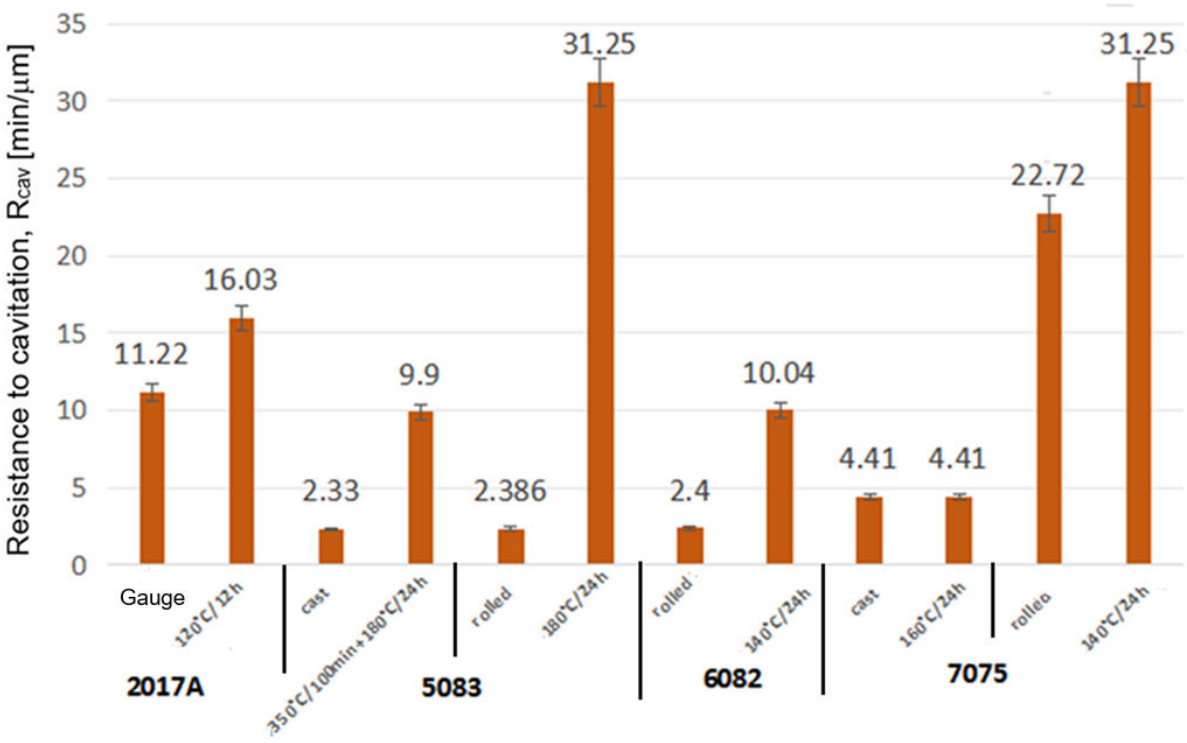

Fig. 11. Histogram comparing the cavitation resistances of alloy 2017A, compared to alloys 5083, 6082 and 7075, control and heat-treated samples

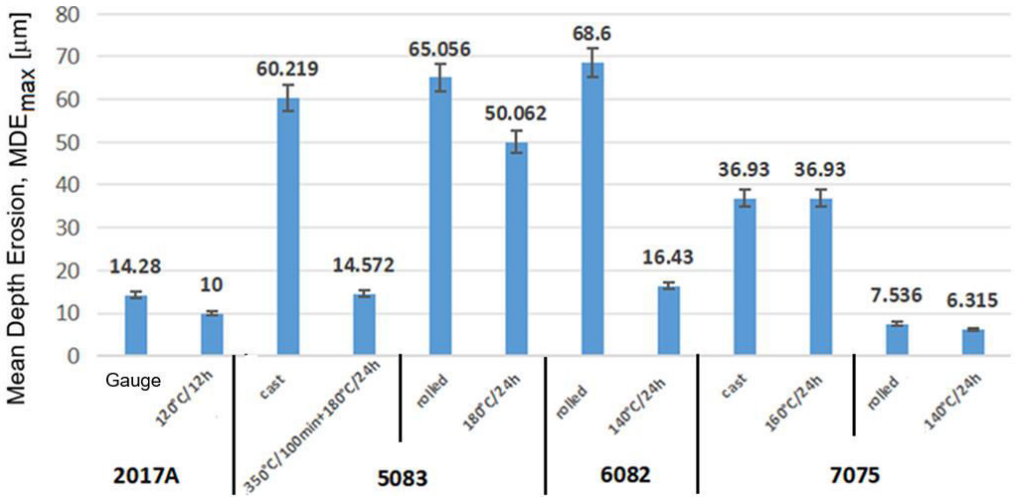

Fig. 12. Histogram comparing erosion depths of alloy 2017A, compared to alloys 5083, 6082 and 7075, control and heat treated samples

Thus, a hierarchy of cavitation resistance can be made within the different series of aluminum alloys, namely:

$$R_{cav}(7075) > R_{cav}(5083) > R_{cav}(2017A) > R_{cav}(6082) \quad (1)$$

and also a hierarchy of calculated penetration depths of cavitation erosion, within the different series of aluminum alloys, as follows:

$$\delta(5083) > \delta(6082) > \delta(2017A) > \delta(7075) \quad (2)$$

3.2 Comparative analysis of the morphology of surfaces tested for cavitation erosion

The cavitation phenomenon encountered in the investigated aluminum alloys is specific to all samples, regardless of the state of the material (control or heat treated). Thus, in the first 15…30 minutes of vibratory cavitation, it respects its specific erosive mechanism through which, in the attacked surface, more elasto-plastic deformations and crack networks are produced and the peaks of roughness and abrasive dust are eliminated [16, 17]. The expulsions of material, with the creation of pitting, are significantly reduced in the mass values recorded by weighing. For this reason, the appearance of the surface looks like a polished/matt one. In the following time intervals, depending on the state of the material, massive expulsions of material occur, leaving large, interconnected cavitations [18-19].

A careful analysis of the propagation of the fracture front through cavitation erosion in the studied aluminum alloys shows that the surfaces subjected to erosion comprise two specific zones, namely an area that is affected by cavitation, with a larger diameter and a concentric zone, inside which suffers a strong erosion phenomenon [20, 21]. This fact is found in all the studied aluminum alloys, the proportion of these zones being influenced by the state of the material, respectively by the aging heat treatment.

To understand the morphological analysis and the evolution of the destruction of the attacked surface, in fig. 13, macro (photographic) images of the eroded surface are presented, taken with the Canon Power Shot A 480 camera, only for the semi-finished states (states without heat treatment) of the 4 types of alloys after 30 minutes and 165 minutes of cavitation.

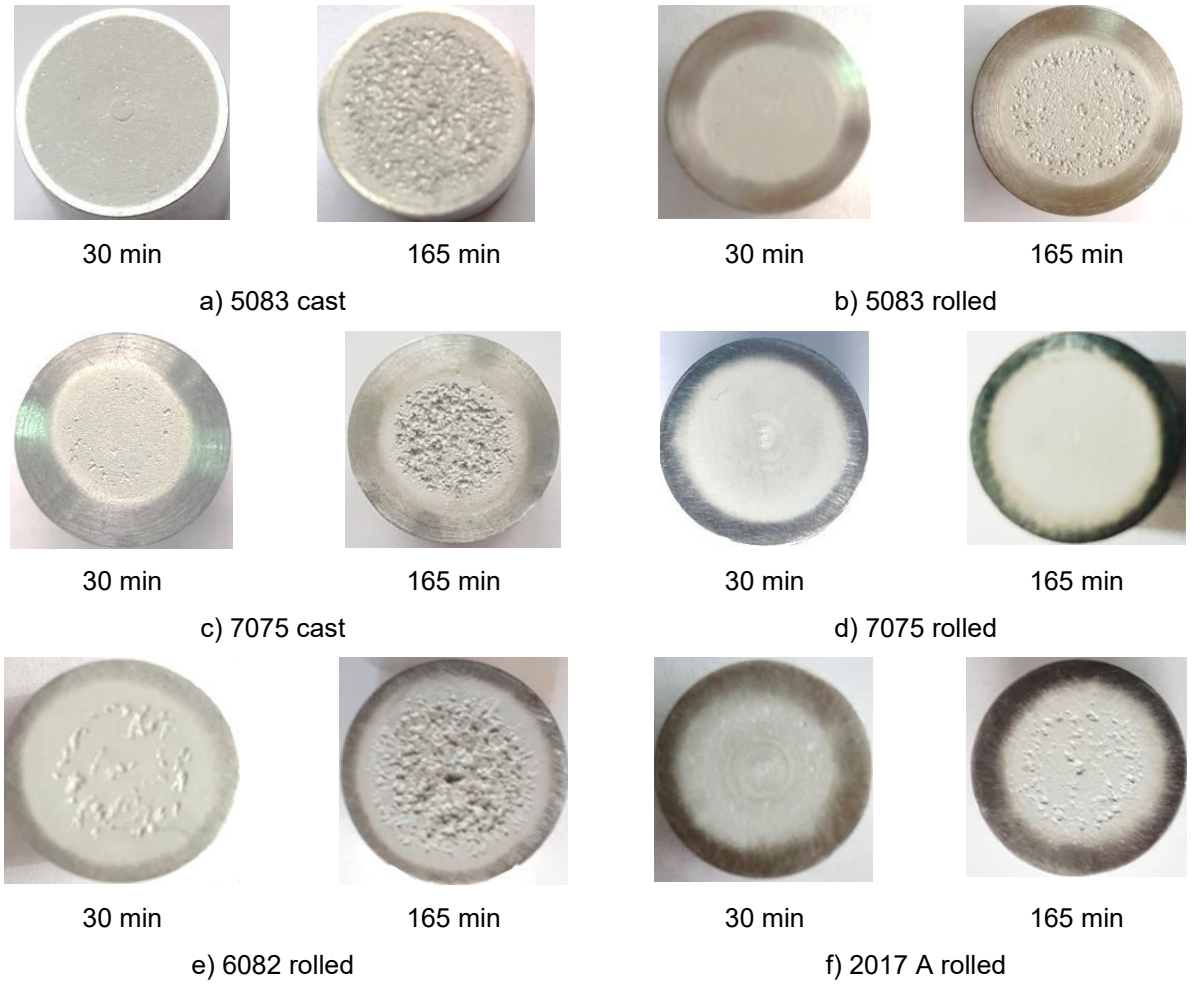

Fig. 13. Images of surface structure degradation by erosion of cavitation vibratory

In the case of alloy 5083, the structural destruction occurring during the cavitation test is generated by the dislocation of Mg5Al8 particles which does not cause significant hardening, leaving the

surface eroded, with numerous secondary cracks. The application of the combination of heat treatments can reduce the maximum cavitation penetration depths, up to about 14 μm to 350°C/100 min + 180°C/24h, in as-cast condition. In the case of rolled samples, regardless of the type of treatments applied erosion manifests itself profoundly by increasing the number and geometric dimensions of pits and caverns.
In the case of alloy 6082, the cavity surfaces are similar to any hardening treatment, with faceted cavities, with propagation of the fracture front in steps, by cleavage, specific to precipitation hardened materials. If in the control sample the total surface affected by the cavitation attack is 85%, it can reach 80% in the heat treated samples, and the surface most affected by the cavitation attack in the control sample is 74% reaching 66% in the aged samples.
In alloy 7075, the cavities are quite large, angular, which are generated by hardening compounds based on (Mg, Mn, Cu). The cavities are coalescent, interconnected, leaving the surface extremely rough after degradation by cavitation erosion. In the as-cast specimens, the control specimen has the largest eroded surfaces, respectively about 68% and 54%, while in the treated specimens these surfaces are 69% and 57%. In the rolled specimens, the proportion of surfaces affected by erosion is different: in the control specimens it is about 80%, reaching 91% in the heat-treated specimens, while the surface most affected by erosion in the control specimen is about 70%, reaching 82% in the heat-treated specimens.
As a general conclusion, the 2017A alloy with or without improvement treatments has a cavitation resistance intermediate to the analyzed aluminum alloys, respectively 7075, 6082 and 5083 and, therefore, a calculated penetration depth intermediate to the alloys considered. It can also be appreciated that the cavitation resistance values of these aluminum alloys are very low compared to those of other classes of metallic materials (stainless steels, INCONEL superalloys, etc. [22-24]), being part of the category of metallic materials not resistant to cavitation erosion.
As a general conclusion, the 2017A alloy with or without improvement treatments has a cavitation resistance intermediate to the analyzed aluminum alloys, respectively 7075, 6082 and 5083 and, therefore, a calculated penetration depth intermediate to the alloys considered. It can also be appreciated that the cavitation resistance values of these aluminum alloys are very low compared to those of other classes of metallic materials (stainless steels, INCONEL superalloys, etc. [22-24]), being part of the category of metallic materials not resistant to cavitation erosion.

4. Conclusions

This paper makes a critical analysis of the comparison of the cavitation resistance of the 2017A aluminum alloy with other aluminum alloys, namely 5083, 6082 or 7075. The analysis allows the formulation of the following conclusions:
1. Alloy 2017A with or without improvement treatments has a cavitation resistance intermediate to the analyzed aluminum alloys, namely 7075, 6082 and 5083 and, therefore, a calculated penetration depth intermediate to the alloys considered. It can also be appreciated that the cavitation resistance values of these aluminum alloys are very low compared to those of other classes of metallic materials (stainless steels, INCONEL superalloys), being part of the category of metallic materials not resistant to cavitation erosion.
2. A possible hierarchy of cavitation resistance within different series of aluminum alloys could be: $R_{cav}(7075) > R_{cav}(5083) > R_{cav}(2017A) > R_{cav(}6082)$.
3. A possible hierarchy of calculated penetration depths of cavitation erosion, within different series of aluminum alloys, can be: $\delta(5083) > \delta(6082) > \delta(2017A) > \delta(7075)$.

References

[1] Bordeasu, Ilare, Cristian Ghera, Cornelia Laura Salcianu, Alexandru-Nicolae Luca, and Robert Stefan Parmanche. "On the Influence of Mechanical Properties of Aluminum Alloys on Their Resistance to Cavitation Erosion". Paper presented at the 13th International Conference on Applied Sciences (ICAS2025), Hunedoara, Romania, May 29-31, 2025. *Journal of Physics: Conference Series* 3153 (2025): 012001.
[2] Istrate, Dionisie, Beatrice-Gabriela Sbarcea, Alin Mihai Demian, Andreea Daniela Buzatu, Laura Salcianu, Ilare Bordeasu, Lavinia Madalina Micu, Cristian Ghera, Bogdan Florea, and Brandusa Ghiban.

"Correlation between Mechanical Properties—Structural Characteristics and Cavitation Resistance of Cast Aluminum Alloy type 5083". *Crystals* 12, no. 11 (2022): 1538.
[3] Istrate, Dionisie, Ilare Bordeasu, Brandusa Ghiban, Bogdan Istrate, Beatrice-Gabriela Sbarcea, Cristian Ghera, Alexandru-Nicolae Luca, Petrisor Ovidiu Odagiu, Bogdan Florea, and Dinu Gubencu. "Correlation between Mechanical Properties-Structural Characteristics and Cavitation Resistance of Rolled Aluminum Alloy Type 5083". *Metals* 13, no. 6 (2023): 1967.
[4] Bordeasu, Ilare, Brandusa Ghiban, Lavinia Madalina Micu, Alexandru-Nicolae Luca, Alin-Mihai Demian, and Dionisie Istrate. "The Influence of Heat Aging Treatments on the Cavitation Erosion Behavior of a Type 6082 Aluminum Alloy". *Materials* 16, no. 17 (2023): 5875.
[5] Bordeasu, I., C. Ghera, D. Istrate, Laura Salcianu, Brandusa Ghiban, Dumitru-Viorel Bazavan, Lavinia-Madalina Micu, Daniel-Catalin Stroita, A. Suta, I. Tomoiaga, and Alexandu-Nicolae Luca. "Resistance and behavior to cavitation erosion of semi-finished aluminum alloy 5083". *Hidraulica Magazine*, no. 4 (2021): 17–24.
[6] Bordeasu, Ilare, Brandusa Ghiban, Lavinia Madalina Micu, Alexandru-Nicolae Luca, Alin-Mihai Demian, and Dionisie Istrate. "The influence of heat aging treatments on the cavitation erosion behavior of a type 6082 aluminum alloy". *Materials* 16, no. 17 (2023): 5875.
[7] Luca, Alexandru-Nicolae, Ilare Bordeasu, Brandusa Ghiban, Cristian Ghera, Dionisie Istrate, and Daniel-Catalin Stroița. "Modification of the cavitation resistance by hardening heat treatment at 450 °C followed by artificial aging at 180°C of aluminum alloy 5083 compared to the state of cast semi-finished product*". Hidraulica Magazine*, no. 1 (2022): 39-45.
[8] Ghera, Cristian, Ilare Bordeasu, Alexandru-Nicolae Luca, Cornelia-Laura Salcianu, Brandusa Ghiban, Ovidiu Odagiu, Alin-Nicusor Sirbu, and Rodica Badarau. "Increasing the resistance to cavitation erosion of 6082 aluminum alloys through thermal aging treatments at 140 °C and holding time of 12 hours". *Solid State Phenomena* 349 (2023): 62–70.
[9] Mitelea, Ion, Ilare Bordeasu, Florin Frant, and Ion-Dragos Utu. "Effect of heat treatment on corrosion and ultrasonic cavitation erosion resistance of AlSi10MnMg alloy". *Materials testing* 62, no. 9 (2020): 921-926.
[10] Istrate, Dionisie. *Heat Treatments Influence on the Performance of an Alloy From Al-Mg System for Marine Applications / Influența tratamentelor termice asupra comportării unui aliaj din sistemul Al-Mg pentru aplicații maritime*. Doctoral thesis. Politehnica University of Bucharest, Romania, 2023.
[11] Luca, Alexandru-Nicolae. *Research on the resistance to cavitation erosion of some aluminum-based alloys with artificial aging heat treatment / Cercetarea rezistenței la eroziunea prin cavitație a unor aliaje cu bază de aluminiu cu tratament termic de îmbătrânire artificială*. Doctoral thesis. Politehnica University of Timișoara, Romania, 2024.
[12] Demian, Alin Mihai. *Research on the cavitation erosion behavior of aluminum alloy type 6082 in correlation with different structural states / Cercetări privind comportamentul la eroziune prin cavitație al aliajului de aluminiu tip 6082 în corelație cu diferite stări structurale*. Doctoral thesis. National University of Science and Technology Politehnica Bucharest, 2026.
[13] Odagiu, Petrișor Ovidiu. *Studies and Experimental Research on Mechanical Behavior and Cavitational Erosion Behavior of an Aluminum Alloy Type 7075 / Studii și cercetări experimentale privind comportarea mecanică și comportarea la eroziunea cavitațională a unui aliaj de aluminiu din seria 7075*. Doctoral thesis. Politehnica University of Bucharest, 2023.
[14] Bordeașu, Ilare. *Monograph of the Cavitation Erosion Research Laboratory of Politehnica University Timișoara (1960–2020) / Monografia Laboratorului de Cercetare a Eroziunii Cavitaționale al Universității Politehnica Timișoara (1960–2020)*. Politehnica Publishing House, Timișoara, 2020 (in Romanian).
[15] ***. *Standard Method of Vibratory Cavitation Erosion Test*. ASTM G-32: West Conshohocken, PE, USA, 2016.
[16] Ahmed, Shemy Mohamed, Kazua Hokkirigawa, Risaburo Oba, and Yasuaki Matsudaira. "Developing stages of ultrasonically produced cavitation erosion and corresponding surface roughness". *JSME Int. J. Ser. 2 Fluids Eng. Heat Transfer Power Fuel. Thermophys. Prop*. 33, no. 1 (1990): 11–16.
[17] Chiu, K-Y, F-T Cheng, and H-C. Man. "Evolution of surface roughness of some metallic materials in cavitation erosion." *Ultrasonics* 43 (2005): 713–716.
[18] Zasada, Dariusz, Judyta Anna Sienkiewicz, and Robert Jasionowski. "Grain size influences the corrosion and cavitation of Ni_3Al intermetallic alloys". *Metallurgija* 54 (2015): 47–50.
[19] Franc, Jean-Pierre, Francois Avellan, Brahim Belahadji, Jean-Yves Billard, Laurence Briançon-Marjollet, Didier Fréchou, Daniel H. Fruman, Ayat Karimi, Jean-Luis Kueny, and Jean-Marie Michel*. Cavitation: Physical Mechanisms and Industrial Aspects / La Cavitation. Mecanismes Physiques et Aspects Industriels*. Presses Universitaires de Grenoble, Grenoble, France, 1995.
[20] Hobbs, John M. "Experience with a 20-KC cavitation erosion test." In *Erosion by Cavitation or Impingement*. *ASTM STP 408*, Atlantic City, USA, 1960.
[21] Hobbs, John M. "Vibratory Cavitation Erosion Testing: Proceedings of a Meeting on 13 June 1963," NEL Report No. 149, National Engineering Laboratory, East Kilbride, Glasgow, 1964.

[22] Manzana, Madalina Elena. *Studies and experimental research on structural changes produced by cavitation–erosion in different metallic materials / Studii și cercetări experimentale privind modificările structurale produse de cavitație-eroziune în diferite materiale metalice*. Doctoral thesis. Politehnica University of Bucharest, 2012 (in Romanian).
[23] Guragata, Constantin Madalin. *Studies and Experimental Researches on the Deformability and Behavior of Cavitational Erosion of INCONEL-718 / Studii și cercetări experimentale privind deformabilitatea și comportarea la eroziunea cavitațională a superaliajului tip INCONEL 718*. Doctoral thesis. Politehnica University of Bucharest, 2021.
[24] Krella, Alicja Krystyna. “Degradation and Protection of Materials from Cavitation Erosion. A Review.” *Materials* 16, no. 5 (2023): 2058.

Comparing Water Quality Evaluations from a Fuzzy Model and a Multi-Parameter Model

M. Eng. **Rosalva MENDOZA RAMÍREZ**[1,*], Dr. **Rodolfo SILVA**[1],
Dr. **Karina SUÁREZ-ALCÁNTARA**[2], M. Eng. **Aníbal SOL BENÍTEZ**[3],
Dr. **Ramón DOMÍNGUEZ MORA**[1], Dr. **Maritza L. ARGANIS JUÁREZ**[1,*],
M. Eng. **Margarita PRECIADO JIMÉNEZ**[4], M. Eng. **Eliseo CARRIZOSA ELIZONDO**[1]

[1] Institute of Engineering, National Autonomous University of Mexico (UNAM)

[2] Academic Unit of the Institute of Materials Research, National Autonomous University of Mexico (UNAM)

[3] External Consultant

[4] Mexican Institute of Water Technology (IMTA)

* rmr@pumas.iingen.unam.mx, MArganisJ@iingen.unam.mx

Abstract: *Water quality in Lake Zirahuén (Mexico) was evaluated using two conceptually different approaches: a classical multi-parameter Water Quality Index (NSF model) and a fuzzy logic–based model. Data from four monitoring sites and three sampling campaigns in 2018 were used, considering biochemical oxygen demand (BOD_5), chemical oxygen demand (COD), and total suspended solids (TSS). The NSF model produced WQI values close to 80/100, classifying the lake as acceptable except for sensitive organisms. In contrast, the fuzzy model yielded values near 50/100, frequently corresponding to the category only suitable for very resistant organisms. The fuzzy model also showed greater variability between sampling campaigns, indicating higher sensitivity to parameter fluctuations. These differences arise from the structural nature of the models: the NSF index applies compensatory averaging, whereas the fuzzy model follows rule-based inference that emphasizes deteriorated conditions. Although neither model indicates extreme pollution, both suggest that current water quality may impose ecological stress, particularly on sensitive aquatic species. The results highlight the importance of incorporating non-compensatory approaches such as fuzzy logic into water quality assessment, particularly in systems where conservation of aquatic life is a management priority.*

Keywords: *Water quality index, fuzzy model, multi-parameter model, water body*

1. Introduction

The water quality assessment uses methodologies based on measurements of physical, chemical, biological, and bacteriological parameters [1, 5]. These components are the inputs for any of the well-known models that give a water quality index (WQI) [6], a value to describe the state of water, and follow up on the changes over time. The reliability of these models will always depend on the accuracy of the measurements, their continuity, and the reduction in uncertainty of external factors, such as having similar conditions in sampling campaigns (start and end of sampling times, control labels, and adequate transportation of samples), adequate calibration of equipment, and so on.
However, since there is no globally applicable index to assess water quality, most countries use indices adapted to the specific conditions of local water bodies (rivers, lakes, and aquifers) [6, 16]. In México, as in other countries, a quick way to assess water quality is through the biochemical oxygen demand at five days (BOD_5), the chemical oxygen demand (COD), and the total suspended solids (TSS) measurements [17]. There are limits determined by different official regulations for each of the three variables, which are related to the respective water quality classifications, expressed in qualitative terms (Table 1) rather than as a number between 0 and 1 or between 0 and 100, which is the way water quality is generally described.

Table 1: BOD_5, COD, and TSS water quality classification scale [17]

CRITERION (mg/l)			CLASSIFICATION
$BOD_5 \leq 3$	COD ≤ 10	TSS ≤ 25	EXCELLENT
$3 < BOD_5 \leq 6$	10 < COD≤ 20	25 < TSS ≤ 75	GOOD
$6 < BOD_5 \leq 30$	20 < COD ≤ 40	75 < TSS ≤ 150	ACCEPTABLE
$30 < BOD_5 \leq 120$	40 < COD ≤ 200	150 < TSS ≤ 400	POLLUTED
$BOD_5 > 120$	COD > 200	TSS > 400	HEAVILY POLLUTED

As the classification labels of these variables are verbal expressions, we thought of using the tools of Fuzzy Logic (FL) to develop a model that, based on logical rules, allows the joint evaluation of the variables to obtain a value that will coincide with the classification ranges established by the National Water Commission and the Ministry of the Environment and Natural Resources (CONAGUA and SEMARNAT, are the respective acronyms in Spanish), for the different water uses (Table 2).
With information from a public database for a water body in Michoacán, Mexico, for 2018, for BOD_5, COD, and TSS, we calculated the water quality index with the fuzzy model. We then compared these values with those obtained in a previous study [18], which used the index developed in the USA by the National Sanitation Foundation (NSF), widely used to assess water quality.

Table 2: WQI classification scale according to the water use [19]

<table>
<tr><th>Value (%)</th><th>General criterion</th><th>Public supply</th><th>General recreation</th><th>Fishing and aquatic life</th><th>Industrial and Irrigation</th><th>Navigation</th></tr>
<tr><td>100</td><td rowspan="3">Not Polluted</td><td rowspan="3">No purification required</td><td rowspan="4">Acceptable for all aquatic sports</td><td rowspan="4">Acceptable for all organisms</td><td>No purification required</td><td rowspan="11">Acceptable</td></tr>
<tr><td>90</td><td rowspan="2">No purification required</td></tr>
<tr><td>85</td><td rowspan="3">Slight purification is required for some processes</td></tr>
<tr><td>80</td><td>Acceptable</td><td>Slight purification required</td><td rowspan="4">Acceptable but not recommended</td></tr>
<tr><td>70</td><td rowspan="3">Slightly Polluted</td><td rowspan="3">Increased need for treatment</td><td>Acceptable, except for susceptible organisms</td></tr>
<tr><td>60</td><td rowspan="2">No treatment is required for industrial use</td></tr>
<tr><td>50</td><td>Doubtful for sensitive organisms</td></tr>
<tr><td>40</td><td rowspan="2">Polluted</td><td>Doubtful</td><td>Doubtful</td><td rowspan="2">Only very resistant organisms</td><td rowspan="2">Treatment is required for most industrial uses</td></tr>
<tr><td>30</td><td rowspan="3">Not acceptable</td><td>Avoid water contact</td></tr>
<tr><td>20</td><td rowspan="3">Heavily Polluted</td><td>Slightly Polluted</td><td rowspan="3">Not acceptable</td><td>Restricted use</td><td>Polluted</td></tr>
<tr><td>10</td><td rowspan="2">Not acceptable</td><td>Not acceptable</td><td>Not acceptable</td></tr>
<tr><td>0</td></tr>
</table>

2. Methodology

2.1 Study Area and Sampling Sites

Lake Zirahuén lies in the basin of the same name, in the state of Michoacán, central México (Fig. 1), between 19°21'10" and 19°29'24" North, and 101°29'37" and 101°49'37" West, 2075 m above sea level. It is an endorheic-type basin, covering 260 km^2 of highlands of the Transverse Volcanic system, with elevations ranging from 2080 m, near the lake, to 3280 m, to the northwest and northeast of the lake. The lake is almost rectangular, covering approximately 10 km^2. There is only one permanent inflow, El Silencio River, which is found in the eastern part of the basin [20] (Fig. 1). There are many settlements in the basin, the most important in terms of population and economic activities are Zirahuén (3263 inhabitants), Santa Clara del Cobre (16748 inhabitants), and Opopeo (11304 inhabitants) [21]. The main economic activities here are tourism, handmade copper crafts, and wooden furniture, respectively. The National Water Commission (NWC) is responsible for the management and protection of all water bodies in México, and has been sampling the water at four sites in Lake Zirahuén from 2012 to the present time. Following the NWC terminology, these sites are Entrada 1, Muelle principal, Entrada 2, and Centro, as seen in Figure 1.

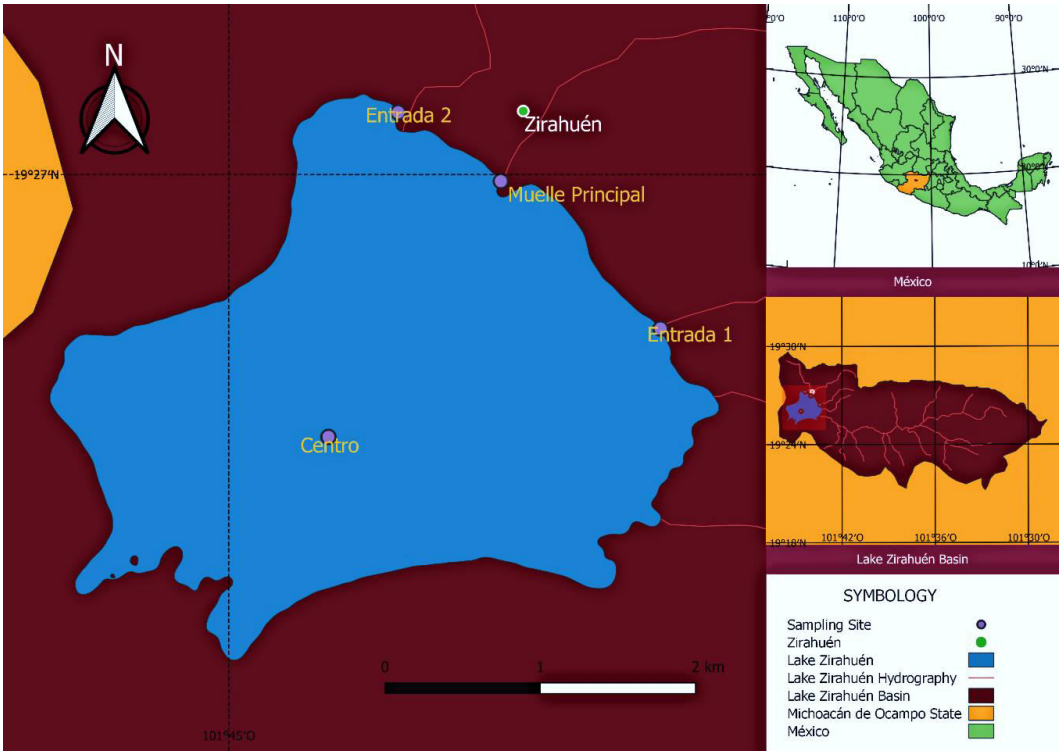

Fig. 1. Location of Lake Zirahuén and sampling sites

2.2 The National Sanitation Foundation (NSF) model

The NSF method was developed in 1970 [2], and is a multi-parameter model that uses nine variables to calculate the WQI: fecal coliforms (FC), dissolved oxygen (DO), biochemical oxygen demand (BOD), turbidity (TU), nitrates (NO_3), potential of hydrogen (pH), total phosphates (TP), change of temperature between air and sample (ΔT), and total dissolved solids (TDS). Each parameter has a weighting, and the value for each measured variable is transformed into a quality value (Q), using a function curve. Q is then multiplied by the weighting of the parameter to give a subtotal, one for each variable (nine in total). These subtotals are summed to obtain the WQI value, which is classified according to the established ranges in Table 2.

2.3 The Fuzzy model (FM)

a) Basic Theory

In 1965 Lofti A. Zadeh developed a form of processing information, in which data could have a degree of partial membership of sets associated with them, calling it Fuzzy Logic (FL) [22]. This means of processing uses validity functions, operations between fuzzy collections, and logic rules. The FM has three stages (Fig. 2): fuzzification, inference process, and defuzzification.

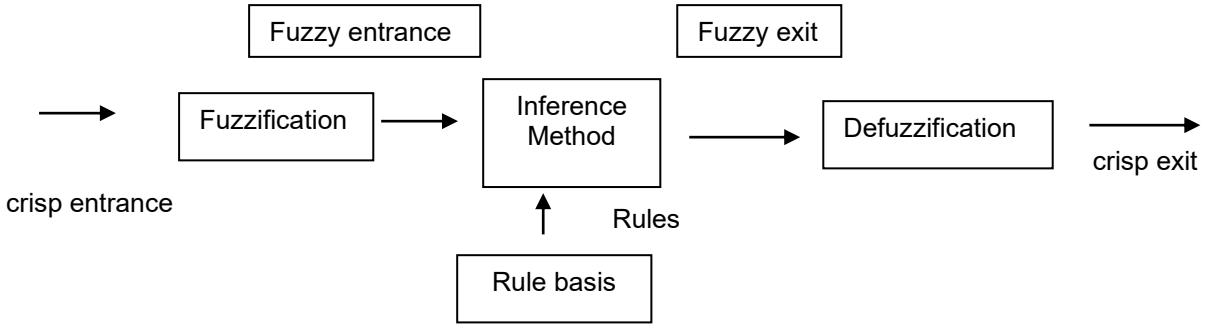

Fig. 2. Fuzzy system [23]

The first stage converts real values (in this case these are the limits of the variables BDO_5, COD, and TSS established in Table 1) into fuzzy values, assigning membership grades with membership functions (triangular, trapezoidal, S -, π -, beta, and Gaussian shape, are the most typical). We used the triangular function (Fig. 3) as a first approach because it is the easiest function to define; it only needs two base points and a third point, which is the peak of the triangle. The second stage uses a mapping process to make decisions or distinguish patterns. The most important are those developed by [24, 26]. We use the Mamdani fuzzy inference system. The third stage in the process takes the fuzzy outputs and converts them into a single value using mathematical methods such as the centroid, bisector, mean value of maximum (mom), the smallest value of maximum (som), and the largest value of maximum (lom). In this case, the centroid method was used.

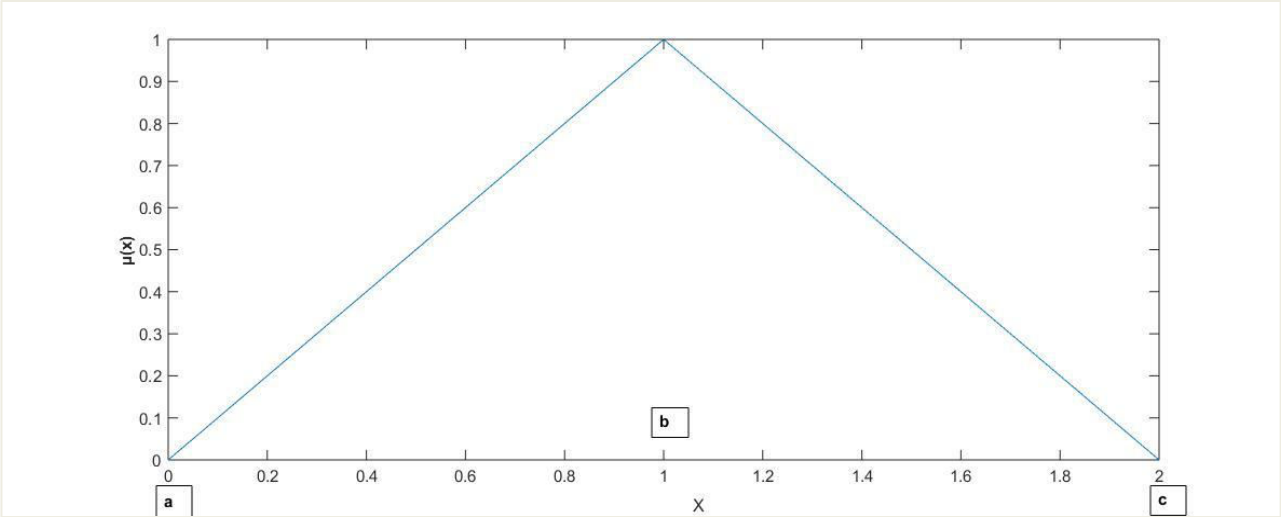

Fig. 3. Triangular membership function

b) Linguistic concepts

The input variables BOD_5, COD, and TSS (ranges shown in Table 1), are fuzzy sets representing linguistic concepts: "E" (excellent), "G" (good)," A" (acceptable)," P" (polluted), and "HP" (heavily polluted). The WQI is the output variable, values shown in Table 2. For Lake Zirahuén, the column corresponding to Fishing and Aquatic Life was taken, and the fuzzy sets were defined with the

linguistic concepts: "AAO" (acceptable for all organisms), "AESO" (acceptable except susceptible organisms), "DSO" (doubtful for sensitive organisms), "OVRO" (only for very resistant organisms), and "NA" (not acceptable).

c) Logical Rules

Logical rules are defined using simple if-then statements, or more complex if-then statements using the and-or connectors. For the output variable, the following cases were defined:

1) "AAO": if the three input variables are "E"
2) "AESO": if the three input variables are "G", or if the input variables are "G", "A" or "E", or if two input variables are "E", or "A", and the third is "E", "G", or "A"
3) "DSO": if the three input variables are "A", or if any of the input variables is "P"
4) "OVRO": if the three input variables are "P", or if two input variables are "P"
5) "NA": if the three input variables are "HP", or if two input variables are "HP"

d) Input and output variables membership functions

With the established limits (see Table 1) and the linguistic concepts, we defined the membership functions for each input variable and the output variable (Figs. 4 and 5).

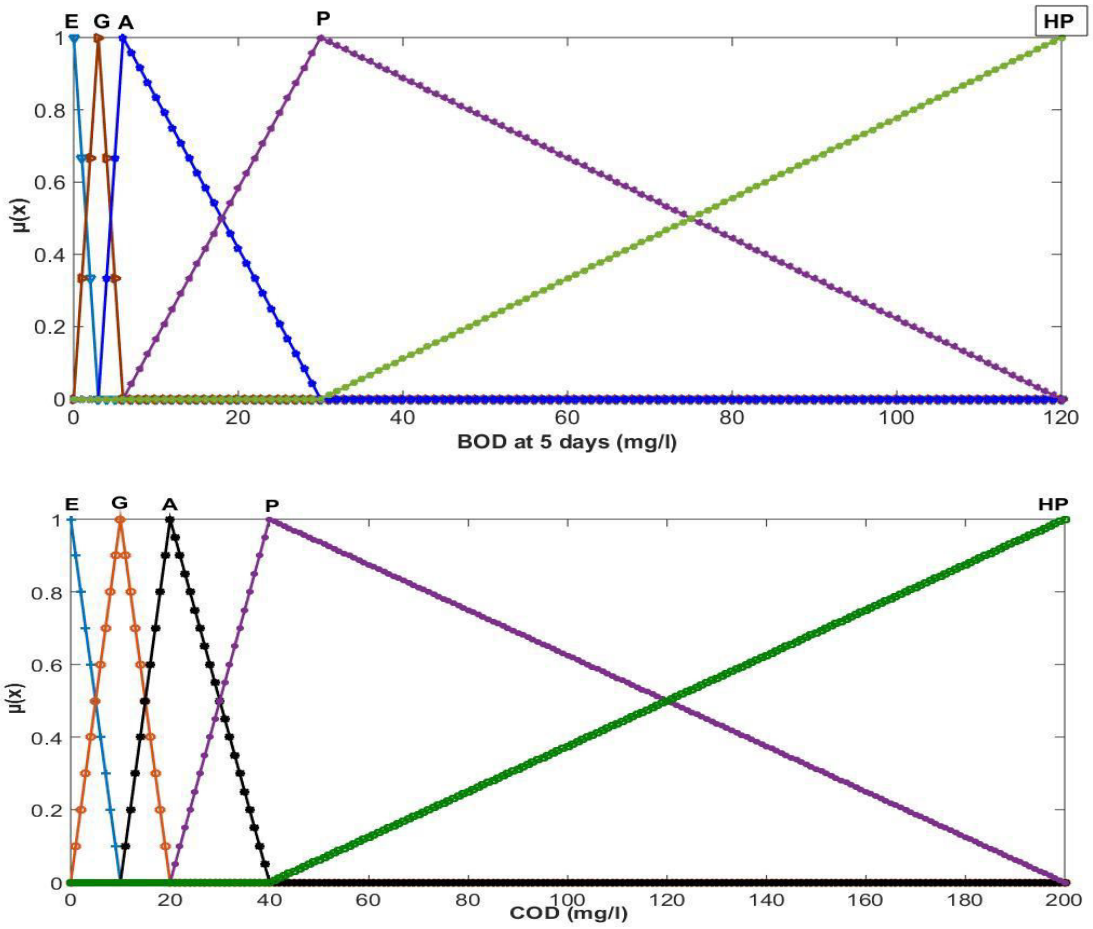

Fig. 4. Membership functions

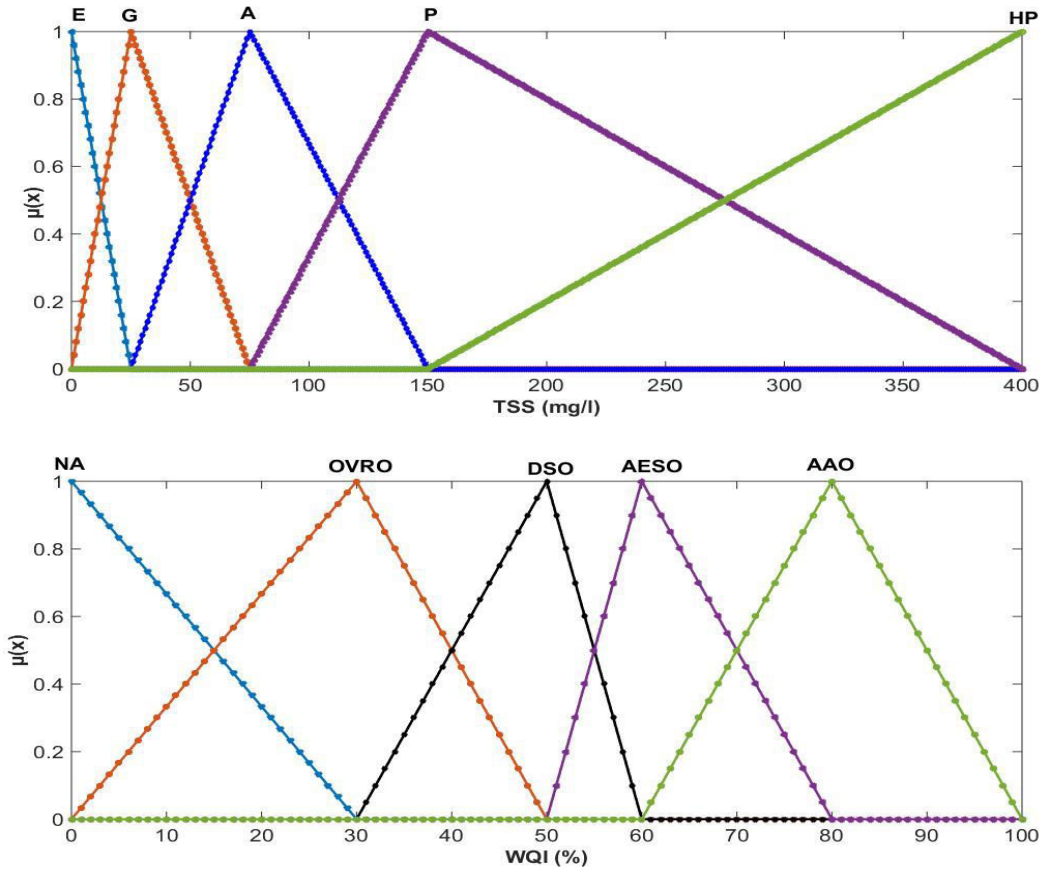

Fig. 5. Membership functions

3. Results

During 2018, three monitoring campaigns were conducted at the four sampling sites of Lake Zirahuén (Fig. 1). The measured concentrations of BOD_5, COD, and TSS are presented in Table 3.

Table 3: 2018 campaigns: Values for each variable

Sampling date	Sampling site	Variables (mg/l)		
		BOD_5	COD	TSS
2018/04/19	Entrada 1	7	44	9
	Muelle principal	7	60	9
	Entrada 2	7	64	9
	Centro	6	64	9
2018/06/21	Entrada 1	3	62	9
	Muelle principal	3	62	9
	Entrada 2	3	21	9
	Centro	3	77	9
2018/11/08	Entrada 1	6	43	9
	Muelle principal	4	45	9
	Entrada 2	6	42	9
	Centro	6	36	9

The numerical value of the WQI allows us to see what classification range this falls into, and which verbal description is given to define the water quality (Table 2), taking into account that the uses of this lake water are fishing and the conservation of aquatic life. Table 4 shows the results obtained with the two models, from which it can be seen that:

Table 4: WQI results with the two models

Sampling site: Entrada 1			
Sampling date	**2018/04/19**	**2018/06/21**	**2018/11/08**
WQI NSF	77	78	77
WQI FM	46	46	46
Sampling site: Muelle principal			
Sampling date	**2018/04/19**	**2018/06/21**	**2018/11/08**
WQI NSF	74	78	79
WQI FM	46	46	46
Sampling site: Entrada 2			
Sampling date	**2018/04/19**	**2018/06/21**	**2018/11/08**
WQI NSF	74	78	75
WQI FM	46	63	46
Sampling site: Centro			
Sampling date	**2018/04/19**	**2018/06/21**	**2018/11/08**
WQI NSF	76	77	76
WQI FM	46	46	52

a) The NSF model:

a.1) In the April campaign, the best WQI value was obtained at the Entrada 1 site, followed by Centro, with Entrada 2 and Muelle principal being the same.
a.2) Entrada 1, Muelle principal, and Entrada 2 tie with 78% (of the possible 100 percent) in the June campaign. The last place is Centro, but with a value of only one percent less.
a.3) The four sites have different values in the November campaign, the best is for Muelle principal (79%), and the worst Entrada 2 (75%).
a.4) Regarding numerical values, the best site is Entrada 1, then Muelle principal, next Centro, and last Entrada 2.
a.5) The water quality for all four sampling sites, in all the sampling campaigns, falls into the category "Acceptable except for sensitive organisms" (60% ≤ WQI < 80%), according to the classification of Table 2.

b) The Fuzzy Model:

b.1) For the four sites, the most common value is 46, the only exceptions being Entrada 2 (63%) in the June campaign, and Centro (52%) in the November campaign.
b.2) The best average value, in terms of percentages, is obtained by Entrada 2 (52), then Centro (48), and then Entrada 1 and Muelle principal, which tie (46).
b.3) According to Table 2: The water quality values are in the category "Only very resistant organisms" for all the campaigns at Entrada 1 and Muelle principal. For Entrada 2 and Centro, the results for one sampling campaign are higher than the other two campaigns. Only Entrada 2, in the June campaign, achieved a rating of "Acceptable, except for susceptible organisms", thus matching the results of the NSF model. The WQI for the Centro sampling site in the November campaign was somewhat higher than the values of the other two campaigns: "Doubtful for sensitive organisms".

c) Similarities

c.1) The only overlap between the two models is that the Centro site in the June campaign had a rating of "Acceptable except for sensitive organisms", which is the rating that encompasses all the values of the four sampling sites with the NSF model.

d) Differences

d.1) Between the maximum and minimum numerical values of the two models, the difference is notable: 5 points for the NSF model and 17 points for the FM.
d.2) With the NSF model, there is no homogeneity in the numerical values for any of the sites. With the FM model, Entrada 1 and Muelle principal have homogeneous values.

d.3) As shown in Table 2, the values obtained with the FM are classified into three categories: values between 30 – 49 % are for "Only very resistant organisms", values between 50 – 59% are "Doubtful for sensitive organisms", and finally values between 60-69% are "Acceptable, except for susceptible organisms". While with the NSF model, the water quality for all four sampling sites, in all the sampling campaigns, falls into the category "Acceptable except for sensitive organisms" (60% ≤ WQI < 80%).
d.4) The NSF model produced consistently higher WQI ratings for the lake compared to the FM.

4. Conclusions

This research compared a classical multi-parameter water quality index (NSF) with a three-input fuzzy logic model for Lake Zirahuén. Although both approaches indicated moderate water quality conditions, the fuzzy model consistently produced lower values and identified more restrictive ecological classifications. The differences arise from the structural nature of the models: the NSF index uses compensatory averaging, while the fuzzy model applies rule-based inference that emphasizes deteriorated parameters. Consequently, the fuzzy model acts as a precautionary indicator, more aligned with ecological threshold responses.
The results suggest that, while general physicochemical conditions may appear acceptable, biological communities could already be under stress. Therefore, relying solely on averaging indices may underestimate ecological risk. This paper highlights the value of fuzzy logic as a complementary tool in water quality assessment, particularly for water bodies where conservation of aquatic life is a priority. The approach can be extended to other lakes and regulatory systems, providing a framework that integrates environmental standards with ecological sensitivity.
Future work should incorporate biological indicators and additional physicochemical parameters to further validate the fuzzy model and refine its rule base.

References

[1] Horton, R. K. "An index number system for rating water quality." *Journal of the Water Pollution Control Federation* 37, no. 3 (1965): 300-306.
[2] Brown R., N. Mcclelland, R. Deininger, and R. Tozer. "A Water Quality Index-Do We Dare?" *Water & Sewage Works* 117, no. 10 (October 1970): 339-343.
[3] Hellawell, J. M. *Biological surveillance of rivers*. Water Research Center, Stevenage, 1978.
[4] Alba-Tercedor, J., and F. Jiménez-Millán. *Evaluation of seasonal variations in the water quality of the Guadalfeo River, based on the study of aquatic macroinvertebrate communities / Evaluación de las variaciones estacionales de la calidad de las aguas del río Guadalfeo, basado en el estudio de las comunidades de macroinvertebrados acuáticos*. Lucdeme III, Icona, Monografía, pp. 48: 91, 1987.
[5] SAFE. "Strategic Assessment of Florida's Environment." *Florida Stream Water Quality Index, Statewide Summary.* 1995. http://www.pepps.fsu.edu/safe/pdf/swq3.pdf. Accessed September 16, 2024.
[6] Uddin, Md. Galal, Stephen Nash, and Agnieszka I. Olbert. "A review of water quality index models and their use for assessing surface water quality." *Ecological Indicators* 122 (March 2021): 107218. https://doi.org/10.1016/j.ecolind.2020.107218.
[7] Winnipeg, M. *Canadian Water Quality Guidelines for the Protection of Aquatic Life: CCME Water Quality Index 1.0.* User's Manual, 2001.
[8] UNEP/GEMS. *Water Quality Outlook.* United Nations Environmental Programme (UNEP)/Global Environmental Monitoring System (GEMS), Burlington, Canada. 2007.
[9] Sharma, Deepshikha, and Arun Kansal. "Water quality analysis of River Yamuna using water quality index in the national capital territory, India (2000–2009)." *Applied Water Science* 1 (2011): 147-157. DOI: 10.1007/s13201-011-0011-4.
[10] Gazzaz, N. M., M. K. Yusoff, A. Z. Aris, H. Juahir, and M. F. Ramli. "Artificial neural network modeling of the WQindex for Kinta River (Malaysia) using Water Quality variables as predictors." *Marine Pollution Bulletin* 64, no. 11 (November 2012): 2409-2420. DOI: 10.1016/j.marpolbul.2012.08.005.
[11] Kocer, M.A.T., and H. Sevgili. "Parameters selection for Water Quality index in the assessment of the environmental impacts of land-based trout farms." *Ecological Indicators* 36 (January 2014): 672-681.
[12] Pataca, L.C.M., M.A.F. Pedrosa, T. R. Zolnikov, and M. P. G. Mol. "Water quality index and sanitary and socioeconomic indicators in Minas Gerais, Brazil." *Environmental Monitoring and Assessment* 192 (2020): 476. https://doi.org/10.1007/s10661-020-08425-9.
[13] Zotou, I., V.A. Tsihrintzis, and G. D. Gikas. "Performance of seven Water Quality indices (WQIs) in a Mediterranean River." *Environmental Monitoring and Assessment* 191 (July 2019): 505.

[14] Fathi, P., E. Ebrahimi Dorche, M. Zare Shahraki, J. Stribling, O. Beyraghdar Kashkooli, A. Esmaeili Ofogh, and A. Bruder. "Revised Iranian Water Quality Index (RIWQI): a tool for the assessment and management of water quality in Iran." *Environmental Monitoring and Assessment* 194, no. 7 (June 2022): 504. doi: 10.1007/s10661-022-10121-9.

[15] Khan, M.H.R.B., A. Ahsan, M. Imteaz, M. Shafiquzzaman, and N. Al-Ansari. "Evaluation of the surface water quality using global water quality index (WQI) models: perspective of river water pollution." *Scientific Reports* 13, no. 1 (2023): 20454. https://doi.org/10.1038/s41598-023-47137-1.

[16] Kumar, D., R. Kumar, M. Sharma, A. Amit Awasthi, and M. Kumar. "Global water quality indices: Development, implications, and limitations." *Total Environment Advances* 9 (March 2024): 200095. https://doi.org/10.1016/j.teadva.2023.200095.

[17] Secretariat of Environment and Natural Resources / Secretaría de Medio Ambiente y Recursos Naturales (SEMARNAT). "Compendium of Environmental Statistics" / "Compendio de Estadísticas Ambientales." National Water Commission, Water Sanitation and Quality Management / Comisión Nacional del Agua, Gerencia de Saneamiento y Calidad del Agua. 2016. https://apps1.semarnat.gob.mx:8443/dgeia/compendio_2016/dgeiawf.semarnat.gob.mx_8080/ibi_apps/WFServlet28b9.html. Accessed September 30, 2024.

[18] Mendoza, R.R., K. Suárez-Alcántara, R. Silva, M. R. Domínguez, B. A. Sol, and E. E. Carrizosa. "Analysis of Water Quality Index in Lake Zirahuén, Michoacán, México." Paper presented at the 40th IAHR World Congress "Rivers – Connecting Mountains and Coasts", Vienna, Austria, August 21-25, 2023. doi: 10.3850/978-90-833476-1-5_iahr40wc-p0041-cd.

[19] Secretariat of Environment and Natural Resources / Secretaría de Medio Ambiente y Recursos Naturales (SEMARNAT). "Water quality classification scale for specific uses, according to its Water Quality Index (WQI)" / "Escala de clasificación de la calidad del agua para usos específicos, según su Índice de Calidad del Agua (ICA)." National Water Commission, Water Sanitation and Quality Management / Comisión Nacional del Agua, Gerencia de Saneamiento y Calidad del Agua. 2022. https://paot.org.mx/centro/ine-semarnat/informe02/estadisticas_2000/compendio_2000/03dim_ambiental/03_02_Agua/data_agua/RecuadroIII.2.2.3.htm. Accessed September 16, 2024.

[20] State Water and Basin Management Commission / Comisión Estatal del Agua y Gestión de Cuencas (CEAC). "Zirahuén Basin" / "Cuenca Zirahuén." 2023. https://ceac.michoacan.gob.mx/areas/subdireccion-de-cuencas/cuenca-zirahuen/. Accessed June 12, 2024.

[21] National Institute of Statistics and Geography / Instituto Nacional de Estadística y Geografía (INEGI). "Population and Housing Census 2020." / "Censo de población y vivienda 2020." México. https://www.inegi.org.mx/programas/ccpv/2020/. 2020. Accessed September 6, 2024.

[22] Zadeh, L.A. "Fuzzy sets." *Information and Control* 8, no. 3 (June 1965): 338–353.

[23] Roveda, S. R. M. M., A. P. M. Bondanca, J. G. S. Silva, J. A. F Roveda, and A. H. Rosa. "Development of a water quality index using a fuzzy logic: A case study for the Sorocaba river." Paper presented at the International Conference on Fuzzy Systems, Barcelona, Spain, July 18-23, 2010. DOI: 10.1109/FUZZY.2010.5584172.

[24] Mamdani, E., and S. Assilian. "An experiment in linguistic synthesis with a fuzzy logic controller." *International Journal of Man-Machine Studies* 7, no. 1 (January 1975): 1-13.

[25] Takagi T., and M. Sugeno. "Derivation of fuzzy control rules from human operator's control actions." Paper presented at the IFAC Symposium on Fuzzy Information, Knowledge Representation and Decision Analysis, Marseille, France, July 19-21, 1983.

[26] Tsukamoto, Y. "An Approach to Fuzzy Reasoning Method." In: Gupta, M., R. Ragade, and R. Yager (eds.). *Advances in Fuzzy Set Theory and Applications*, pp. 137-149. North-Holland Publishing Company, Netherlands, 1979.

Advanced Chemical-Engineered Biochar for the Simultaneous Removal of Toxic Heavy Metals and Complex Organic Pollutants from Water

Assoc. Prof. Ph.D. **Deniz ŞAHİN**[1,*], Assoc. Prof. Ph.D. Eng. **Ștefan ŢĂLU**[2,*]

[1] Gazi University, Faculty of Science, Department of Chemistry, 06560 Teknikokullar Yenimahalle/Ankara, Turkey

[2] Technical University of Cluj-Napoca, The Directorate of Research, Development and Innovation Management (DMCDI), Constantin Daicoviciu Street, no. 15, Cluj-Napoca, 400020, Cluj county, Romania

* dsahin42@hotmail.com (Deniz Şahin); stefan_ta@yahoo.com (Ștefan Țălu)

Abstract: *The co-occurrence of heavy metals and organic pollutants in aquatic environments has become a critical global concern due to their persistence, toxicity, and complex interactions in multi-contaminant systems. Conventional water treatment technologies often exhibit limited efficiency under simultaneous contamination conditions and may involve high operational costs or secondary pollution. In this context, engineered biochars (E-BCs) has emerged as a promising multifunctional material for sustainable water remediation. This review comprehensively evaluates recent advances in the design, modification, and application of engineered biochar for the simultaneous removal of heavy metals and organic pollutants from water. Various engineering strategies, including metal/metal oxide doping, heteroatom functionalization, magnetic modification, nano-composite formation, and chemical activation, are systematically discussed. The fundamental mechanisms governing pollutant removal are critically analyzed, including ion exchange, surface complexation, electrostatic attraction, precipitation, π–π interactions, hydrogen bonding, hydrophobic interactions, and pore-filling effects. Particular emphasis is placed on competitive and synergistic adsorption behaviors in multi-pollutant systems. Furthermore, the influence of environmental parameters such as pH, temperature, ionic strength, and natural organic matter on adsorption performance is examined. Regeneration capacity, structural stability, environmental safety, and practical applicability in real wastewater matrices are also evaluated. Finally, current challenges and future research directions are highlighted to support the rational development of next-generation multifunctional biochar materials. Engineered biochar demonstrates significant potential as a cost-effective, environmentally friendly, and highly efficient solution for integrated water purification, particularly in complex contamination scenarios.*

Keywords: *Aquatic environments, engineered biochar, heavy metals, organic pollutants, water purification*

1. Introduction

Water contamination has emerged as one of the most critical environmental challenges of the 21st century due to rapid industrialization, agricultural intensification, and urban expansion [1,2]. Aquatic environments increasingly receive complex mixtures of pollutants, including heavy metals, pharmaceuticals, pesticides, dyes, and other persistent organic contaminants [3,4]. Unlike single-contaminant systems traditionally investigated in laboratory studies, real wastewater matrices typically contain multiple classes of pollutants simultaneously, leading to complex physicochemical interactions and increased ecological risks [5]. Among these contaminants, heavy metals such as lead (Pb^{2+}), cadmium (Cd^{2+}), chromium (Cr^{6+}), mercury (Hg^{2+}), and arsenic (As^{3+}/ As^{5+}) are of particular concern due to their toxicity, persistence, and non-biodegradable nature [6,7]. Heavy metals can accumulate in sediments and biota, enter the food chain, and cause severe health effects including neurotoxicity, carcinogenicity, and organ damage [8,9]. Concurrently, organic pollutants, including pesticides, antibiotics, endocrine-disrupting compounds, and polycyclic aromatic hydrocarbons (PAHs), are increasingly detected in surface water, groundwater effluents [10,11]. These organic contaminants may exhibit persistence, bioaccumulation potential, and antibiotic resistance induction effects [12]. The co-existence of heavy metals and organic pollutants in aquatic systems presents a more complicated environmental scenario than individual contamination. Their interactions may alter adsorption behavior, toxicity, speciation, and degradation pathways [13,14]. For instance, heavy metals may compete for active sites on adsorbents, while organic molecules may block pores or form complexes with metal ions, thereby

affecting removal efficiency [15,16]. Therefore, remediation strategies capable of simultaneously removing both pollutant categories are urgently required.

Conventional water treatment technologies such as chemical precipitation [17,18], ion exchange [19], membrane filtration [20-25], coagulation-flocculation [26,27], electrochemical processes [28-31], advanced oxidation processes [32,33], and biological treatments [34,35] have been extensively applied. Although these methods can achieve high removal efficiencies under optimized conditions, they often suffer from limitations including high operational cost, sludge generation, membrane fouling, secondary pollution, and reduced efficiency in multi-contaminant systems. Adsorption has gained significant attention as an attractive alternative due to its simplicity, high efficiency, reusability potential, and economic feasibility [36,37].

In recent years, biochars (BCs), a carbon-rich material produced through the pyrolysis of biomass under limited oxygen conditions, has emerged as a promising adsorbent for environmental remediation [38]. Biochar possesses several advantageous properties, including high surface area, well-developed porosity, surface functional groups (–OH, –COOH, $–NH_2$), and relative environmental compatibility [39]. Pristine biochar has demonstrated effectiveness in removing either heavy metals or organic pollutants individually from aqueous systems [40,41]. However, its performance in simultaneous removal scenarios is often limited due to insufficient surface functionality, low affinity for certain contaminants, and restricted active sites [42].

To overcome these limitations, significant research efforts have focused on the development of E-BCs, which involves physical, chemical, or nanomaterial-based modification to enhance adsorption capacity and selectivity. Engineering strategies include metal oxide loading (e.g., Fe_3O_4, MnO_2, TiO_2), acid/base activation, heteroatom doping (N, S, P), magnetic modification, and composite formation with graphene oxide or nanoparticles. These modifications can increase specific surface area, introduce new functional groups, enhance redox activity, and improve structural stability. Particularly, metal-doped biochars have shown enhanced affinity toward heavy metals through surface complexation, ion exchange, and precipitation mechanisms.

Peng et al. developed a FeS/Fe_3O_4 co-modified biochar via a facile one-step synthesis strategy and applied it for peroxymonosulfate (PMS) activation to degrade quinclorac (QNC) in aqueous systems. The engineered material achieved complete removal (100%) of QNC under optimized laboratory conditions and maintained a high degradation efficiency of 99.31% in real irrigation water, demonstrating strong resistance to interference from coexisting anions and natural organic matter. Ecotoxicity assessment further indicated that the transformation products exhibited lower toxicity compared to the parent herbicide. Their characterization results confirmed the homogeneous dispersion of FeS and Fe_3O_4 nanoparticles on the biochar matrix, providing abundant Fe^{2+} sites for PMS activation and reactive oxygen species (ROS) generation. The Fe^{3+} formed during the reaction was continuously reduced by sulfur species, sustaining an efficient Fe^{2+}/Fe^{3+} redox cycle. Radical quenching and mechanistic analyses revealed the coexistence of •OH, $SO_4•^-$, $^1O_2$, and $O_2•^-$, indicating the simultaneous involvement of radical and non-radical pathways. Density functional theory (DFT) calculations further supported PMS adsorption and charge redistribution processes, while electrochemical tests highlighted the contribution of electron transfer mechanisms to catalytic performance. Overall, Peng et al. demonstrated that co-modified biochar can effectively enhance PMS-based advanced oxidation processes for the removal of refractory organic pollutants in real water matrices [43].

Meanwhile, E-BCs containing aromatic domains and π-electron-rich structures exhibit strong interactions with organic pollutants via π–π stacking, hydrogen bonding, hydrophobic interactions, and pore-filling effects. Li et al. investigated the adsorptive removal of tetracycline (TC) and Hg(II) using ball-milled magnetic nanobiochars (BMBCs) derived from wheat straw. They demonstrated that BMBC700, prepared at 700 °C, could adsorb ≥ 99% of TC and Hg(II) within 12 hours. The maximum adsorption capacities were 268.3 mg/g for TC and 127.4 mg/g for Hg(II). Li and colleagues reported that the adsorption efficiency decreased with increasing ionic strength but increased when the solution temperature rose from 25 °C to 45 °C. Mechanistic analyses showed that TC removal was mainly governed by electrostatic interactions, hydrogen bonding, and Cπ–Cπ interactions, whereas Hg(II) adsorption was primarily controlled by electrostatic attraction, Hg–Cπ bond formation, and surface complexation. They also found that BMBC700 exhibited good recyclability and the advantage of magnetic separation [44].

Additionally, biochar-based nanocomposites integrated with photocatalytic materials such as TiO_2 or ZnO have demonstrated dual adsorption-degradation capabilities, offering synergistic removal performance. Khang et al. demonstrated the synthesis of a BDH/ZnO/TiO_2 nanocomposite via a hydrothermal method, where biochar derived from pyrolyzed biomass was activated with H_3PO_4 and combined with TiO_2 (anatase, 20-35 nm) and ZnO (wurtzite, 100-240 nm). The resulting material exhibited a significantly increased surface area (approximately 5.5 times higher than raw biochar) and enhanced porosity (14.761-34.143 Å). The nanocomposite showed superior photocatalytic and adsorption performance under UV irradiation (365 nm, 100 min) for 10 ppm methylene blue, achieving 98.57% removal and maintaining over 95% efficiency after three regeneration cycles, outperforming the individual TiO_2 (58.52%) and ZnO (40.38%) components. Adsorption data fitted the Freundlich isotherm model, with a maximum adsorption capacity of 52.21 $mg \cdot g^{-1}$, indicating synergistic dual functionality in adsorption and photodegradation [45].

These multifunctional materials hold considerable promise for the remediation of complex wastewater matrices. However, despite notable advancements, several critical challenges remain unresolved. The underlying mechanisms governing simultaneous adsorption of multiple contaminants are not yet fully elucidated, particularly under competitive multi-pollutant conditions. Furthermore, adsorption performance is highly sensitive to environmental factors, including pH, ionic strength, temperature, and the presence of natural organic matter (NOM) [46]. In addition, the long-term regeneration potential, structural integrity, and environmental implications of engineered biochar require comprehensive and systematic investigation to ensure both efficacy and sustainability in practical applications.

This review aims to provide a comprehensive assessment of engineered biochar for the simultaneous removal of heavy metals and organic pollutants from water. The synthesis strategies, physicochemical characteristics, adsorption mechanisms, performance evaluation, influencing factors, regeneration potential, and practical applications are discussed. Furthermore, current limitations and future research perspectives are highlighted to guide the rational design of next-generation multifunctional biochar materials for sustainable water remediation.

2. Methodology of the Review

This review study is prepared by reviewing more than 200 peer-reviewed articles, graduate theses, and meeting proceedings on EPs published from different countries across the world, available from 2020 to 2026. Documents were collected through an exhaustive search in recognized sources of peer-reviewed and other types of scientific information, such as Google Scholar, Science Direct, PubMed, Springer, Wiley, and MDPI. While searching the literature, certain keywords, such as 'engineered biochar', 'removal of heavy metals from water', 'removal of heavy metals and organic pollutants from water' were used. Articles with common information were excluded from the citation list.

3. Engineered Biochars (E-BCs): Synthesis and Characteristics

The performance of engineered biochar (E-BC) is intrinsically linked to its physicochemical properties, including surface area, pore structure, functional group composition, crystallinity, and morphology, which critically influence adsorption capacity, selectivity, and stability. Systematic characterization of these properties is essential to understand contaminant removal mechanisms and optimize biochar design for environmental remediation applications.

Pristine biochar, typically produced through pyrolysis of biomass under limited oxygen conditions, possesses intrinsic adsorption capabilities derived from its porous structure and limited surface functional groups. However, these natural physicochemical properties often constrain performance in complex wastewater treatment, particularly when multiple contaminants coexist. In contrast, E-BC is modified through physical, chemical, or nanomaterial-based strategies to enhance adsorption capacity, selectivity, and stability.

Approaches such as metal doping (e.g., Fe, Mn, Mg), acid/base activation, magnetic modification, and incorporation of nanocomposites introduce additional functional groups, increase surface area, and improve structural properties, rendering engineered biochar a more versatile and effective material for environmental remediation [47].

3.1. Chemical activation

Chemical activation is one of the most widely applied strategies to enhance the physicochemical properties of biochar, particularly its surface area, pore volume, porosity, cation exchange capacity (CEC), and surface functional groups [48]. This approach generally involves treating biomass or pristine biochar with acids (e.g., H_2SO_4, HCl, HNO_3, H_3PO_4), alkalis (e.g., KOH, NaOH), metal salts, or oxidizing agents such as $KMnO_4$ and Fe(III) under controlled thermal conditions and often in an inert atmosphere [49-54]. Activation can be conducted via one-step or two-step processes: in the one-step method, pyrolysis and chemical activation occur simultaneously, whereas in the two-step method, biochar is first produced by pyrolysis and subsequently subjected to chemical activation followed by secondary heat treatment [55]. Comparative studies indicate that the two-step process generally promotes greater surface area and pore structure development than the one-step route. Acid treatments typically enrich oxygen-containing functional groups, while alkaline modification enhances carbon content and microporosity; oxidizing agents further enlarge pore size and specific surface area. Beyond simple acid-base treatments, chemical modification also includes coating and impregnation techniques to produce biochar-based composites. In these methods, high-surface-area biochar serves as a scaffold for clays, carbonaceous materials (e.g., amino-functional polymers, chitosan, carbon nanotubes, graphene oxide), metal oxides, and functional nanoparticles [56,57]. Metal salts may be introduced either by pre-treating the biomass prior to pyrolysis or by post-synthesis impregnation, leading to the in-situ formation of metal hydroxides or nano-metal oxides within the biochar matrix. Although nanoparticles possess high surface reactivity and multiple active sites, their instability can limit direct application; immobilization onto biochar effectively overcomes this drawback while improving porosity, functional group diversity, thermal stability, and contaminant affinity.

More recently, oxygen plasma activation has emerged as an environmentally friendly and efficient alternative to conventional chemical treatments. In this process, oxygen gas is ionized under dielectric barrier discharge conditions, generating reactive species such as electrons and oxygen ions that interact with the biochar surface. This interaction introduces additional oxygen-containing functional groups and increases surface reactivity without extensive chemical consumption.

For example, Wang et al. demonstrated the effectiveness of oxygen plasma treatment as a green activation strategy for raw biochar subsequently applied as an electrode material in electric double-layer capacitors (EDLCs) and capacitive deionization (CDI) systems. Plasma treatment significantly enhanced electrochemical performance, increasing the specific capacitance from 80 to 97.5 F g^{-1}. In addition, the desalination capacity of plasma-activated biochar was approximately 1.2 times higher than that of untreated biochar. These improvements were attributed to the modulation of surface functional groups, surface charge, and textural characteristics induced by plasma activation [58]. These chemical and plasma-based modification strategies enable the tailored design of biochars with enhanced adsorption performance for environmental applications.

3.1.1. Acidic, Alkaline, and Oxidative Modification

Acid treatment primarily aims to remove mineral impurities and metals from the biochar surface while introducing oxygen-containing functional groups such as carboxyl (–COOH), hydroxyl (–OH), phenolic, lactonic, and carbonyl moieties [59]. Common acids used include HCl, HNO_3, H_2SO_4, H_3PO_4, citric acid, and oxalic acid. Acid oxidation generally increases hydrophilicity and may enhance microporosity and specific surface area, although the extent of these changes strongly depends on acid type and concentration. In some cases, substantial improvements in BET surface area have been reported; for example, sulfuric acid activation increased surface area more than 250-fold compared to pristine biochar [60]. However, strong acid treatment can also damage pore structures or reduce mineral components essential for certain adsorption mechanisms. For instance, while HCl modification effectively decreases ash content and removes surface metals, it may not be ideal for heavy metal adsorption, where mineral-mediated precipitation plays a key role. Additionally, excessive oxidation may weaken π–π interactions, potentially reducing adsorption of aromatic organic compounds. Liu et al. investigated the adsorption performance of chemically modified biochars derived from walnut shell (WSC) and wood powder (WPC) prepared by limited-oxygen pyrolysis. The biochars were activated with $ZnCl_2$, KOH, H_2SO_4, and H_3PO_4 and tested for methylene blue (MB) removal. The modified materials exhibited mesoporous structures,

while alkaline activation significantly enhanced pore development and specific surface area, particularly for KOH-modified biochar. The presence of oxygen-containing functional groups further increased the number of active adsorption sites. Wood-derived biochar showed superior performance compared to shell-derived biochar (WPC > WSC), and the effectiveness of activating agents followed the order $ZnCl_2$ > KOH > H_3PO_4 > H_2SO_4. The maximum adsorption capacities reached 850.9 mg g^{-1} for $ZnCl_2$-modified WPC and 701.3 mg·g^{-1} for KOH-modified WSC, highlighting the potential of chemically activated biochars for dye removal from aqueous systems [61]. Jiang et al. developed a phosphoric acid-modified biochar through the co-pyrolysis of agricultural straw and industrial tire wear particles (TWPs) for Cr(VI) removal from aqueous solutions. The optimized material (PBC-3) achieved 90.43% removal efficiency with an adsorption capacity of 10.851 mg·g^{-1}. The adsorption mechanism involved electrostatic attraction, surface complexation, and redox reactions, where Cr(VI) was partially reduced to Cr(III) or metallic Cr and immobilized on the biochar surface, while another fraction interacted with oxygen-containing groups to form CrO_3. The adsorbent also showed good stability and reusability under different environmental conditions, demonstrating the potential of waste-derived biochars for heavy metal remediation [62].

Alkaline activation, typically using KOH or NaOH, is another effective modification strategy [63]. Base treatment often promotes higher aromaticity, increases the N/C ratio, decreases the O/C ratio, and enhances pore development. It may also reduce certain acidic oxygen-containing groups (e.g., C=O) while enriching hydroxyl functionalities. NaOH is considered less corrosive and thermally stable compared to KOH in some applications. Significant surface area enhancement has been observed following alkaline treatment; for example, NaOH-modified coconut biochar exhibited improved surface roughness and adhesion properties. At NaOH concentrations of 4% and 6%, the increased surface roughness enhanced peel strength, reaching 15.6 N and 15.9 N, respectively. However, when the concentration increased to 8%, excessive surface etching reduced the peel strength to 3.7 N. These results indicate that moderate alkaline treatment can enhance surface characteristics and interfacial adhesion, whereas excessive treatment may reduce the effective surface area and adhesion performance [64]. In another study, Su et al. investigated the performance of KOH-modified biochar (KBC) for Zn removal and stabilization in bioretention systems using batch experiments and density functional theory (DFT) calculations. KBC removed 89.0–97.5% of Zn from influent water, mainly through complexation and precipitation, with precipitation being the dominant mechanism. Approximately 67% of Zn was immobilized in the residual fraction, indicating enhanced stabilization. Moreover, KBC significantly suppressed secondary Zn release under acidic and saline runoff conditions, reducing it by 43.6% and 37.08%, respectively. These results suggest that KOH-modified biochar can effectively control Zn-contaminated runoff and mitigate secondary metal release under conditions such as acid rain or snowmelt [65]. Beyond acid and alkaline activations, oxidizing agents such as H_2O_2, $KMnO_4$, and O_3 are used to introduce additional reactive oxygen species onto biochar surfaces. Oxidant-modified biochars often demonstrate improved thermal stability and strong affinity for pollutants. For example, Chang and Li reported that $KMnO_4$-modified biochar derived from cotton stem exhibited abundant surface functional groups and increased surface area, achieving a maximum Pb(II) adsorption capacity of 144.49 mg·g^{-1} at pH 5 [66]. Chemical modification using acid, alkaline, or oxidant treatments effectively enhances biochar surface chemistry and pore structure, improving the removal of metal(loid)s and organic pollutants from wastewater. Large-scale soil applications may be limited by the costs associated with chemical reagents, equipment, and energy requirements.

3.1.2. Iron modification

Iron modification has emerged as one of the most effective and commonly applied approaches to enhance the performance of biochar in large-scale environmental remediation. This is mainly attributed to the natural abundance of iron, its relatively low cost, and its lower environmental risk compared with many other metal-based modifiers. This approach is mainly applied to improve the separation and recyclability of biochar, while simultaneously enhancing its decontamination capacity through interactions between the incorporated and target contaminants [67]. Fe-modified biochars can be synthesized through different preparation techniques such as co-pyrolysis,

precipitation, thermal reduction, and ball-milling, which are generally categorized as either biomass pre-treatment or post-treatment of iron materials [68-73] (Figure 1).

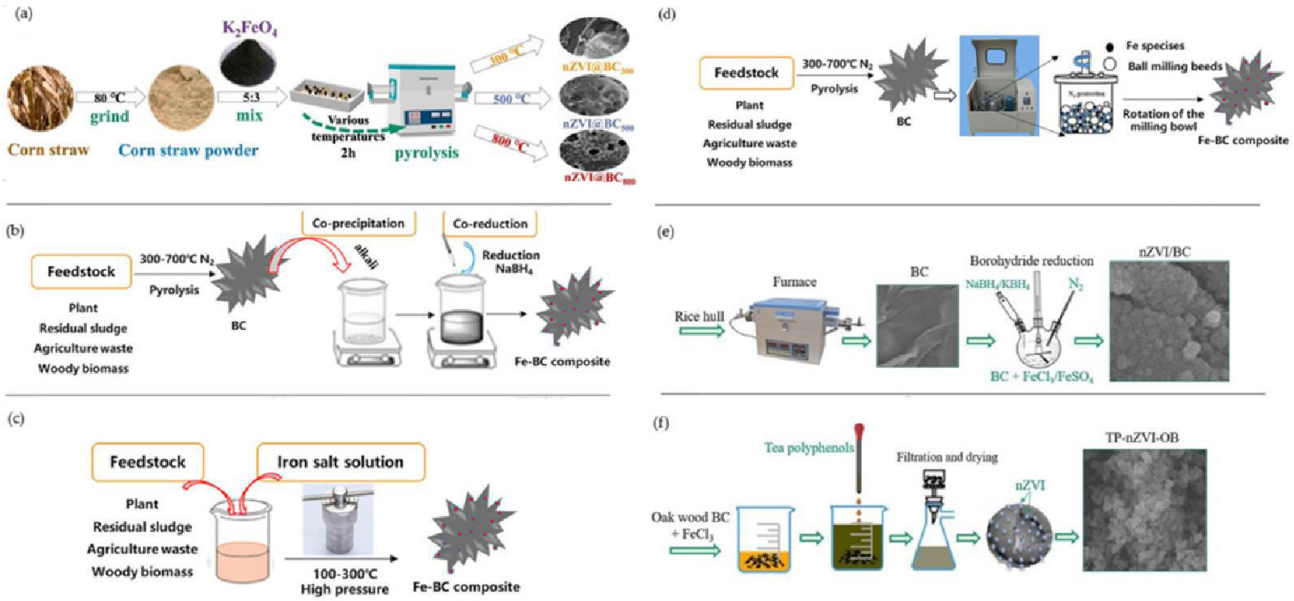

Fig. 1. Methods for preparing iron-based biochar materials: (a) one-step pyrolysis method. Reproduced with permission from ref. [70]. Copyright © 2024 Elsevier, (b) co-precipitation method, (c) hydrothermal carbonization method. Reproduced with permission from ref. [71]. Copyright © 2021 Elsevier; (d) ball milling method (e) chemical reduction method. Reproduced with permission from ref. [72]. Copyright © 2022 Elsevier, and (f) green synthesis Reproduced with permission from ref. [73]. Copyright © 2020 Elsevier.

Various iron compounds, including iron oxides (e.g., hematite (Fe_2O_3) and goethite (α-FeOOH)), iron sulfide (FeS), and nano zero-valent iron (nZVI), have been used to modify biochar [74, 75]. For example, Zhu et al. synthesized α-FeOOH-modified wheat straw biochar (α-FeOOH@BC), which exhibited maximum adsorption capacities of 63 mg g^{-1} for Cd(II) and 78 mg g^{-1} for As(III) [76]. Similarly, Kim et al. modified rice husk biochar through ball-milling with iron-based materials, magnetite (Fe_3O_4) and pyrite (FeS_2), followed by re-pyrolysis at 600 °C to produce Fe_3O_4-BC and FeS_2-BC. In dual-element aqueous systems, Fe_3O_4-BC achieved 99.62% Cd and 62.39% As removal, while FeS_2-BC removed 81.73% Cd and 55.54% As. In comparison, unmodified biochar showed slightly lower efficiencies (99.04% Cd and 54.31% As), indicating the enhancement provided by iron-based modification [77]. Beyond adsorption, Fe-modified biochar can also facilitate redox reactions that reduce the toxicity of contaminants such as As(III), Cr(VI), and U(VI) [78]. Materials modified with nZVI, FeS, or FeOOH can provide reductive species such as Fe^0, Fe(II), or S(II), enabling the transformation of hazardous compounds into less toxic forms. For instance, Zhou et al. reported that nZVI-modified biochar achieved an adsorption capacity of 54.4 mg·g^{-1} for Cr(VI) while simultaneously reducing it to the less toxic Cr(III) [79]. Similarly, Liu et al. also observed that FeS- and starch-modified peanut shell biochar effectively reduced U(VI) to stable U(IV) species, highlighting the role of Fe^0 and S(II) in the reduction mechanism [80]. Due to its electron-transfer capacity, persistent free radicals, and oxygen-containing functional groups, Fe-modified biochar can activate oxidants such as H_2O_2, peroxomonosulfate (HSO_5^-, PMS), peroxodisulfate ($S_2O_8^{2-}$, PDS), and ozone to generate reactive oxygen species (ROS), including •OH, $^1O_2$, and SO_4•$^-$ (Equations (1), (2), (3), (4))). These species contribute to the degradation of various organic pollutants, including tetracycline, bisphenol A, metronidazole, and phthalate esters [81-84]. Therefore, Fe-modified biochar is also widely investigated as a catalyst in advanced oxidation processes, particularly in Fenton-like and persulfate activation systems [85]. For example, Herath et al. developed developed a metal oxide–biochar composite (Fe_2TiO_5/BC) for the simultaneous removal of Pb^{2+}, Cr^{6+}, F^-, and methylene blue (MB) from aqueous solutions. Under acidic conditions (pH 3), partial iron leaching promoted Photo-Fenton degradation of MB. Band gap analysis of Fe_2TiO_5, BC, and Fe_2TiO_5/BC indicated improved photocatalytic activity compared with

conventional TiO_2-based systems. Under UV irradiation (365 nm), MB removal occurred through a combined adsorption–photocatalytic mechanism at pH 3–6. The composite also showed high removal efficiencies for Cr^{6+}, Pb^{2+}, F^-, and MB even in the presence of multiple competing ions in simulated water systems [86].

$$H_2O_2 + Fe^{2+} \rightarrow OH^- + \bullet OH + Fe^3 \quad (1)$$

$$HSO_5^- + Fe^{2+} \rightarrow SO_4^{\bullet-} + OH^- + Fe^{3+} \quad (2)$$

$$HSO_5^- + Fe^{2+} \rightarrow SO_4^{2-} + \bullet OH + Fe^{3+} \quad (3)$$

$$S_2O_8^{2-} + Fe^{2+} \rightarrow SO_4^{\bullet-} + SO_4^{2-} + Fe^{3+} \quad (4)$$

Despite these advantages, conventional iron-based Fenton catalysts tend to aggregate and may suffer from iron ion leaching, which can reduce catalytic efficiency [87]. To address this limitation, various carbon-based supports such as reduced graphene oxide (rGO), carbon nanotubes, and activated carbon have been employed to improve the dispersion of active iron species and enhance catalytic stability [88].

3.1.3. Metal oxides and metal salts

The incorporation of metal oxides or metal salts onto biochar can significantly improve its adsorption performance by introducing additional functional active sites on the surface. Among various metals used for modification, Fe is the most widely studied and has been discussed in detail in Section 3.1.2. In addition to Fe, manganese (Mn) has attracted considerable attention because of its natural abundance, relatively simple preparation procedures, and environmentally friendly characteristics [89]. For instance, Jia et al. synthesized a series of Mn-coated biochars with different Mn-to-biochar mass ratios using $MnSO_4 \cdot H_2O$ as the precursor. The prepared materials exhibited maximum adsorption capacities of 0.94 $mg \cdot g^{-1}$ for Sb(III) and 0.73 $mg \cdot g^{-1}$ for Sb(V). Furthermore, Mn-modified biochar has shown excellent catalytic activity in persulfate activation systems [90]. In addition, Liu et al. reported that Mn-modified nMnOx@RBC biochar achieved nearly 100% removal efficiency of 4-chloro-3-methylphenol (CMP), which was mainly attributed to the generation of reactive oxygen species such as $SO_4\bullet^-$, •OH, and $^1O_2$, promoting the degradation of CMP [91]. Besides Fe and Mn, a variety of other metals have also been explored for biochar modification, including magnesium (Mg) [92], aluminum (Al) [93], copper (Cu) [94], cerium (Ce) [81], lanthanum (La) [95], zirconium (Zr) [96], and bismuth (Bi) [97]. These studies demonstrate that incorporating different metal species into biochar enhances adsorption performance and catalytic activity, highlighting the versatility of metal-modified biochars.

3.1.4. Nonmetallic heteroatoms

Doping biochar with non-metallic heteroatoms has recently gained increasing attention as an effective strategy to tailor the electronic structure and surface chemistry of biochar, thereby improving its adsorption and catalytic capabilities for pollutant removal [47]. Among the various heteroatoms explored, nitrogen (N), sulfur (S), and boron (B) are the most frequently used elements for biochar modification. In addition, phosphorus-doped [98] and iodine-doped biochars [99] have also been reported for the removal of contaminants from aqueous systems.

Nitrogen is the most studied heteroatom in biochar doping, where it integrates into the carbon framework in various configurations, markedly affecting surface chemistry and catalytic properties.

Nitrogen in doped biochar generally exists as amine functional groups, pyridinic N, pyrrolic N, graphitic N, and nitrogen oxide species ($–NO_x$) [100] (Figure 2). Graphitic nitrogen facilitates electron mobility within the carbon matrix, which improves catalytic efficiency during processes such as persulfate activation [101]. In contrast, pyrrolic and pyridinic nitrogen species can donate electrons and generate structural defects, providing additional active sites on the biochar surface. Amine-type nitrogen groups can also serve as coordination sites for metal(loid) ions through chelation interactions [102]. Owing to these characteristics, N-doped biochar has been widely investigated for the removal of various contaminants including antibiotics [103], phenolic compounds [104], dyes [105-107], and heavy metals[108-112].

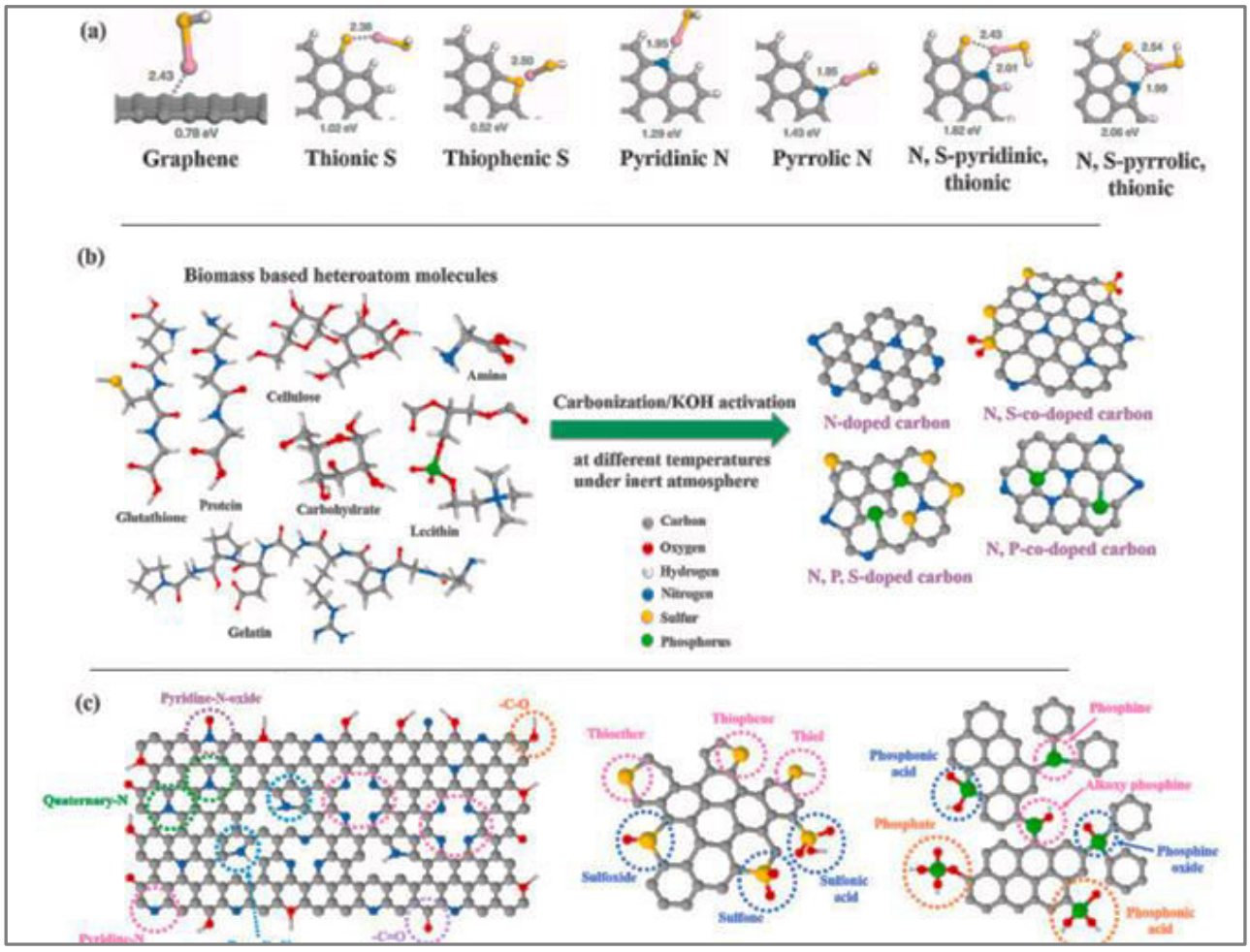

Fig. 2. (a) Model of binding energy of undoped graphene, S-doped graphene, N-doped graphene, and N, S-co-doped graphene with LiSH interaction, (b) schematic illustration of heteroatoms self-doped porous carbon derived from biomass sources; Types of N, P and S in biomass. Reproduced with permission from Ref. [100] Copyright © 2024 Elsevier.

Nitrogen doping enhances biochar properties such as pore structure, surface area, conductivity, catalytic activity, and adsorption capacity, while nitrogen-containing functional groups can actively promote catalytic reactions like ester hydrolysis [113,114]. Similarly, sulfur doping introduces functional groups (C–S, C–S–C, C=S, C–S–O, $–SO_3^{2-}$, $–SO_4^{2-}$) that improve adsorption and catalytic behavior [107,115,116]. For example, Ahmed et al. showed that sulfur-modified sawdust biochar significantly increased Cd adsorption (up to 9-fold), with maximum capacities of 39.38, 20.84, and 34.14 mg g^{-1} depending on the sulfur source, via mechanisms including electrostatic attraction, Cd–π interactions, surface complexation, and ion exchange [117].

Boron doping similarly alters electronic structure, increases defects and active sites, and improves surface chemistry [118]. Boron-modified corn-straw biochar exhibited a high surface area (898 m^2 g^{-1}) and enhanced Fe(II) adsorption via surface complexation, ion exchange, and co-precipitation [118]. Boron incorporation is typically achieved during pyrolysis using boric acid, borax, or boron carbide, or via hydrothermal carbonization followed by doping. For instance, Xue et al. [119] prepared a boron-doped biochar by initially converting *Zoysia sinica* into hydrothermal carbon (HC) through hydrothermal treatment at 180 °C for 4 h. The resulting HC then served as a precursor material for subsequent boron doping and carbonization. Pyrolysis is the most common method for boron incorporation due to its simplicity, scalability, and efficiency. In this process, biomass or pre-activated biochar is thermally treated to integrate boron species, typically sourced from boric acid, sodium tetraborate decahydrate (borax), or boron carbide, into the carbon framework.

Liu et al. [120] demonstrated that when boric acid is mixed with ethanol, a chemical reaction occurs leading to the formation of triethyl borate. During thermal treatment, this compound interacts with hydroxyl groups present in cellulose, hemicellulose, and lignin within the biomass structure.

3.1.5. Carbon nanomaterials

Carbon nanomaterials such as graphene, graphene oxide, carbon nanotubes, and graphitic carbon nitride are widely employed as functional modifiers in the synthesis of biochar-based composites [121]. These materials exhibit a strong affinity toward a wide range of pollutants; therefore, incorporating carbon nanomaterials into biochar structures has attracted considerable attention as a strategy to improve adsorption capacity for toxic contaminants. Among these materials, graphene is a two-dimensional structure composed of sp^2-hybridized carbon atoms arranged in a hexagonal lattice. This unique configuration provides several outstanding physicochemical properties, including high electron mobility, strong π–π interactions, excellent mechanical strength, high biocompatibility, and a remarkably large specific surface area. Owing to these characteristics, graphene demonstrates strong adsorption potential for both organic and inorganic contaminants. Consequently, graphene-modified biochar composites have been explored as effective sorbents for environmental remediation. However, despite their high adsorption capacity, the production of graphene-based biochar often requires extensive pretreatment processes, which significantly increase the cost and limit their feasibility for large-scale applications [122,123].
Graphene oxide (GO) has been extensively investigated as a functional modifier for biochar. Several studies have demonstrated that GO-modified biochar can effectively remove heavy metals such as Cd(II), Cr(VI), As(III) and As(V), and Pb(II), as well as organic contaminants including atrazine. These materials typically interact with pollutants through mechanisms such as complexation, electrostatic attraction, and strong binding with oxygen-containing functional groups present on the graphene-based biochar surface [124]. For example, Liu et al. developed a graphene-modified biochar (GB) supported nanoscale zero-valent iron composite (GB/nZVI) for the simultaneous removal of Cd(II) and As(III) under aerobic conditions. The composite exhibited high sorption capacities of 363 $mg \cdot g^{-1}$ for As(III) at pH 4 and 92.8 $mg \cdot g^{-1}$ for Cd(II) at pH 7, calculated based on the nZVI content. These values were considerably higher than those achieved using GB or nZVI individually, indicating a strong synergistic interaction between the two components. In this system, GB promoted the oxidation of nZVI to iron oxyhydroxides, which also facilitated the conversion of approximately 35% of As(III) to As(V). Moreover, the presence of As(III) further improved Cd(II) removal, reaching 131.8 $mg \cdot g^{-1}$ [125].
Despite these advantages, carbon nanomaterial-coated biochars face limitations, including the lack of comprehensive studies on their long-term stability and environmental impacts in soil systems, which hinders large-scale implementation [126]. Furthermore, many coatings are non-biodegradable and costly to synthesize, limiting their economic feasibility for environmental applications.

3.1.6. Clay minerals

Natural clay minerals such as bentonite, montmorillonite, sepiolite, vermiculite, zeolite, kaolinite, and illite (Figure 3) are abundant, inexpensive, and nontoxic materials widely explored for heavy metal removal due to their layered structures, large surface areas, and ion-exchange capacities. For example, bentonite and montmorillonite exhibit strong electrostatic attraction toward metal ions, while vermiculite and sepiolite provide additional adsorption sites through interlayer interactions and surface complexation. Kaolinite and illite generally show lower adsorption capacities due to tightly bound layers and restricted cation exchange, but their performance can be enhanced via surface modifications or incorporation into biochar composites.
Several studies illustrate the potential of these materials: Ramola et al. demonstrated nearly complete Pb removal using bentonite-biochar composites [127], while Zhang et al. reported effective removal of multiple heavy metals using montmorillonite-based biochar composites [128]. Deng et al. highlighted phosphate removal using sepiolite-modified biochar [129], and Al-Swadi et al. showed pH-dependent adsorption improvements on kaolinite-modified biochar [130].
Integrating clay minerals with biochar enhances porosity, cation exchange capacity, and adsorption efficiency, making clay-biochar composites promising materials for water remediation [131].

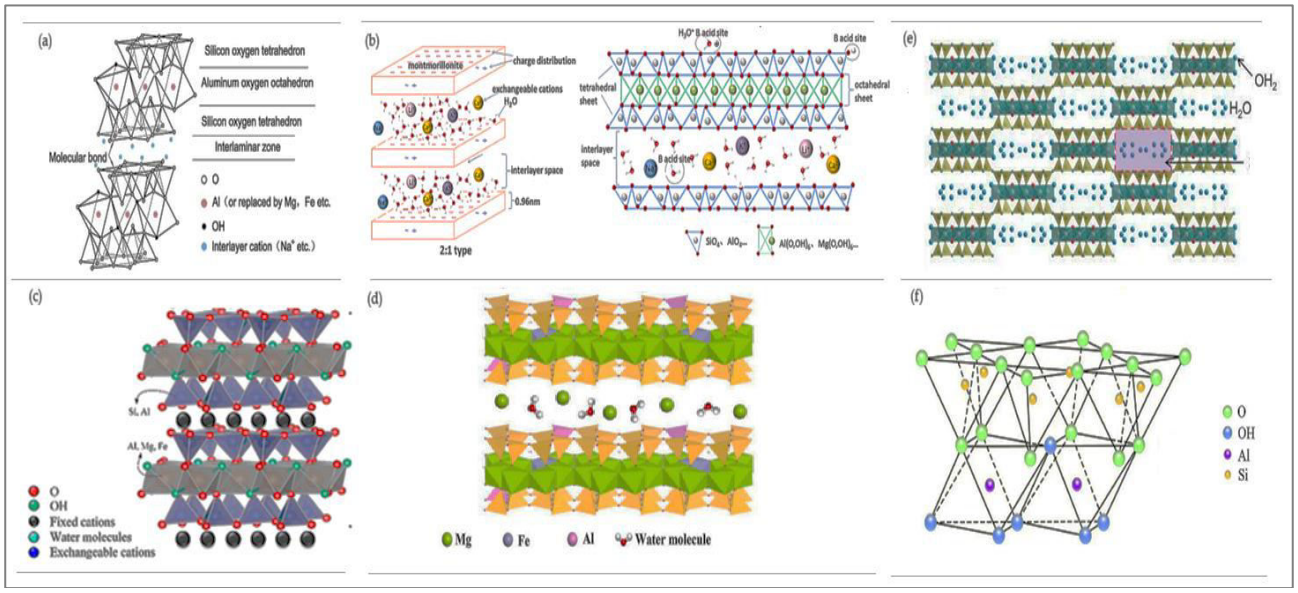

Fig. 3. Crystal structures of (a) bentonite, (b) montmorillonite (MMT), (c) illite, (d) vermiculite, (e) sepiolite and (f) kaolinite. (a) Reproduced with permission from Ref. [132] Copyright © 2024 Elsevier. (b) Reproduced with permission from Ref. [133] Copyright © 2025 Elsevier. (c) Reproduced from [125] under the Creative Commons CC BY license 4.0. (d) Reproduced with permission from Ref. [134] Copyright © 2022 Elsevier. e) sepiolite Reproduced with permission from Ref. [135] Copyright © 2024 Elsevier and (f) Reproduced with permission from Ref. [136] Copyright © 2022 Elsevier

3.1.7. Layer double hydroxides (LDHs)

Layered double hydroxides (LDHs) are effective adsorbents due to their layered structure and strong anion-exchange capability [137]. However, dense stacking can limit adsorption efficiency [138]. To overcome this, LDH nanoparticles are often combined with biochar, resulting in BC/LDH composites with enhanced surface area, functional groups, stability, and overall adsorption performance [139-41]. For example, MgAl-LDH/biochar from engineered wood sawdust efficiently removed Pb and Cr ions [142] (Figure 4a), while ZnCo-LDH/biochar showed improved photocatalytic degradation of antibiotics due to reduced particle aggregation [143]. Wang et al. further demonstrated that E-Mg/Al-LDH-BC removed Pb(II) and Cd(II) via cation exchange, surface complexation, mineral precipitation, and electrostatic interactions [144] (Figure 4b). These results highlight the potential of LDH-biochar composites as multifunctional materials for water remediation.

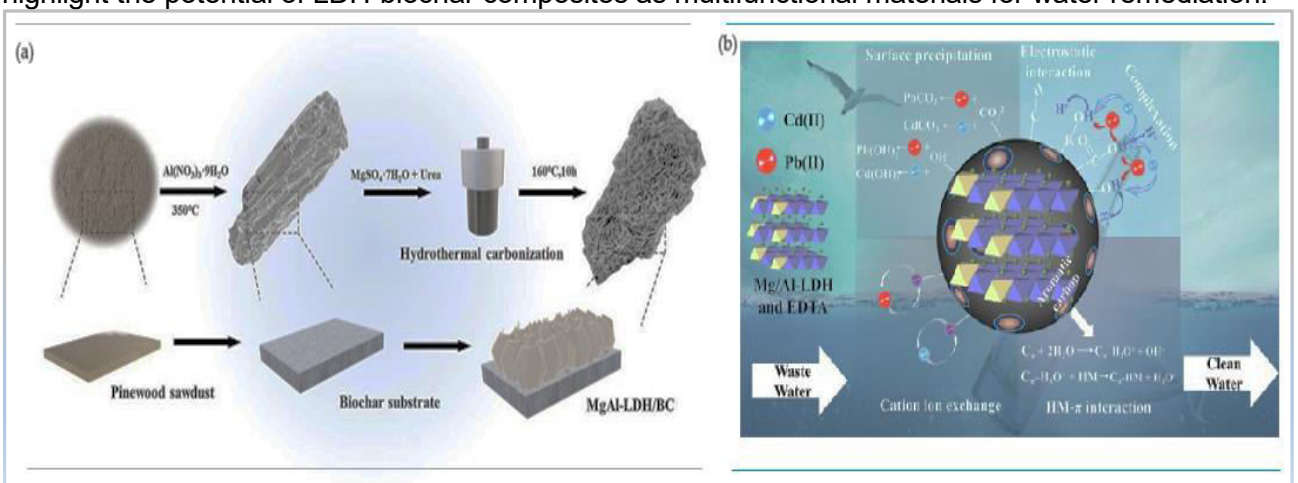

Fig. 4. (a) Preparation of MgAl-LDH/BC and illustration of its structure. Reproduced with permission from Ref. [142] Copyright © 2020 Elsevier. (b) Scenario diagram of the removal mechanism. Reproduced with permission from Ref. [144] Copyright © 2024 Elsevier.

3.1.8. Organic surfactants

Organic surfactants can also modify biochar surface properties, influencing surface area, functional groups, and hydrophobicity. Surfactant molecules attach through electrostatic, hydrogen-bonding, π–π, and hydrophobic interactions, forming mono- or bilayers that enhance adsorption of both inorganic and organic pollutants (Figure 5). For instance, CTAB-functionalized peanut shell biochar improved Cr(VI) removal from 37.47% (pristine) to 79.35% [146]. Similarly, SDS/SAP-modified biochar (SDMBC) significantly increased adsorption capacities for Pb(II), Cd(II), and various organics, maintaining performance even in mixed pollutant systems [145]. Broccoli-derived biochar modified with H_2SO_4 and CTAB achieved removal efficiencies of up to 99.9% for dyes and 98.6% for Pb^{2+} [147]. Non-ionic surfactants like Triton X-100 have been used to improve Pb(II) uptake while sometimes reducing polymer adsorption [148]. These studies illustrate that surfactant modification can tailor biochar properties and create new adsorption pathways, enhancing its versatility for water treatment.

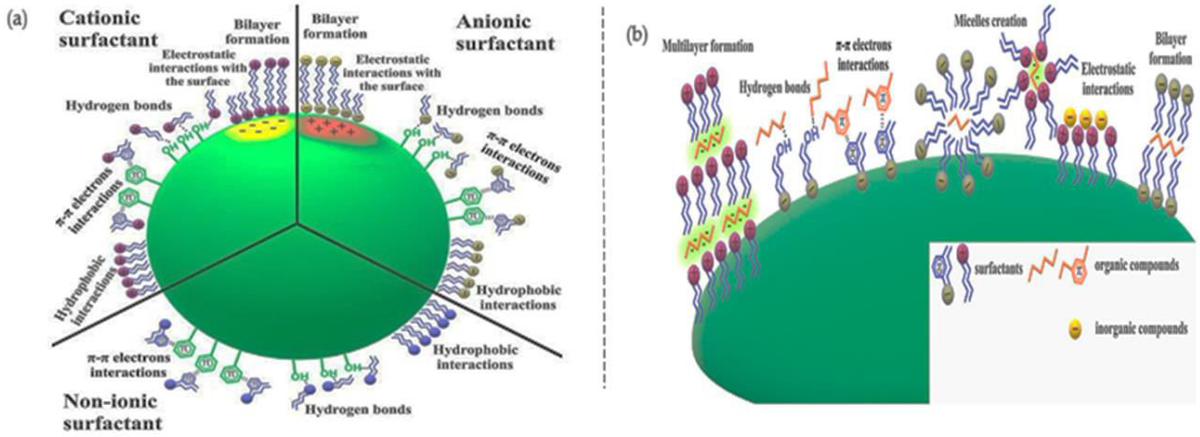

Fig. 5. (a) Possible adsorption mechanisms of surfactants with various ionic character on biochar surface. (b) Possible mechanisms of organic and inorganic compounds adsorption on surfactant-modified biochar surface. Reproduced from [145] under the Creative Commons CC BY license 4.0.

These studies demonstrate that surfactant modification can significantly alter the physicochemical properties of biochar and create new adsorption pathways, thereby improving its effectiveness for the removal of a wide range of organic pollutants and heavy metals from aqueous environments. Similar advancements in adsorption and sensor-based monitoring techniques have been reported for water treatment systems, highlighting the potential of engineered materials for enhanced contaminant removal [149-153].

4. Conclusions

Chemical modification enhances biochar's adsorption, surface functionality, and catalytic activity. Acidic, alkaline, oxidative treatments, and incorporation of metals or metal oxides enable efficient removal of heavy metals and organic pollutants. While laboratory-scale studies show high efficiency and tunable properties, challenges remain in scaling up, ensuring stability, and cost optimization. Chemically modified biochars thus offer a versatile and promising solution for sustainable water and wastewater treatment.

Conflicts of Interest: The authors declare no conflict of interest.
ORCIDs: D. Şahin, https://orcid.org/0000-0003-3519-4434. Ș. Țălu, https://orcid.org/0000-0003-1311-7657.

References

[1] Ejiohuo, Ovinuchi, Helen Onyeaka, Adenike Akinsemolu, Ozioma Forstinus Nwabor, Kehinde Favour Siyanbola, Phemelo Tamasiga, and Zainab T. Al-Sharif. "Ensuring Water Purity: Mitigating Environmental Risks and Safeguarding Human Health." *Water Biology and Security* 4, no. 2 (2025): 100341. https://doi.org/10.1016/j.watbs.2024.100341.

[2] Mozaffari, Nastaran, Ștefan Ţălu, Niloofar Mozaffari, Mika Sillanpää, Viola Vambol, and Sergij Vambol. “Chapter 2: Pharmaceuticals Measurements and Estimation Methods.” In *Hospital Wastewater Treatment: Global Scenario and Case Studies*, chapter 2, 10–26. Eds. N. A. Khan, V. Vambol, S.j Vambol, N. Mozaffari, N. Mozaffari. London, IWA Publishing, July 2022. https://doi.org/10.2166/9781789062625_0013.

[3] Ravi, Gudiguntla, Niranjan Patra, and Ștefan Ţălu. “Efficient Sunlight-Driven Degrdation of Methylene Blue using Hydrothermally Synthesized Copper Oxide/Zinc Oxide Hybrid Composites.” *Next Materials*, no. 9 (2025): 101128. https://doi.org/10.1016/j.nxmate.2025.101128.

[4] Adam, A. Bilyaminu, J. B. Mu'azu, O. adeshewa titilayo, Passali D. B., A. Emmanuel Ba'aku, J. Gani, and M. Yahaya Abubakar. “The Role of Organic Pollutants in Water Pollution: A Review.” *Journal of Chemical Technology* 1 (2025): 142–159. https://doi.org/10.22034/JCHEMTECH.2025.528420.1006.

[5] Barka, Evridiki, Constantinos Noutsopoulos, and Andriani Galani Barka. “Removal of Contaminants of Emerging Concern from Wastewater Using an Integrated Column System Containing Zero Valent Iron Nanoparticles.” *Water* 15, no. 3 (2023): 598. https://doi.org/10.3390/W15030598.

[6] Georgin, Jordana, Dison Stracke Franco, Ramo Pfingsten, Claudete Gindri, et al. “A Review of the Antibiotic Ofloxacin: Current Status of Ecotoxicology and Scientific Advances in Its Removal from Aqueous Systems by Adsorption Technology.” *Chemical Engineering Research and Design* 193 (2023): 99–120. https://doi.org/10.1016/j.cherd.2023.03.025.

[7] Mahmoud, Alaa El Din, Manal Fawzy, and Nadeem Ahmad Khan. *Artificial Intelligence and Modeling for Water Sustainability: Global Challenges.* Boca Raton, CRC Press, 2023.

[8] Kaur, Manmeet, et al. “A Review on Heavy Metal Accumulation and Toxicity in Biotic and Abiotic Components.” *IOP Conference Series: Earth and Environmental Science* 889 (2021): 012062. https://doi.org/10.1088/1755-1315/889/1/012062.

[9] Ding, Chunlian, Jianxin Chen, Feng Zhu, et al. “Biological Toxicity of Heavy Metal(loid)s in Natural Environments: From Microbes to Humans.” *Frontiers in Environmental Science* 10 (2022): 920957. https://doi.org/10.3389/fenvs.2022.920957.

[10] Gao, Zhongyuan, Shiyi Zhang, Chengzhong Fu, Jun Xiang, et al. “Non-Target Screening and Priority Assessment of Organic Pollutants in Tropical Island Watershed Water.” *Ecotoxicology and Environmental Safety* 303 (2025): 118872. https://doi.org/10.1016/j.ecoenv.2025.118872.

[11] Morin-Crini, Nadia, Eric Lichtfouse, Guorui Liu, et al. “Worldwide Cases of Water Pollution by Emerging Contaminants: A Review.” *Environmental Chemistry Letters* 20 (2022): 2311–2338. https://doi.org/10.1007/s10311-022-01447-4.

[12] Madesh, S., Sanjai Gopi, Avra Sau, et al. “Chemical Contaminants and Environmental Stressors Induced Teratogenic Effect in Aquatic Ecosystem: A Comprehensive Review.” *Toxicology Reports* 13 (2024): 101819. https://doi.org/10.1016/j.toxrep.2024.101819.

[13] Abbasi, Sedigheh, Davoud Dastan, Ștefan Ţălu, Muhammad Bilal Tahir, Md. Elias, Lin Tao, and Zhi Li. “Evaluation of the Dependence of Methyl Orange Organic Pollutant Removal Rate on the Amount of Titanium Dioxide Nanoparticles in MWCNTs-TiO_2 Photocatalyst Using Statistical Methods and Duncan's Multiple Range Test.” *International Journal of Environmental Analytical Chemistry* 104, no. 9 (2024): 2180–2194. https://doi.org/10.1080/03067319.2022.2060085.

[14] Ricardo, Ivo A., Edna A. Alberto, Afonso H. Silva Junior, Domingos P. Macuvele, Natan Padoin, Cintia Soares, et al. “A Critical Review on Microplastics, Interaction with Organic and Inorganic Pollutants, Impacts and Effectiveness of Advanced Oxidation Processes Applied for Their Removal from Aqueous Matrices.” *Chemical Engineering Journal* 424 (2021): 130282. https://doi.org/10.1016/j.cej.2021.130282.

[15] Atugoda, Thilakshani, Meththika Vithanage, Hasintha Wijesekara, et al. “Interactions between Microplastics, Pharmaceuticals and Personal Care Products: Implications for Vector Transport.” *Environment International* 149 (2021): 106367. https://doi.org/10.1016/j.envint.2020.106367.

[16] Saini, Ankita, and Sunil Kumar Saini. “Polymer Composites for Environmental Pollution and Remediation.” In *Polymer Composites: From Computational to Experimental Aspects*, 151–180. Singapore, Springer, 2024. https://doi.org/10.1007/978-981-97-0888-8_8.

[17] Ko, Young Gun. “Hybrid Method Integrating Adsorption and Chemical Precipitation of Heavy Metal Ions on Polymeric Fiber Surfaces for Highly Efficient Water Purification.” *Chemosphere* 363 (September 2024): 142909. https://doi.org/10.1016/j.chemosphere.2024.142909.

[18] Ahmad, Arslan, Sam Rutten, Martijn Eikelboom, et al. “Impact of Phosphate, Silicate and Natural Organic Matter on the Size of Fe(III) Precipitates and Arsenate Co-Precipitation Efficiency in Calcium Containing Water.” *Separation and Purification Technology* 235 (2020): 116117. https://doi.org/10.1016/j.seppur.2019.116117.

[19] Fu, Zheng-Jun, Shang-Kun Jiang, Xin-Yi Chao, et al. “Removing Miscellaneous Heavy Metals by All-in-One Ion Exchange–Nanofiltration Membrane.” *Water Research* 222 (2022): 118888.

[20] Şahin, Deniz, Okan Taş, and Senay Taşcıoğlu. "Determination of Pb(II) Ions in Wastewater by Differential Pulse Polarography Combined with Surfactants and Membrane Filtration Process." *Fresenius Environmental Bulletin* 26, no. 12 (2017): 7128–7136.

[21] Şahin, Deniz, and Senay Taşcıoğlu. "Removal of Cu(II) Ions from Single Component and Cd(II)-Containing Solutions by Micellar Enhanced Ultrafiltration Utilizing Micellar Effects on Complex Formation." *Desalination and Water Treatment* 57, no. 24 (2016): 11143–11153. https://doi.org/10.1080/19443994.2015.1042059.

[22] Şahin, Deniz. "Membrane Filtration–Flame Atomic Absorption Spectrometry for Determination of Trace Amounts of Copper Ions in Water Samples." *Academia Journal of Scientific Research* 7, no. 4 (2019): 239–243. https://doi.org/10.15413/ajsr.2018.0207.

[23] Şahin, Deniz, and Senay Taşcıoğlu. "Removal of Pb(II) Ions from Aqueous Solution Using Complexation–Ultrafiltration." *Polish Journal of Chemical Technology* 20, no. 2 (2018): 80–84. https://doi.org/10.2478/pjct-2018-0026.

[24] Şahin, Deniz. "Determining the Trace Amounts of Zinc by Membrane Filtration–Sensitized Flame Atomic Absorption Spectrometry in Water Samples." *Romanian Biotechnological Letters* 23, no. 5 (2018): 13941–13947. https://doi.org/10.26327/RBL2018.203.

[25] Şahin, Deniz, and Senay Taşcıoğlu. "Separation of Cu(II) Ions from Single-Component and Cd(II)-Containing Solutions by LM-MEUF Utilizing Micellar Effects of CTAB and TX100 on Complex Formation." *Desalination and Water Treatment* 118 (2018): 143–152. https://doi.org/10.5004/dwt.2018.22317.

[26] Hailu, Awraris, and Feleke K. Sishu. "Application of Enhanced Coagulation in Drinking Water Treatment from the Degraded Catchment to Reduce NOM: A Major DBP Precursor." *Water Supply* 25, no. 2 (2025): 303–314. https://doi.org/10.2166/ws.2025.010.

[27] Pivokonsky, Martin, Katerina Novotna, Radim Petricek, et al. "Fundamental Chemical Aspects of Coagulation in Drinking Water Treatment—Back to Basics." *Journal of Water Process Engineering* 57 (January 2024): 104660. https://doi.org/10.1016/j.jwpe.2023.104660.

[28] Li, Hongna, Yunlong Tian, Wen Liu, et al. "Impact of Electrokinetic Remediation of Heavy Metal Contamination on Antibiotic Resistance in Soil." *Chemical Engineering Journal* 400 (2020): 125866. https://doi.org/10.1016/j.cej.2020.125866.

[29] Huang, Liping, Huilin Wan, Shiping Song, Deqiang Liu, and Gianluca Li Puma. "Complete Removal of Heavy Metals with Simultaneous Efficient Treatment of Etching Terminal Wastewater Using Scaled-Up Microbial Electrolysis Cells." *Chemical Engineering Journal* 439 (2022): 135763. https://doi.org/10.1016/j.cej.2022.135763.

[30] Pathak, Atin K., Richa Kothari, V. V. Tyagi, and Sanjeev Anand. "Integrated Approach for Textile Industry Wastewater for Efficient Hydrogen Production and Treatment through Solar PV Electrolysis." *International Journal of Hydrogen Energy* 45 (2020): 25768–25782. https://doi.org/10.1016/j.ijhydene.2020.03.079.

[31] Zhang, Yonghao, Liankai Gu, and Ying Zhang. "Energy-Efficient Reuse of Bio-Treated Textile Wastewater by a Porous-Structure Electrochemical PbO_2 Filter: Performance and Mechanism." *Environmental Research* 231 (2023): 116254. https://doi.org/10.1016/j.envres.2023.116254.

[32] Sun, Shaobin, Hong Yao, Wanyi Fu, Shan Xue, and Wen Zhang. "Enhanced Degradation of Antibiotics by Photo-Fenton Reactive Membrane Filtration." *Journal of Hazardous Materials* 386 (2020): 121955. https://doi.org/10.1016/j.jhazmat.2019.121955.

[33] Pan, Xuqin, Zhepei Gu, Weiming Chen, and Qibin Li. "Preparation of Biochar and Biochar Composites and Their Application in a Fenton-Like Process for Wastewater Decontamination: A Review." *Science of the Total Environment* 754 (2021): 142104. https://doi.org/10.1016/j.scitotenv.2020.142104.

[34] Yeasmin, Farzana, Md. Rasheduzzaman, Mohammed Manik, and Mahbubul Hasan Mehedi. "Activated Sludge Process for Wastewater Treatment." In *Advanced and Innovative Approaches of Environmental Biotechnology in Industrial Wastewater Treatment*, 23–50. Singapore, Springer, 2023. https://doi.org/10.1007/978-981-99-2598-8_2.

[35] Prasad, Yagna K. "Sedimentation in Water and Used Water Purification." In *Handbook of Water and Used Water Purification*, 29–54. Cham, Springer Nature, 2020.

[36] Omidvar, Akbar. "Removal of Toxic Heavy Metal Ions from Waste Water Using Superchalcogens: A Theoretical Study." *Journal of Environmental Chemical Engineering* 9 (2021): 104787.

[37] Siipola, Virpi, Stephan Pflugmacher, Henrik Romar, Laura Wendling, and Pertti Koukkari. "Low-Cost Biochar Adsorbents for Water Purification Including Microplastics Removal." *Applied Sciences* 10 (2020): 788. https://doi.org/10.3390/app10030788.

[38] Fahmy, Tamer Y. A., Yehia Fahmy, Fardous Mobarak, Mohamed El-Sakhawy, and Ragab Abou-Zeid. "Biomass Pyrolysis: Past, Present, and Future." *Environment, Development and Sustainability* 22 (2020): 17–32. https://doi.org/10.1007/s10668-018-0200-5.

[39] Sakhiya, Anil Kumar, and Abhijeet Anand. "Production, Activation and Application of Biochar in Recent Times." *Biochar* (2020). https://doi.org/10.1007/s42773-020-00047-1.

[40] Wei, Ming, Bing Wang, Pan Wu, et al. "Electrolytic Manganese Residue–Biochar Composite for Simultaneous Removal of Antimony and Arsenic from Water: Adsorption Performance and Mechanisms." *Journal of Cleaner Production* 437 (2024): 140623. https://doi.org/10.1016/j.jclepro.2024.140623.

[41] Jiang, Tao, Bing Wang, and Masud Hassan. "Green Synthesis of Natural Limonite-Modified Biochar Catalyst for Peroxymonosulfate Activation in Efficient Degradation of Carbamazepine in Water." *Journal of Environmental Chemical Engineering* 13 (2025): 115522. https://doi.org/10.1016/j.jece.2025.115522.

[42] Mohsenzadeh, Abas, Maria Persson, Anita Pettersson, and Flemming Jappe Frandsen. "Biochar for the Removal of Microplastics from Water: A Comprehensive Scoping Review." *Microplastics* 4, no. 4 (2025): 99. https://doi.org/10.3390/microplastics4040099.

[43] Peng, Zhengjie, Shikai Li, Hao He, Yujiao Wen, et al. "FeS and Fe_3O_4 Co-Modified Biochar to Build a Highly Resistant Advanced Oxidation Process System for Quinclorac Degradation in Irrigation Water." *Journal of Environmental Management* 348 (2023): 119492. https://doi.org/10.1016/j.jenvman.2023.119492.

[44] Li, Ronghua, Yichen Zhang, Hongxia Deng, et al. "Removing Tetracycline and Hg(II) with Ball-Milled Magnetic Nanobiochar and Its Potential on Polluted Irrigation Water Reclamation." *Journal of Hazardous Materials* 384 (2020): 121095. https://doi.org/10.1016/j.jhazmat.2019.121095.

[45] Khang, Tran Minh, Tran Thi Bich Quyen, Luong Huynh Vu Thanh, et al. "Synthesis of ZnO/TiO_2–Biochar from Durian Husk for Efficient Dye Adsorption and Degradation." *Journal of Chemical Technology & Biotechnology* 100, no. 10 (2025): 2217–2229. https://doi.org/10.1002/jctb.70038.

[46] Pervez, Md. Nahid, Tao Jiang, Jaydev Kumar Mahato, et al. "Surface Modification of Graphene Oxide for Fast Removal of Per- and Polyfluoroalkyl Substances (PFAS) Mixtures from River Water." *ACS EST Water* 4, no. 7 (2024): 2968–2980. https://doi.org/10.1021/acsestwater.4c00187.

[47] Zhao, Junqi, Yunqiu Jiang, Xinyu Chen, et al. "Unlocking the Potential of Element-Doped Biochar: From Tailored Synthesis to Multifunctional Applications in Environment and Energy." *Biochar* 7 (2025): 77. https://doi.org/10.1007/s42773-025-00467-x.

[48] Liu, Zhixin, Ziyi Xu, Linfeng Xu, et al. "Modified Biochar: Synthesis and Mechanism for Removal of Environmental Heavy Metals." *Carbon Research* 1, no. 1 (2022): 8. https://doi.org/10.1007/s44246-022-00007-3.

[49] Surip, S. N., Ahmed Saud Abdulhameed, Zaharaddeen N. Garba, et al. "H_2SO_4-Treated Malaysian Low Rank Coal for Methylene Blue Dye Decolourization and COD Reduction: Optimization of Adsorption and Mechanism Study." *Surface and Interfaces* 21 (2020): 100641. https://doi.org/10.1016/j.surfin.2020.100641.

[50] Jawad, Ali H., Mondira Bardhan, Md. Atikul Islam, et al. "Insights into the Modeling, Characterization and Adsorption Performance of Mesoporous Activated Carbon from Corn Cob Residue via Microwave-Assisted H_3PO_4 Activation." *Surface and Interfaces* 21 (2020): 100688. https://doi.org/10.1016/j.surfin.2020.100688.

[51] Jawad, Ali H., Ahmed Saud Abdulhameed, et al. "Statistical Modeling of Methylene Blue Dye Adsorption by High Surface Area Mesoporous Activated Carbon from Bamboo Chip Using KOH-Assisted Thermal Activation." *Energy Ecology and Environment* 5, no. 6 (2020): 456–469. https://doi.org/10.1007/s40974-020-00177-z.

[52] Yan, Lilong, Yue Liu, Yudan Zhang, et al. "$ZnCl_2$ Modified Biochar Derived from Aerobic Granular Sludge for Developed Microporosity and Enhanced Adsorption to Tetracycline." *Bioresource Technology* 297 (2020): 122381. https://doi.org/10.1016/j.biortech.2019.122381.

[53] Zhang, Dawei, Kejing Zhang, Xiaolan Hu, et al. "Cadmium Removal by $MgCl_2$ Modified Biochar Derived from Crayfish Shell Waste: Batch Adsorption, Response Surface Analysis and Fixed Bed Filtration." *Journal of Hazardous Materials* 408 (2021): 124860. https://doi.org/10.1016/j.jhazmat.2020.124860.

[54] Liu, Huidong, Guoren Xu, and Guibai Li. "Preparation of Porous Biochar Based on Pharmaceutical Sludge Activated by NaOH and Its Application in the Adsorption of Tetracycline." *Journal of Colloid and Interface Science* 587 (2021): 271–278. https://doi.org/10.1016/j.jcis.2020.12.014.

[55] Panwar, N. L., and Ashish Pawar. "Influence of Activation Conditions on the Physicochemical Properties of Activated Biochar: A Review." *Biomass Conversion and Biorefinery* 12 (2022): 925–947.

[56] Srivatsav, Prithvi, Bhaskar Sriharsha Bhargav, Vignesh Shanmugasundaram, et al. "Biochar as an Eco-Friendly and Economical Adsorbent for the Removal of Colorants (Dyes) from Aqueous Environment: A Review." *Water* 12 (2020): 3561. https://doi.org/10.3390/w12123561.

[57] Wang, Yi, Ya-Jie Hu, Xiang Hao, et al. "Hydrothermal Synthesis and Applications of Advanced Carbonaceous Materials from Biomass: A Review." *Advanced Composites and Hybrid Materials* 3 (2020): 267–284. https://doi.org/10.1007/s42114-020-00158-0.

[58] Wang, Keliang, Bocong Zheng, Junwoo Lee, Thomas Schuelke, Jin Hong, and Qi Hua Fan. "Enhanced Capacitance and Desalination Performance with Plasma-Activated Biochar Electrodes." *Energy Technology* 11, no. 7 (2023): 2300043. https://doi.org/10.1002/ente.202300043.

[59] Wang, Jia, Jiayi Cai, Siqi Wang, et al. "Biochar-Based Activation of Peroxide: Multivariate-Controlled Performance, Modulatory Surface Reactive Sites and Tunable Oxidative Species." *Chemical Engineering Journal* 428 (2022): 131233. https://doi.org/10.1016/j.cej.2021.131233.

[60] Awasthi, Sanjeev Kumar, Manish Kumar, Surendra Sarsaiya, et al. "Multi-Criteria Research Lines on Livestock Manure Biorefinery Development towards a Circular Economy: From the Perspective of Life Cycle Assessment and Business Model Strategies." *Journal of Cleaner Production* 341 (2022): 130862. https://doi.org/10.1016/j.jclepro.2022.130862.

[61] Liu, Can, Wendong Wang, and Rui Wu. "Preparation of Acid- and Alkali-Modified Biochar for Removal of Methylene Blue Pigment." *ACS Omega* 5, no. 48 (2020): 30906–30922. https://doi.org/10.1021/acsomega.0c03688.

[62] Jiang, Man, Qi Xu, Caiping Hu, et al. "Mechanistic Insights into Cr(VI) Removal by Acid-Modified Biochar via Coupled Redox and Complexation Processes." *New Journal of Chemistry* 50 (2026): 3542–3554. https://doi.org/10.1039/D5NJ03816B.

[63] Feng, Qianwei, Miao Chen, Pan Wu, et al. "Simultaneous Reclaiming Phosphate and Ammonium from Aqueous Solutions by Calcium Alginate–Biochar Composite: Sorption Performance and Governing Mechanisms." *Chemical Engineering Journal* 429 (2022): 132166.

[64] Han, Yoojung, and Changsang Yun. "Effect of the Alkaline Surface Modification of the Substrate Fabric on the Peel Strength of 3D Printed Composite Fabrics." *Fashion and Textiles* 12 (2025): 25. https://doi.org/10.1186/s40691-025-00436-9.

[65] Su, Zenghui, Ping Sun, Youyuan Chen, et al. "The Influence of Alkali-Modified Biochar on the Removal and Release of Zn in Bioretention Systems: Adsorption and Immobilization Mechanism." *Environmental Pollution* 310 (2022): 119874. https://doi.org/10.1016/j.envpol.2022.119874.

[66] Chang, Fuhua, and Haoyu Li. "Preparation of High-Efficient $KMnO_4$ Modified Biochar for Heavy Metal Removal from Municipal Wastewater." *Arabian Journal of Chemistry* 17, no. 5 (2024): 105756. https://doi.org/10.1016/j.arabjc.2024.105756.

[67] Feng, Zhuqing, Rongfang Yuan, Wan Fei, et al. "Preparation of Magnetic Biochar and Its Application in Catalytic Degradation of Organic Pollutants: A Review." *Science of the Total Environment* 765 (2021): 142673. https://doi.org/10.1016/j.scitotenv.2020.142673.

[68] Yang, Xing, Marvin Hinzmann, He Pan, et al. "Pig Carcass-Derived Biochar Caused Contradictory Effects on Arsenic Mobilization in a Contaminated Paddy Soil under Fluctuating Controlled Redox Conditions." *Journal of Hazardous Materials* 421 (2022): 126647.

[69] Yang, Xing, Sabry M. Shaheen, Jianxu Wang, et al. "Elucidating the Redox-Driven Dynamic Interactions between Arsenic and Iron-Impregnated Biochar in a Paddy Soil Using Geochemical and Spectroscopic Techniques." *Journal of Hazardous Materials* 422 (2022): 126808.

[70] Qu, Jianhua, Jiaqi Xue, Mingze Sun, et al. "Superefficient Non-Radical Degradation of Benzo[a]pyrene in Soil by Fe–Biochar Composites Activating Persulfate." *Chemical Engineering Journal* 481 (2024): 148585. https://doi.org/10.1016/j.cej.2024.148585.

[71] Li, Xiang Qin, Jia Yang, Yan Li, et al. "Preparation and Application of Fe/Biochar (Fe-BC) Catalysts in Wastewater Treatment: A Review." *Chemosphere* 274 (2021): 129766. https://doi.org/10.1016/j.chemosphere.2021.129766.

[72] Ahmad, Shakeel, Xiaomei Liu, and Jingchun Tang. "Biochar-Supported Nanosized Zero-Valent Iron (nZVI/BC) Composites for Removal of Nitro and Chlorinated Contaminants." *Chemical Engineering Journal* 431 (2022): 133187. https://doi.org/10.1016/j.cej.2021.133187.

[73] Zhang, Yuting, Xinqian Jiao, Na Liu, Jing Lv, and Yadong Yang. "Enhanced Removal of Aqueous Cr(VI) by a Green Synthesized Nanoscale Zero-Valent Iron Supported on Oak Wood Biochar." *Chemosphere* 245 (2020): 125542. https://doi.org/10.1016/j.chemosphere.2019.125542.

[74] Ye, Tiancai, Tianci Liu, Hulong Yi, et al. "In Situ Arsenic Immobilization by Natural Iron (Oxyhydr) Oxide Precipitates in As-Contaminated Groundwater Irrigation Canals." *Journal of Environmental Sciences* 153 (2024): 143–157. https://doi.org/10.1016/j.jes.2024.04.005.

[75] Lyu, Honghong, Jingchun Tang, Mengke Cui, Bin Gao, and Boxiong Shen. "Biochar/Iron (BC/Fe) Composites for Soil and Groundwater Remediation: Synthesis, Applications, and Mechanisms." *Chemosphere* 246 (2020): 125609.

[76] Zhu, Sihang, Ting Qu, Muhammad Irshad, and Jianying Shang. "Simultaneous Removal of Cd(II) and As(III) from Co-Contaminated Aqueous Solution by α-FeOOH Modified Biochar." *Biochar* 2 (2020): 81–92.

[77] Kim, Seo Yeon, Jin Ju Lee, and Goontaek Lee. "Comparative Efficacies of Iron Oxide-Modified Biochar and Pyrite-Modified Biochar for Simultaneous Passivation of Cadmium and Arsenic in Aqueous

Solutions and Lettuce (*Lactuca sativa* L.) Cultivation." *Applied Biological Chemistry* 68 (2025): 13. https://doi.org/10.1186/s13765-025-00988-w.

[78] Amen, Rabia, Hamna Bashir, Irshad Bibi, et al. "A Critical Review on Arsenic Removal from Water Using Biochar-Based Sorbents: The Significance of Modification and Redox Reactions." *Chemical Engineering Journal* 396 (2020): 125195. https://doi.org/10.1016/j.cej.2020.125195.

[79] Zhou, Hongyi, Mengyao Ye, Yongkang Zhao, et al. "Sodium Citrate and Biochar Synergistic Improvement of Nanoscale Zero-Valent Iron Composite for the Removal of Chromium(VI) in Aqueous Solutions." *Journal of Environmental Sciences* 115 (2022): 227–239. https://doi.org/10.1016/j.jes.2021.05.044.

[80] Liu, Renrong, Hai Wang, Li Han, Baowei Hu, and Muqing Qiu. "Reductive and Adsorptive Elimination of U(VI) Ions in Aqueous Solution by SFeS@Biochar Composites." *Environmental Science and Pollution Research* 28 (2021): 55176–55185. https://doi.org/10.1007/s11356-021-14835-0.

[81] Dong, Cheng-Di, Chiu-Wen Chen, Thanh-Binh Nguyen, et al. "Degradation of Phthalate Esters in Marine Sediments by Persulfate over Fe–Ce/Biochar Composites." *Chemical Engineering Journal* 384 (2020): 123301. https://doi.org/10.1016/j.cej.2019.123301.

[82] Zhu, Qijia, Kai Zhang, Jiani Xu, Xinyu Wei, Lixia Shi, Sumita, Cong Li, and Eric Lichtfouse. "Performance and Mechanism of Fe_3O_4-Loaded Biochar Activating Persulfate to Degrade Acid Orange 7." *Water* 15, no. 10 (2023): 1849. https://doi.org/10.3390/w15101849.

[83] Luo, Xuewen, Minxian Shen, Junhong Liu, et al. "Resource Utilization of Piggery Sludge to Prepare Recyclable Magnetic Biochar for Highly Efficient Degradation of Tetracycline through Peroxymonosulfate Activation." *Journal of Cleaner Production* 294 (2021): 126372. https://doi.org/10.1016/j.jclepro.2021.126372.

[84] Hublikar, Leena V., K. S. Nivedhitha, Bipin S. Chikkatti, et al. "Functionalized Biochar–Metal Oxide Nanocomposites for the Catalytic Degradation of Recalcitrant Pollutants in Wastewater Treatment." *RSC Advances* 16 (2026): 12186–12214. https://doi.org/10.1039/d5ra07670f.

[85] Herath, Amali, Chanaka Navarathna, Shannon Warren, et al. "Iron/Titanium Oxide–Biochar (Fe_2TiO_5/BC): A Versatile Adsorbent/Photocatalyst for Aqueous Cr(VI), Pb^{2+}, F^- and Methylene Blue." *Journal of Colloid and Interface Science* 614 (May 2022): 603–616. https://doi.org/10.1016/j.jcis.2022.01.067.

[86] Liu, Xiaochen, Yuan Yao, Jun Lu, Juan Zhou, and Quanyuan Chen. "Catalytic Activity and Mechanism of Typical Iron-Based Catalysts for Fenton-Like Oxidation." *Chemosphere* 311 (2023): 136972. https://doi.org/10.1016/j.chemosphere.2022.136972.

[87] Feng, Qianwei, Bing Wang, Miao Chen, et al. "Invasive Plants as Potential Sustainable Feedstocks for Biochar Production and Multiple Applications: A Review." *Resources, Conservation and Recycling* 164 (2021): 105204.

[88] Zeng, Shaoyi, Kunquan Li, Xia Xu, et al. "Efficient Catalytic Degradation of Tetracycline via Persulfate Activation with Plant-Based Biochars: Insight into Endogenous Mineral Self-Template Effect and Pyrolysis Catalysis." *Chemosphere* 337 (2023): 139309.

[89] Shaheen, Sabry M., Natasha Mosa, Ahmed, et al. "Manganese Oxide–Modified Biochar: Production, Characterization and Applications for the Removal of Pollutants from Aqueous Environments—A Review." *Bioresource Technology* 346 (2022): 126581. https://doi.org/10.1016/j.biortech.2021.126581.

[90] Jia, Xiaocen, Jianwei Zhou, Jing Liu, et al. "The Antimony Sorption and Transport Mechanisms in Removal Experiments by Mn-Coated Biochar." *Science of the Total Environment* 724 (2020): 138158. https://doi.org/10.1016/j.scitotenv.2020.138158.

[91] Liu, Tong, Kangping Cui, Yihan Chen, et al. "Removal of Chlorophenols in the Aquatic Environment by Activation of Peroxymonosulfate with nMnOx@Biochar Hybrid Composites: Performance and Mechanism." *Chemosphere* 283 (2021): 131188. https://doi.org/10.1016/j.chemosphere.2021.131188.

[92] Zheng, Yulin, Yongshan Wan, Jianjun Chen, Hao Chen, and Bin Gao. "MgO Modified Biochar Produced through Ball Milling: A Dual-Functional Adsorbent for Removal of Different Contaminants." *Chemosphere* 243 (2020): 125344. https://doi.org/10.1016/j.chemosphere.2019.125344.

[93] Luo, Jin-Zhi, Yan-Yan Cai, Jin Yu, and Jun-Feng Huang. "Development and Optimization of a Polysilicon–Aluminum Alkali Mineral-Enhanced Biochar Composite for Effective Heavy Metal Removal in Acidic Environments." *Journal of Cleaner Production* 460 (2024): 142568.

[94] Zhong, Quanfa, Qintie Lin, Runlin Huang, et al. "Oxidative Degradation of Tetracycline Using Persulfate Activated by N and Cu Codoped Biochar." *Chemical Engineering Journal* 380 (2020): 122608.

[95] Zhang, Zixin, Xinhui Liu, and Jiaofeng Gu. "Lanthanum-Modified Biochar Reducing Arsenic Bioavailability in Soil and Accumulation in Rice: Characterization, Performance, and Mechanism." *Environmental Technology & Innovation* 40 (2025): 104552. https://doi.org/10.1016/j.eti.2025.104552.

[96] Zhang, Yufei, and Yifeng He. "Synthesis of Zirconium-Based MOF–Biochar Composites for Efficient Congo Red Removal from Industrial Wastewater." *Water* 17, no. 19 (2025): 2814.

[97] Liao, Jun, Xiaoshan He, and Yong Zhang. "Bismuth Impregnated Biochar for Efficient Uranium Removal from Solution: Adsorption Behavior and Interfacial Mechanism." *Science of the Total Environment* 819 (2022): 153145. https://doi.org/10.1016/j.scitotenv.2022.153145.

[98] Pan, Jing, Haowang Deng, Ziyan Du, et al. "Design of Nitrogen-Phosphorus-Doped Biochar and Its Lead Adsorption Performance." *Environmental Science and Pollution Research* 29, no. 19 (2022): 28984–28994. https://doi.org/10.1007/s11356-021-17335-3.

[99] Bai, Bing, Qingyang Liu, He Li, Dan Liu, Haichao Wang, Chengliang Zhang, Zheng Yang, and Jingjing Yao. "Sorption of Iodine on Biochar Derived from the Processing of Urban Sludge and Garden Waste at Different Pyrolysis Temperatures." *Molecules* 29, no. 13 (2024): 3007.

[100] Gopalakrishnan, Arthi, and Sushmee Badhulika. "Effect of Self-Doped Heteroatoms on the Performance of Biomass-Derived Carbon for Supercapacitor Applications." *Journal of Power Sources* 480 (2020): 228830. https://doi.org/10.1016/j.jpowsour.2020.228830.

[101] Zhang, Jian, Ni Zhang, Filip M. G. Tack, et al. "Modification of Ordered Mesoporous Carbon for Removal of Environmental Contaminants from Aqueous Phase: A Review." *Journal of Hazardous Materials* 418 (2021): 126266. https://doi.org/10.1016/j.jhazmat.2021.126266.

[102] Alshreef, Abdulasalam Amhamed Mohamed Hıssen, Ayhan Kocaman, and Amr Salem S. Abu. "Desalination and Water Treatment." *Desalination and Water Treatment* 325 (2026): 101673. https://doi.org/10.1016/j.dwt.2026.101673.

[103] Yang, Yuxuan, Chi Yanxiao, Kunlun Yang, et al. "Iron/Nitrogen Co-Doped Biochar Derived from Salvaged Cyanobacteria for Efficient Peroxymonosulfate Activation and Ofloxacin Degradation: Synergistic Effect of Fe/N in Non-Radical Path." *Journal of Colloid and Interface Science* 652 (2023): 350–361.

[104] Liu, Yanyang, Liqing Li, Zheshan Duan, et al. "Chitosan Modified Nitrogen-Doped Porous Carbon Composite as a Highly Efficient Adsorbent for Phenolic Pollutants Removal." *Colloids and Surfaces A: Physicochemical and Engineering Aspects* 610 (2021): 125728.

[105] Hou, Yanrui, Sinian Yan, Gege Huang, et al. "Fabrication of N-Doped Carbons from Waste Bamboo Shoot Shell with High Removal Efficiency of Organic Dyes from Water." *Bioresource Technology* 303 (2020): 122939. https://doi.org/10.1016/j.biortech.2020.122939.

[106] Li, Zhenhao, Bo Xing, Yan Ding, Yunchao Li, and Shurong Wang. "A High-Performance Biochar Produced from Bamboo Pyrolysis with In-Situ Nitrogen Doping and Activation for Adsorption of Phenol and Methylene Blue." *Chinese Journal of Chemical Engineering* 28, no. 11 (2020): 2872–2880.

[107] Zheng, Xiaogang, Yuanliang Zhou, Xinhui Liu, Xiaojin Fu, Hao Peng, and Sihao Lv. "Enhanced Adsorption Capacity of MgO/N-Doped Active Carbon Derived from Sugarcane Bagasse." *Bioresource Technology* 297 (2020): 122413. https://doi.org/10.1016/j.biortech.2019.122413.

[108] Chu, Bei, Yoshimasa Amano, and Motoi Machida. "Preparation of Bean Dreg Derived N-Doped Activated Carbon with High Adsorption for Cr(VI)." *Colloids and Surfaces A: Physicochemical and Engineering Aspects* 586 (2020): 124262. https://doi.org/10.1016/j.colsurfa.2019.124262.

[109] Chen, Feng, Mou Zhang, Lulu Ma, et al. "Nitrogen and Sulfur Codoped Micro-Mesoporous Carbon Sheets Derived from Natural Biomass for Synergistic Removal of Chromium(VI): Adsorption Behavior and Computing Mechanism." *Science of the Total Environment* 730 (2020): 138930. https://doi.org/10.1016/j.scitotenv.2020.138930.

[110] Zhang, Nahui, Xuelei Jiang, Dezhang Ren, et al. "A Magnetic Amino-Enriched Hydrothermal Carbon Production with Molasses as Carbon Source." *Journal of Environmental Chemical Engineering* 10 (2022): 107073. https://doi.org/10.1016/j.jece.2021.107073.

[111] Lin, Shiwei, Xiong Yang, Lihu Liu, et al. "Electrosorption of Cadmium and Arsenic from Wastewaters Using Nitrogen-Doped Biochar: Mechanism and Application." *Journal of Environmental Management* 301 (2022): 113921. https://doi.org/10.1016/j.jenvman.2021.113921.

[112] Jiang, Siyu, Lili Yan, Runkai Wang, et al. "Recyclable Nitrogen-Doped Biochar via Low-Temperature Pyrolysis for Enhanced Lead(II) Removal." *Chemosphere* 286 (2022): 131666.

[113] Fu, Shilong, Ming Li, Wiebren de Jong, and Ruud Kortlever. "Tuning the Properties of N-Doped Biochar for Selective CO_2 Electroreduction to CO." *ACS Catalysis* 13, no. 15 (2023): 10309–10323. https://doi.org/10.1021/acscatal.3c01773.

[114] Ke, Linyao, Qiuhao Wu, Nan Zhou, et al. "Lignocellulosic Biomass Pyrolysis for Aromatic Hydrocarbons Production: Pre- and In-Process Enhancement Methods." *Renewable and Sustainable Energy Reviews* 165 (2022): 112607. https://doi.org/10.1016/j.rser.2022.112607.

[115] Wan, Zhonghao, Zibo Xu, Yuqing Sun, et al. "Stoichiometric Carbocatalysis via Epoxide-Like C–S–O Configuration on Sulfur-Doped Biochar for Environmental Remediation." *Journal of Hazardous Materials* 428 (2022): 128223. https://doi.org/10.1016/j.jhazmat.2022.128223.

[116] Banerjee, Paramita, G. P. Das, and Ranjit Thapa. "Computationally Exploring the Role of S-Dopant and S-Linker in Activating the Catalytic Efficiency of Graphene Quantum Dot for ORR." *Catalysis Today* 370 (June 2021): 36–45. https://doi.org/10.1016/j.cattod.2021.03.001.

[117] Ahmed, M. M. M., Chih-Hao Liao, and S. Venkatesan. "Sulfur-Functionalized Sawdust Biochar for Enhanced Cadmium Adsorption and Environmental Remediation: A Multidisciplinary Approach and Density Functional Theory Insights." *Journal of Environmental Management* 373 (2025): 123586.

[118] Sui, Long, Chunyu Tang, Qing Du, et al. "Preparation and Characterization of Boron-Doped Corn Straw Biochar: Fe(II) Removal Equilibrium and Kinetics." *Journal of Environmental Sciences* 106 (2021): 116–123. https://doi.org/10.1016/j.jes.2021.01.001.

[119] Xue, Shan, Jiangyao Tan, and Xiaoyu Ma. "Boron-Doped Activated Carbon Derived from Zoysia sinica for Rhodamine B Adsorption: The Crucial Roles of Defect Structures." *FlatChem* 34 (2022): 100390. https://doi.org/10.1016/j.flatc.2022.100390.

[120] Liu, Fan, Jing Ding, Qingliang Zhao, Guanshu Zhao, Kun Wang, Lili Li, and Shuyan Guan. "Insight into the Self-Driven O_2 Activation and Interfacial Electron Transfer for Micropollutant Degradation by Boron-Doped Biochar: Role of Boron Moieties and Persistent Free Radicals." *Separation and Purification Technology* 330 (2024): 125444. https://doi.org/10.1016/j.seppur.2023.125444.

[121] Zhang, Ailin, Xin Li, Jia Xing, and Guoren Xu. "Adsorption of Potentially Toxic Elements in Water by Modified Biochar: A Review." *Journal of Environmental Chemical Engineering* 8 (2020): 104196. https://doi.org/10.1016/j.jece.2020.104196.

[122] Karce, Houssam Eddine, Selmane Boumessaidia, Ahmed Bahloul, et al. "Efficient Removal of Methylene Blue by a Biochar from Neem Tree Shell Wastes Using Adsorption Technology." *Biomass Conversion and Biorefinery* (2024): 1–16. https://doi.org/10.1007/s13399-024-06072-5.

[123] Mandal, Sandip, Shengyan Pu, Lingling He, Ma Hui, and Deyi Hou. "Biochar Induced Modification of Graphene Oxide & nZVI and Its Impact on Immobilization of Toxic Copper in Soil." *Environmental Pollution* 259 (2020): 113851. https://doi.org/10.1016/j.envpol.2019.113851.

[124] Hamid, Yasir, Lei Liu, Usman Muhammad, et al. "Functionalized Biochars: Synthesis, Characterization, and Applications for Removing Trace Elements from Water." *Journal of Hazardous Materials* (2022): 129337. https://doi.org/10.1016/j.jhazmat.2022.129337.

[125] Liu, Kai, Fangbai Li, Jianghu Cui, Shiyun Yang, and Liping Fang. "Simultaneous Removal of Cd(II) and As(III) by Graphene-Like Biochar-Supported Zero-Valent Iron from Irrigation Waters under Aerobic Conditions: Synergistic Effects and Mechanisms." *Journal of Hazardous Materials* 395 (2020): 122623.

[126] Stephen, Joseph, Annette L. Cowie, Lukas Van Zwieten, et al. "How Biochar Works, and When It Doesn't: A Review of Mechanisms Controlling Soil and Plant Responses to Biochar." *GCB Bioenergy* 13, no. 11 (2021): 1731–1764. https://doi.org/10.1111/gcbb.12885.

[127] Ramola, Sudipta, Tarun Belwal, and Cun Jun Li. "Improved Lead Removal from Aqueous Solution Using Novel Porous Bentonite- and Calcite-Biochar Composite." *Science of the Total Environment* 709 (2020): 136171. https://doi.org/10.1016/j.scitotenv.2019.136171.

[128] Zhang, Tingting, Wei Wang, Yunliang Zhao, et al. "Removal of Heavy Metals and Dyes by Clay-Based Adsorbents: From Natural Clays to 1D and 2D Nano-Composites." *Chemical Engineering Journal* 420 (2021): 127574. https://doi.org/10.1016/j.cej.2020.127574.

[129] Deng, Wangde, Dong-Qing Zhang, Xiaoxian Zheng, and Xingyao Ye. "Adsorption Recovery of Phosphate from Waste Streams by Ca/Mg-Biochar Synthesis from Marble Waste, Calcium-Rich Sepiolite and Bagasse." *Journal of Cleaner Production* 288 (2020): 125638.

[130] Al-Swadi, Hamed A., Abdullah S. Al-Farraj, Mohammad I. Al-Wabel, Munir Ahmad, Jahangir Ahmad, Mohammed Awad Mousa, Muhammad Imran Rafique, and Muhammad Usama. "Kaolinite-Composited Biochar and Hydrochar as Low-Cost Adsorbents for the Removal of Cadmium, Copper, Lead, and Zinc from Aqueous Solutions." *Sustainability* 15, no. 22 (2023): 15978. https://doi.org/10.3390/su152215978.

[131] Li, Hui, Feng Zheng, Jing Wang, et al. "Facile Preparation of Zeolite-Activated Carbon Composite from Coal Gangue with Enhanced Adsorption Performance." *Chemical Engineering Journal* 390 (2020): 124513. https://doi.org/10.1016/j.cej.2020.124513.

[132] Zhou, Haitao, Huanggang Wang, Jian-Chun Wu, et al. "Boosting the Mechanical and Electrochemical Performance of MnO_2 Dry Electrode with Bentonite for Ampere-Hour Aqueous Zn-Ion Batteries." *Batteries & Supercaps* 8, no. 8 (2025): e202400757. https://doi.org/10.1002/batt.202400757.

[133] Shi, Yan, Xin Wang, Changping Feng, and Shipeng Yang. "Nano-Clay Montmorillonite Removes Tetracycline in Water: Factors and Adsorption Mechanism in Aquatic Environments." *iScience* 27, no. 2 (2024): 108952. https://doi.org/10.1016/j.isci.2024.108952.

[134] Wang, Xiaoli, and Hejing Wang. "Structural Analysis of Interstratified Illite-Smectite by the Rietveld Method." *Crystals* 11, no. 3 (2021): 244. https://doi.org/10.3390/cryst11030244.

[135] Zhuang, Guanzheng, Jiajun Zhang, Jinrong Chen, Qian Liu, Wenxiao Fan, and Qiang Li. "Application of Nanofibrous Clay Minerals in Water-Based Drilling Fluids: Principles, Methods, and Challenges." *Minerals* 14, no. 8 (2024): 842. https://doi.org/10.3390/min14080842.

[136] Yuan, Bingxiang, Weijie Chen, Zihao Li, and Jin Zhao. "Sustainability of the Polymer SH Reinforced Recycled Granite Residual Soil: Properties, Physicochemical Mechanism, and Applications." *Journal of Soils and Sediments* 23, no. 8 (2022). https://doi.org/10.1007/s11368-022-03294-w.

[137] Chen, Qincheng, Zhiwen Cheng, Xiaoying Li, et al. "Degradation Mechanism and QSAR Models of Antibiotic Contaminants in Soil by MgFe-LDH Engineered Biochar Activating Urea-Hydrogen Peroxide." *Applied Catalysis B: Environmental* 302 (2022): 120866. https://doi.org/10.1016/j.apcatb.2021.120866.

[138] Lyu, Peng, Guanghui Wang, Yelin Cao, et al. "Phosphorus Modified Biochar Cross-Linked Mg-Al Layered Double-Hydroxide Composite for Immobilizing Uranium in Mining Contaminated Soil." *Chemosphere* 276 (2021): 130116. https://doi.org/10.1016/j.chemosphere.2021.130116.

[139] Chao, Yang, Guanhua Zhang, Yue Meng, et al. "Direct Z-Scheme CeO_2@LDH Core-Shell Heterostructure for Photodegradation of Rhodamine B by Synergistic Persulfate Activation." *Journal of Hazardous Materials* 408 (2021): 124908. https://doi.org/10.1016/j.jhazmat.2020.124908.

[140] Yang, You, Zekai Shi, Yunhe Li, et al. "Magnetic Cobalt Ferrite Biochar Composite as Peroxymonosulfate Activator for Removal of Lomefloxacin Hydrochloride." *Separation and Purification Technology* 272 (2021): 118889. https://doi.org/10.1016/j.seppur.2021.118889.

[141] Mukarram, Zubair, Ihsanullah Ihsanullah, Hamidi Abdul Aziz, et al. "Sustainable Wastewater Treatment by Biochar/Layered Double Hydroxide Composites: Progress, Challenges, and Outlook." *Bioresource Technology* 319 (2021): 124128. https://doi.org/10.1016/j.biortech.2020.124128.

[142] Wang, Huabin, Siqi Wang, Zhulei Wang, et al. "Engineered Biochar with Anisotropic Layered Double Hydroxide Nanosheets to Simultaneously and Efficiently Capture Pb^{2+} and CrO_4^{2-} from Electroplating Wastewater." *Bioresource Technology* 306 (2020): 123118.

[143] Peyman, Gholami, Alireza Khataee, Reza Darvishi Cheshmeh Soltani, et al. "Photocatalytic Degradation of Gemifloxacin Antibiotic Using Zn-Co-LDH@Biochar Nanocomposite." *Journal of Hazardous Materials* 382 (2020): 121070. https://doi.org/10.1016/j.jhazmat.2019.121070.

[144] Wang, Yifan, Jianen Li, Liang Xu, et al. "EDTA Functionalized Mg/Al Hydroxides Modified Biochar for Pb(II) and Cd(II) Removal: Adsorption Performance and Mechanism." *Separation and Purification Technology* 335 (2024): 126199. https://doi.org/10.1016/j.seppur.2023.126199.

[145] Tian, Kun, Chunping Li, and Lianchun Wang. "SAP Nanomicelle-Functionalized Biochar: A Multifunctional and Sustainable Adsorbent for Efficient Removal of Dyes and Heavy Metals." *ACS Omega* 10, no. 50 (2025). https://doi.org/10.1021/acsomega.5c06590.

[146] Murad, Hafiza Afia, Mahtab Ahmad, and Jochen Bundschuh. "A Remediation Approach to Chromium-Contaminated Water and Soil Using Engineered Biochar Derived from Peanut Shell." *Environmental Research* 204, Part B (2022): 112125. https://doi.org/10.1016/j.envres.2021.112125.

[147] Nessiani, Rahele Khosravi, Meysam Naseri, and Khadijeh Ahmadzadeh. "Advanced Simultaneous Adsorption of Heavy Metals and Organic Dyes from Aqueous Solutions Using CTAB-Functionalized Broccoli Waste Biochar: A Sustainable Approach for Water Remediation." *Desalination and Water Treatment* 324 (2025): 101553. https://doi.org/10.1016/j.dwt.2025.101553.

[148] Gęca, Marlena, Ahmed M. Khalil, Mengqi Tang, Arvind K. Bhakta, Youssef Snoussi, Piotr Nowicki, Małgorzata Wiśniewska, and Mohamed M. Chehimi. "Surface Treatment of Biochar—Methods, Surface Analysis and Potential Applications: A Comprehensive Review." *Surfaces* 6, no. 2 (2023): 179–213. https://doi.org/10.3390/surfaces6020013.

[149] Ţălu, Ștefan, and Deniz Şahin. "Advances in Membrane Adsorption Techniques for the Removal of Radioactive Materials." *Hidraulica Magazine*, no. 4 (December 2025): 7–26.

[150] Şahin, Deniz. "Advances in Sensorics for Ecological Monitoring: Trends, Challenges, and Future Perspectives." *Hidraulica Magazine*, no. 4 (December 2025): 53–68.

[151] Das, Abhijeet, and Satchidananda Mishra. "Smart and Sustainable Water Management: Policy, Technology, and Innovation Pathways for Resource Resilience." *GRN Tech Research on Sustainability* 5, no. 5 (2025). https://doi.org/10.1007/s44173-025-00022-8.

[152] Hossen, Md. Anowar, and M. G. Mostafa. "Emerging Pollutants in Aquatic Environment: A Global Challenge." *Water Practice and Technology* 20, no. 8 (2025): 1763–1783. https://doi.org/10.2166/wpt.2025.097.

[153] Vagi, Maria C., Andreas S. Petsas, and Maria Kostopoulou. "Potential Effects of Persistent Organic Contaminants on Marine Biota: A Review on Recent Research." *Water* 13, no. 18 (2021): 2488. https://doi.org/10.3390/w13182488.

Pedagogical Valences of Computer-Assisted Instruction (CAI) in relation to Integrated Waste Management (IWM)

MA stud. **Ioana-Elisabeta CIORUȚA**[1,2], PhD Eng. IT exp. **Bogdan V. CIORUȚA**[3-5,*], MA stud. **Gabriela-Ionela HEREȘ**[6], Assoc. Prof. PhD Eng. habil. **Mirela-Ana COMAN**[7,8], Eng. IT exp. **Alexandru L. POP**[3,5]

[1] Technical University of Cluj-Napoca - North University Centre of Baia Mare, Faculty of Letters - Department of Specialty with Psychopedagogical Profile, Construction and Curricular Innovation (MA prog.), 76 Victoriei Str., 430083, Baia Mare, Romania

[2] "Little Prince" Extended Program Kindergarten, 8B Cuza Vodă Str., 430034, Baia Mare, Romania

[3] Technical University of Cluj-Napoca - North University Centre of Baia Mare, Office of Informatics, 62A Victor Babeș Str., 430083, Baia Mare, Romania

[4] Technical University of Cluj-Napoca - North University Centre of Baia Mare, Department of Mathematics and Computer Science, 76 Victoriei Str., 430072, Baia Mare, Romania

[5] Technical University of Cluj-Napoca - North University Centre of Baia Mare, Faculty of Letters - Department of Specialty with Psychopedagogical Profile, 76 Victoriei Str., 430083, Baia Mare, Romania

[6] Technical University of Cluj-Napoca - North University Centre of Baia Mare, Department of Mathematics and Computer Science, Computer Science and Software Engineering (MA prog). 76 Victoriei Str., 430072, Baia Mare, Romania

[7] Technical University of Cluj-Napoca - North University Centre of Baia Mare, Faculty of Engineering - Department of Mineral Resources, Materials and Environmental Engineering, 62A Victor Babeș Str., 430083, Baia Mare, Romania

[8] University of Agricultural Sciences and Veterinary Medicine from Cluj-Napoca, 3-5 Calea Mănăștur, 4000372, Cluj-Napoca, Romania

* bogdan.cioruta@staff.utcluj.ro

Abstract: *The transition to a circular economy in Romania faces significant challenges, requiring not only technological innovation but also a structural reform in environmental engineering education. This paper explores the pedagogical valences of Computer-Assisted Instruction (CAI) as a strategic pillar in training specialists for Integrated Waste Management (IWM). We propose the "IWM-CAI 4.0" methodology, an experiential learning framework grounded in Scenario-Based Learning (SBL) and Problem-Based Learning (PBL). The proposed methodology integrates professional software suites - such as SimaPro for Life Cycle Assessment, ArcGIS for spatial modeling, and STAN for material flow analysis - to bridge the gap between academic theory and Industry 4.0 requirements. By utilizing 10 progressive digital case folders and performance analytics, the framework evolves students from compliance specialists into architects of the circular economy. The paper demonstrates that reconfiguring specialist training through CAI is a strategic imperative to ensure that future engineers are "ready-to-operate" in a digitalized global industrial ecosystem.*

Keywords: *Circular economy, environmental engineering education, performance analytics, CAI*

1. Introduction

The transition toward a circular economy - where waste management occupies a leading position (with focus on using resources efficiently, reducing waste, waste valorisation, and protecting the environment) [1, 2] - within today's information-driven consumer society represents one of the 21st century's greatest challenges. It demands not only technological innovation to manage municipal waste generation (according to Eurostat data [3]), but also a profound paradigm shift in both civic and professional education, with sustainable solutions that balance economic growth with environmental responsibility over the decades [4-6].

In this context, Computer-Assisted Instruction (CAI) - as a pedagogical and applied discipline, bearing profound implications for both remediation technologies and the management of protected

areas [7, 8] - can also serve as a strategic pillar in developing the core competencies of future specialists in Integrated Waste Management (IWM) strategies. Within the EU, the legislative framework established by the circular economy package mandates member states, including Romania, to meet ambitious recycling targets and drastically reduce landfill disposal.

The success of these policies depends critically on public awareness and technical expertise - factors that can be optimized through the use of interactive digital learning platforms, which are the hallmark of CAI. The pedagogical potential of CAI in this field lies in its ability to transform abstract concepts - such as Life Cycle Assessment (LCA) or the impact of methane emissions often associated with IWM - into visual and immersive learning experiences. For instance, digital simulations within CAI enable learners to grasp complex waste streams without the inherent risks of direct contact with hazardous materials.

In Romania, IWM remains a sensitive issue, as the country faces constant pressure from European authorities due to low separate collection rates. Physical infrastructure deficiencies are compounded by a major educational gap, where traditional information methods seem to have reached their limits. In this regard, implementing CAI solutions within the Romanian educational system and professional training programs could accelerate the adoption of environmental standards (as presented in Fig. 1). By leveraging gamification algorithms and adaptive testing modules, learning becomes personalized, addressing the specific needs of various age groups and professional sectors. A significant advantage of CAI is its scalability; while physical workshops are geographically and logistically constrained, an e-learning platform focused on IWM can disseminate best practices in real-time, bridging the knowledge gap between regions in Romania.

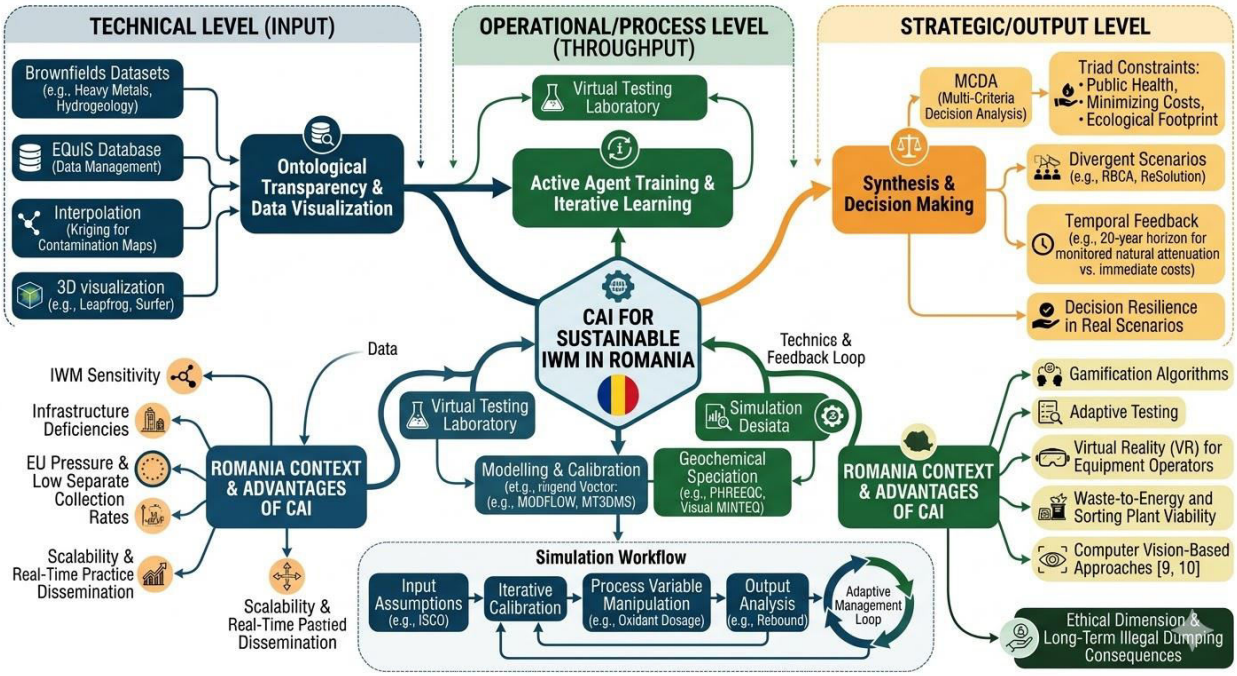

Fig. 1. Integrated workflow of CAI in IWM - from ontological transparency to strategic decision resilience (source: generated with Gemini 3 flash)

From a pedagogical perspective, CAI facilitates the development of critical thinking. Students and future digital citizens can use modeling software to observe how source-sorting decisions directly impact the economic viability of a sorting plant or a waste-to-energy facility, thereby linking ecology with economics via computer vision-based approaches [9, 10]. In the EU, best practices from countries like Germany or the Netherlands demonstrate that using Virtual Reality (VR) to train IWM equipment operators reduces human error and optimizes processing times. Romania can adopt these sustainable models to professionalize its workforce in the sanitation sector. Furthermore, the ethical dimension of IWM is more effectively explored through interactive digital case studies; these can vividly illustrate the long-term consequences of illegal dumping, providing a temporal perspective that traditional textbooks cannot convey with the same emotional impact.

The current context of early 2026, shaped by the accelerated post-pandemic digitalization, provides fertile ground for integrating CAI into national and local environmental policies. It is no longer enough to discuss what must be done or adopted; CAI demonstrates precisely how to take the correct steps, providing immediate feedback and behavioral corrections in a virtual environment before real-world application. This paper aims to demonstrate that IWM in Romania is not just a logistical challenge but also one of digital pedagogy, where the focus lies on the visible implications of CAI. We believe that only by exploiting the potential of CAI can we build a bridge between strict EU requirements and local socio-economic realities, fostering both responsible citizens and truly competent specialists.

2. Literature Review and Research Methodology

The analysis and interpretation of recent scientific literature highlight a paradigm shift in engineering education, moving from unidirectional knowledge transmission models toward technology-mediated, constructivist learning frameworks. In the specialized field of Environmental Engineering and Protection in Industry (EEPI), this transition is driven by the need to align university curricula with European Green Deal objectives and Industry 4.0 requirements. Recent studies indicate that IWM can no longer be taught as a series of isolated processes, but rather as a complex system with unique dynamics. Over the last decade, foundational research in instructional design has been adapted to the specifics of technical disciplines; consequently, CAI in environmental engineering must go beyond simple graphical interfaces and integrate computational engines capable of running pollutant-transport simulations or mass and energy balances. This approach, defined in the literature as Simulation-Based Learning (SBL), is widely regarded as the gold standard for developing decision-making competencies in IWM.

Regarding IWM, scholarly literature emphasizes the difficulty students face in conceptualizing the waste hierarchy dynamically. Furthermore, several recent studies demonstrate that the use of serious games and 'what-if' scenarios improves the retention rate of circular economy concepts by up to 40% compared to traditional courses lacking CAI support. Simultaneously, a significant segment of current research focuses on the application of the digital twins strategy in IWM education. The reviewed literature indicates that the virtual replication of a sorting plant or a sanitary landfill allows students to interact with real-world technical parameters - such as flow rates, waste composition, and biogas emissions - without leaving the classroom. This approach, centered on an extended laboratory showcasing various operational scenarios, effectively addresses the limited physical infrastructure in many universities while providing access to cutting-edge technologies via cloud computing.

The literature review indicates that integrating fuzzy logic modules into student assessments for EEPI disciplines allows for a much finer diagnosis of design errors. In IWM, where a calculation error in a landfill's liner system can be catastrophic, the capacity of CAI to identify and correct erroneous reasoning in real-time is documented as a major educational advantage. Complementing this, another identified research vector is the use of Augmented Reality (AR) to visualize invisible waste streams, such as underground methane emissions or leachate migration. The spatial visualization of complex data (GIS integrated into CAI) helps future specialists develop the necessary technical intuition for monitoring and environmental impact assessment (EIA). This convergence between geospatial data and CAI is transforming how the territorial planning of IWM infrastructure is taught.

Furthermore, an analysis of the current state of affairs reveals a significant barrier within our country: the resistance to change among teaching staff and the lack of fully integrated course prototypes associated with IWM. Although individual tools are available - such as computational software, databases, and communication platforms - the literature indicates a deficiency in instructional design models capable of weaving them into a coherent workflow specific to the EEPI specialization. In addition, integrating engineering ethics into IWM through CAI represents a vital research direction; simulations can be programmed to present ethical dilemmas, such as choosing between a low-cost but long-term risky solution and a sustainable but capital-intensive one. Specialized literature emphasizes that the virtual environment is the ideal space for fostering Corporate Social Responsibility (CSR) skills among future engineers.

The current state of knowledge confirms that the efficiency of future IWM systems directly depends on the quality of the instructional design implemented in universities today. Through the strategic use of CAI, we can train specialists capable not only of monitoring pollution but of designing intrinsically clean industrial systems, thereby closing material loops in a sustainable and scientifically grounded manner.

3. Conceptual Framework and Proposed Work Scenarios

The conceptual framework we propose for the EEPI specialization (see Fig. 2) integrates the principles of systemic instructional design, creating a hybrid adaptive learning ecosystem. Rather than a mere sequence of standalone courses, this proposed methodology constitutes a computer-aided workflow that mirrors the real-world design and decision-making stages of an IWM system for experiential learning.

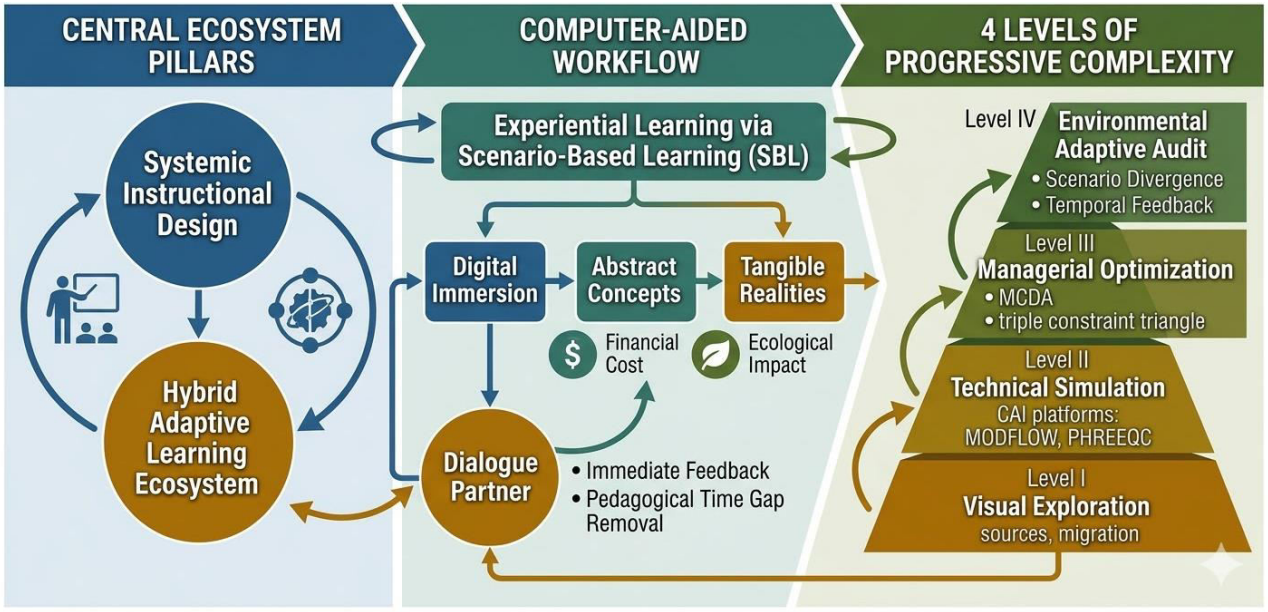

Fig. 2. Integrated workflow of CAI in IWM - a hybrid adaptive learning ecosystem for EEPI students (source: generated with Gemini 3 flash)

The central pillar of this methodology is Scenario-Based Learning (SBL). In the initial stage, students or future specialists do not merely receive theoretical information; they are placed within a specific industrial context via CAI dedicated platforms. This digital immersion serves to anchor abstract environmental protection concepts into tangible technical realities, where every variable introduced into the system carries both a financial cost and a measurable ecological impact.
The framework is structured across 4 levels of progressive complexity: *visual exploration* (i), *technical simulation* (ii), *managerial optimization* (iii), and *environmental adaptive audit* (iv). At each level, the software acts not just as a computational tool but as a dialogue partner providing immediate feedback, eliminating the time gap between design errors and pedagogical correction, allowing for the iterative refinement of the technical solutions proposed by EEPI engineers.

3.1 Case studies - from local context to global impact

The proposed case studies are digitized as Digital Case Folders (DCF) containing GIS maps, chemical analysis bulletins, and historical monitoring data. The 10 scenarios are ordered by progressive complexity, as follows:

1) **Waste Audit in an Educational or Public Institution** (basic level)
   - Focus - physical characterization and waste composition;
   - CAI pedagogical task - using mobile apps for field data collection and automated generation of composition charts; this is the first step in understanding the waste generator concept.

2) **Dual Collection Systems in Urban Areas** (operational level)
   - Focus - logistics and transport;
   - CAI pedagogical task - route optimization for waste fraction collection to minimize fuel consumption and CO_2 emissions, introducing the concept of efficiency in source separation.
3) **Industrial Composting of Biodegradable Waste** (process level)
   - Focus - biochemical transformation and parameter control (*moisture*, *temperature*, *pH*, *C/N ratio*);
   - CAI pedagogical task - simulating composting evolution based on various additives and digital monitoring of end-product (compost) quality.
4) **Remediation of Contaminated Sites** (remediation level)
   - Focus - soil and groundwater contamination;
   - CAI pedagogical task - 3D modeling of the pollutant plume and simulating remediation techniques (*bioremediation vs. encapsulation*) to select the solution with the lowest residual impact.
5) **Construction and Demolition Waste Management** (circularity level)
   - Focus - recovery of inert materials and their reintegration into the economic cycle;
   - CAI pedagogical task - simulating optical sorting algorithms to maximize the purity of aggregates destined for recycling.
6) **Industrial Symbiosis in a Logistics Park (**systemic level)
   - Focus - resource exchange between distinct legal entities;
   - CAI pedagogical task - designing a material flow network where unit A's waste (e.g., *residual heat* or *ash*) becomes unit B's resource, using material flow analysis soft.
7) **Waste-to-Energy Valorization** (thermodynamic conversion level)
   - Focus - incineration with energy recovery and flue gas treatment;
   - CAI pedagogical task - calculating energy efficiency and simulating emission filtration systems to ensure compliance with best available techniques (BAT) and BREF standards.
8) **WEEE management** (value recovery level)
   - Focus - extraction of critical raw materials and rare earth elements;
   - CAI pedagogical task - modeling hydrometallurgical recovery processes and performing life cycle assessment to compare primary mining with urban mining.
9) **National Deposit-Refund Systems** (macro-economic level)
   - Focus - financial flows, social behavior, and digital traceability;
   - CAI pedagogical task - simulating the impact of DRS on national recycling rates using agent-based modeling (ABM) to predict consumer behavior.
10) **Smart Waste City 4.0 with IoT and AI Integration** (dynamic/predictive level)
   - Focus - real-time smart city waste management;
   - CAI pedagogical task - configuring an integrated and adaptive network of sensor-equipped bins communicating with autonomous vehicles; students must manage the system during a peak event (*an urban festival*), optimizing resources via IoT/AI.

3.2 Specific Software - the digital engineer's toolkit

Within the proposed methodology, the role of software transcends basic user proficiency. Students are trained to correlate input parameters with the underlying mathematical models of the algorithms. The focus is placed on data interoperability across various software suites, including:

- **LCA dedicated software** (e.g., *SimaPro* or *GaBi*) - used for evaluating environmental impacts throughout the entire product life cycle - from raw material extraction to the final disposal of the resulting waste.
- **Geographic Information Systems** (e.g., *QGIS* and *ArcGIS*) - utilized for the spatial modeling of diverse waste streams and the identification of optimal locations for transfer stations or eco-compliant landfills.
- **Process simulators** (e.g., *STAN for Material Flow Analysis*) - employed to perform mass balances and identify resource losses within the thermal, mechanical, or biological treatment processes of various waste categories.

3.3 Pedagogical task-centered instruction - the 10 engineering deliverables

The methodology prioritizes task-centered instruction (TCI); each CAI module culminates in a professional-grade technical document or digital model. These deliverables reflect the transition from basic technical execution to strategic expertise:

1) **Physico-Chemical Waste Stream Characterization** (analytical level)
   - CAI pedagogical task - correlating lab data with the European Waste Catalogue (EWC) codes.
   - Deliverable - a technical report generated from a relational database that automatically validates waste as hazardous/non-hazardous based on critical substance concentrations.
2) **Legislative Compliance Audit** (normative level)
   - CAI pedagogical task - auditing an industrial facility against the Waste Framework Directive and national legislation.
   - Deliverable - an interactive audit report featuring stoplight indicators (compliant/non-compliant) and an automated timeline for corrective actions.
3) **Waste Management Plan Development** (operational level)
   - CAI pedagogical task - designing the waste flow for a specific industrial sector (e.g., *paint* or *tire manufacturing*).
   - Deliverable - a digital strategic document with dynamic templates that automatically calculate Key Performance Indicators (KPIs) and 5-year reduction targets.
4) **Leachate Collection System Sizing** (technical level)
   - CAI pedagogical task - hydraulic design of the drainage network for a sanitary landfill.
   - Deliverable - a computational model (*advanced Excel* or *CAD-integrated*) simulating leachate volumes based on local precipitation patterns.
5) **Mass and Energy Balance for a Sorting Plant (**systemic level)
   - CAI pedagogical task - identifying the recovery efficiency of recyclable materials;
   - Deliverable - a dynamic diagram (created in software like *STAN*) highlighting system losses and resulting secondary material flows.
6) **Environmental Impact Study related to the Dispersion Assessment** (evaluative level)
   - CAI pedagogical task - estimating emissions impact from a hazardous waste incinerator;
   - Deliverable - an isoconcentration map generated through mathematical modeling (e.g., *AERMOD*) for key atmospheric pollutants (*NO_x*, *dioxins*).
7) **Life Cycle Assessment for products/packaging** (strategic level)
   - CAI pedagogical task - comparing the environmental footprint of two packaging options (e.g., fossil-based plastic vs. bioplastic);
   - Deliverable - a sustainability report generated in LCA software (e.g., *open LCA*) quantifying global warming potential (GWP) and resource depletion.
8) **Pay-As-You-Throw Infrastructure Design** (socio-economic level)
   - CAI pedagogical task - modeling tariff structures and collecting logistics based on volume or weight;
   - Deliverable - a financial and logistical simulation demonstrating economic viability and its impact on citizen disposal behavior.
9) **Regional Industrial Symbiosis Strategy** (integrative level)
   - CAI pedagogical task - mapping waste streams within an industrial cluster to identify resource-sharing opportunities;
   - Deliverable - a resource interconnection matrix and calculation of the industrial park's carbon footprint reduction through circular economy loops.
10) **Waste 4.0 Predictive Management Dashboard** (advanced/dynamic level)
   - CAI pedagogical task - configuring a real-time waste monitoring system for a smart city ecosystem.
   - Deliverable - a dashboard prototype utilizing virtual sensor data to optimize collection routes and predict bin fill levels via machine learning algorithms.

This hierarchy ensures that EEPI students evolve from compliance specialists into architects of the circular economy. The final tasks (8-10) require a high level of synthesis, positioning the student as a senior consultant capable of making data-driven decisions within interdependent systems.

3.4 Problem-based scenarios - challenges in a controlled environment

Problem-based learning (PBL) serves as the engine of critical thinking (see Fig. 3); through CAI, we can introduce data noise or unforeseen events that force the student to re-evaluate and subsequently re-adapt the entire management strategy.

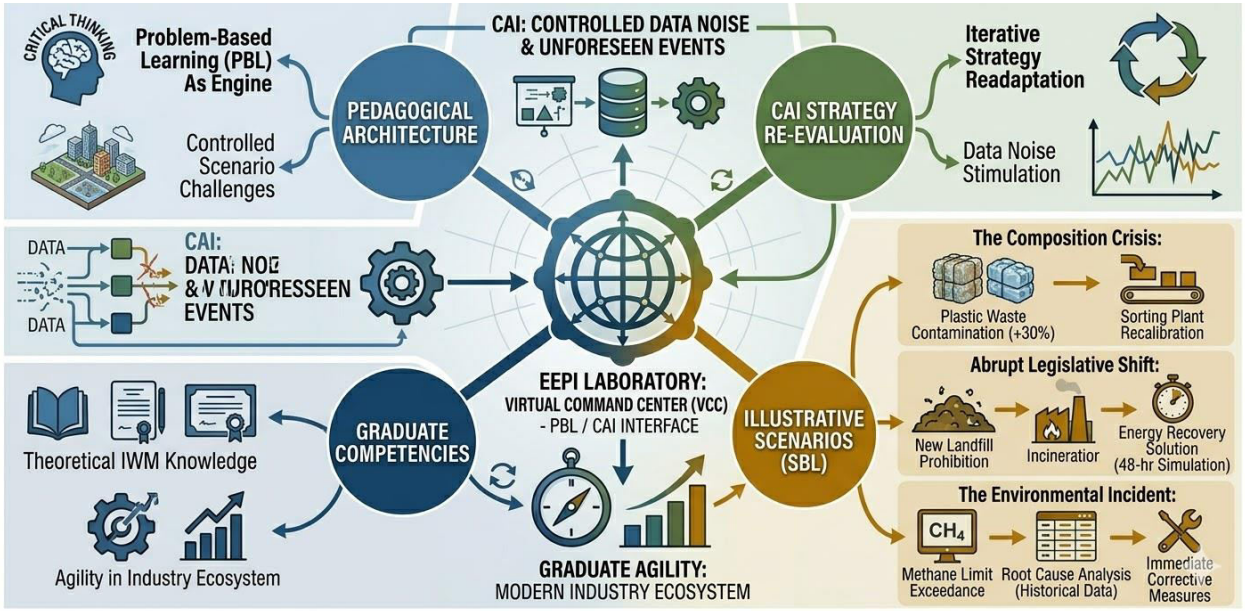

Fig. 3. Integrated workflow of CAI in IWM - a problem-based learning engine for critical thinking development (source: generated with Gemini 3 flash)

Consequently, the following sections detail several illustrative examples of PBL:

- ***The composition crisis*** - "*The contamination rate of collected plastic waste has suddenly increased by 30%. How do you recalibrate the sorting plant to maintain the quality of the secondary raw materials?*"
- ***Abrupt legislative shift*** - "*A new regulation prohibits the landfilling of high-calorific waste. Propose an energy recovery solution within a simulated timeframe of 48 hours*."
- ***The environmental incident*** - "*The monitoring system indicates an exceedance of methane emission limits. Identify the root cause by analyzing historical temperature and pressure data from the landfill body and propose immediate corrective measures*."

This pedagogical architecture transforms the EEPI laboratory into a virtual command center; in this context, the proposed methodology guarantees that the graduate will possess not only theoretical knowledge of IWM but also the agility to navigate the ecosystem of modern industry.

4. Competency assessment in IWM within the CAI ecosystem

Assessment within the EEPI specialization, mediated by CAI, must transcend conventional multiple-choice testing. We propose a system based on performance analytics, where the learning platform records not only the final output but the student's entire decision-making trajectory. This granularity allows for the identification of the exact moment a technical rationale (e.g., *selecting a hazardous waste treatment method*) becomes suboptimal or legally non-compliant.

A central tool in this phase is the integrated competency assessment matrix (ICAM); this matrix divides student performance into three vectors (see Table 1): *technical accuracy* (calculations and models), *regulatory compliance*, and *sustainability solution*. Through CAI, these rubrics become interactive, providing the student with a radar chart of their competencies immediately upon task completion. Some notable examples of digital metrics:

- ***Modeling fidelity index*** - the proximity of the student's simulation to real-world data from certified environmental reports (e.g., *residual error in pollutant dispersion modeling*).
- ***Algorithmic efficiency*** - the ability to select the shortest and most cost-effective technological flow to achieve the recycling targets mandated by the scenario.
- ***Anomaly response time*** - the speed and accuracy of intervention during a simulated environmental incident at a composting facility.

Table 1: A comparative analysis - traditional vs. CAI-enhanced IWM instruction

Instructional & pedagogical factor	Traditional IWM approach (classic)	CAI-enhanced IWM framework (IWM-CAI 4.0)
1. *Knowledge model*	Unidirectional transmission of isolated waste management processes	Technology-mediated, constructivist system mirroring real-world dynamics
2. *Instructional design*	Reliance on traditional textbooks and geographical/ logistical constraints	Scenario-based and problem-based learning via digital platforms
3. *Practical Immersion*	Abstract conceptualization of the waste hierarchy and LCA	Digital immersion and VR for risk-free interaction with hazardous waste
4. *Technical tooling*	Manual calculations or basic graphical interfaces	Integration of SimaPro (LCA), ArcGIS (GIS), and STAN (MFA) for high-fidelity modeling
5. *Ethical & strategic depth*	Theoretical discussion of environmental ethics	Interactive simulations of illegal dumping consequences and CSR dilemmas
6. *Feedback loop*	Delayed assessment with a pedagogical time gap	Immediate feedback and real-time behavioral/design corrections
7. *Competency metric*	Static scores based on the final technical report	Performance analytics - tracking the entire decision-making trajectory
8. *Assessment focus*	Correctness of the final "paper" output	Modeling fidelity index, algorithmic efficiency, and anomaly response time
9. *Career readiness*	Theoretical specialist in a world of practical needs	Ready-to-operate architect of the circular economy with a digital project portfolio

The goal of this methodology is the creation of a digital project portfolio that certifies the graduate's ability to operate complex IWM tools. In our vision, the final examination is not a simple written paper, but the defense of a waste management master plan, fully generated and optimized through CAI. This portfolio has become a powerful employability tool; an EEPI specialist who can present a potential employer with LCA models developed in *SimaPro* or risk maps created in *QGIS* gains an immediate competitive advantage.

5. Conclusions and (re)configuring specialist training as a strategic imperative

The reconfiguration of IWM through the lens of CAI is not a mere technological update, but a structural reform of how we perceive environmental engineering. This article demonstrates that utilizing problem-based scenarios and specialized software transforms learning from a process of memorizing technological flows into a continuous exercise in systemic optimization. Adopting CAI allows universities to keep pace with the dynamic nature of EU legislation, turning waste management courses into living organisms that are permanently updated. Developing cross-disciplinary digital competencies paves the way for the adoption of the Waste Management 4.0 concept, where IoT sensors, Big Data, and AI will govern the circular infrastructure of the future.

We believe that the success of this conceptual framework depends on the institutional courage to invest in faculty training and specialized software licensing. Without these assets, the specialist remains a theoretician in a world desperately in need of practical, rapid, and scientifically grounded solutions. The future of IWM is digital, and education must be the first sector to validate this reality.

References

[1] Bhardwaj, Nitesh, Sushman Sharma, and Kesha Patel. "Circular Economy and Sustainable Waste Management." *International Journal of Innovative Science and Research Technology* 10, no. 2 (December 2025): 837-839. 10.38124/ijisrt/25dec678.

[2] Tume, Suiven John Paul, and Agbor Ebai Maurice Tambe. "Building a Local Circular Economy Through Waste Valorisation in Bamenda, Cameroon." *Journal of Waste Management & Recycling Technology* 4, no. 2 (2026): 1-11. 10.47363/JWMRT/2026(4)165.

[3] The National Institute for Environmental Protection and Research / Istituto Superiore per la Protezione e la Ricerca Ambientale (ISPRA). *Report on Municipal Waste 2023. Summary data*. Report no. 394 bis/2023, September 2024.

[4] Datta, Deepshikha, Sayantan Sarkar, Saista Parvin, Sk Mehebub Alom, Esha Mandal, Soheli Biswas, and Bimal Das. "Waste Management and Circular Economy Strategies", pp. 157–185. In: Hossain, I., Ghosal, I., Haque, A.K.M.M. (eds.). *Green Policies for a Sustainable World*. Cham, Springer, 2026. 10.1007/978-3-032-08828-4_7.

[5] Jenčo, Ján, and Michaela Hletková Ploszeková. "Waste hierarchy as an obstacle to the transition to the circular economy." Paper presented at Waste Forum 2025 Symposium, Hustopeče, Czech Republic, October 12-14, 2025.

[6] Falah, T.R. Fahsul, Muhammad Hatta Jamil, Eymal B Demmalino, Ariady Arsal, and Yenita Sandra Sari. "Waste Management and Circular Economy Approach in Sinjai Regency." *Journal of Cultural Analysis and Social Change* 10, no. 3 (2025): 949-962. 10.64753/jcasc.v10i3.2532.

[7] Cioruța, Bogdan-Vasile, Ioana-Elisabeta Cioruța, Gabriela-Ionela Hereș, and Alexandru Leonard Pop. "Pedagogical Implications of Computer-Assisted Instruction in Reconfiguring Content for Soil Remediation Technologies." *Hidraulica Magazine*, no. 4 (December 2025): 84-94.

[8] Cioruța, Ioana-Elisabeta, Bogdan-Vasile Cioruța, Gabriela-Ionela Hereș, Mirela-Ana Coman, and Alexandru Leonard Pop. "Pedagogical Valences of Computer-Assisted Training in the context of Adaptive Ecological Management of Protected Areas." *Hidraulica Magazine*, no. 4 (December 2025): 119-126.

[9] Sanjeev, A M. "Computer Vision Approaches for Waste Segregation: A Survey of Methods, Datasets, and Challenges." *International Journal for Multidisciplinary Research* 7, no. 6 (November-December 2025): IJFMR250664204. 10.36948/ijfmr.2025.v07i06.64204.

[10] Gagnao, Mj, Mark Leonel De Isidro, Ronelo Galaura, Jyrillen Segobre, Jamaica Mae Gamala, and Reiner Jun Alminaza. "Smart Waste Management System Using Computer Vision." *Komputasi: Jurnal Ilmiah Ilmu Komputer dan Matematika* 22, no. 2 (2025): 99-107. 10.33751/komputasi.v22i2.44.

Numerical Study on the Dynamics of Hydraulic Systems Controlled by Proportional Valves

Associate professor **Fănel Dorel ȘCHEAUA**[1,*]

[1] "Dunărea de Jos" University of Galati, MECMET Research Center

* fanel.scheaua@ugal.ro

Abstract: *In order to ensure efficiency in modern hydraulic actuation this study presents a numerical hydraulic actuation system analysis, using the numerical analysis method for modelling and simulation. The study aims to develop a rigorous mathematical model that describes the dynamic behaviour of the hydraulic components, represented by proportional valves and hydraulic cylinders. Based on this model, nonlinear differential equations are formulated that characterize the evolution of pressure, flow rate and actuator displacement velocity. While the numerical simulations can be performed for different operating conditions, including the variation of constructive parameters and control signals, the obtained results allow highlighting the influence of hydraulic parameters on the stability and performance of the system, as well as validating the efficiency of the numerical method used. The paper demonstrates that the numerical analysis environment represents an accessible and efficient for the theoretical analysis of hydraulic systems, providing a solid basis for their design and optimization.*

Keywords: *Hydraulic actuation, fluid flow parameters, modern techniques, numerical analysis*

1. Introduction

In the context of the accelerated development of control technologies and the need for energy optimization, the analysis of the dynamic behaviour of hydraulic systems has become essential. The study of hydrodynamic phenomena, pressure and flow variations, as well as the interaction between mechanical and hydraulic components allows the design of more efficient, more stable and easier to control systems. At the same time, the complexity of internal processes — such as fluid compressibility, pressure losses, valve nonlinearities and actuator dynamics — requires the use of advanced modelling and simulation methods.

Numerical simulation is today an indispensable tool in the analysis of hydraulic drives, as it allows the investigation of the system behaviour without the need of expensive physical prototypes or laborious experiments. The numerical analysis platforms, due to accessibility, syntax and numerical integration tools, provide an efficient environment for developing mathematical models and performing precision simulations. Through it, multiple operating scenarios, parametric optimizations and control strategies can be quickly analyzed.

The present work aims to develop a rigorous numerical model for a hydraulic drive system and to investigate its behaviour under various operating conditions. Both the theoretical foundations of the modelling and the numerical implementation are presented, along with the interpretation of the obtained results. Thus, the work provides a solid foundation for understanding and optimizing modern hydraulic systems.

Hydraulic drive systems are essential technical solutions in many industrial fields due to their ability to transmit and control large forces with high precision. This type of system uses an incompressible fluid to transfer energy from the power source to an execution element, ensuring stable and predictable linear or rotary movements. Due to their high energy density, flexibility in configuration and operational reliability, hydraulic drives are frequently found in mobile equipment, construction machinery, automated industrial systems, as well as in lifting, pressing or positioning applications. In addition, the robustness of the components and the ability to operate in difficult conditions make hydraulic systems a preferred option where performance and safety are a priority 0, 0, 0.

2. The hydraulic system model

A model of a hydraulic system for driving a linear motor with a return spring powered by a proportional valve from a pressure source and volumetric flow of hydraulic agent is proposed for analysis, while a fluid reservoir is connected to the discharge branch. This construction represents one of the simplest linear motor drive schemes that can achieve an axial translation of a mass or an equipment working body.
The hydraulic system is modelled by an assembly of interconnected mechanical and hydraulic elements represented by the hydraulic spring rod cylinder or linear actuator motor with elastic return, being powered by a 4/3 proportional distributor for which the specific equations to be considered within the numerical model will be written 0, 0, 0.
Considering the mechanical dynamics of the piston the equations of motion are:

$$m\frac{d^2x}{dt^2} = A \cdot p - k \cdot x - F_f$$
$$F_f = b \cdot v + F_C \tanh\left(\frac{v}{\varepsilon}\right) \quad (1)$$

where:

m –piston mass;

A – piston surface;

p – pressure in the supply chamber;

k – spring constant;

Ff – friction force;
b - coefficient of viscous friction;

Fc - Coulomb force.

When the system starts operating, the equations describing the dynamics of the hydraulic pressure must be considered, because the pressure value in the cylinder evolves according to:

$$\frac{dp}{dt} = \frac{\beta}{V}(Q - Av) \quad (2)$$

where:

β – bulk modulus of the working fluid;

V – chamber volume depending on the piston position;

Q – valve flow rate;

Av – volumetric flow rate due to piston displacement.
The 4/3 proportional valve model can be introduced into the calculation through the fluid flow rate corresponding to the connection that supplies the cylinder chamber and for the main sequences corresponding to the valve, for both the supply and the discharge of the working fluid on the admission/return branches which are modelled as follows:

I. Supply (positive opening):

$$Q_a = K_v u\sqrt{\frac{2(p_s - p)}{\rho}} \quad (3)$$

II. Discharge (negative opening):

$$Q_e = -K_v |u| \sqrt{\frac{2(p - p_b)}{\rho}} \tag{4}$$

where:

Kv - valve flow coefficient;

p_s – source pressure or hydraulic system supply pressure;

p_b – back-up pressure.

The proportional valve control is achieved through a control function *u(t)* which is defined as a step signal between 0.1 and 0.8 s which allows the analysis of the system response to a transient command.
The numerical simulation is performed by solving the system of ordinary differential equations (ODE) which is solved by means of a Runge-Kutta solver with adaptive step, suitable for moderately rigid systems, while in the initial conditions the piston is declared at the retracted position and the pressure is equal to the back-pressure 0, 0.
Numerical results are expected for the piston position, indicating the increase in position value and the movement of the piston in the cylinder due to the pressure generated by the valve.
The maximum position is provided which coincides with the piston stop to prevent the mechanical stroke from being exceeded.
Also, with reference to the piston speed, the transient response of the system and the effect of friction must be shown as well as the increase in pressure in the cylinder reflecting the fluid supply through the valve. The back-pressure limitation prevents the pressure from falling below the physical minimum value.
It should be highlighted that the model includes important nonlinearities related to Coulomb friction forces, back-pressure limitation, as well as fluid flow proportional to the square root of the pressure difference, and this approach allows a realistic simulation of the response of a hydraulic cylinder actuated by a 4/3 proportional valve 0, 0, 0.
The model is scalable, meaning that it can be extended with temperature models, temperature-dependent viscosity, or valves with neutral zones.

3. Numerical analysis for hydraulic fluid flow

Based on the above nonlinear dynamic model for the hydraulic actuation system a numerical analysis is developed in order to investigate the interaction between hydraulic pressure dynamics and mechanical translational motion parameters of the cylinder piston.
The system is described using a lumped-parameter approach, considering fluid compressibility, variable chamber volumes and piston dynamics.
The adopted model has the ability to simulate the position, velocity and pressure in the cylinder for the axial movement of the spring-loaded hydraulic piston and includes the nonlinearity of the circulated fluid flow through the directional valve.
The proposed framework provides a flexible and computationally efficient basis for parametric analysis and control-oriented study of hydraulic actuation systems 0, 0, 0, 0.
The results of the numerical analysis are presented in terms of position, velocity and pressure of the cylinder piston, and are shown in Figure 1.

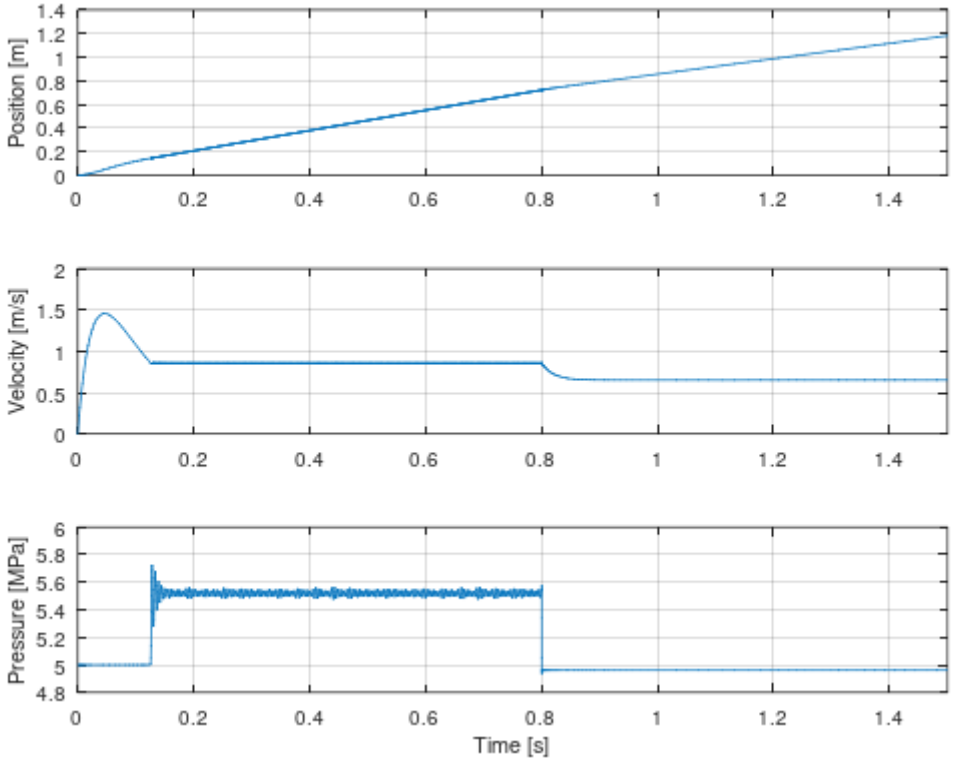

Fig. 1. The obtained results from numerical analysis

The simulation of the hydraulic cylinder was performed for the time interval *t=[0,1.5]* s with the initial conditions presenting the situation in which the piston is at the initial position *x0=0* m, the initial velocity v0=0 m/s and the pressure equal to the back-pressure *p0=pb*, the valve control was performed by means of a step signal of amplitude 0.6 in the range of 0.1-0.8 s and the graph for the piston position *x(t)* shows the rapid increase immediately after the valve opens at *t=0.1 s.*
The position increases approximately linearly during the acceleration phase, then stabilizes as the piston approaches the end of its maximum stroke xmax=0.15 m, while this curve reflects the balance between the hydraulic force generated by the pressure and the mechanical resistance forces (spring + friction).
The velocity *v(t)* exhibits a transient response characteristic of mechanical systems with mass and damping. Initially, the piston accelerates rapidly due to the increasing pressure, reaching a maximum level, while later the velocity decreases when the friction and spring pressure forces become comparable to the actuating force.
Observation of this curvature allows the estimation of the system response time and the effect of friction on the dynamic performance.
The pressure *p(t)* increases with the opening of the valve, reaching a maximum during the active phase of the control signal and after the valve closing, the pressure gradually decreases to the back-pressure value, being emphasized the pressure limitation below the visible pressure limit, confirming the protection implementation: *dpdt=0* for *p≤pb.* This limitation prevents the simulation of physically impossible states and reflects the real behavior of the hydraulic system.
The position and velocity graph provides information about the mechanical response, including acceleration and the friction effect, while the pressure graph allows the performance of the 4/3 proportional valve to be evaluated and back-pressure constraints to be verified.
These results are fundamental for the design and control of hydraulic systems and can be used in the optimization of valve parameters, piston mass or friction coefficients.

4. Conclusions

A numerical model of a hydraulic actuator system was developed in this work that can be

implemented to correctly describe the mechanical and hydraulic dynamics of a cylinder with a 4/3 proportional valve, including the effects of Coulomb friction forces, viscous friction and pressure limits.

The importance of pressure protection is shown by the possibility of ensuring the pressure values limitation within safe limits, thus ensuring the numerical stability conditions for the simulation and thus functionality which is essential for the realistic simulation of hydraulic systems.

The characteristics of the proportional valve were highlighted in the model through the valve flow rate coefficient and the supply pressure that determine the piston response velocity and the maximum reached pressure level.

The practical utility of the model allows the analysis of the transient response of the cylinder to specific commands, the evaluation of maximum to minimum velocities and pressure level which can be used for optimizing the system parameters or designing hydraulic control.

Acknowledgments

The research within this paper was conducted within Fluid Mechanics Laboratory, Engineering Sciences and Management Department, Engineering and Agronomy Faculty of Braila, "Dunarea de Jos" University of Galati and with the support of Machine Mechanics and Technological Equipments - MECMET Research Center, "Dunarea de Jos" University of Galati, Engineering and Agronomy Faculty of Braila and received no external funding.

References

[1] Axinti, G., and A.S. Axinti. *Hydraulic and pneumatic drives – Components and systems, Functions and features/Acţionări hidraulice şi pneumatice – Componente și sisteme, Funcții și caracteristici*. Vol. 1. Chişinău, Tehnica-Info Publishing House, 2008.

[2] Axinti, G., and A.S. Axinti. *Hydraulic and pneumatic drives – Bases of Calculation, Design, Operation, Reliability and Drive Diagrams/Acţionări hidraulice şi pneumatice – Baze de Calcul, Proiectare, Exploatare, Fiabilitate și Scheme de Acționare*. Vol. 3. Chişinău, Tehnica-Info Publishing House, 2009.

[3] Scheaua, F*. Fluid mechanics and hydraulic equipment/Mecanica fluidelor și echipamente hidraulice*. Galați, GUP - Galati University Press, ISBN 978-606-696-233-9, 2022.

[4] Wu, Yu-Ting, Zhen Qin, Amre Eizad, Sung-Ki Lyu, and Choon-Man Lee. "Numerical investigation of flow characteristics in a viscous damping system with symmetrical hydraulic cylinders." *International Journal of Precision Engineering and Manufacturing* 22, no. 4 (2021): 579-597.

[5] Algar, Antonio, Javier Freire, Robert Castilla, and Esteban Codina. "Simulation of hydraulic cylinder cushioning." *Sustainability* 13, no. 2 (2021): 494.

[6] Wu, Jia-Bin, Li Li, Yong-Kang Yan, Pin-Jian Wang, and Wei Wei. "An energy-saving position control strategy for deep-sea valve-controlled hydraulic cylinder systems." *Journal of Marine Science and Engineering* 10, no. 5 (2022): 567.

[7] Li, Yanchao, Ruichuan Li, Junru Yang, Xiaodong Yu, and Jikang Xu. "Review of recent advances in the drive method of hydraulic control valve." *Processes* 11, no. 9 (2023): 2537.

[8] Khan, Haroon Ahmad, So-Nam Yun, Eun-A Jeong, Jeong-Woo Park, and Byung-Il Choi. "A novel design and performance evaluation technique for a spool-actuated pressure-reducing valve." *Actuators* 10, no. 9 (September 2021): 232.

[9] Li, Ruichuan, Qiyou Sun, Xinkai Ding, Yisheng Zhang, Wentao Yuan, and Tong Wu. "Review of flow-matching technology for hydraulic systems." *Processes* 10, no. 12 (2022): 2482.

[10] Jiang, Wenguang, Cheng Zhang, Pengshuo Jia, Guishan Yan, Rui Ma, Gexin Chen, Chao Ai, and Tiangui Zhang. "A study on the electro-hydraulic coupling characteristics of an electro-hydraulic servo pump control system." *Processes* 10, no. 8 (2022): 1539.

Implications of Computer-Aided Instruction (CAI) in Reconfiguring the Contaminated Site Management Pedagogy

PhD Eng. IT exp. **Bogdan V. CIORUȚA**[1-3,*], MA stud. **Ioana-Elisabeta CIORUȚA**[4,5], Assoc. Prof. PhD Eng. habil. **Mirela-Ana COMAN**[6,7], Eng. IT exp. **Alexandru L. POP**[1,3], MA stud. **Gabriela-Ionela HEREȘ**[8]

[1] Technical University of Cluj-Napoca - North University Centre of Baia Mare, Office of Informatics, 62A Victor Babeș Str., 430083, Baia Mare, Romania

[2] Technical University of Cluj-Napoca - North University Centre of Baia Mare, Department of Mathematics and Computer Science, 76 Victoriei Str., 430072, Baia Mare, Romania

[3] Technical University of Cluj-Napoca - North University Centre of Baia Mare, Faculty of Letters - Department of Specialty with Psychopedagogical Profile, 76 Victoriei Str., 430083, Baia Mare, Romania

[4] Technical University of Cluj-Napoca - North University Centre of Baia Mare, Faculty of Letters - Department of Specialty with Psychopedagogical Profile, Construction and Curricular Innovation (MA prog.), 76 Victoriei Str., 430083, Baia Mare, Romania

[5] "Little Prince" Extended Program Kindergarten, 8B Cuza Vodă Str., 430034, Baia Mare, Romania

[6] Technical University of Cluj-Napoca - North University Centre of Baia Mare, Faculty of Engineering - Department of Mineral Resources, Materials and Environmental Engineering, 62A Victor Babeș Str., 430083, Baia Mare, Romania

[7] University of Agricultural Sciences and Veterinary Medicine from Cluj-Napoca, 3-5 Calea Mănăștur, 4000372, Cluj-Napoca, Romania

[8] Technical University of Cluj-Napoca - North University Centre of Baia Mare, Department of Mathematics and Computer Science, Computer Science and Software Engineering (MA prog). 76 Victoriei Str., 430072, Baia Mare, Romania

* bogdan.cioruta@staff.utcluj.ro

Abstract: *This paper analyses the pedagogical and practical valences of Computer-Assisted Instruction (CAI) within the context of integrated management of contaminated sites and waste, a field characterized by high technical and decisional complexity. We propose a conceptual reference framework (CRF) based on a triad of digital competencies - cognitive, operative, and strategic - designed to transform the educational process from a passive information flow into an interactive and adaptive experience. The study explores how the integration of specialized software platforms facilitates the simulation of invisible physico-chemical processes, allowing learners to test management hypotheses in a controlled, risk-free "sandbox" environment. Through progressive work scenarios, ranging from basic auditing to global waste governance, this research demonstrates that CAI develops systemic thinking and decisional resilience. Ultimately, the paper argues that the future of environmental expertise depends on a paradigm shift toward technology-mediated, constructivist learning models.*

Keywords: *Contaminated sites, instructional design, digital competencies, environmental protection*

1. Introduction

The management of contaminated sites represents one of the most complex challenges in contemporary environmental engineering, involving a heterogeneous mix of technical, legislative, and socio-economic variables [1-3]. The transition from traditional approaches to integrated management requires not only advanced technological solutions but also a highly skilled workforce capable of operating within a decision-making landscape marked by uncertainty [4, 5]. In this context, the training of future specialists can no longer be limited to conventional didactic methods; the complexity of pollutant transport phenomena in soil and groundwater demands training models that allow for the visualization and manipulation of virtual scenarios.

This is where the pedagogical valences of Computer-Assisted Instruction (CAI) intervene - an applied discipline that transforms the learning process from a passive flow of information into an interactive and adaptive experience for diverse situations (Fig. 1). The pedagogical essence of CAI in this field resides in its ability to simulate physico-chemical processes invisible to the naked eye.

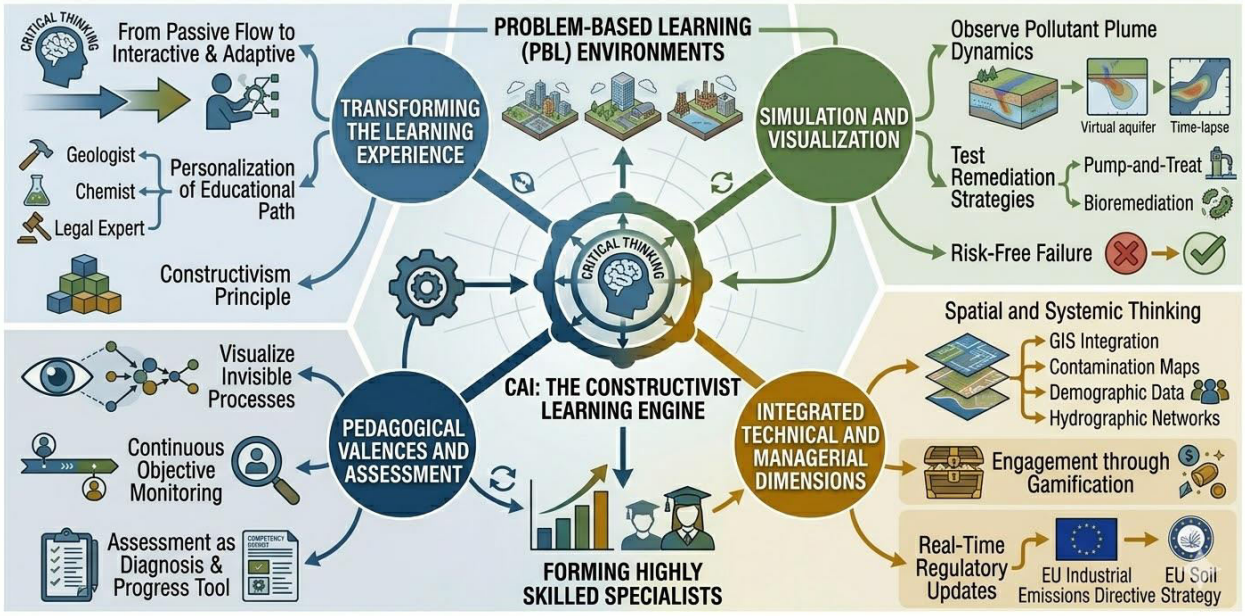

Fig. 1. Integrated workflow of CAI in CSMP - from passive flow to interactive and adaptive learning path (source: generated with Gemini 3 flash)

Through simulation software, students and practitioners can observe the dynamics of a pollutant plume under the influence of various remediation strategies - such as pump-and-treat or bioremediation - without the costs or risks associated with a real site. Instructional design applied to environmental management must be based on the principle of constructivism. CAI facilitates this by creating problem-based learning (PBL) environments, where the user is placed in front of a virtual contaminated site and must select, based on the provided data, the most effective investigation and remediation techniques. Key benefits for specialist training as follows:

- ***Personalization of the educational path*** - intelligent instruction systems can adapt the difficulty level and content according to the user's profile - whether geologist, chemist, or legal expert - ensuring an optimal learning curve for every specialization in the integrated management team.
- ***Learning by failure in a controlled environment*** - in real-world site management, a wrong decision can lead to ecological disasters or massive financial losses. In a CAI virtual environment, the learner can test the limits of a technical solution, understanding the consequences of failure without compromising environmental integrity.
- ***Spatial and systemic thinking*** - integrating Geographic Information Systems (GIS) into CAI platforms adds a critical spatial dimension to environmental education. The ability to overlay contamination maps, demographic data, and hydrographic networks develops the systemic thinking essential for a holistic approach to contaminated sites.
- ***Engagement through gamification*** - using gamification elements can increase motivation, transforming dry tasks - such as legislative compliance analysis or environmental auditing - into engaging learning experiences.
- ***Real-time regulatory updates*** - digital platforms allow for the instantaneous integration of new EU standards (such as the *Industrial Emissions Directive* or the *EU Soil Strategy*), ensuring training remains synchronized with administrative and technical realities.

A major pedagogical advantage is objective and continuous assessment. CAI platforms can monitor every step of the user during a site management simulation, providing immediate feedback and detailed analysis of acquired competencies.

This monitoring transforms assessment from a mere grade into a tool for diagnosis and educational progress. Introducing CAI into the integrated management of contaminated sites (IMCS) represents a pedagogical paradigm shift. It responds to the need for forming experts capable of managing environmental complexity through solid digital competencies, critical thinking, and strategic simulation capabilities.

2. Current State of Knowledge and Literature Review: The Convergence of E-Learning and Environmental Remediation

The evolution of specialized literature in the field of contaminated sites has undergone a visible transition, moving from purely technical studies on adsorption processes or chemical oxidation to complex analyses of decision support systems, even for risk-based management [6, 7]. Recent research highlights that the primary barrier to implementing integrated management is not a lack of technology, but rather a deficit in transdisciplinary competencies. Foundational works indicate that numerical modeling of pollutant transport represents the gold standard in risk assessment; however, the pedagogy behind these models often remains opaque to non-specialists.

Research in the field of CAI has demonstrated that the use of interactive computer simulations (ICS) significantly reduces the retention time of abstract concepts, such as hydrodynamic dispersion or in-situ biodegradation. Comparative studies between control groups (traditional instruction) and experimental groups (CAI-based) in environmental engineering reveal up to a 40% increase in the ability to solve unforeseen field problems, from regulation and mapping exposure to priority treatment, and remediation strategies [8-10]. This environmental digital literacy is now recognized as an essential meta-competency in the curricula of prestigious universities.

A significant segment of recent literature explores the use of Virtual Reality (VR) and Augmented Reality (AR) as extensions of CAI. These technologies allow the learner to be immersed in a living contaminated site, where monitoring data from sensors is projected in real-time over the visual environment. While promising, these approaches raise questions regarding instructional design: *How can we prevent cognitive overload when a site manager is simultaneously exposed to geochemical data, budgetary constraints, and legislative pressures within a virtual environment?*

The methodology proposed for this article is based on a mixed model, integrating the quantitative analysis of technical efficiency with the qualitative evaluation of the learning process. The starting point is the site management systemic architecture (SMSA), which is transposed into a digital training environment. The research is structured across 3 methodological pillars, as follows:

- ***Data modeling*** - in the first phase, real datasets from decommissioned industrial sites are utilized. These data (e.g., *heavy metal concentrations*, *hydrogeological parameters*, and *industrial activity history*) are processed to create the geometry of the problem; the methodology involves using spatial interpolation algorithms to generate contamination maps that serve as interactive teaching material within the CAI platform.
- ***Instructional scenario design*** - the second phase applies the ADDIE model (Analysis, Design, Development, Implementation, Evaluation) adapted for environmental engineering; in this context, decision trees are constructed where each user choice (e.g., *choosing a permeable reactive barrier instead of excavation*) triggers a simulation of the cost-benefit evolution and long-term residual impact. This method allows for the testing of management hypotheses within a sandbox structure.
- ***Evaluation and validation*** - the third pillar uses dual Key Performance Indicators (KPIs). On one hand, the accuracy of the technical solution proposed by the learner is measured (e.g., *reaching threshold values for pollutants within a given timeframe*). On the other hand, the user experience is evaluated through Likert-scale questionnaires and think-aloud protocols to determine the extent to which the CAI interface facilitated the understanding of complex environmental phenomena.

An innovative aspect of this methodology is the introduction of instructional life cycle analysis (ILCA). This evaluates not only the immediate success of a training session but also the sustainability of the competencies acquired over time. The goal is to observe whether specialists trained through CAI manifest greater decisional resilience in the face of real-world accidental pollution scenarios compared to those trained through classical methods.

The methodological framework is validated through a series of expert-review iterations, where senior environmental protection specialists and instructional design experts audit the coherence between learning objectives and the technical complexity of the simulations. This rigorous approach ensures that the CAI platform is not only a visualization tool but a robust educational ecosystem capable of generating authentic expertise in integrated environmental management.

3. Development of a Conceptual Reference Framework and Generation of Sustainable Work Scenario Proposals

3.1 From perception to phenomenological understanding (cognitive or input level)

The cognitive level constitutes the foundation upon which the entire expertise is built. In the management of contaminated sites, the primary barrier is the invisibility of the phenomenon; pollutants migrate through opaque media (*soil*, *rock*, *aquifers*). The role of CAI at this level is to provide ontological transparency. By utilizing advanced data visualization, the platform transforms spreadsheets containing thousands of concentrations into intuitive 3D models. This stage is not only about viewing, but about pattern recognition.
Pedagogically, this level is grounded in cognitive load theory; the specialist learns to decode the signature of a pollution event. For instance, understanding how a dense non-aqueous phase liquid accumulates at the base of an aquifer on an impermeable layer requires a spatial representation that no theoretical lecture can match. In this particular case, CAI facilitates assisted observational learning, where the user can virtually section the site along any plane to understand the relationship between lithology and pollutant distribution.

3.2 Mastering models and simulation of interventions (operative or process level)

The transition to the operative level marks the transformation of the learner from a passive observer into an active agent. At this stage, the integration of MODFLOW and PHREEQC becomes essential. The conceptual framework proposes that CAI functions as a virtual testing laboratory. The specialist does not merely run a model but learns to calibrate it.
This stage is critical for demystifying the software; the user understands that a model's output depends strictly on the quality of the input assumptions (the garbage-in, garbage-out principle). The primary pedagogical valence of this level is iterative experimental learning. Within a CAI environment, the specialist can simulate, for example, in-situ chemical oxidation; the user manipulates process variables: *oxidant dosage*, *the number of injection points*, and *the radius of influence*. If the model shows a concentration rebound, the learner must analyze desorption processes from the soil matrix. This direct interaction with transport and reaction mechanisms transforms theoretical biochemical knowledge into applicable technical competencies.

3.3 Synthesis and multi-criteria decision-making (strategic or output level)

The strategic level represents the apex of the triad, where environmental engineering intersects with project management; at this stage, CAI platforms no longer evaluate if the pollutant was removed, but how it was removed. The specialist is presented with multi-criteria decision analysis scenarios. In integrated management, success is not defined solely by reaching cleanup thresholds, but by optimizing a triple constraint triangle: public health protection, cost minimization, and the reduction of the ecological footprint of the intervention itself. From an instructional design perspective, this level employs the divergent scenarios method. The learner proposes a strategy, and the CAI system simulates the outcomes over a 20-year horizon. This temporal feedback is vital. The manager learns to think long-term, understanding, for example, that a low-cost solution today (such as monitored natural attenuation) could lead to immense legal costs in the future if the contaminant plume migrates under residential properties.
The proposed conceptual reference framework (CRF) architecture ensures an organic connection between the mentioned 3 levels through continuous feedback loops. What the learner discovers at the strategic level (e.g., *that a specific technology is cost-prohibitive*) forces a return to the operative level to optimize the technical design in MODFLOW, which, in turn, necessitates a re-evaluation of the initial cognitive data. This circularity mimics the adaptive management process utilized in large-scale environmental projects.

This CRF transforms CAI into a support system for the development of hybrid intelligence. The future manager of contaminated sites will not be a mere executor but an architect of solutions, capable of navigating fluidly between the rigor of differential transport equations and the pragmatism of economic decisions. CAI becomes the backbone of a new professional culture in environmental protection: one that is more transparent, precise, and, ultimately, more responsible toward our natural heritage.

3.4 Sustainable Work Scenarios for Computer-Assisted Instruction (CAI)

The following scenarios integrate the previously discussed software ecosystem into a coherent educational pathway, ranging from local technical issues to global environmental governance.

1) **Seepage assessment at a former fuel distribution station** (technical level)
   - Focus - identifying the contamination source and subsurface migration pathways;
   - CAI pedagogical task - utilizing 3D visualization software to overlay chemical analysis results onto a digital soil model; the future specialists learn to delineate the critical intervention zone through spatial interpolation, defining the soil volume for remediation.
2) **Integrated leachate management in a non-compliant landfill** (compliance level)
   - Focus - groundwater protection and liquid emission monitoring;
   - CAI pedagogical task - simulating the operation of a reverse osmosis treatment plant based on precipitation fluctuations; the user learns to balance storage volumes with treatment capacity, preventing accidental discharges into natural water bodies.
3) **Brownfield redevelopment into a residential area** (strategic level)
   - Focus - human health risk assessment and future resident safety;
   - CAI pedagogical task - running a risk calculation model to determine target cleanup concentrations; the concept of use-based safety is introduced, optimizing remediation costs according to the future land use.
4) **Aquifer remediation via permeable reactive barriers** (advanced level)
   - Focus - reactive transport processes and in-situ chemical kinetics;
   - CAI pedagogical task - integrating a PHREEQC module to predict the lifespan of the reactive material; the learner understands how chemical reactions can alter barrier permeability over time, requiring predictive maintenance.
5) **Transboundary water pollution management** (regional level)
   - Focus - water quality monitoring and early warning protocols;
   - CAI pedagogical task - operating a virtual crisis platform where IoT sensor data are used to model the propagation of a pollution wave between neighboring states; the task targets technical coordination and timely official notification.
6) **Ecodesign and life cycle assessment (LCA) for production streams** (systemic level)
   - Focus - reducing environmental impact from cradle to grave;
   - CAI pedagogical task - using LCA software to compare the carbon footprint and toxicity of two alternative materials; the learner understands the direct link between design decisions and the complexity of end-of-life waste.
7) **Circular economic systems in an industrial park** (integrated level)
   - Focus - industrial symbiosis and the recovery of waste as secondary raw materials;
   - CAI pedagogical task - managing a resource exchange network within a flow simulator; the user must maintain park profitability while minimizing final waste disposal by transforming outputs into inputs for neighboring facilities.
8) **Climate change impact on isolated historical sites** (global level)
   - Focus - resilience of remediation measures against extreme weather events;
   - CAI pedagogical task - simulating a major flood or sea-level rise scenario over a contaminated site; the task is to redesign protection systems to prevent pollutant remobilization under projected future climate conditions.
9) **Global governance of plastic waste and microplastics** (ethical and policy level)
   - Focus - international pollutant flows and extended producer responsibility;
   - CAI pedagogical task - a multiplayer simulation exercise where learners represent global actors that negotiate an environmental treaty.

3.5 Domain-specific software - the digital engineer's toolkit

To ensure Integrated Contaminated Site Management (ICSM) according to modern standards, the use of specialized software is no longer optional but a critical necessity (Fig. 2). These tools allow for the transformation of massive volumes of geochemical, hydrogeological, and topographic data into coherent decision-making models. From a CAI perspective, these platforms serve as digital laboratories where specialists can simulate interventions without real-world risks. The integration of these solutions into the training and operational process enables a holistic approach to the site.
Instead of analyzing soil, water, and air in isolation, integrated software allows for the visualization of complex interactions between these media. This capacity for synthesis is essential for the Operative pillar of the competency triad, providing the user with the necessary leverage to manipulate environmental variables within a controlled framework.

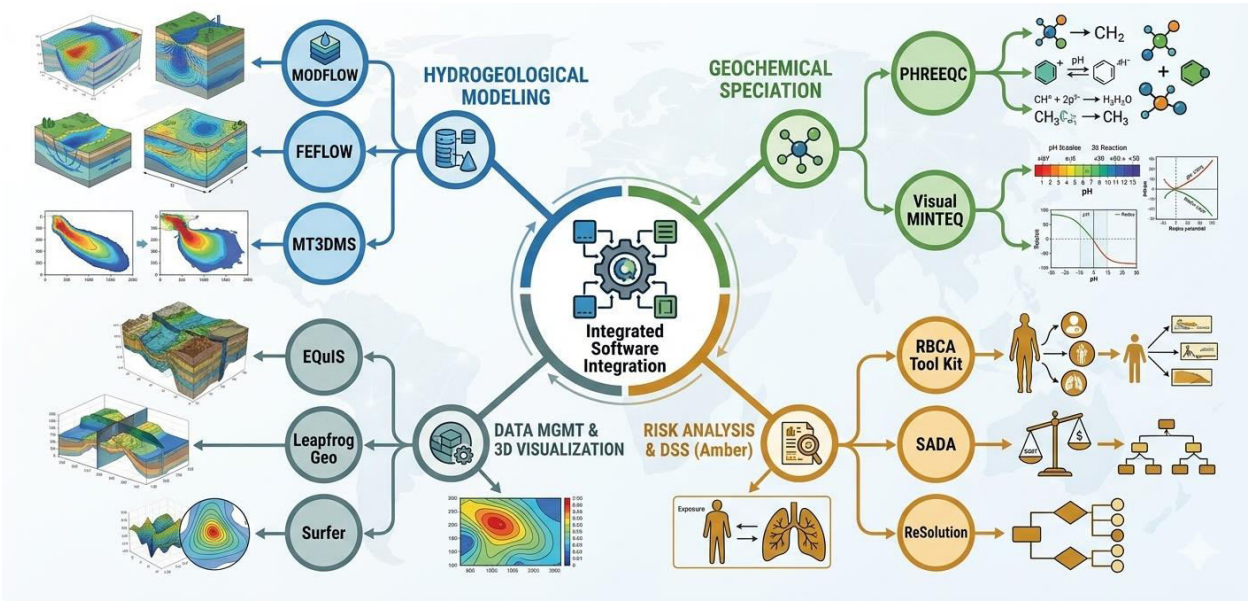

Fig. 2. Integrated workflow of CAI in CSMP - the digital toolset proposed
(source: generated with Gemini 3 flash)

The integration of professional software tools within a CAI framework allows for the digital replication of complex environmental phenomena. These instruments are categorized into 4 functional groups:

1) ***Hydrogeological and pollutant transport modeling*** - serve as computational engines that predict the trajectory and velocity of contaminants within groundwater systems.
   - *MODFLOW (via groundwater modeling system)* - the global standard for groundwater flow simulation. In a CAI context, the user learns to define boundary conditions and observe how well pumping alters the direction of a contaminant plume.
   - *FEFLOW* - an advanced finite-element modeling tool, ideal for sites with complex or fractured geology. It enables the simulation of heat transport and chemical reactions coupled with fluid dynamics.
   - *MT3DMS* - often used as an extension for MODFLOW, this software is specifically dedicated to chemical species transport, allowing for the calculation of advection, dispersion, and adsorption/decay reactions.
2) ***Geochemical and speciation modeling*** - essential digital tools for understanding the chemical state and mobility of a pollutant based on environmental parameters such as pH and redox potential.
   - *PHREEQC* - a versatile geochemical calculation tool. Learners can simulate how the injection of an oxidizing agent interacts not only with the target pollutant but also with native soil minerals.
   - *Visual MINTEQ* - used to determine chemical equilibrium in aqueous solutions; it is vital for designing leachate treatment plants or managing acid mine drainage.

3) ***Risk analysis and decision support systems*** - these programs bridge the gap to the strategic pillar, evaluating impacts on human health and remediation costs.
   - *RBCA (risk-based corrective action) tool kit* - assists site managers in determining if contamination requires immediate intervention or if the human health risk is acceptable based on exposure scenarios (inhalation, ingestion).
   - *SADA (spatial analysis and decision assistance)* - freeware that integrates GIS, geostatistics, and risk analysis modules, ideal for training students in visualizing data uncertainty.
   - *ReSolution* - dedicated to optimizing remediation strategies, allowing for cost comparisons between different technologies throughout the project's life cycle.
4) ***Data management and 3D visualization*** - integrated management requires a digital memory of the site, where thousands of data points are logically organized.
   - *EQuIS (EarthSoft)* - the world's most widely used environmental data management system, ensuring data integrity from tablet-based field collection to regulatory reporting.
   - *Leapfrog Geo/Hydro* - enables the creation of highly dynamic 3D geological models. Pedagogically, it is revolutionary as it allows for instantaneous cross-sectional slicing, facilitating the understanding of subsurface structures.
   - *Surfer (Golden Software)* - a geostatistical tool used for generating isoconcentration maps. It is often the first software a learner interacts with to visualize the extent of a pollution plume.

The value of these software solutions in the IMCS increases exponentially when they are used in combination. For instance, a learner can extract raw data from an EQuIS database, construct the geological model in Leapfrog, run the hydraulic simulation in MODFLOW, and finally evaluate the community risk using RBCA (Risk-Based Corrective Action). This interoperability represents the "holy grail" of integrated contaminated site management. From an educational perspective, the task of CAI is not to teach every single button of each program, but to train the specialist on how to transfer information between these platforms to ultimately achieve a faithful representation of field reality. The use of software enables "what-if" analysis; the environmental manager can simulate extreme climate scenarios and observe in real-time how site risks are redistributed.
This predictive capability transforms contaminated site management from a reactive activity into a proactive and resilient one. Dedicated software tools represent the backbone upon which modern integrated management rests. Without them, decisions would remain based on intuition or dangerous simplifications. Their integration into the CAI pathway ensures that the next generation of experts will possess not only theoretical knowledge but also the practical ability to navigate the digital complexity of environmental protection.

4. Strategic Perspectives and Best Practices for CAI-CSM Competency Assessment

The transition to a circular economy in Romania requires a structural reform in environmental engineering education, moving from memorizing technological flows to continuous systemic optimization. Assessment mediated by CAI offers a dynamic perspective permanently updated to reflect EU legislation and local socio-economic realities.

1) ***Transition to performance analytics*** via:
   - *From testing to tracking* - shift from traditional multiple-choice testing to a system based on performance analytics.
   - *Granular monitoring* - record the student's entire decision-making trajectory to identify the exact moment a technical rationale becomes suboptimal or non-compliant.
   - *Integrated matrix* - utilizes the ICAM to devide performance into technical accuracy, regulatory compliance, and sustainability.
   - *Visual feedback* - provides interactive rubrics that offer students immediate feedback via radar charts upon task completion.
2) ***Key digital metrics for engineering excellence*** via:
   - *Modeling fidelity index* - measures the proximity of student simulations to real-world data from certified environmental reports.

- *Algorithmic efficiency* - evaluate the ability to select the most cost-effective technological flows to achieve mandatory recycling targets.
- *Anomaly response time* - test the speed and accuracy of interventions during simulated environmental incidents, such as methane emission limit exceedances.
- *Problem-based scenarios* - use what-if challenges and data noise to force students to re-evaluate and re-adapt management strategies.

3) ***Professional deliverables and industry readiness*** via:
   - *Task-centered instruction* - ensure each CAI module culminates in a professional-grade technical document or digital model.
   - *Software interoperability* - assesses the student's ability to correlate input parameters across suites like SimaPro, ArcGIS, and STAN.
   - *Digital portfolios* - foster the creation of a digital project portfolio that certifies the graduate's ability to operate complex IWM tools.
   - *Employability advantage* - use LCA models and GIS risk maps as powerful tools for students to gain a competitive edge in the job market.
4) ***Ethical and strategic evaluation*** via:
   - *Temporal Perspectives* - use interactive digital case studies to illustrate the long-term consequences of illegal dumping, which traditional textbooks cannot convey.
   - *Corporate Social Responsibility* - utilize virtual environments to foster CSR skills by presenting ethical dilemmas between low-cost and sustainable solutions.
   - *Strategic capstone* - replace simple written exams with the defense of a comprehensive waste management master plan, fully optimized through CAI.
   - *Smart city integration* - evaluate the configuration of IoT/AI networks for real-time waste monitoring and predictive management.

Table 1: Comparative synthesis related to traditional vs. CAI-enhanced instruction in CSM

Instructional factor	Traditional scenario (classic)	CAI-enhanced scenario (Industry 4.0)
1. ***Knowledge acquisition***	Passive, lecture-based; focused on memorizing static remediation standards and protocols	Active, constructivist; based on navigating complex, high-volume data ecosystems
2. ***Problem-solving logic***	Linear and theoretical; limited to simplified textbook examples with predictable outcomes	Non-linear and systemic; utilizing what-if analyses to anticipate climate change impacts
3. ***Modeling & simulation***	Abstract conceptualization; inability to visualize subsurface contaminant migration in real-time	Digital Twins and 3D modeling; real-time visualization of plume dynamics and remediation efficacy
4. ***Technical tooling***	Manual calculations; reliance on static maps and historical reports	Software-mediated (GIS, MODFLOW, SimaPro); integration of IoT data for site monitoring
5. ***Risk management***	Purely theoretical discussion of safety and environmental hazards	Immersive simulations; testing intervention strategies in risk-free, high-fidelity virtual environments
6. ***Feedback mechanism***	Delayed (after grading); often disconnected from the active decision-making phase	Real-time, iterative feedback; immediate correction of design flaws through algorithmic validation
7. ***Competency assessment***	Static, based on the final report's technical correctness at a specific point in time	Dynamic, assessment of the entire decision-making trajectory and adaptive resilience
8. ***Learning outcome***	Theoretical expert with fragmented knowledge of site management components	Decisional strategist capable of transforming massive data into coherent, actionable models

5. Conclusions

The introduction of CAI into the IMCS marks a fundamental pedagogical paradigm shift, transitioning from a passive information flow to an interactive and adaptive experience. This approach addresses the high technical and decisional complexity of contemporary environmental engineering, providing future specialists with the capacity to operate within a landscape marked by uncertainty. By utilizing specialized software platforms, invisible physico-chemical processes become transparent through intuitive 3D simulations and models.
The proposed CRF is built upon a triad of digital competencies - cognitive, operative, and strategic - designed to guide the learner from recognizing pollution patterns to calibrating numerical models and making strategic decisions. Utilizing computational engines such as MODFLOW or PHREEQC allows for the testing of remediation hypotheses in a controlled sandbox environment, eliminating the ecological and financial risks associated with real-world errors. The interoperable integration of modeling, risk analysis, and visualization tools represents the holy grail of integrated management, transforming massive volumes of data into coherent decision-making models. This methodology develops systemic thinking and decisional resilience, preparing experts to anticipate climate change impacts through what-if analyses. The future of environmental expertise depends on the adoption of these technology-mediated, constructivist learning models that merge scientific rigor with decisional pragmatism for a responsible protection of our natural heritage.

References

[1] Swartjes, Frank A. "Introduction to Contaminated Site Management", pp 3–89. In: Swartjes, F. (ed.). *Dealing with Contaminated Sites*. Dordrecht, Springer, 2011. 10.1007/978-90-481-9757-6_1.
[2] Dupuis, Johann, and Peter Knoepfel. *The Politics of Contaminated Sites Management*. Cham, Springer, 2015. 10.1007/978-3-319-11307-4.
[3] Vidojević, Dragana, Nemanja Jevtić, Aleksandra Tomic, and Bozidar Djokic. "Improved management of contaminated sites in Serbia." Paper presented at International Conference on Contaminated Sites 2020 (ICCS 2020), Trnava, Slovak Republic, June 10–12, 2020 (initial date, postponed).
[4] Yu, Jingjing, Tian Liang, Huilong Luo, Panpan Wang, Bin Yang, Lina Wang, and Fasheng Li. "Case Analysis and Environmental Management Significance of Contaminated Site Reuse in China from 2011 to 2021." *Research of Environmental Sciences* 35, no. 5 (2022): 1110-1119. 10.13198/j.issn.1001-6929.2022.02.03.
[5] Samlani, Nouha, Cristina Deperon Maluf, Reginaldo Bertolo, and Tannaz Pak. *A New Data-Driven Framework for Operationalising Complexity in Contaminated-Site Management*. Preprint article, 2026. 10.2139/ssrn.6349411.
[6] Marcomini, Antonio, Glenn Walter Suter II, and Andrea Critto. *Decision Support Systems for Risk-Based Management of Contaminated Sites*. 1st edition. New York, Springer, 2009. 10.1007/978-0-387-09722-0.
[7] Agostini, Paola, Lisa Pizzol, Andrea Critto, Marco D'Alessandro, Alex Zabeo, and Antonio Marcomini. "Regional risk assessment for contaminated sites Part 3: Spatial decision support system." *Environment International* 48 (2012): 121-32. 10.1016/j.envint.2012.07.005.
[8] Litauriya, Disha. "From Regulation to Remediation: Strengthening Rule of Law in the Governance of Pollution Affected and Contaminated Sites in India." *International Journal of Research and Analytical Reviews* 6, no. 12 (2025): 5315-5322. 10.55248/gengpi.06.1225.4222.
[9] Vacca, Daniela, Enrico Olla, Giovanna Pala, Stefano Tersigni, and Luigi Minerba. "An experimental approach to mapping exposure in contaminated sites." *Rivista Italiana di Economia Demografia e Statistica* 80, no. 3 (2026): 273-284. 10.71014/sieds.v80i3.459.
[10] Trobec, Tajan, Barbara Lampič, Blaž Repe, Katja Vintar Mally, Nejc Bobovnik, and Lea Rebernik. "A Data-driven Approach to Assess the Need for Priority Treatment of Potentially Contaminated Sites (PCSs) in Slovenia." *European Journal of Geography* 17, no. 1 (2026): 72-92. 10.48088/ejg.t.tro.17.1.072.092.

FLUIDAS

NATIONAL PROFESSIONAL ASSOCIATION OF HYDRAULICS AND PNEUMATICS IN ROMANIA

fluidas@fluidas.ro